

TDP-43 based biomarker development in amyotrophic lateral sclerosis

by

Dr. Emily Feneberg

A thesis submitted to the University of Oxford for the degree of

DOCTOR OF PHILOSOPHY

Green Templeton College

Nuffield Department of Clinical Neurosciences

University of Oxford

For *my family*

Abstract

Amyotrophic lateral sclerosis is a devastating neurodegenerative disease which is clinically and aetiologically heterogenous. However, TDP-43 neuropathology is a unifying hallmark found in 97% of ALS cases. Understanding the common pathological pathways downstream of TDP-43 dysregulation is essential for the development of novel drug targets, and the development of a TDP-43 based biomarker for clinical translation would have profound implications for early diagnosis and monitoring of disease progression.

The work presented in the first part of this thesis addresses the need to develop TDP-43 as a unifying disease-specific biomarker. Mass spectrometry was used to detect TDP-43 from insoluble protein fractions extracted from ALS *post mortem* tissue with TDP-43 pathology which led to the discovery of ALS disease-specific TDP-43 peptides. These peptides were then validated in an independent targeted proteomic experiment which, for the first time, allowed the quantification of disease-relevant peptides. This enabled the measurement of an ALS-specific TDP-43 peptide signal that reflects sites of pathological truncation and an increased C-terminal TDP-43 protein ratio. This now provides a platform with which to investigate ALS biofluids with the aim to ultimately develop a disease-specific TDP-43 *in vivo* assay for patient stratification.

In the second part of the thesis I describe the use of affinity-enrichment mass spectrometry to investigate the human wild-type and M337V mutant TDP-43 interactome in a low expression (BAC)-transgenic mouse motor neuron model. I demonstrate that the C-terminal mutation of TDP-43 disrupts specific protein-protein interactions associated with human wild-type TDP-43. In response to oxidative stress, wild-type TDP-43 interactions shift towards proteins that are relevant to cellular stress pathways, while mutant TDP-43 is bound

to proteins that are independently linked to pathways known to drive ALS pathogenesis. The key interactions that were disrupted by the M337V mutation involve proteins that are important for stress granule formation and extracellular vesicle secretion. Furthermore, I was able to demonstrate correlative phenotypic abnormalities in stress granule assembly and exosome secretion in motor neurons from the human TDP-43 (BAC)-transgenic mouse model and also in human iPSC-derived motor neurons with the same TDP-43 M337V mutation.

In conclusion, work in this thesis provides significant novel data to support the further development of TDP-43 as an *in vivo* biomarker in ALS. Analysis of the TDP-43 interactome in a physiologically relevant mouse model has defined core cellular pathways matched to relevant phenotypes which will be important for the identification of pathways relevant for drug target development.

Declaration

Except where acknowledgement is made, all the work presented in this thesis was performed by the author in the Nuffield Department of Clinical Neurosciences, University of Oxford. The work reported in this thesis has not been submitted for any other degrees in this or any other University of Institute of learning.

Acknowledgement

I would like to thank Professor Martin Turner for his scientific support and encouragement throughout my DPhil. His ability to always inspire me as a scientist, clinician and person, will ever serve as an example for me. I am thankful to Professor Kevin Talbot who led me through the science of MND and to whom I owe an incredible gain of knowledge. He has been inspirational as a leader and made my time at Oxford University very valuable. I would like to thank Dr. Elizabeth Gray who always planned my projects with great experience, strategically and emotionally supported me throughout my DPhil and who very much helped me shape my scientific planning and career development.

I would also like to thank the Target Discovery Institute, Professor Benedikt Kessler, Dr Roman Fischer and Philip Charles who added their incredible proteomic experience to my projects. I would like to thank Professor Olaf Ansorge who provided me with *post mortem* tissue and to whom I owe detailed knowledge about TDP-43 neuropathology. I also want to thank Dr David Gordon for initiating the mouse embryonic stem cell cultures and sharing it with me. I am grateful to Dr Lynn Ossher and the clinic team who made every Monday enjoyable.

I would like to thank Dr Alexander Thompson and Dr Jakub Scaber who patiently introduced me to a new medical system, became incredibly important peers and made my time at Oxford unforgettable. I am grateful to Dr Ana Candalija, Chaitra Sathyaprakash, Paola Barbagallo and Lucy Farrimond who have enriched my DPhil with their support and friendship.

Above all, I am extremely grateful to my parents and my sister for their loving support and interest in my work.

Finally, I would like thank our ALS patients. Undoubtedly, the source of learning about ALS is inexhaustibly, when talking to patients and I will always remember their bravery in such a difficult condition. My research would have not been possible without their help. I would like to thank the MND Association for making this such an incredible community and the Lady Edith Wolfson Fellowship Fund and the Medical Research Council for generously supporting this work.

Abbreviations

AD	Alzheimer's Disease
ALS	Amyotrophic lateral sclerosis
ALSFRS	Amyotrophic lateral sclerosis functional rating scale
BAC	Bacterial artificial chromosome
CFTR	Cystic fibrosis transmembrane conductance regulator
Chat	Choline Acetyltransferase
CHMP2B	Charged Multivesicular Body Protein 2B
C9orf72	Chromosome 9 open reading frame 72
CSF	Cerebrospinal fluid
C-Terminus	Carboxyl-(COOH)-terminus
CTF	C-terminal fragment
CTL	Healthy control
Ctrl	Healthy control
DNA	Deoxyribonucleic acid
DDT	Dithiothreitol
EEC	El Escorial criteria
EGFP	Enhanced green fluorescent protein
eIF	Eukaryotic translation initiation
ELISA	Enzyme-linked immunosorbent assay
ESC	Embryonic stem cell
ESCRT	Endosomal sorting complex required for transport
EV	Extracellular vesicle
FTD	Frontotemporal dementia
FTLD	Frontotemporal lobar degeneration

FUS	Fused in sarcoma
GFP	Green fluorescent protein
GRN	Granulin
HEK293T	Human embryonic kidney 293 cells
hnRNP	Heterogeneous nuclear ribonucleoprotein
hiPSC	human induced pluripotent stem cells
IP	Immunoprecipitation
IAA	Iodoacetamide
kDa	Kilodalton
KIF5A	Kinesin heavy chain isoform 5A
LATE	Limbic-predominant age-related TDP-43 encephalopathy
LC-MS/MS	Liquid chromatography tandem mass spectrometry
LMN	Lower motor neuron
M337V	Methionine-to-valine substitution at position 337
MN	Motor neuron
MS	Mass spectrometry
NaAs	Sodium arsenite
NTA	Nanoparticle tracking analysis
N-Terminus	Amino-(NH2)-terminus
Pabpc/PABPc	Cytoplasmic Polyadenylate/Poly(A)-binding protein
PFN1	Profilin 1
PLS	Primary lateral sclerosis
PMA	Primary muscular atrophy
PD	Parkinson’s Disease
PRM	Parallel reaction monitoring
Rab11	Rab-GTPase11a

Rab7	Rab-GTPase7
RNA	Ribonucleic acid
RRM	RNA recognition motif
SOD1	Superoxide dismutase
SQSTM1	Sequestosome 1
TDP-43	TAR DNA binding protein 43
TOF	Time of flight
TUBA4A	Tubulin alpha-4 chain
Tuj1	Beta-Tubulin III
UMN	Upper motor neuron
Unc119	Uncoordinated-119
VCP	Valosin containing protein
VPS41	Vacuolar protein sorting-associated protein 41 homolog
WB	Western immunoblot
WT	Wild-type
YPet	Yellow fluorescent protein

Table of Contents

Abstract *3*

Declaration *5*

Acknowledgement *6*

Abbreviations *8*

Table of Contents *11*

List of Figures *18*

List of Tables *21*

Chapter 1: Introduction *22*

1.1. The syndrome of amyotrophic lateral sclerosis **22**

1.1.1. The nature and diagnosis of amyotrophic lateral sclerosis 22

1.1.1.1. The core syndrome of amyotrophic lateral sclerosis 22

1.1.1.2. The diagnosis of amyotrophic lateral sclerosis 24

1.1.1.3. The clinical spectrum of amyotrophic lateral sclerosis 25

1.1.1.4. Progression and survival 26

1.1.2. Patterns of progression 27

1.1.2.1. Focality and spread of symptoms 27

1.1.2.2. Mechanisms of disease evolution 28

1.1.3. Epidemiology 31

1.2. TDP-43 an unifying disease-specific marker in ALS **33**

1.2.1. TDP-43 pathology in ALS 33

1.2.1.1. Neuropathology 33

1.2.1.2. The pathological signature of TDP-43 34

1.2.2. Genetics underlying TDP-43 pathology 37

1.2.2.1. TARDPB 38

1.2.2.2. C9orf72 39

1.2.2.3. Other genes associated with TDP-43 pathology 40

1.3. TDP-43 and its role in ALS pathogenesis 41

1.3.1. The cellular functions of TDP-43 41

1.3.2. TDP-43 in ALS pathobiology 43

1.3.2.1. Nuclear to cytoplasmic mislocalization 43

1.3.2.2. Protein-protein interactions 46

1.3.3. TDP-43 disease models 48

1.3.3.1. TDP-43 transgenic cellular and animal models 48

1.4. Functional dysregulation of TDP-43 in ALS 51

1.4.1. Aggregation and spreading 51

1.4.1.1. Liquid-liquid phase separation 51

1.4.1.2. Propensity for the formation of aggregates 52

1.4.2. Stress granule formation 53

1.4.3. Clearance of pathologic TDP-43 54

1.4.4. Intra- and extracellular trafficking in ALS 56

1.4.4.1. Nucleocytoplasmic transport 56

1.4.4.2. Endosomal trafficking 57

1.4.4.3. Extracellular release of TDP-43 58

1.5. Measuring TDP-43 in ALS 59

1.5.1. Neurochemical biomarkers in ALS 59

1.5.1.1. Neurofilaments 60

1.5.1.2. Disease-specific biomarkers in ALS 61

1.5.2. A TDP-43-based biomarker 63

1.5.2.1. Disease-associated TDP-43 isoforms in biofluids 63

1.5.2.2. Quantitative measurement of TDP-43 in CSF and blood 67

1.5.2.3. Limitations of the quantification of TDP-43 in human 69

1.5.3. Mass spectrometric analysis 70

1.6. Aims of the thesis 72

Chapter 2: Methods and Materials 73

2.1. Enrichment of TDP-43 and detection of TDP-43 peptides by mass spectrometry 73

2.1.1. Patient samples and *post mortem* tissue 73

2.1.3. Immunoprecipitation 73

2.1.4. Immunoblotting 74

2.1.5. Silver Staining 75

2.1.6. Serial extraction of soluble and insoluble protein fractions from tissue 76

2.1.7. Sample preparation for mass spectrometry – in-solution digest 77

2.1.8. Sample preparation for mass spectrometry – in-gel digest 78

2.1.9. Mass spectrometry and analysis 79

2.1.10 Digestion and peptide generation 80

2.2. Quantification of TDP-43 peptides by targeted mass spectrometry 83

2.2.1. Heavy isotope-labelled peptides 83

2.2.2. Sample preparation for parallel reaction monitoring 83

2.2.3. Parallel reaction monitoring 83

2.2.4. Statistical analysis 85

2.3. Studying the human TDP-43 interactome by mass spectrometry 86

2.3.1. Motor neuron cultures from mouse embryonic stem cells 86

2.3.2. Mass spectrometry and bioinformatics 87

2.3.3. Gene ontology (GO) enrichment analysis 88

2.3.3. Immunohistochemistry and confocal microscopy 89

2.4. Validation of proteomic data and studying cellular pathways derived from the human TDP-43 interactome 90

2.4.1. Co-Immunoprecipitation for immunoblotting 90

2.4.2. Cloning human TDP-43 constructs 92

2.4.2.1. cDNA Plasmid constructs 92

2.4.2.2. Subcloning of chemically component cells 94

2.4.2.3. DNA extraction 94

2.4.2.4. Restriction digests of plasmid DNA 95

2.4.2.5. Sanger sequencing 95

2.4.2.6. Site-directed mutagenesis 96

2.4.2.7. Ligation 96
2.4.3. Human cellular models 96
2.4.4. Ultrafiltration liquid chromatography and extracellular vesicle characterization 98
2.4.5. Quantification and statistical analysis 99

Chapter 3: Detection of pathological TDP-43 peptides by mass spectrometry 100

3.1. Introduction and Aims 100

3.2. Results 101

3.2.1. Enrichment of TDP-43 for mass spectrometric detection 101
3.2.1.1. Specificity of antibodies for affinity enrichment of human TDP-43 102
3.2.1.2. Efficiency of antibodies for affinity enrichment of human TDP-43 104
3.2.1.3. Antibody-based methods are limited for the enrichment of TDP-43 from human biofluids 104
3.2.1.4. Serial fractionation of ALS post mortem tissue with TDP-43 pathology enables the detection of disease-specific TDP-43 forms 106
3.2.2. Detection of TDP-43 and its pathological peptides by mass spectrometry 109
3.2.2.1. TDP-43 was not detected in human biofluids 109
3.2.2.2. Serial fractionation of ALS post mortem tissue enables the detection of TDP-43 113
3.2.2.3. TDP-43 is detected in the disease-specific low molecular weight fractions 116
3.2.2.4. Mass spectrometry has the potential to detect truncation of TDP-43 fragments by semi-specific peptide identification 119

3.3. Conclusion 120

Chapter 4: Quantification of TDP-43 peptides and its pathological forms in ALS 122

4.1. Introduction and Aims 122

4.2. Results 123

4.2.1. Construction of heavy isotope-labelled TDP-43 peptides for the quantification of TDP-43 123
4.2.1.2. Biochemical characteristics of heavy isotope-labelled TDP-43 peptides 123
4.2.1.1. Heavy isotope-labelled TDP-43 peptides for the quantification of TDP-43 and pathological truncation sites 128

4.2.2. Quantification of endogenous TDP-43 peptides by targeted mass spectrometry 129
4.2.2.1. Pre-analytical screening of samples and digest sufficiency 131
4.2.2.2. Quantification of endogenous TDP-43 peptides in tryptic and chymotryptic digested urea fractions across diagnostic groups 133
4.2.3. The C-terminal end of TDP-43 is increased in ALS urea fractions 136
4.2.3.1. Absolute quantification shows a disease-specific peptide signature in ALS 136
4.2.3.2. The absolute amount of disease-specific TDP-43 peptides in ALS cortex tissue was higher compared to controls 139
4.2.4. C-terminal fragments are increased in ALS urea fractions by immunoblotting 141
4.3. Conclusion 143
Chapter 5: The interactome of human TDP-43 in a cellular model of ALS 146
5.1. Introduction and aims 146
5.2. Results 147
5.2.1. The characterisation of motor neurons derived from human YPet-tagged TDP-43 (BAC)-transgenic mESCs 147
5.2.1.1. MESC-derived motor neurons express human wild-type and M337V mutant TDP-43 147
5.2.1.2. Differentiated mouse embryonic stem cells express neuronal and motor neuronal marker and low levels of human TDP-43 148
5.2.1.3. Low-level expression of human TDP-43$^{M337V/-}$ in (BAC)-transgenic motor neuron cultures leads to reduced survival in response to oxidative stress 150
5.2.2. Co-Immunoprecipitation of human YPet-tagged TDP-43 and identification of protein-protein interactions by mass spectrometry 152
5.2.2.1. Affinity enrichment of human YPet-tagged TDP-43 from mouse motor neuron lysates 152
5.2.2.2. Mass spectrometric analysis of the human TDP-43 interactome 154
5.2.2.3. Human wild-type and mutant TDP-43 have a shared background proteome and genotype-specific interacting proteins that are unique binding partners 154
5.2.3. The ALS-associated C-terminal mutation M337V alters the normal interactome of human TDP-43 156
5.2.3.1. C-terminal mutation of TDP-43 leads to a reduction in protein-protein interactions 156

5.2.3.2. Gene ontology enrichment analysis reveals impairment of the normal cellular function of human wild-type TDP-43 and links the M337V mutation to ALS associated pathways 157

5.2.3.3. The physiological function of TDP-43 demonstrated by human TDP-43^{WT} interactors is disturbed by the M337V mutation 159

5.3. Conclusion 162

Chapter 6: The interactome of human TDP-43 reveals important cellular pathways with implications for possible therapeutic targets in ALS 165

6.1. Introduction and Aims 165

6.2. Results 167

6.2.1. Validation of the TDP-43^{WT} interactor Poly(A)-binding protein in mouse motor neurons 167

6.2.1.1. The TDP-43^{WT} interaction with Poly(A)-binding protein is disrupted by the M337V mutation in mouse motor neurons 167

6.2.2. The M337V mutation alone is not sufficient to cause an interruption of exogenous expressed TDP-43 and PABPc binding in HEK293T cells 171

6.2.2.1. Expression of exogenous TDP-43 constructs in HEK293T cells 171

6.2.2.2. The interaction of TDP-43 with Poly(A)-binding protein is not abrogated by the M337V mutation, when expressed exogenously in HEK293T cells 173

6.2.2.3. The binding of Poly(A)-binding to N-terminal truncated TDP-43 is reduced 176

6.2.2.4. Interaction of Poly(A)-binding protein to TDP-43 is RNA dependent 178

6.2.2.5. Immunoprecipitation of TDP-43 from human fibroblasts derived from an ALS patient with the heterozygous TDP-43$^{M337V/-}$ mutation is impaired 178

6.2.3. Phenotypic characterization of *TDP-43$^{M337V/-}$* motor neurons reveal impaired functions relevant to identified pathways containing human TDP-43 interactors 181

6.2.3.1. Reduced formation of stress granules in response to oxidative stress treatment 181

6.2.3.2. Reduced vesicle secretion in response to stress treatment 187

6.2.3.3. Extracellular vesicles secretion is decreased in human iPSC-derived motor neurons from an ALS patient with the heterozygous TDP-43$^{M337V/-}$ mutation 190

6.3. Conclusion 191

7. Discussion *195*

7.1. The current understanding of ALS and the relevance of studying TDP-43 as a disease-specific marker in ALS **195**

7.2. The concept of measuring disease-specific TDP-43 from human *post mortem* tissue **197**

7.3. The detection and quantification of TDP-43 peptides discriminate ALS from other diseases **199**

7.4. Implications for future TDP-43 assay developments **200**

7.5. Studying the interactome of human TDP-43 in a mouse motor neuronal model elucidates pathways for the understanding of ALS pathogenesis **201**

7.6. A C-terminal M337V mutation of TDP-43 alters the interactome of TDP-43 ..... **202**

7.7. Towards the identification of protein-protein interactions linking phenotypes of M337V mutant TDP-43 mouse motor neurons **204**

7.8. Closing remarks **205**

8. Publications arising from this research period *206*

8.1. Original articles **206**

8.2. Review articles **206**

References *207*

List of Figures

Fig. 1.1. Cellular and molecular processes mediating neurodegeneration in ALS (Kiernan *et al*., The Lancet, 2011) 30

Fig. 1.2. Schematic of full-length TDP-43 illustrating the important domains and C-terminal fragments found in ALS/FTD (modified from Feneberg *et al*., Mol Neurobiol, 2018) 35

Fig. 1.3. TDP-43 pathology and trafficking in ALS and FTLD (modified from Feneberg et al., Mol Neurobiol, 2018) 64

Fig. 2.1. Specific and semi-specific peptide detection by LC-MS/MS and the underlying hypothesis of endogenous truncation 82

Fig. 2.2. Workflow for parallel reaction monitoring 84

Fig. 2.3. Human TDP-43 constructs for transient transfection of HEK293T cells 93

Fig. 3.1. Affinity enrichment of human TDP-43 from (BAC)-transgenic mouse brain homogenates and human biofluids 103

Fig. 3.2. Serial fractionation of ALS *post mortem* tissue with TDP-43 pathology enables the detection of disease-specific TDP-43 forms 108

Fig. 3.3. In-Gel size separation of immunoprecipitations from biofluids does not separate a TDP-43 molecular weight band at 48kDa 110

Fig. 3.4. Serial fractionation of ALS *post mortem* tissue enables the detection of TDP-43 by mass spectrometry 115

Fig. 3.5. TDP-43 is detected in the disease-specific low molecular weight TDP-43 fractions 117

Fig. 4.1. Characteristics of heavy isotope-labelled TDP-43 peptides 127

Fig. 4.2. Pre-analytical screening and digest sufficiency for parallel reaction monitoring 132

Fig. 4.3. Quantification of TDP-43 peptides 134

Fig. 4.4. Quantification of TDP-43 peptides in human post mortem cortex tissue 138

Fig. 4.5. Absolute amounts of TDP-43 peptides in human *post mortem* cortex tissue (fmol) 140

Fig. 4.6. Quantification of C-terminal TDP-43 fragments in soluble and insoluble protein fractions.....142

Fig. 5.1. Characterisation of motor neuron cultures from (BAC)-transgenic mouse embryonic stem cells that express human wild-type and M337V mutant TDP-43 at low levels 149

Fig. 5.2. Human *TDP-43*$^{M337V/-}$ (BAC)-transgenic motor neurons in response to oxidative stress.....151

Fig. 5.3. Human YPet-tagged TDP-43 is sufficiently immunoprecipitated from (BAC)-transgenic motor neuron lysates.....153

Fig. 5.4. LC-MS/MS identification of proteins that bind to human TDP-43 and how the M337V mutation affects its binding capacity.....155

Fig. 5.5. The TDP-43 interactome is altered by the C-terminal TDP-43 mutation 158

Fig. 5.6. The physiological function of TDP-43 demonstrated by human TDP-43^{WT} interactors and its potentially distinct condition-dependent functions 161

Fig. 6.1. The interaction of mouse Poly(A)-binding protein to human TDP-43 is disrupted by the M337V mutation in mouse motor neurons 169

Fig. 6.2. Cloning for expression of human full-length TDP-43, M337V mutant TDP-43 and N-terminal truncated C-terminal TDP-43 in HEK293T cells.....172

Fig. 6.3. The interaction of Poly(A)-binding protein and human TDP-43 is unaltered by the M337V mutation, when transiently expressed in HEK293T cells 175

Fig. 6.4. The interaction of Poly(A)-binding protein to N-terminal truncated TDP-43 is reduced in HEK293T cells.....177

Fig. 6.5. Immunoprecipitation of TDP-43 from human ALS fibroblasts with a heterozygous *TDP-43 M337V* mutation is impaired 180

Fig. 6.6. Time course of Poly(A)-binding protein-positive stress granule formation in response to 0.5mM NaAs treatment in *TDP-43*$^{WT/-}$ and *TDP-43*$^{M337V/-}$ mouse motor neurons 184

Fig. 6.8. Human YPet-tagged TDP-43 does not co-localize with Poly(A)-binding protein-positive stress granules 186

Fig. 6.9. In response to stress extracellular vesicle secretion is decreased in *TDP-43*$^{M337V/-}$ mouse and ALS iPSC-derived motor neurons 189

List of Tables

Table 2.1. TDP-43 primary antibodies 75

Table 2.2. Proteases and cleavage sites 81

Table 2.3. Primary antibodies for immunohistochemistry 90

Table 2.4. Protocol for restriction enzymes 95

Table 2.5. Oligomers for Sanger Sequencing 95

Table 2.6. Oligomers for site-directed mutagenesis 96

Table 3.1. Mass spectrometric results from TDP-43 IP from serum and in-solution digest 112

Table 3.2. Mass spectrometric results from TDP-43 IP from CSF and in-solution digest 112

Table 3.3. Detection of TDP-43 peptides from in-solution digest of urea fractions 114

Table 3.4. Detection of semi-specific TDP-43 peptides from in-gel digest of urea fractions 118

Table 4.1. Characteristics of all heavy isotope-labelled peptides (on the next page) 123

Table 4.2. Characteristics of final heavy isotope-labelled peptide selection for absolute quantification 126

Table 4.3. Clinical data and tissue regions of ALS *post mortem* tissue 130

Table 6.1. Cell number and viability per plate 188

Chapter 1: Introduction

1.1. The syndrome of amyotrophic lateral sclerosis

1.1.1. The nature and diagnosis of amyotrophic lateral sclerosis

1.1.1.1. The core syndrome of amyotrophic lateral sclerosis

Amyotrophic lateral sclerosis (ALS) is the commonest phenotype within the broader term motor neuron disease. It is an adult-onset neurodegenerative condition associated with the loss of upper motor neurons in the brain and corticospinal tract and the lower motor neurons of the brainstem nuclei and spinal cord anterior horns, resulting in progressive muscle weakness and paralysis, with a median survival of 30 months from symptom onset usually secondary to respiratory muscle insufficiency (van Es *et al.*, 2017). There is no obvious risk factor to develop ALS, instead patients often have a lean past medical history and the disease more often develops in middle age between 50 and 60 years (Al-Chalabi and Hardiman, 2013). However the number of genes associated with ALS significantly increased over the last two decades attributing genetics a substantial contribution to the development of ALS (Al-Chalabi *et al.*, 2017). ALS is a clinical motor syndrome, but its pathology is not restricted to the motor system, which is best demonstrated by its clinical overlap with the behavioural variant of frontotemporal dementia (FTD) (Strong *et al.*, 2017). The discovery of cytoplasmic TDP-43 inclusion in neurons and glia cells in both ALS and FTD has revealed a common pathological hallmark (Neumann *et al.*, 2006). Importantly the C9*orf*72 gene repeat expansion as a frequent cause of both diseases has further strengthened the link between ALS and FTD (Balendra and Isaacs, 2018).

Amyotrophic lateral sclerosis was described by Jean-Martin Charcot (1825–93) in 1865 and named ten years later in his book “Clinical lectures of the central nervous system”

(Charcot, 1865, 1875). Prior to Charcot, in 1862, Clarke (1817 – 1880) and Radcliffe (1822–89) had described the clinical characteristics of lower motor neuron (LMN) and upper motor neuron (UMN) degeneration in a description of a highly paralysed ALS patient with weakness and atrophy of the muscles, but also signs of rigidity and increased muscle tone:

"*..., the arms were found to be wasted to the last degree…and somewhat pronated and flexed, the relics of the muscles being tense and rigid, and altogether disobedient to the will."*
(page 216, line 8-11) (Radcliffe and Clarke, 1862).

They went on to describe the involvement of bulbar muscles, with the cause of death was specified as respiratory failure occurring in the early morning hours:

"*... the palsied and wasted state of the tongue, for the difficult deglutition, for the occasional trouble of breathing, for the mode of dying."*
(page 215, line 16-18) (Radcliffe and Clarke, 1862)

Despite prominent motor involvement, the "mind and intelligence" were noted to be unaffected in this patient. Detailed *post mortem* analysis of the central nervous system revealed a rather intact structure of the brain, while a majority of atrophic cells were observed in the anterior horn of the grey matter, suggesting the degeneration of the LMNs.

1.1.1.2. The diagnosis of amyotrophic lateral sclerosis

The diagnosis of ALS is made clinically and based on the unique regional patterns of UMN and LMN involvement. The disease presents with a heterogenous site of first symptom onset, approximately one third bulbar, one third upper limb and one third lower limb. A minority of cases commence with dementia, respiratory or truncal weakness. The diagnosis is usually made in ALS reference centres, when patients are seen by specialised neurologists. This contributes to a delay in diagnosis to up to one year from symptom onset (Zoccolella *et al.*, 2006), though mis-referral in primary care and over-concern over the exclusion of implausible mimic disorders are other avoidable sources of delay (Turner and Talbot, 2013). Clinical diagnostic certainty criteria have been established to categorize ALS patients at the time of diagnosis, historically (and increasingly questionably) for the purpose of enrolment into clinical study trials. The first diagnostic consensus criteria were defined in El Escorial in Spain in 1994 (Brooks, 1994). The diagnosis of ALS according to the El Escorial criteria (EEC) require the presence of evidence of LMN degeneration (clinical, electrophysiological, or neuropathological examination) and of clinical UMN degeneration, as well as the progression of the motor syndrome within a region or to other regions determined by patient history or examination. According to these criteria patients are categorized into clinically definite, probable, possible or suspected ALS based on the number of body regions (bulbar, cervical, thoracic and lumbar) in which there are combined UMN and LMN signs. Most clinical trials demand the definite or probable ALS category for confident inclusion, but at the same time this selects more advanced cases in which the therapeutic window is already narrowed. Furthermore, patients in the possible and even suspected categories die never having progressed to the 'higher' categories and with confirmed ALS on *post mortem* histopathology (Traynor *et al.*, 2000). In 2019 the revised Airlie House consensus guidelines for design and implementation of ALS clinical trials still advise enrolment of

ALS patients based on the Revised EEC 1998, who have also a short interval from disease onset to trial entry (Brooks *et al.*, 2000; van den Berg *et al.*, 2019). The clinical criteria according to El Escorial describe severity of clinical presentation as a result of the pathology involved, and not to the underlying diagnosis of ALS, but when symptoms are restricted to one body region or anatomically and neuronally circumscribed, the differentiation from mimic disorders is often more challenging and ALS as a diagnostic term is often avoided (Mitchell *et al.*, 2010).

1.1.1.3. The clinical spectrum of amyotrophic lateral sclerosis

Although the majority of ALS cases present with the classic pattern of combined UMN and LMN involvement, some UMN-predominant and LMN-predominant syndromes populate either side of a spectrum. 'Pure' UMN involvement is termed primary lateral sclerosis (PLS), but the line between this and UMN-predominant ALS is blurred up to four years from symptom onset. LMN-predominant ALS was historically termed progressive muscular atrophy (PMA), but within the spectrum of ALS more broadly (Visser *et al.*, 2007) (Chio *et al.*, 2011b). PMA patients typically have cortical spinal tract pathology and lower motor neuron ubiquitinated inclusions as seen in ALS (Ince *et al.*, 2003). PLS is a very slowly-progressive, typically symmetric spastic paresis with a median duration of up to 19 years and therefore clinically a more distinct entity to ALS (Pringle *et al.*, 1992). Subtyping of ALS can include regionally-limited phenotypes such as flail-arm syndrome or bulbar palsy (Wijesekera *et al.*, 2009). The most striking of all these more distinct forms is that patients have a longer survival compared to classic ALS (Chio *et al.*, 2011b). The spectrum of ALS further comprises cases where symptoms exceed the motor system and affect cognitive domains. At least one third of patients with ALS have detectable mild cognitive or behavioural impairment, with up to 15% fulfilling

criteria for the behavioural variant of FTD (Lomen-Hoerth *et al.*, 2002; Goldstein and Abrahams, 2013; Crockford *et al.*, 2018; Lule *et al.*, 2019). Cognitive changes may also be associated with PLS and PMA (de Vries *et al.*, 2019). An important aspect of discussing the ALS disease-spectrum is, whether or not different disease aetiologies or modifiers underlie these subtypes and should be recognized as different entities, when for example new therapeutic targets are developed or tested (Rosenfeld and Swash, 2006). On the other hand, it is suggested that distinguishing between ALS outliers and other disease entities remains subjective - exemplified in arbitrary distinctions between UMN-predominant ALS versus PLS, or between LMN-predominant ALS and PMA. Instead using the focality of symptom onset and the rate of anatomical spread that ultimately proves to be important for evaluating the disease evolution (Ravits and La Spada, 2009).

1.1.1.4. Progression and survival

The clinical syndrome of ALS is heterogenous and the natural history depends on many factors, also some clinical features indicate a slow or fast progressing form of ALS. The time of the presentation of the first symptom from diagnosis, the site of onset, whether symptoms remain regional localised or spread rapidly to other anatomical segments, the timing of involvement of respiratory and bulbar muscles, and the age of the patient all help to define the course of disease (Talbot, 2014). While the rate of progression can vary between individuals, it stays remarkably linear for the duration of the disease within an individual (Ravits and La Spada, 2009). Several models use clinical measures such as muscle strength, forced vital capacity or the ALS functional rating scale (ALSFRS) to determine the progression rate and also predict survival (Armon *et al.*, 2000) (Magnus *et al.*, 2002). However, to predict survival in individual ALS patients is much more difficult and relies on many clinical, cognitive, and genetic predictors defined at diagnosis (Westeneng *et al.*, 2018). Therefore, methods to assess individual survival rates are still

complex, often rely on subjective rating scales and can be lengthy as result. An objective marker to measure disease activity and outcomes for e.g. new treatment trials which depend on survival or rate of change would be of great benefit. Neurochemical biomarkers are currently not included in the diagnostic criteria, but are useful and easily accessible markers to predict disease progression and monitor effects under treatment (Otto *et al.*, 2012). Moreover, biomarkers could ultimately enable a diagnostic test in individuals for earlier diagnosis and facilitate access to therapeutic trails, for those suspected to have ALS. This highlights the need towards the development of a biomarker with the best diagnostic and prognostic value for ALS.

1.1.2. Patterns of progression

1.1.2.1. Focality and spread of symptoms

There is consensus that ALS has a focal onset to symptoms, starting in the bulbar or spinally-innervated territories, including cervical, thoracic or lumbar regions (de Carvalho and Swash, 2006). A study in 100 ALS patients demonstrates that in 98% of cases the disease starts in one region, where UMN and LMN involvement are maximal and then spread outward and towards caudal regions (Ravits *et al.*, 2007). The severity of UMN and LMN involvement are independent of each, also a slight dominance of LMN is normal (a single UMN innervates many LMNs). The pattern of spreading is explained by the differing somatotopic anatomy of the upper and lower motor system (Ravits and La Spada, 2009): a contiguous LMN spread in the spinal cord would first be expected from the hand region to the contralateral side (shortest distance) and subsequent to the ipsilateral caudal foot region (thoracic span arm to leg about 26 cm). From the UMN hand region the spread is first anticipated towards the ipsilateral foot then contralateral to the arm (3 to 6 cm). An exemption is pseudobulbar palsy where bi-focal signs underlie from

the start. The onset of symptoms can be discrete and the onset side correlates with neuron numbers affected.

1.1.2.2. Mechanisms of disease evolution

The mechanisms behind the onset of a degenerative focal lesion and subsequent spread is yet not known. An ubiquitous cause, such as gene mutations of ubiquitous expressed proteins (e.g. superoxide dismutase-1, SOD1; C9*orf*72 repeat expansion), versus a local and multiple hit cause, where molecular changes such as toxic protein products accumulate to a threshold of cellular tolerance depending on the type of cell are debated (Kanouchi *et al.*, 2012). A motor nerve is in a complex interplay with other cells and non-autonomous mechanisms caused by surrounding astrocytes and glial cells might be important mediators of the disease, as well as excitotoxicity and axonal transport deficits (Fig. 1.1.) (Kiernan *et al.*, 2011; Thompson and Turner, 2019). When symptomatic neurons accumulate beyond one region, symptoms become more widespread. However, spreading of disease can also occur trans-synaptic by increased glutamate excitotoxicity or the dying back of long axons. More controversial is the proposed prion-like nature of misfolded proteins resulting in a contiguous spread of ALS pathology in horizontal or vertical regions. Prion disease is characterized by the misfolding of a protein, known as prion or proteinaceous infectious particle, which renders it prone for spreading and transmission in a cell independent way to propagate disease (Walker and Jucker, 2015). Common features of prion proteins are sequence regions of low complexity and their ability to assemble into amyloid fibrils and ß-sheets (Eisenberg and Jucker, 2012). The fact that the conversion of proteins into insoluble aggregates is a hallmark of many neurodegenerative diseases (Jucker and Walker, 2013) and that many aggregate prone proteins in ALS have also low complexity domains (LCD), which render them aggregation prone (King *et al.*, 2012), is reminiscent of prion disease. However, a major

difference in ALS protein toxicity is that it is dosage-dependent (Bolognesi *et al.*, 2016) rather than aggregate-dependent (Arnold *et al.*, 2013). TDP-43 aggregates do also not stain for the typical thioflavin staining compared to classical amyloid plaques (Kwong *et al.*, 2008). In addition, the distribution of inclusions in ALS follows a stereotypical progression (Brettschneider *et al.*, 2013), weather this is caused by axonal transmission of the pathological protein TDP-43 from one site to other regions or just a sign of sequential affection of brain regions is not yet clear, but excludes a random contiguous transmission. In the context of the distribution of TDP-43 proteinopathy other forms of the intercellular transmission such as extracellular vesicles or exosomes are also important (Feiler *et al.*, 2015). TDP-43 has been identified in exosomes in the CSF of ALS patients, however without detecting the pathological forms of TDP-43 (Feneberg *et al.*, 2014). The transmission of pathological TDP-43 via exosomes in cellular models has to be interpreted with appropriate consideration of the fact that these models are based on overexpression, and therefore can induce dosage-dependent toxicity (Feiler *et al.*, 2015).

Fig. 1.1. Cellular and molecular processes mediating neurodegeneration in ALS (Kiernan *et al*., The Lancet, 2011)

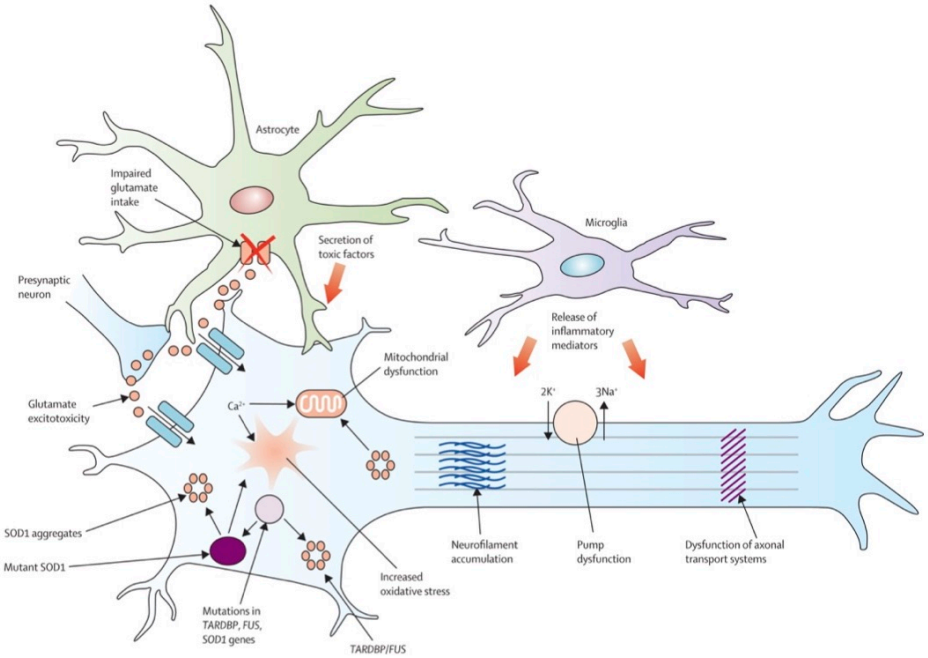


Fig. 1.1. The mechanisms underlying neurodegeneration in ALS are multifactorial and operate through inter-related molecular and genetic pathways. Specifically, neurodegeneration in ALS might result from a complex interaction of glutamate excitotoxicity, generation of free radicals, cytoplasmic protein aggregates, SOD1 enzymes, combined with mitochondrial dysfunction, and disruption of axonal transport processes through accumulation of neurofilament intracellular aggregates. Mutations in *TARDBP* and *FUS* result in formation of intracellular aggregates, which are harmful to neurons. Activation of microglia results in secretion of proinflammatory cytokines, resulting in further toxicity. Ultimately, motor neuron degeneration occurs through activation of calcium-dependent enzymatic pathways. ALS=amyotrophic lateral sclerosis.

1.1.3. Epidemiology

Multiple studies have determined a similar incidence of ALS across distinct geographical regions. Since 1990, registries have been founded to prospectively include ALS patients based on diagnostic consensus criteria. Three independent studies are highlighted: a study across Europe 1998-1999; a study conducted in Ireland 1995-2004; and one in Southern Germany 2010-2014. The first study assessed the incidence rate in six different regions across Europe: Ireland, Lancashire (UK), Lombardy (Italy), Piemonte (Italy), Puglia (Italy) and Scotland (Logroscino *et al.*, 2010). It included all of the different clinical subtypes of ALS such as the extremes of UMN involvement (termed PLS), LMN involvement (historically termed PMA) and body region-of-onset-defined syndromes (e.g. bulbar palsy). Rates for the European population were calculated combining all six registers resulting in 1028 individuals diagnosed with ALS of a total of 47.7 million person-years population. This resulted in an annual incidence rate of 2.16 per 100.000 person-years (male 3.0 and female 2.4). The rate of incidence increased from the age of 40 years and decreased in very old age. Incidences between regions were higher in Ireland and more ALS cases presenting with bulbar muscle weakness were also reported in this region. The Irish ALS register alone showed an annual average incidence rate of 2.6 per 100000 persons-years over six years in a 4 million population (O'Toole *et al.*, 2008). The incidence rate between 1995-1997 and 2002-2004 proved stable. The onset of the disease in the spinal region was almost twice as high in men, but onset in the bulbar region in men and women was equal. Therefore, bulbar-onset ALS in a prevalent cohort only accounted for one third of the numbers in an incident cohort (O'Toole *et al.*, 2008). The German study observed an age-adjusted incident rate of 3.1 per 100.000 person-years from 2009-2010 and 2012–2013 in a population of 8 million. This study deciphered a peak of incidence for ALS with a spinal-onset at earlier age 55-59 years compared with bulbar-onset at 75-79 years. This was confirmed in a separate study, which showed that

those over 80 years old presented more often with bulbar-onset of ALS, also associated with a shorter survival (Santos *et al.*, 2018). The prevalence in the German cohort was 8 per 100.000 person-years, totalling 6400 patients living with ALS in Germany. Due to a predicted ageing population, a significant increase in ALS incidence is projected for 2050. Beyond Europe, between 1997 and 2002 China calculated a lower incidence rate of 0.6 per 100.000 person-years on the limited basis of using a computer database and confirmation of diagnosis by hospitals at a later stage of inclusion. Epidemiologic studies in China have been inconsistent to date, but it is generally concluded that ALS is less frequent in China compared to both Europe and Japan (Doi *et al.*, 2014). The Chinese age peak is older at 60-64 years and the male to female ratio is 1.72:1 (Fong *et al.*, 2005). Hereditary cases are less frequently reported in literature from Asian countries with fewer cases of common European mutations, including *C9orf72* which is only found in 1/14 of all familial ALS cases compared to approximately 1/3 in European familial cases (Zou *et al.*, 2017).

1.2. TDP-43 an unifying disease-specific marker in ALS

Ubiquitinated cytoplasmic aggregates of the nuclear 43kDa transactive response DNA binding protein, TDP-43, is the histopathological hallmark of 97% of all cases of ALS (Neumann *et al.*, 2006; Chen-Plotkin *et al.*, 2010). TDP-43 pathology is found in 50% of the cases with frontotemporal lobar degeneration (FTLD). FTLD is used to describe the pathology, while FTD is used as an umbrella term for many different clinical syndromes underlying FTLD (Josephs *et al.*, 2011). TDP-43 pathology most commonly is associated with the clinical syndrome of behavioural variant FTD, which also often overlaps with ALS (Lomen-Hoerth *et al.*, 2002).

1.2.1. TDP-43 pathology in ALS

1.2.1.1. Neuropathology

Antibodies to ubiquitin first revealed the nature of the cellular protein inclusions found in ALS (Leigh *et al.*, 1991). Ubiquitin-immunoreactive inclusions were found in anterior horn cells of ALS derived spinal cords, mostly dense and round in form or irregular, in loosely arranged bundles, likened to skeins of wool. In contrast, relatively few inclusions were present in the pyramidal neurons of the motor cortex. Ubiquitin modification of the proteins found in these accumulations suggest that those have been resistant to degradation via the proteolytic pathway. Neumann et al. discovered that the main underlying protein of the inclusions present in both ALS and FTLD brains is TDP-43 (Neumann *et al.*, 2006).

The pathology of TDP-43 in ALS and FTLD is characterized by its mislocalization from the nucleus to the cytoplasm of neurons and glia cells where it is found posttranslational modified by phosphorylation and ubiquitination and N-terminal cleaved into smaller C-

terminal fragments (CTF) (Fig. 1.2. A). Neuropathological studies on the brain from ALS patients have shown that the phosphorylated form of TDP-43 can be found distributed in a relatively stereotyped spectrum of anatomical patterns which has led to the definition of four neuropathological stages (Brettschneider *et al.*, 2013). Stage 1 involves the spinal cord and the motor cortex, stage 2 and 3 involve the frontal and temporal lobe structures while in stage 4 a widespread cerebral pathology including the neocortex and allocortex is observed. All stages describe neuropathological patterns at *post mortem* and yet there is no evidence that the burden of TDP-43 pathology relates to clinical severity of disease or functional decline (Cykowski *et al.*, 2017). To date, only few case studies exist to describe a possible timescale of TDP-43 pathology development. In an autopsy case within an early disease phase, TDP-43 inclusions were only found in neurons, but not in glia cells, possibly suggesting an early cell-type dependent burden of disease (Kon *et al.*, 2019). In addition to different TDP-43 pathology *post mortem* stages, subtypes of characteristic staining of TDP-43 classified as FTLD-TDP type A-E can be distinguished (Lee *et al.*, 2017; Mackenzie and Neumann, 2017). Each subtype is characteristic for a certain clinical syndrome within the FTLD-ALS spectrum. TDP-43 type B is observed in most cases with ALS and reflects the early ubiquitin-description of round cytoplasmic inclusions and dystrophic neurites which are present in all cortical layers, while skein-like inclusions are typically seen in the spinal cord.

1.2.1.2. The pathological signature of TDP-43

Serial fractionation led to the extraction of insoluble proteins which specifically recovers pathological TDP-43 from affected brain regions (Fig. 1.2. B). Immunoblotting of sarkosyl-insoluble urea-soluble fractions showed the disease-specific signature for TDP-43.

Fig. 1.2. Schematic of full-length TDP-43 illustrating the important domains and C-terminal fragments found in ALS/FTD (modified from Feneberg *et al*., Mol Neurobiol, 2018)

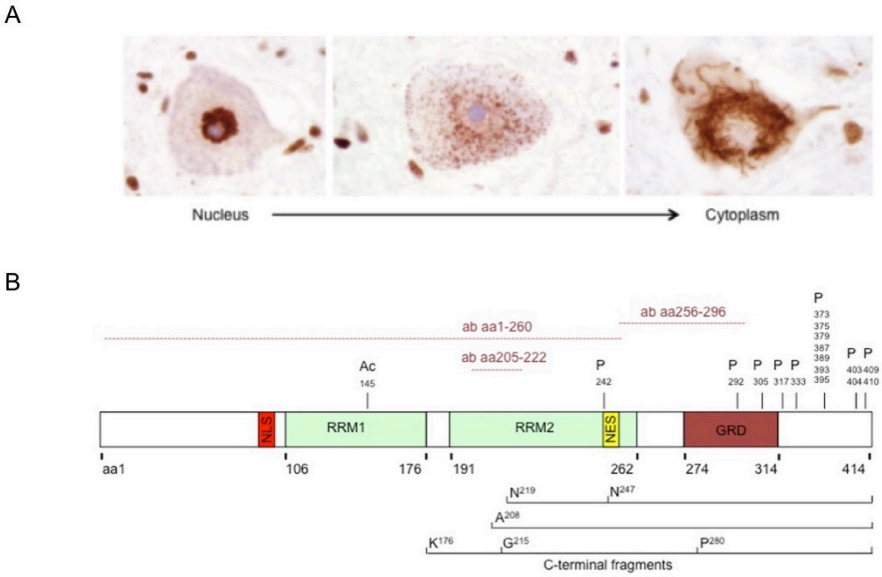


Fig. 1.2. A TDP-43 mislocalization from the nucleus into the cytoplasm and aggregate formation in motor neurons of the spinal cord of ALS **B** NLS nuclear localization signal, RRM RNA-recognition motifs, NES nuclear export signal, GRD Glycine-rich domain, P phosphorylation sites, Ac acetylation site and C-terminal fragments from Arginin A208 extracted from a 22kDa gel band of sarkosyl-insoluble, urea-soluble FTLD-TDP brains, Aspargin N219 and N247 extracted from a 23kDa band of FTLD-TDP (Neumann *et al*. 2006) and from Lysin K176, Glycin G215, Prolin P280 extracted from 23-25kDa bands of ALS brain fractions (Kametani *et al*. 2016). Abbreviations: Aa, amino acid; ab, antibody binding-site

This includes a high molecular weight smear, phosphorylated full-length TDP-43 with a molecular mass size of 45-50kDa and 60kDa and truncated forms at 24-26kDa, identified as C-terminal fragments of TDP-43 (Neumann *et al.*, 2006). The mechanisms of fragmentation of TDP-43 are still not fully understood but there is evidence that C-terminal fragments are different among neuropathological subtypes of FTLD-TDP. While shorter fragments are observed in FTLD-TDP types A-C, longer C-terminal fragments may predominate in a recently described FTLD-TDP subtype E (Lee *et al.*, 2017). By mass spectrometric analysis of the 23kDa band in urea-soluble fractions from FTLD-TDP brains, cleavage sites at amino acids 219, 247 and 208 of TDP-43 were reported (Igaz *et al.*, 2009; Nonaka *et al.*, 2009). Fragments of the size of 25kDa and 35kDa can be explained by caspase- or calpain-dependent truncation, however the presence of multiple C-terminal fragments argues for possible other mechanisms (Zhang *et al.*, 2009; Yamashita *et al.*, 2012; Berning and Walker, 2019). On a transcriptional level, alternative splicing of TDP-43 can lead to a 35kDa TDP-43 isoform, which is often found in ALS spinal cords suggesting that alternative splicing is altered in ALS (Xiao *et al.*, 2015). It is important to note that induced cleavage of TDP-43 in cellular models leads to rapid degradation of its fragments, while overexpression of C-terminal fragments or secondary changes such as RNA depletion impairs degradation and leads to the formation of inclusions, suggesting a two-hit model leading to accumulation of fragments into inclusions (Pesiridis *et al.*, 2011). It has been reported from human tissue that the presence of C-terminal fragments in sarkosyl-insoluble urea-soluble fractions of the spinal cord is less frequent and more variable compared with fractions of brain tissue (Neumann *et al.*, 2006; Igaz *et al.*, 2008). A possible explanation could be that cleavage of TDP-43 in spinal motor neurons does either not exist or spinal motor neurons have mechanisms to clear pathological fragments. TDP-43 can also be acetylated, but this is only found in the

spinal cord of ALS patients and not in the brain, where C-terminal fragments predominate (Cohen *et al.*, 2015).

Importantly, both the higher molecular weight bands and the lower truncated forms of TDP-43 are phosphatase-sensitive, implying disease-associated hyperphosphorylation (Neumann *et al.*, 2006). Many phosphorylation sites have been described for TDP-43, and ubiquitin-positive inclusions stain strongly for TDP-43 phosphorylated at serine residues 409/410 of the C-terminal glycine-rich domain of the protein (Hasegawa *et al.*, 2008; Kametani *et al.*, 2009). However, the timeline of the major pathological TDP-43 changes in phosphorylation, ubiquitination and aggregation has not yet been elucidated. Phosphorylation of TDP-43 can be an early event followed by mislocalization and aggregation, or is thought to be a secondary event after aggregate formation for the purpose of degradation processes (Neumann *et al.*, 2009; Nonaka *et al.*, 2016). A detailed biochemical study revealed different biochemical properties of pathological TDP-43 isolated from brains of FTLD and ALS patients (Laferriere *et al.*, 2019). Different pathological strains of TDP-43 were shown to underlie neuropathological subtypes of FTLD-TDP. Among those the most toxic form was associated with type A, which is often related with shorter disease durations. This suggests that not TDP-43 burden, but the pathological TDP-43 propensity correlates with clinical presentation.

1.2.2. Genetics underlying TDP-43 pathology

TDP-43 pathology is found in 97% of ALS cases, with cases linked to superoxide dismutase 1 (SOD1) and Fused in Sarcoma (FUS) accounting for the other 3% (though clinically indistinguishable). In at least 10% of ALS patients there is a positive family history with a definable underlying genetic component (Al-Chalabi *et al.*, 2017). Most of

the known genetic mutations have TDP43 pathology as a common underlying marker. *SOD1* gene mutations are the notable exception, accounting for approximately 20% of familial ALS cases, but lacking the classical TDP-43 pathology, suggesting that other common pathways are sufficient to cause the disease (Rosen *et al.*, 1993; Mackenzie *et al.*, 2007; Chio *et al.*, 2008). The fact that most familial FTD cases also have underlying TDP-43 pathology strengthens the view that ALS and FTD lie in a spectrum of disease linked by TDP-43 proteinopathy (Liscic *et al.*, 2008).

1.2.2.1. TARDPB

Support for a direct mechanistic link between TDP-43 and neurodegeneration comes from the identification of mutations in the *TAR-DNA binding protein* (*TARDBP*) gene in familial ALS, clinically and pathologically identical to sporadic ALS cases (Gitcho *et al.*, 2008; Sreedharan *et al.*, 2008). However, *TARDBP* mutations in ALS are rare and account for only about 4% of familial ALS and only a tiny percentage of sporadic cases (Kuhnlein *et al.*, 2008; Daoud *et al.*, 2009). *TARDBP* mutations are also found in a small percentage of ALS and FTD cases, but even less frequently in pure FTD. The *TDP-43 N267S* mutation has been found independently in patients with ALS or FTD, suggesting a common pathogenic role in both diseases (Benajiba *et al.*, 2009; Borroni *et al.*, 2009). Most of the ALS-causing genotypes of *TARDBP* are heterozygous missense mutations located in the C-terminal region of TDP-43, though one truncating mutation has been described. These findings suggest a fundamental pathological function for misprocessing of TDP-43 in ALS and FTD (Kabashi *et al.*, 2008; Van Deerlin *et al.*, 2008). In cell lines derived from patients with C-terminal TDP-43 mutations an increased cleavage of TDP-43 and phosphorylation can be observed. In some cases, missense mutations result in the exchange of amino acids such as threonine or serine, which enhance the substitution of phosphate groups (Sreedharan *et al.*, 2008).

1.2.2.2. C9orf72

The *C9orf72* mutation is the most common genetic cause found in approximately 40% of familial ALS, 25% of familial FTD, and 7% of sporadic ALS cases (Majounie *et al.*, 2012). The discovery of the *C9orf72* hexanucleotide GGGGCC repeat expansion in 2011 was a second molecular basis for a common underlying disease mechanism in ALS and FTLD (DeJesus-Hernandez *et al.*, 2011; Renton *et al.*, 2011). The *C9orf72* mutation is located in a non-coding region of chromosome 9 and follows an autosomal dominant inheritance pattern. The suggested pathomechanisms for *C9orf72* are:

1. Haploinsufficiency by impaired expression or splicing of the *C9orf72* gene.
2. Toxic RNA gain of function by sequestration of RNA binding proteins to transcripts with expanded repeats into RNA foci that can be found in the nucleus and cytoplasm (Donnelly *et al.*, 2013; Mizielinska *et al.*, 2013).
3. Toxicity of dipeptides which are sense and antisense products of the abnormal expanded GGGGCC repeat expansion of *C9orf72* generated through a non-canonical process called 'repeat associated non-ATG' (RAN) translation (Ash *et al.*, 2013; Gendron *et al.*, 2013; Mori *et al.*, 2013).

The second and third potential mechanisms highlight the importance of RNA metabolism for disease development. The underlying neuropathology in *C9orf72* mutation cases is a classical ALS pathology with TDP-43 inclusions (Cooper-Knock *et al.*, 2012). Most cases present with TDP-43 pathology type B, while a subset of cases also have comma-shaped neuronal cytoplasmic inclusions and numerous dystrophic neurites characteristic of FTLD-TDP type A (Mackenzie *et al.*, 2014). Noticeable frontal and temporal cortex involvement are more common in *C9orf72* ALS cases compared to *non-C9orf72* ALS, while FTLD cases also have motor cortex TDP-43 pathology (Hsiung *et al.*, 2012). In addition to TDP-43 pathology, a characteristic feature of *C9orf72*-positive patients is the

presence of neuronal cytoplasmic inclusions in the cerebellum, hippocampus and neocortex that are *negative* for TDP-43, but positive for proteins of the ubiquitin proteasome system (UPS) such as ubiquitin, ubiquilin and p62 (Al-Sarraj *et al.*, 2011; Brettschneider *et al.*, 2012). These inclusions are now identified as dipeptides and so far, seem to not correlate with the extend of neurodegeneration or clinical phenotype (Mackenzie *et al.*, 2013; Gomez-Deza *et al.*, 2015; Mackenzie *et al.*, 2015). However, that TDP-43 pathology alone is essential for the development of ALS/FTD in *C9orf72* cases comes into question in a case of a patient with early FTD where *in vivo* pure dipeptide pathology was found in the absence of TDP-43 (Mackenzie and Neumann, 2016; Vatsavayai *et al.*, 2016). Studies have reproduced *C9orf72* pathology in transgenic animals resulting in different degrees of neurodegeneration and phenotypes (Peters *et al.*, 2015; Liu *et al.*, 2016). Dipeptide toxicity was studied in cellular models expressed by synthetic genes without GGGGCC repeats (May *et al.*, 2014). These show aberrant dendritic arborization and apoptosis of neurons, activation of the ubiquitin proteasome system and decrease of the transport factor Unc119 under GA expression. Models for the *C9orf72* repeat-length-dependent dipeptide production show defects in nucleocytoplasmic transport and expression of arginine-containing dipeptides impairs the formation of membrane-less organelles such as stress granules by interacting with RNA-binding proteins and proteins with low-complexity domains (Freibaum *et al.*, 2015; Lee *et al.*, 2016).

1.2.2.3. Other genes associated with TDP-43 pathology

SOD1 does not lead to the typical TDP-43 proteinopathy, but there is evidence that SOD1 in some extend interacts with TDP-43 and in more detailed analysis increases pathological TDP-43 modifications (Jeon *et al.*, 2019). ALS mutations in *FUS* – another RNA-binding protein - do not lead to TDP-43 pathology, however given its close

similarity in function common mechanism are likely to underlie its pathogenicity (Vance *et al.*, 2009). Most other rare gene mutations show TDP-43 pathology, also not always proven to colocalize with the gene product (Kwiatkowski *et al.*, 2009; Toth and Atkin, 2018). Many of these rare ALS-causing genes have a role in intracellular trafficking and degradation. A mutation in the *valosin-containing protein (VCP)* gene is present in 1-2% cases of familial ALS and is involved in pathways of the endoplasmic reticulum, the Golgi-apparatus and endosomal trafficking. An *optineurin* gene mutation is present in 4% of the Japanese ALS population and has an additional role in exocytosis. *Sequestosome 1* (*SQSTM1)* directly connects polyubiquitination and autophagosomes. ALS genes are further involved in RNA processing (*hnRNP1A*), intracellular transport (*KIF5A, PFN1, TUBA4A*) and autophagy or inflammation (Kim *et al.*, 2013; Tanaka and Hasegawa, 2016; Brenner *et al.*, 2018; Brenner *et al.*, 2019). The latter includes the *serine/threonine-protein kinase 1 gene (TBK1)* that also links ALS and FTD.

1.3. TDP-43 and its role in ALS pathogenesis

1.3.1. The cellular functions of TDP-43

TDP-43 is named by its function to bind to the TAR DNA, which is also known to be the promoter region of the human immunodeficiency virus 1a regulatory motif in order to repress its transcription (Ou *et al.*, 1995). TDP-43 belongs to a family of heterogeneous nuclear ribonucleoproteins (hnRNP) which bind to nuclear nascent RNA polymerase II transcripts and package heterogeneous nuclear RNAs into particles. Each hnRNP contains RNA-binding motifs with a preference to certain transcripts (Krecic and Swanson, 1999). TDP-43 consists of a RNA-binding domain composed of tandem RNA-recognition motifs (RRM) separated by a 14-amino-acid linker (Lukavsky *et al.*, 2013). A common feature of all hnRNPs is an additional region of “unusual amino acid

distributions" that support them in their function to bind to RNA and further promote protein-protein interactions (Krecic and Swanson, 1999). This region was later confirmed to be a glycine-rich amino acid domain of the C-Terminus of TDP-43 that is able to promote protein interactions including with other hnRNPs due to its hydrophobic nature of amino acid repeats (Cartegni *et al.*, 1996). Even before TDP-43 had been known for its function to bind RNA, the RRM 1 of TDP-43 was already found as a regulator of alternative splicing of exon 9 of the cystic fibrosis transmembrane conductance regulator (CFTR) transcript. TDP-43 gene silencing leads to an upregulation of CFTR by exon 9 inclusion whereas TDP-43 recruitment to the 3' splice sites of exon 9 inhibits its recognition and promotes exon 9 exclusion (Buratti *et al.*, 2001). Further studies on how TDP-43 regulates transcription showed that TDP-43 preferentially binds to long UG-rich RNA motifs and intronic sites that are over 100 kilobase long. The binding to long RNA transcripts possibly requires more than one RRM which TDP-43 only can deliver as a protein homodimer (Polymenidou *et al.*, 2011; Tollervey *et al.*, 2011). Cross-linking–immunoprecipitation is a method to identify where a protein exactly binds to RNA transcripts. TDP-43 binds upstream of silenced exons and downstream of enhanced exons. Through this "flanking" of exons TDP-43 regulates alternative splicing which is mediated by the glycine-rich domain at the C-Terminus of TDP-43 (D'Ambrogio *et al.*, 2009). TDP-43 regulates itself through binding to its own 3'untranslated RNA non-continuous UG repeat region (Ayala *et al.*, 2011) and it is capable of regulating specific transcripts of proteins many of which are involved in neuronal survival indicating its important role within the brain (Tollervey *et al.*, 2011). It also binds to long non-coding nuclear RNAs including transcripts of *NEAT1* and *MALAT1*, both involved in paraspeckle formation and regulation of other splicing factors. A detailed RNA-protein interaction map gives evidence that TDP-43 is crucial for maintaining the levels and splicing patterns of more than 1000 RNAs (Polymenidou *et al.*, 2011). Some of these transcripts have a

role in synaptic function such as the subunit 2A of the NMDA receptor (Grin2a), the ionotropic glutamate receptor 6 (Grik2/GluR6), the calcium-activated potassium channel alpha (Kcnma1), the voltage-dependent calcium channel (Cacna1c) and the synaptic cell-adhesion molecules neurexin 1, 3 (Nrxn1, Nrxn3) and neuroligin 1 (Nlgn1). Loss of TDP-43 leads to a significant reduction of these transcripts. Furthermore, the C-Terminus of TDP-43 forms a complex with nuclear Drosha and cytoplasmic Dicer, which regulate miRNAs (Kawahara and Mieda-Sato, 2012). MiRNAs are also gene expression modulators and influence cytoplasmic mRNA translation, therefore TDP-43 has an indirect influence on cytoplasmic translation.

1.3.2. TDP-43 in ALS pathobiology

1.3.2.1. Nuclear to cytoplasmic mislocalization

The pathological hallmark of TDP-43 proteinopathy is the nuclear clearance of TDP-43 in conjunction with cytoplasmic inclusions (Neumann *et al.*, 2006). The loss of normal nuclear TDP-43 expression and the concomitant cytoplasmic inclusions of aggregated, phosphorylated and ubiquitinated TDP-43 prompts the discussion of a loss-of-function of TDP-43 versus a gain-of-function as potential disease mechanisms in ALS (Lee *et al.*, 2011). As cytoplasmic mislocalization is limited to a proportion of neurons in the cortex and spinal cord of ALS patients the role of upstream loss-of-function of TDP-43 as the primary cause in the pathogenesis of ALS has been suggested (Van Deerlin *et al.*, 2008). Nuclear clearance of TDP-43 may be an early event in the absence of mislocalization and cytoplasmic inclusions that often undergo a maturation process (Mori *et al.*, 2008). In ALS spinal cord tissue with TDP-43 pathology a dysregulation of genes that are regulated by alternative splicing of TDP-43 can be observed. Interestingly many of these genes are independently linked to neurological disorders or ALS, suggesting common pathological

pathways (Xiao *et al.*, 2011). A detailed study of extracted motor neurons from spinal cords of sporadic ALS and *C9orf72*-positive ALS patients by laser-capture-microscopy was able to demonstrate that the TDP-43 dependent splicing alterations are a key feature of those motor neurons exhibiting prominent mislocalization, but not in normal motor neurons (Highley *et al.*, 2014). Again, this involved the pathological splicing of gene transcripts many of them linked to ALS pathogenesis (including *FUS, Optineurin, Ataxin, VCP, Ubiquilin, Profilin, GRN, hnRNPA1, SQSTM1*). A mouse model that expresses human TDP-43 with a mutation in its nuclear localisation signal leading to nuclear clearing and cytoplasmic mislocalization of TDP-43 induced neuronal death in the absence of cytoplasmic phosphorylated and ubiquitinated TDP-43 inclusions supporting the idea that loss-of-function of TDP-43 causes neurodegeneration (Igaz *et al.*, 2011). Indeed, cytoplasmic mislocalization of human TDP-43 is sufficient to downregulate mouse endogenous TDP-43 and subsequently alter gene expression levels. The perturbation of nuclear TDP-43 levels therefore result in an abnormal function of TDP-43 directly arguing for a loss-of-function model. In addition to nuclear clearance and cytoplasmic mislocalization of TDP-43, TDP-43 can be found N-terminally truncated in the cytoplasm of neurons and glia cells. The corresponding C-terminal fragments are predominantly found in the cortex of ALS patients (Igaz *et al.*, 2008), but how these fragments affect TDP-43 pathology has only been studied in cellular overexpression models (Igaz *et al.*, 2009). Overexpression of C-terminal fragments, that still include RRM2 and the glycine-rich-domain, promotes the formation of cytoplasmic aggregates with post-translationally modified fragments. In the presence of these aggregates alternative splicing of the *CFTR* gene transcript, which is regulated by TDP-43, becomes dysregulated and are an indicator of abnormal function of TDP-43.

Adding to this complexity TDP-43 itself underlies a tight auto-regulative control, where the loss of nuclear TDP-43 possibly contributes to an increased synthesis of TDP-43 by arrest of its negative feedback loop possibly enhancing cytoplasmic accumulation. In contrast, overexpression of exogenic TDP-43 supresses TDP-43 production decreasing normal nuclear TDP-43 levels. However, this can be disrupted when aggregate formation impairs the C-terminal regions required for negative feedback (Ayala *et al.*, 2011; Igaz *et al.*, 2011). To dissect the pathological role of nuclear loss of TDP-43 on pathobiology more closely, transgenic mouse models were generated that recapitulate ALS by age-dependent motor neuron degeneration and motor deficits in the absence of cytoplasmic inclusions. This is mainly achieved by expressing wild-type or mutant human *TDP-43* transgenes at closer to physiological TDP-43 levels (Arnold *et al.*, 2013). Apart from other results this model demonstrates the importance of containing physiological TDP-43 levels under transgene expression by showing that alternative pre-mRNA splicing is affected by slight changes of expression levels of either mouse or transgenic TDP-43. Only under strict control of human mutant TDP-43 expression, a specific loss-of-function effect of the mutation on the splicing of direct exon targets of transcripts from *Kcnip2, Abhd14a, Ctnnd1, and Atp2b1* is demonstrated. Most other changes occur indirectly through an enhancement of normal endogenous TDP-43. The creation of knock-in mouse models enables to study the effect of point mutations in strategic regions of *TDP-43* without expression of a transgene (Fratta *et al.*, 2018). A point mutation in the RRM2 decreases the ability of TDP-43 to bind RNA (loss-of-function) and induces the inclusion of exons similar to the effect of TDP-43 knock-down experiments. In contrast, a mutation in the C-terminal glycine-rich domain leads to altered splicing through an increased exon exclusion under normal RNA-binding conditions (gain-of-function). The exclusion of exons seems to be promoted by the direct binding of TDP-43 to UGUGUG-rich motifs within exon to intron boundaries. As the majority of ALS mutations are located in the C-

terminal low complexity domain, this mechanism is an important disease relevant mechanism. The mechanism of skipping otherwise expressed and highly conserved exons in a gain-of-function mutation is now called "skiptik" exons. These skipping events often lead to a frameshift or the termination of transcripts, resulting in unstable transcripts and degradation. This in contrast to what has been reported to loss-of-function mutations (RRM mutations) where otherwise repressed exons are included called "cryptic" exons (Ling *et al.*, 2015). The gain-of-function mutation and exon skipping lead to an increase in TDP-43 mRNA levels within the mouse spinal cord tissue, in accordance with disturbed autoregulation of TDP-43. This was sufficient to cause an impaired motor phenotype in this model, also TDP-43 protein levels were unchanged and cytoplasmic inclusions or nuclear clearing was absent.

1.3.2.2. Protein-protein interactions

Three main studies focused TDP-43 protein-protein interactions and how these interactions can be altered in the presence of a pathogenic mutation. Protein interactions are mediated through its hydrophobic C-terminal domain and this is where most mutations in ALS are located. The first study used overexpression of human FLAG-tagged TDP-43 in human HEK293T cells in its wild-type form or with two disease-causing mutations (Freibaum *et al.*, 2010). In this study 126 proteins interacted with overexpressed wild-type FLAG-tagged TDP-4. This study was able to demonstrate protein-protein interactions that were composed of nuclear proteins including other hnRNP, serine/arginine-rich splicing factors, small nuclear ribonucleoproteins, an ATP-dependent RNA helicase and nuclear RNA export factors. Furthermore, a cluster was observed for proteins that are enriched in the cytoplasm and involved in functions such as translation initiation, elongation factors and ribosomal subunits. Poly(A)-binding protein c (PABPc), a protein important for transcription and translation regulation, was

found to link these two distinct protein interaction networks. This study was not able to identify any alteration of protein-protein interactions by overexpression of human FLAG-tagged TDP-43 with C-terminal mutations (A315T and M337V). This finding was in contradiction to another study where C-terminal TDP-43 mutations led to an increase in a protein-protein interaction with FUS (Ling *et al.*, 2010). The nature of TDP-43 as a RNA-binding protein suggests that protein interactions are RNA-dependent and the colocalization of TDP-43 in RNA granules corroborates this function in RNA metabolism (Freibaum *et al.*, 2010).

However, the presence of RNA may have differential effects on binding as some protein-protein interactions can also be disrupted by RNA (Blokhuis *et al.*, 2016). Biotin-GFP-tagged constructs of wildtype *TDP-43* and *TDP*-43 with the C-terminal mutation *M337V* in conjunction with a bacterial biotin ligase were expressed in N2A cells to perform a pull-down of the biotin-GFP-TDP-43 and subsequent protein identification of biotinylated bait proteins by mass spectrometry analysis (Blokhuis *et al.*, 2016). At the same time the interactome of other relevant ALS mutations (including *ATXN2 31Q, 39Q, FUS R521C, OPTN E478G, TDP-43 M337V and UBQLN2 P497H*) were investigated. This study used RNase treatment prior to immunoprecipitation to abrogate RNA-dependent protein interactions. This study noted a significant overlap (60%) of binding proteins seen in the previous study by Freibaum et al. and validated interactors such as hnRNPA2B1 and hnRNPA1, hnRNPH, hnRNPK, hnRNPQ, interleukin enhancer binding factor 3, Matrin 3, PABPc and probable ATP-dependent RNA helicase DDX5, many of which have been independently linked to neurodegeneration. Of note, PABPc was identified despite prior RNase treatment of cell lysates, although its binding was previously described as RNA-dependent. FUS seems to be a common interactor with ALS related proteins such as TDP-43 and Ataxin 2. The interaction of wild-type TDP-43 to

mutant FUS was further verified by colocalization of both proteins in cytoplasmic FUS-positive inclusions or TDP-43-positive inclusions in human ALS spinal cords (Blokhuis *et al.*, 2016). This suggests that both RNA-binding proteins have a common contribution to pathology. The reverse immunoprecipitation of a different RNA-binding protein, RBM45, was able to confirm the interaction of both TDP-43 and FUS (Li *et al.*, 2016).

1.3.3. TDP-43 disease models

1.3.3.1. TDP-43 transgenic cellular and animal models

Over-expressing human wild-type and mutant TDP-43 in human cellular and animal models has been used to study the pathologic biological functions of mutations and disease. Human cellular models were used to demonstrate a pathogenic role of newly identified mutations to develop disease-specific TDP-43 pathology and toxicity ranging from immortalized rodent or human cells, neuronal-like cells or hiPSC (Sreedharan *et al.*, 2008; Freibaum *et al.*, 2015; Tanaka and Hasegawa, 2016). Non-human yeast models have led to key identifications of the pathogenicity of the low-complexity domain of TDP-43 promoting liquid-liquid phase separation and stress granule formation (Molliex *et al.*, 2015). Smaller animal models, such as drosophila, were used to study the effects of pathologic TDP-43 cost-effectively within neuronal networks allowing phenotypic characterisations (Feiguin *et al.*, 2009). Transgenic human wild-type TDP-43 zebrafish were used to study nucleocytoplasmic defects with real time imaging by expression of fluorophores (Svahn *et al.*, 2018). Rodent models allow to study cell-type specific changes caused by TDP-43 mutations. Dependent on the expression promotor this can lead to the development of motor or behavioural phenotypes that in a broader term are reminiscent of an ALS- or FTD-like phenotype (Wegorzewska *et al.*, 2009). Mostly mice are used, but transgenic TDP-43 rat models also recapitulate certain phenotypes relevant

to ALS, also with a much higher variation and are therefore limited to more complicated research procedures such as the application of pharmaceutics (McGoldrick *et al.*, 2013). However, over-expression models are limited as the effect of dose-dependent toxicity of TDP-43 is well known (Ayala *et al.*, 2011). Therefore, the need for more 'physiological' disease models has become important. Human induced pluripotent stem cells (hiPSC) from patients with ALS have provided the opportunity to study disease mechanisms without the influence of an external transgene. The differentiation of hiPSC-derived motor neurons allows to study potential cell-selective vulnerability at the same time *in vitro*. It is the only model to study sporadic ALS (Fujimori *et al.*, 2018), but is commonly used to study the effect of genetic mutations. So far hiPSC-models of different ALS gene mutations have identified (Lee *et al.*, 2016) pathologic pathways and this will open new advances for treatment in ALS (Kiskinis *et al.*, 2014; Shi *et al.*, 2018). The study of transcriptional and phenotypic changes in mutant *SOD1* hiPSC-derived motor neurons showed an increased oxidative stress reaction, reduced mitochondrial function, altered subcellular transport, and activation of the ER stress and unfolded protein response pathways. Some of these features, such as impaired stress response, are similar in hiPSC-derived motor neurons from patients with the *C9orf72* mutation (Almeida *et al.*, 2013; Kiskinis *et al.*, 2014).

HiPSC-derived motor neurons from ALS patients with a C-terminal *TARDBP* (*M337V*) mutation showed an increase in soluble full-length and insoluble C-terminal TDP-43 fragments. Importantly this was observed in the absence of pathological mislocalization of TDP-43 demonstrating the difference to overexpression models of the mutant TDP-43 protein. Additional pathologic features were present, such as increased vulnerability and decreased survival of the mutant motor neurons compared to healthy controls, but the maturation and differentiation seemed unaffected by the mutation (Bilican *et al.*, 2012).

Not all experiments allow the use of hiPSC-derived models. This includes affinity-enrichment mass spectrometry analysis of target proteins to study protein-protein interactions. In stem cell models the protein product of a heterozygous mutation cannot be differentiated from the normal protein using affinity-enrichment, while the expression of tagged target-proteins allows specific detection. Interaction data of human TDP-43 can be obtained using targeted bacterial artificial chromosome (BAC) for transgenesis enabling the expression of the transgene from its native genomic environment. An exogenous tag enables highly specific affinity purification of human TDP-43 and selective depletion of the endogenous mouse TDP-43 while expressed in a cellular model relevant to pathology (Poser *et al.*, 2008; Hubner *et al.*, 2010). A mouse model expressing a single copy stably-integrated BAC transgene of human TDP-43 with a C-terminal fluorescence protein tag (YPet) led to low expression levels of the transgene (Gordon *et al.*, 2019). By expressing human wild-type or mutant TDP-43 in this model, the effects of the C-terminal mutation M337V were studied. Mutant heterozygous mice developed motor function deficits with reduced grip strength and a reduced latency to fall from the rotarod at the age of six months and progressing through to 18 months. The survival was nearly 50% reduced by two years in mutant mice compared to non-transgenic mice. There was a clear dose-effect of mutant TDP-43 as both survival and motor deficits were more severe in homozygous compared to heterozygous mutant mice. There was a reduced size of lumbrical neuromuscular endplates of 9-month old mutant TDP-43 mice. Also, TDP-43 levels were increased in the insoluble protein fractions extracted from mutant mice, there were no cytoplasmic TDP-43 inclusions in symptomatic lumbar spinal cord motor neurons, suggesting that aggregate formation is not necessary for disease initiation. The mouse embryonic stem cells (mESC) used to make the BAC mice can be further applied to differentiate motor neurons *in vitro.* One hour of 0.5mM sodium arsenite treatment induces oxidative stress and leads to the formation of stress granules in differentiated

motor neurons. Heterozygous *TDP-43$^{M337V/-}$* ESC-derived motor neurons showed a significant reduction of stress granules per neuron compared to heterozygous *TDP-43$^{WT/-}$* motor neurons, representing a robust phenotype (Gordon *et al.*, 2019). The generation of motor neurons from mouse ESC provides a unique tool to compare the effect of human wild-type TDP-43 or TDP-43 M337V under conditions close to physiological expression patterns with the advantage of the generation of high-throughput motor neuron cell cultures.

1.4. Functional dysregulation of TDP-43 in ALS

1.4.1. Aggregation and spreading

1.4.1.1. Liquid-liquid phase separation

The glycine-rich domain of TDP-43 is a low-complexity domain that has a similar amino acid sequence to prions in yeast models, so that the term prion-like domain has become established. Primarily the glycine-rich domain is important for protein-protein interactions and supports alternative splicing as reviewed above. Established using the RNA-binding protein FUS, it was recently shown that the low-complexity domains are important to form membrane-less granules by liquid-liquid phase separation (Kato *et al.*, 2012). Hydrogel droplet formation demonstrates that the reversible aggregation of this protein is dependent on its low-complexity domain. These droplets are further capable to form polymer-like structures similar to amyloid fibrils. This polymer formation retains other proteins with low-complexity domains (including TDP-43), but is also important for the association of mRNAs. Whereas the binding itself follows a certain pattern by which the 3'untranslated region of the mRNAs is recognized by the RRM (Kato *et al.*, 2012), phase separation of TDP-43 through its low-complexity domain contributes to its

self-aggregation and this can be promoted by C-terminal pathogenic mutations. In disease this process is enhanced through the presence of additional C-terminal fragments of TDP-43 (Molliex *et al.*, 2015). Under normal conditions there seem to be mechanisms that prevent TDP-43 from self-aggregation. Recently it has been suggested that the N-terminal region of TDP-43 is essential to retain its physiological form through the formation of homo-oligomers (Afroz *et al.*, 2017). N-terminal homo-oligomerization of nuclear TDP-43 prevents the low-complexity domains of TDP-43 to interact and self-aggregate. Homo-oligomerization of TDP-43 also explains the alternative splicing of long intronic UG-rich sequences, which is impossible for its monomer.

1.4.1.2. Propensity for the formation of aggregates

Many different mechanisms have been described to enhance aggregate formation of TDP-43 within models of ALS. Post-translational modification is an important regulatory mechanism to maintain protein homeostasis of TDP-43. While ubiquitination of proteins marks them for degradation, dysregulation of the ubiquitin proteasome system can enhance the aggregation of TDP-43 (Osaka *et al.*, 2016). The presence of ubiquitinated and phosphorylated TDP-43 in cytoplasmic inclusions in ALS possibly reflects an imbalance of this system. In ALS TDP-43 is found phosphorylated at serine 409/410, but multiple other phosphorylation sites have been described from *in vivo* extractions of TDP-43 aggregates (Hasegawa *et al.*, 2008; Kametani *et al.*, 2016). It has been shown that phosphorylation of TDP-43 increases oligomerization and fibrillization of TDP-43 and hyperphosphorylation can directly induce mislocalization and accumulation of TDP-43 in model systems (Nonaka *et al.*, 2016). Another contributor to pathological modifications of proteins is increased oxidative stress reactions associated with old age and many neurodegenerative conditions (Guil *et al.*, 2006). Oxidative stress activates integrated stress response pathways including phosphorylation and inactivation of the

eukaryotic translation initiation factor (eIF2A) while activating the serine/threonine-protein phosphatase to dephosphorylate eIF2A (GADD34). GADD34 also interacts with TDP-43 and casein kinase 1 to enhance phosphorylation of TDP-43, suggesting that oxidative stress can directly alter TDP-43 post-translational modifications (Goh *et al.*, 2018). Oxidative stress also induces reactive oxygen species that are capable of cysteine oxidation and disulphide-bond formations of TDP-43 (Cohen *et al.*, 2012). Results from an *in vitro* cellular model show that sodium arsenite treatment, an oxidative stressor, leads to an increase of insoluble TDP-43 and reduced alternative splicing of CFTR exon 9 by the generation of high molecular weight species caused by cystein oxidation. These changes affect the RRM 2 of TDP-43 that cause conformational changes leading to aberrant intra- and inter-molecular cross-links. Lysine acetylation is another modification that controls cellular protein processes and enhance aggregation of proteins in many neurodegenerative diseases. (Cohen *et al.*, 2015). Acetylation of TDP-43 seems to be restricted to the spinal cord of ALS patients, where it also promotes insolubility and aggregate formation.

1.4.2. Stress granule formation

TDP-43 is able to undergo liquid-liquid phase separation resulting in the formation of membraneless granules. This seems to be an essential function for the regulation of mRNA expression, processing and sorting under various forms of cellular stress. In TDP-43 over-expression models stress granule formation has been reported to be increased and associated with toxic aggregate formation, giving rise to the theory that stress granules seed TDP-43 aggregation (Liu-Yesucevitz *et al.*, 2010; Chew *et al.*, 2019). Other models show an impairment of stress granule assembly, suggesting a protective role of stress granules (McDonald *et al.*, 2011). Therefore, the relevance of stress granules to the

disease is still uncertain and may depend on the cellular model as well as expression levels of TDP-43 itself (Khalfallah *et al.*, 2018). Pathological confirmation of TDP-43 may also change the dynamics of stress granule formation rather than induce a complete lack of stress granule formation. Physiological stress granule formation requires a dynamic alteration in global RNA metabolism – with efficiency of RNA-binding proteins to bind RNA - which is then followed by the formation of a stable stress granule ‘‘core’’ (Markmiller *et al.*, 2018). PABPc, which is also an interactor of TDP-43, is found in the “shell” of stress granules, which characteristically forms in a dynamic behaviour requiring a rapid exchange of RNA-binding proteins between the cytosol and stress granule (Markmiller *et al.*, 2018). It can be argued that the loss of interactive TDP-43 through change of confirmation or mutations impairs the immediate assembly of stress granules (Kedersha and Anderson, 2002). A recent model in which TDP-43 proteinopathy is driven by optogenetic control has demonstrated that pathological aggregation of TDP-43 may occur independently of stress granule formation (Mann *et al.*, 2019). Also, the interplay with other proteins such as chaperonin-containing T complex (CCT complex) are important to inhibit (Leitner *et al.*, 2012; Jain *et al.*, 2016) or assemble stress granules in case for the chaperones HSP90b1 andHSP90ab1 (Matsumoto *et al.*, 2011). The stress granule marker PABPc can be found in cytoplasmic inclusions of pathological TDP-43 aggregates in neurons in ALS *post mortem* tissue, suggesting a role of stress granules in disease, however these findings are limited to end stage disease (Taylor and Dillin, 2011; McGurk *et al.*, 2014).

1.4.3. Clearance of pathologic TDP-43

A pathological hallmark of TDP-43 pathology is ubiquitination. The ubiquitin proteasome system is important for the degradation of soluble or misfolded, insoluble proteins, while larger aggregates are cleared by autophagy (Scotter *et al.*, 2014). Many

genes that are associated with ALS code for proteins of the ubiquitin proteasome pathway. It is therefore likely that mutations in these genes inhibit TDP-43 clearance resulting in a common pathology of TDP-43 accumulation (Jantrapirom *et al.*, 2018). The same effect is observed by chemical inhibition of the proteasome in primary neurons, which causes mislocalization of TDP-43 to the cytoplasm and subsequent phosphorylation and ubiquitination, recapitulating human disease aggregate formation (van Eersel *et al.*, 2011). Moreover, the clearance of TDP-43 underlies a tight control of the endosomal-lysosomal and autophagy pathway. The endosomal sorting complexes required for transport (ESCRTs) guide integral membrane proteins into intralumenal vesicles and multivesicular bodies. TDP-43 is found in multivesicular bodies that are subsequently fused with lysosomes for further degradation (Filimonenko *et al.*, 2007). Yeast models, where conserved cellular processes can be studied, have shown that the proteolytic activity and uptake of endosomal vesicles in multivesicular bodies is reduced in the presence of overexpressed TDP-43 (Leibiger *et al.*, 2018). Autophagy is a mechanism to retain cellular protein homeostasis, to remove insoluble proteins and aggregates or even organelles via macroautophagy (Glick *et al.*, 2010). It is tightly controlled by the cell and its function can be protective or detrimental for cell survival. There is evidence that TDP-43 itself regulates mRNA levels of the *autophagy related gene 7* (*ATG7*) and that depletion of TDP-43 leads to an impairment in autophagy resulting in accumulation of ubiquitinated proteins and autophagy protein p62 (Bose *et al.*, 2011). TDP-43 influences the mTOR complex 1 pathway by activating mRNA translation of RPTOR. Both are involved in the activation of autophagosome and lysosome biogenesis. TDP-43 deficiency leads to an enhanced autophagy-lysosome biogenesis, which is followed by accumulation of immature autophagic vesicles (Ying *et al.*, 2016).

In spinal cord, p62 was found in cytoplasmic inclusions of TDP-43 (Sasaki, 2011) and different markers of autophagy have been found colocalized to TDP-43 inclusions independent of ubiquitin in FTLD brains (Hiji *et al.*, 2008). Many gene mutations that are associated with ALS are involved in autophagy pathways and there is evidence that the dysfunction of these pathways lead to increased TDP-43 accumulation (Chang *et al.*, 2017). Therapeutic interventions that activate autophagy using rapamycin or tamoxifen describe promising effects on the clearance of TDP-43 aggregates and may be beneficial in disease (Caccamo *et al.*, 2009; Wang *et al.*, 2012). Importantly, *C9orf72* repeat expansion impairs autophagy most likely through the formation of complexes with several rab-GTPase that are involved in autophagosome formation (Webster *et al.*, 2016; Corbier and Sellier, 2017).

1.4.4. Intra- and extracellular trafficking in ALS

Many genes that are associated with ALS affect cellular trafficking therefore intra- and extracellular transport deficits in ALS could reflect a common pathomechanism. Trafficking processes that have been linked to the pathogenesis of ALS include endosomal trafficking and autophagy, axonal and nucleocytoplasmic transport. Additionally, the secretion of extracellular vesicles has become extremely important for many neurodegenerative diseases and are potential mediators of disease (Thompson *et al.*, 2016).

1.4.4.1. Nucleocytoplasmic transport

Over-expression of the pathological C-terminal fragment of TDP-43 induces pathological protein aggregation and impairment of the nucleocytoplasmic transport (Woerner *et al.*, 2016). Many proteins with disordered and low-complexity sequences were found to be recruited to aggregates including a nuclear export protein (THO), which in normal

conditions shuttles between the nucleus and the cytoplasm. It was shown that cytoplasmic aggregates caused mislocalization of nuclear core complexes, which impaired nuclear transport through a decrease of nuclear mRNA export in the cytoplasm and subsequent protein synthesis. It was therefore concluded that RNA transport is disturbed by proteotoxicity of cytoplasmic aggregates. This finding was corroborated by another study that determined aggregate-specific interacting partners of overexpressed C-terminal TDP-43 fragments by BioID, a proximity labelling of protein (Chou *et al.*, 2018). Many aggregates consisted of nucleoporins and nuclear export factors. Importantly phenylalanine-glycine repeat-containing nuclear-pore proteins, which contain a flexible low-complexity domain, were found to co-aggregate with TDP-43. This subsequently led to the mislocalization of proteins of the nuclear basal lamina and transmembrane nucleoporins. This was recapitulated with mutant TDP-43 in the absence of cytoplasmic aggregates, suggesting a disturbance of nucleoporins in early disease phase. Nuclear pore proteins were also identified as interactors of toxic poly-dipeptides produced from mutant *C9orf72* and may reflect a common pathogenic pathway (Freibaum *et al.*, 2015).

1.4.4.2. Endosomal trafficking

The endosomal sorting complex required for transport (ESCRT) as described above is relevant for the clearance of toxic TDP-43 products. The endo-lysosomal pathway is regulated by different rab-GTPases where RAB5 regulates early endosomes, RAB11-recycling endosomes, and RAB7 late endosomes/lysosomes (Schwenk *et al.*, 2016). TDP-43 has been shown to negatively regulate the activation of VPS4B, which downregulates cell surface receptors and RAB11 mediated endocytosis. The consequence of TDP-43 knock-down was a VSPB4-activated lysosomal degradation pathway, decreased uptake of recycling endosomes and the downregulation of cell surface adhesion receptors such as ERB B4. ERB B4 is involved in trophic signalling pathways and loss of ERB B4

caused dendrite loss. This links TDP-43 pathology to other ALS genes of the ESCRT, including ErbB4 and CHMP2B.

1.4.4.3. Extracellular release of TDP-43

TDP-43 has been identified in exosomes isolated from ALS patient cerebrospinal fluid (CSF) by immunoblotting (Feneberg *et al.*, 2014). However, there was no evidence of the pathological forms of TDP-43 and further investigations are hampered by the limited amount of vesicles that can be extracted from CSF. From a cellular model using HEK293T cells there is evidence that TDP-43 is transported in exosomes, secreted and intercellularly transmitted (Feiler *et al.*, 2015). Furthermore, an experimental approach to quantify TDP-43 dimers and oligomers via luciferase activation was capable of measuring oligomerization after TDP-43 overexpression and stress activation. Conditioned media was able to seed oligomerization of TDP-43 in non-transfected cells possibly through transmission of exosomes, which contained toxic TDP-43 oligomers. This has also been reproduced in a neuronal culture and there was evidence that transmission might be trans-synaptic. This model also provided evidence for a prion-like seeding of TDP-43 pathology, when ALS brain homogenates induced TDP-43 oligomerization in normal HEK293T cells. Evidence for the propagation of TDP-43 proteinopathy by exosomes came from direct isolation of exosomes from ALS brains, which seeded aggregation of TDP-43 in normal cells (Iguchi *et al.*, 2016). However, inhibition of exosome secretion in a TDP-43 mutant animal model exacerbated the disease phenotype, suggesting that exosome secretion is beneficial for neuronal survival possibly through clearance of pathological TDP-43.

1.5. Measuring TDP-43 in ALS

1.5.1. Neurochemical biomarkers in ALS

The diagnosis of ALS and FTD is made clinically and an objective neurochemical biomarker has not yet been included in the diagnostic certainty criteria for ALS and FTD (Brooks *et al.*, 2000; Rascovsky *et al.*, 2011; Feneberg *et al.*, 2018a). The median interval between onset of symptoms and ALS diagnosis applying diagnostic criteria described above is 9.3 months (Zoccolella *et al.*, 2006). This is when a potential window for effective treatment has already narrowed and a more objective and rapid diagnostic test might facilitate access to therapeutic trials (Feneberg *et al.*, 2018a). A neurochemical biomarker would ideally also measure disease progression and assess response to treatment in clinical study trials (Otto *et al.*, 2012; van den Berg *et al.*, 2019). Use of subjective clinical outcome measures such as progression rate, survival or a change in functional scores such as the revised ALS Functional Rating Score (ALSFRS-R) can lead to failure of therapeutic trials (Proudfoot *et al.*, 2016).

A new important role of biomarkers arises from new advances in gene therapies. The first *SOD1* genetic cases of ALS are now being approached with antisense oligonucleotides or viral-vector-based gene therapies and antisense oligonucleotide treatments are under development for the most frequent mutation *C9orf72*. Understanding the evolution of ALS and FTLD in regards of disease onset, even before obvious clinical signs have established, then becomes essential (Miller *et al.*, 2013; Benatar *et al.*, 2019). This includes the understanding of an early or pre-symptomatic disease phase, which may be divided further into a pre-manifest and a prodromal stage. Given that the pre-manifest stage is defined by the lack of evidence of any signs or symptoms of the disease it can by definition only be detected by a reliable biomarker (Benatar *et al.*, 2019). This creates a

new challenge in biomarker development with the establishment of studies for longitudinal measurements to assess the pre-symptomatic disease progression, onset and progression of disease.

Biomarkers can be classified into two categories: 1) specific biomarkers reflecting underlying pathology or genetics and 2) markers that reflect pathological processes such as axonal damage due to neurodegeneration, inflammation or blood-brain barrier dysfunctions. The advantage of a biomarker that reflects disease-specific change is its pre-symptomatic existence, independent of secondary damage. A disease-specific biomarker indicates pathological pathways before cellular damage occurs and it further provides evidence of a specific drug target engagement (Feneberg *et al.*, 2018a).

1.5.1.1. Neurofilaments

As generic markers of neuronal loss associated with neurodegeneration, there has been much progress in validating neurofilaments as diagnostic and prognostic biomarkers in ALS and FTLD. Neurofilaments are cytoskeletal proteins of neurons, important for the growth and stability of long axons with a polymer structure consistent of neurofilament light or heavy chains (Khalil *et al.*, 2018). Following neuronal damage, neurofilaments are released into the CSF and concentrations of neurofilament light and the phosphorylated heavy chain can be reliable measured by immunoassays in CSF and blood. Neurofilament light chain and phosphorylated heavy chain concentrations are significantly increased in biofluids of ALS patients and are assessed for their use in predicting diagnosis and prognosis (Rosengren *et al.*, 1996; Reijn *et al.*, 2009; Tortelli *et al.*, 2012; Boylan *et al.*, 2013). A large prospective study on 455 patients demonstrated the diagnostic value of neurofilaments in the CSF. Neurofilament light and heavy chain levels in 253 patients with ALS were higher compared to important differential diagnoses

such as multifocal motor neuropathy, other neurodegenerative diseases and neurological control patients (Steinacker *et al.*, 2016). There was no significant difference between sporadic and genetic ALS or PLS cases and neurofilament levels correlated moderately with disease progression and duration. Sensitivity and specificity for neurofilament light chain levels in CSF and blood and heavy chain levels in CSF was high in patients with early symptomatic ALS in a larger multicentric study (Feneberg *et al.*, 2018b). Neurofilaments were elevated in ALS patients within 6 months of disease onset and this was independent of clinical diagnostic certainty categories. Neurofilament levels are promising markers to monitor the response to treatments demonstrated by their stability over the course of disease and robust correlation with disease progression (Lu *et al.*, 2015). In people who are at risk to develop ALS, when carrying an ALS-associated gene mutation, neurofilament levels increase in the symptomatic phase, but an extensive longitudinal study provides evidence that in a circumscribed pre-symptomatic phase neurofilament levels rise before the appearance of the first clinical symptom or sign (Weydt *et al.*, 2016; Benatar *et al.*, 2018).

1.5.1.2. Disease-specific biomarkers in ALS

Ideally a disease-specific biomarker detects changes that are upstream of irreversible neurodegenerative processes such as axonal damage to monitor:

1. disease-specific changes to enable diagnostic accuracy in an early/ pre-symptomatic phase
2. disease-specific pathological processes/pathways for drug target evaluation
3. drug target engagement and treatment effects.

1.5.1.2.1. Dipeptides in *C9orf72*

The sense and antisense non-ATG translation of the *C9orf72* hexanucleotide repeat expansion results in five different dipeptide products including poly-GP, which is the most prominent in human disease (Schludi *et al.*, 2015). Important advances have been made to measure dipeptides in CSF from patients with the underlying mutation. Using a highly sensitive Meso-Scale Discovery immune-assay platform poly-GP dipeptide concentrations in C9orf72 carriers were 35 times higher compared to non-carriers. Importantly poly-GP was already detectable in asymptomatic *C9orf72* expansion carriers compared to healthy controls and patients with other neurodegenerative diseases. The levels of poly-GP did not correlate to the levels of neurofilaments, which is important as poly-GP levels seem to be independent of disease progression markers (Lehmer *et al.*, 2017). Addressing the need for a pharmacodynamic biomarker for antisense oligonucleotide gene therapy, poly-GP levels measured by the same immune-assay decrease significantly in response to treatment (Gendron *et al.*, 2017).

1.5.1.2.2. Progranulin

Mutation in the *Progranulin (GRN)* gene are a common cause of inherited FTLD, but rare in ALS. Most mutations are nonsense mutations, deletions, or splice-site mutations that generate premature stop codons and lead to nonsense-mediated decay of its mRNA resulting in low levels of its gene product progranulin (Cruts *et al.*, 2006; Schymick *et al.*, 2007). There have been advances to therapeutically up-regulate protein levels of progranulin to restore its function (Sha *et al.*, 2017). One example is the drug nimodipine, which is a calcium channel blocker and aims to increase progranulin secretion by lowering intracellular calcium levels. Progranulin is measurable in blood and CSF and is stable during disease progression (Nicholson *et al.*, 2014). Therefore, it is an ideal biomarker to monitor drug effects within individuals. On a case basis it has been shown

that nimodipine increases progranulin levels, when treating a patient with a loss of function *GRN* gene mutation (Feneberg *et al.*, 2016).

1.5.2. A TDP-43-based biomarker

The development of a TDP-43-based biomarker would reflect the most consistent molecular finding in ALS and FTLD and be potentially valuable to monitor disease activity (Feneberg *et al.*, 2018a).

1.5.2.1. Disease-associated TDP-43 isoforms in biofluids

The distribution of the pathological isoforms of TDP-43 has been established from human *post mortem* tissue and the disease-specific characteristics of TDP-43 are well-described. All TDP-43 antibodies applied in biofluid studies so far bind to aa1-260, 205-222 or 256-296 of TDP-43 (Zhang *et al.*, 2008) and therefore have the potential to detect full-length TDP-43, C-terminal fragments or phosphorylated full-length TDP-43 (Fig. 1.3.). Antibodies, which bind to the phosphorylated Serine at aa409/410 of the C-Terminus of TDP-43, are likely to detect both phosphorylated truncated and full-length forms of TDP-43 (Feneberg *et al.*, 2018a).

Fig. 1.3. TDP-43 pathology and trafficking in ALS and FTLD (modified from Feneberg et al., Mol Neurobiol, 2018)

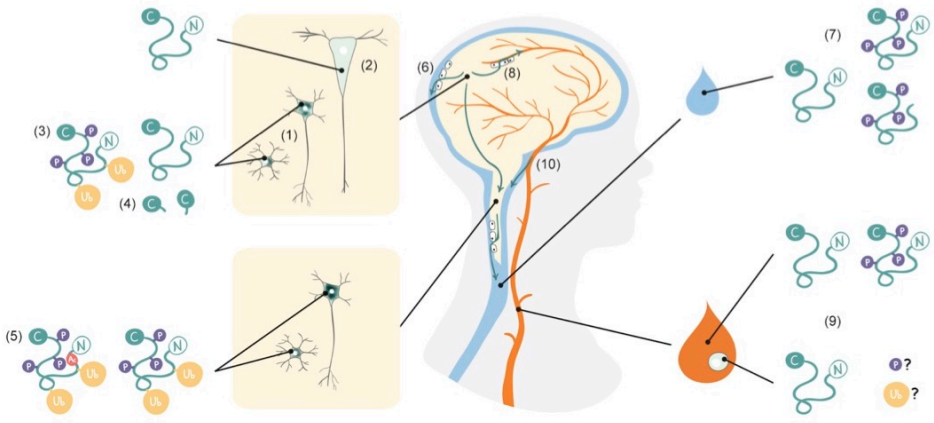


Fig. 1.3. (1) Neuronal and glial aggregates of TDP-43 are formed by mislocalization of the normal nuclear protein to the cytoplasm. (2) In contrast to spinal motor neurons, in Betz cells only sparse cytoplasmic deposits of TDP-43 can be found. (3) Aggregated TDP-43 is pathologically altered by phosphorylation and ubiquitination and (4) additional C-terminal fragments of TDP-43 are detected in the brain. (5) In addition to phosphorylation and ubiquitination acetylated TDP-43 is found in the spinal cord of ALS. (6) The CSF compartment is in direct contact with the central nervous system and enables brain-derived proteins to transfer along the brain-CSF barrier. (7) Both, normal full-length and phosphorylated TDP-43 are detected while the N-terminal end of TDP-43 has not yet been detected in CSF. (8) A tight epithelial barrier separates blood from brain. (9) A proportion of the full-length and phosphorylated TDP-43 can be measured in blood and lymphomonocytes which (10) might also derive from CSF by diffusion along the blood-CSF barrier.

However, the length of C-terminal fragments present in ALS tissue has not been fully elucidated, making it possible that not all fragments can be detected by current available antibodies, and immunohistochemical staining revealed nonspecific binding of phosphorylation dependent antibodies to the physiological nuclear TDP-43 (Kwong *et al.*, 2014). Therefore, it is not clear if in the presence of all forms of TDP-43 the binding of the current antibodies is specific for pathological TDP-43.

The ubiquitous presence of normal TDP-43 demands a technique that specifically detects the brain-specific form of TDP-43. This is even more challenging in complex biofluids such as CSF and blood where measurements interfere with highly abundant proteins such as albumin and immunoglobulins (Feneberg *et al.*, 2018b). The protein exchange between the brain and blood is highly regulated through epithelial tight junctions and brain-derived proteins are expected to be much lower abundant in blood, while the CSF compartment is in direct contact with the brain and therefore best reflects brain-derived proteins (Begley and Brightman, 2003). But depending on their hydrodynamic radius proteins diffuse along the blood-CSF barrier and blood-derived proteins may influence CSF TDP-43 homeostasis (Felgenhauer, 1974; Johanson *et al.*, 2011). In the CSF the pathological signature of TDP-43 seen in immunoblots of *post mortem* tissue has been only partially reproduced in CSF from patients with ALS and FTLD (Steinacker *et al.*, 2008). A polyclonal antibody recognizing aa1-260 of TDP-43 detected a 45kDa band. This molecular weight was slightly higher than the expected molecular weight of 43kDa of native TDP-43 and suggests the presence of post-translational modified full-length TDP-43. However, this shift has not yet been confirmed with a phosphorylation-dependent antibody for TDP-43. Also, a C-terminal antibody detected full-length TDP-43, lower molecular weight bands specific to ALS and FTD have not been detected in CSF. The significance of the main finding that TDP-43 is detected at higher level in ALS and FTD is unclear, given that the same immunoreactivity

for suggested phosphorylated full-length TDP-43 was also detected in disease controls (Steinacker *et al.*, 2008).

Blood lymphocytes of ALS patients are an alternative source of pathologically altered TDP-43 (De Marco *et al.*, 2011). Nuclear-cytoplasmic fractions of blood lymphocytes from ALS patients and *TDP-43* mutation carriers compared to asymptomatic first-degree relatives with and without mutations and healthy controls show an increase of the cytoplasmic TDP-43 band on immunoblots indicating pathological mislocalization. This shift was not observed in a patient with a *SOD1* mutation confirming that this sub-group of ALS is associated with a different molecular pathway (Feneberg *et al.*, 2018a). A study compared the TDP-43 biochemical profile in blood and CSF, to see whether CSF TDP-43 reflects brain-derived TDP-43, or predominantly reflects the physiological full-length form derived from blood (Feneberg *et al.*, 2014). The study demonstrated that similar 2-D immunoreactive patterns of TDP-43 at 45kDa were present in CSF and serum, whereas in brain tissue of ALS patients with TDP-43 pathology, a higher and more acidic pattern was observed at 50kDa suggesting post-translational modifications in addition to the full-length form of TDP-43. Therefore, this study did not show evidence of a brain-specific TDP-43 pattern in CSF. However, TDP-43 was detected in exosome fractions isolated from CSF. Exosomes directly derive from endosomal transport pathways and are released into the extracellular compartment. Across neurodegenerative diseases exosomes offer potential for the identification of intracellular mislocalized proteins (Thompson *et al.*, 2016). Evidence using an *in vitro* over-expression model described the transmission of TDP-43 via exosomes obtained from primary cortical neurons that may contain the pathologically phosphorylated form of TDP-43 (Iguchi *et al.*, 2016).

1.5.2.2. Quantitative measurement of TDP-43 in CSF and blood

Given the indications of altered TDP-43 in biofluids subsequent studies have attempted to quantify the degree of TDP-43 and the pathological altered TDP-43 using either a monoclonal or polyclonal TDP-43 antibody against amino acid regions 1-260, 205-222 and 256-296 or phosphorylation-dependent antibodies to aa409/410 of TDP-43 (Feneberg *et al.*, 2018a). Nearly all studies used enzyme-linked immunosorbent assay (ELISA) to measure TDP-43.

The first quantification of TDP-43 in the CSF of ALS patients used an ELISA technique against full-length TDP-43 with a commercially available chemiluminescent substrate to enhance the TDP-43 signal (Kasai *et al.*, 2009). TDP-43 levels in apparently sporadic ALS patients were significantly higher compared to neurological and healthy control subjects. This elevation was accentuated in an early phase of ALS. The elevation of TDP-43 did not correlate with the level of the revised EEC nor with the site of disease onset (limb versus bulbar). The same methodology was used to measure TDP-43 levels in the CSF of ALS patients compared to other neurodegenerative diseases such as Parkinson's disease and neuroinflammatory disease (Noto *et al.*, 2011). Mean TDP-43 levels were higher in the ALS group than in all the control groups. Despite the overall picture of higher TDP-43 in other studies, lower TDP-43 levels were here found to correlate with a shorter survival. A commercially available ELISA with a biotin-streptavidin method for the detection of TDP-43 has since been used to distinguish a group of FTD patients from a smaller group of ALS patients and *C9orf72* repeat expansion carriers of both subgroups (Junttila *et al.*, 2016). TDP-43 levels were higher in ALS patients, regardless of genotype or clinical features. Another study group used an ELISA with a full-length TDP-43 coating antibody for ventricular CSF obtained *post mortem* at the time of autopsy and lumbar CSF samples, applying a biotin-streptavidin detection method for the latter

(Kuiperij *et al.*, 2017). For each ventricular CSF sample neuropathology was confirmed as FTLD-TDP, FTLD-Tau or AD, with and without TDP-43 pathology at autopsy. The lumbar CSF was obtained from a patient group determined as FTLD-TDP or AD either by autopsy, by genetics (*GRN*, *C9orf72* and *MAPT*) or clinically. Remarkably this is the first study reporting *lower* TDP-43 levels in patients with neurodegenerative diseases of FTLD-TDP and AD compared to controls. This study might suggest lower levels of TDP-43 are a feature of neurodegeneration in general, as lower levels were not restricted to TDP-43 proteinopathies (Kuiperij *et al.*, 2017). Of note, a possible breakdown of the CSF barrier *post mortem* is likely to have an influence on the quantification of TDP-43 in the ventricular CSF samples.

The first study to quantify the full-length TDP-43 isoform in plasma included an initial patient cohort clinically diagnosed with FTD and Alzheimer's disease (AD) (Foulds *et al.*, 2008). In this study, 22% of AD patients and 46% of FTD patients were above the detection limit of the assay, with most healthy control samples (92%) falling below this level. A subsequent study by the same group included plasma samples from autopsy confirmed cases, and quantified both full-length and phosphorylated TDP-43 as the detection antibody (Foulds *et al.*, 2009). Full-length TDP-43 concentrations did not differ between FTD and AD patients, including when patients documented to have TDP-43 pathology were considered as an independent group. Phosphorylated TDP-43 levels were non-significantly higher in FTD patients with TDP-43 pathology than FTD with Tau pathology, but not in clinical AD patients with TDP-43 pathology. Phosphorylated plasma TDP-43 levels in FTD cases were positively correlated with the severity of TDP-43 pathology. Overall a wide variation in individual levels was observed. In a separate study, plasma levels of TDP-43 in a large cohort of 219 ALS patients were measured by ELISA using a chemiluminescent substrate (Verstraete *et al.*, 2012). By this method 28%

of ALS patients and 21% of control subjects were over the detection limit. Overall, TDP-43 levels in ALS, including three patients with *TARDBP* mutations, were increased compared to healthy control subjects.

Another study measured full-length and phosphorylated TDP-43 in plasma in FTD non-mutation carriers compared to a small subgroup of FTD patients with a *C9orf72* repeat expansion, *GRN* mutation carriers and healthy controls (Suarez-Calvet *et al.*, 2014). This study applied a commercially available ELISA with a biotinylated detection antibody against the phosphorylated TDP-43 and streptavidin-conjugated chemiluminescence. Concentrations were normalised to a control sample and given as relative units compared to this internal standard on each plate. Higher levels of phosphorylated TDP-43 were found in FTD *C9orf72* and *GRN* mutation carriers compared to FTD non-mutation carriers and healthy controls. Interestingly full-length TDP-43 levels were found to be negatively correlated with phosphorylated TDP-43, meaning that it was lower in mutation carriers compared to non-mutation carriers and controls. No difference was found when investigating a smaller CSF sample group of 20 FTD patients and 5 FTD mutation carriers compared to controls. A different methodology uses phage-displayed single chain antibody fragments directed against TDP-43 from an established library (Sheets *et al.*, 1998; Williams *et al.*, 2017). These antibodies were originally tested against immunoprecipitated TDP-43 from homogenate samples of the motor cortex from healthy controls, ALS and FTLD-TDP brains, to assess their specificity and could be promising to be used in biofluids.

1.5.2.3. Limitations of the quantification of TDP-43 in human

The pathologic forms of TDP-43 are established from human *post mortem* studies, however the quantification of TDP-43 isoforms in the CSF and plasma of ALS/FTLD patients has been inconsistent. Although a range of antibodies can be used to detect TDP-

43 in biofluids (Goossens *et al.*, 2015), an unacceptably high level of variability of detection in samples from ALS and FTLD patients has been reported. Quantification of TDP-43, in particular its phosphorylated form in CSF, appears limited by very low concentrations or low binding affinity of the antibodies in the presence of high abundant immunoglobulins and albumin (Feneberg *et al.*, 2018a). To date, it is not clear if TDP-43 rises due to degeneration of nerve cells and release of intracellular proteins or if it is reduced due to aggregate formation. Many earlier studies are contradicted by later studies with confirmed TDP-43 pathology or proof of a pathogenic gene mutations (Noto *et al.*, 2011; Suarez-Calvet *et al.*, 2014; Kuiperij *et al.*, 2017). The detailed characterisation of samples in times of established biofluid biobanks increases the possibility of more reliable results.

1.5.3. Mass spectrometric analysis

To overcome the problems arising from non-specificity of commercially available antibodies for TDP-43, label-free proteomics using mass spectrometry is a promising alternative approach. For so-called "bottom-up" proteomics, proteins are cleaved into peptides by enzymatic digest. Liquid-chromatography tandem mass spectrometry (LC-MS/MS) is the gold-standard for peptide detection. Peptides are then assigned to proteins using proteome databases and search engines. With the most recent instruments that couple a quadrupole mass filter to an Orbitrap analyser, more than 2500 proteins of a mammalian cell lysate can be identified (Michalski *et al.*, 2011). The procedure is to separate peptides by liquid-chromatography ionization, peptide ions are then separated in the mass spectrometer using quadrupole mass filters, time of flight (TOF) mass analysers, linear ion traps, and Orbitrap analysers. In tandem mass spectrometry a quadrupole mass filter selects a defined mass window around a precursor ion of choice, ions are activated in a collision cell and resulting fragments are analysed in the TOF part of the instrument.

While the linear ion trap retains a chosen mass-dependent ion population to allow separation and fragmentation of the trapped precursor ions in time.

To achieve proteomic identification of target proteins preparation of samples prior to mass spectrometry (MS) is essential. 1D- or 2D-immunoblotting gels are used for the separation of proteins and MS identification of individual gel bands (Brewis and Brennan, 2010). Affinity-enrichment of a bait protein using protein tags can enrich target proteins and proteins that interact with the target protein (bait), when interactions are contained prior to affinity-enrichment, e.g. by using low detergent buffers. Importantly, specific interactors of a protein can be investigated, when comparing the proteome of the target to direct tagged control strains, by eliminating background proteins from true interactors (Keilhauer *et al.*, 2015). The processing of MS data by downstream bioinformatic protocols strengthens the reliability of results. New targeted proteomic approaches such as parallel reaction monitoring (PRM) or selective-reaction-monitoring are able to absolutely quantify proteins and are a good alternative to immunoassays (Oeckl *et al.*, 2018). A stable isotope-labelled version of the peptide that is uniquely formed by proteolysis of the target protein is added to the sample and these internal standard peptides are then used to precisely quantify the absolute levels of the corresponding endogenous peptides (Gerber *et al.*, 2003). A disadvantage is that pre-analytical differences within samples, for example digest efficiency is not assessed and requires standardized sample preparation, also the target peptides of a protein need to be known to generate the isotope-labelled version. An advantage of this method is that peptide sequences offer an opportunity for antibody production, which then selectively recognize the protein sequences. When the protein sequence is representing a disease-specific protein, this can be used to assess its relevance for future treatment options (such as immunisation studies, which target toxic protein species).

1.6. Aims of the thesis

Core aims of this thesis are the characterisation and quantification of disease-specific TDP-43 and the identification of key pathways, which are affected in ALS, to develop a TDP-43 pathology specific biomarker.

Objectives include:

1. Identify TDP-43 from biofluids and *post mortem* tissue with systematic screening for the relevant brain-derived disease-specific TDP-43 peptides by mass spectrometry (Chapter 3).
2. Assessment of the specificity of the disease-specific TDP-43 peptides in brain tissue across diagnostic groups using targeted mass spectrometry (Chapter 4).
3. Characterise how pathological TDP-43 alters protein-protein interactions and how this affects cellular pathways using a (BAC)-transgenic mouse model expressing human wild-type and M337V mutant TDP-43, with validation in ALS human cellular models (Chapter 5).
4. Determine how mutant-induced interactome changes correlate with phenotypic alterations in mESC-derived motor neurons and human iPSC-derived motor neurons from patients with *TARDBP* mutations (Chapter 6).

Chapter 2: Methods and Materials

2.1. Enrichment of TDP-43 and detection of TDP-43 peptides by mass spectrometry

2.1.1. Patient samples and *post mortem* tissue

CSF and serum were obtained from The Oxford Study for Biomarkers in MND ('BioMOx') and an on-going collection in a multicentre biomarker resource strategy in ALS (AMBRoSIA). Both provide a resource of longitudinal biofluids and clinical data in well-characterized phenotypes of ALS, healthy and disease controls. Patients with ALS were recruited from the Oxford ALS Centre (Oxford, UK). For CSF sample collection, ethical approval was obtained from South Central Oxford Ethics Committee B (08/H0605/85), NRES Central Committee South Central–Berkshire (14/SC/0083 and 10/H0505/71). All participants provided written consent. The human *post mortem* tissue, cortices and spinal cords, were donated to the Oxford Thomas Willis Brain Bank, Department of Neuropathology, Oxford University from donors for or from whom a written informed consent for a brain autopsy and the use of the material and clinical information for research purposes has been obtained by the respective institution.

2.1.3. Immunoprecipitation

Immunoprecipitation of TDP-43 with Protein A/G magnetic beads (ThermoFisher MS compatible IP KIT) was performed using a polyclonal full-length N-terminal TDP-43 antibody (10782-2-AP, Proteintech) or monoclonal full-length TDP-43 antibody (H00023435-M01, Abnova). To establish the method immunoprecipitations were performed using whole brain homogenates

of a bacterial artificial chromosome (BAC)-transgenic mouse carrying human YPet-tagged *TDP-43^{M337V}*/- or a C57BL/6 mouse. Frozen tissue was homogenized with RIPA buffer (ThermoFisher) using steel beads in a TissueLyser system (Qiagen) and centrifuged at 21,000g for 30 minutes at 4°C. For biofluid immunoprecipitations pooled CSF and serum samples from a group of ALS patients and healthy controls were used. Protein amount was determined by BCA assay (ThermoFisher). Immunoprecipitation was performed with an equal amount of 1000µg protein per reaction and 10µg of antibody per 25µl of magnetic beads. Samples were pre-cleaned to avoid nonspecific reaction to beads. The negative immunoprecipitation (IP) was done by using either rabbit IgG or mouse IgG1 isotype control dependent on the respective TDP-43 antibody used in the positive IP. For crosslinking 50µl beads were incubated with 10µg of the antibody for 2 hours, then 500µl crosslinking buffer (13mg DMP in 2ml 0.2M triethanolamine) was added and incubated for 45 minutes at room temperature. The reaction was quenched with 500ml 50mM Ethanolamine and incubated for 1 hour at room temperature with gentle agitation. Beads were collected and washed with 500µl PBS and 1M glycine was used to remove excess antibody, before immunoprecipitation continued as above.

2.1.4. Immunoblotting

All samples were denatured in LDS-sample buffer with 10x reducing agent ((NuPage, ThermoFisher) and heated for 5 minutes at 95°C. Samples were separated on precast 4-12% or 10% Bis-Tris gels (NuPage, ThermoFisher) in running buffer (NuPage MES or MOPS SDS running buffer (20x), ThermoFisher) at 130V. Gels were transferred onto polyvinylidene difluoride (PVDF) membrane using the iBlot 2 dry blotting system (Life Technologies). The membrane was blocked using 10% BSA, protein free blocking buffer (ThermoFisher) or TBS blocking buffer (Licor) for 1 hour at room temperature and primary

antibodies were added in 1% of the respective blocking buffer. The membrane was incubated overnight at 4°C, washed for 10 minutes in TBS with 1% Tween for three times and incubated in secondary antibody for 1 hour at room temperature. Immunoreactive bands were detected using ECL Prime western blotting detection reagents (GE Healthcare) with film development or using a ChemiDoc MP Imaging System (Bio-Rad), or directly referred to fluorescent imaging (Odyssey FC imaging System, Licor).

Table 2.1. TDP-43 primary antibodies

Description	aa binding	Company	CatNo	Capture	Detection	Dilution WB
rabbit polyclonal TDP-43	1-260	Proteintech	10782-2-AP	IP	WB	1:1000
mouse monoclonal TDP-43	205-222	Abnova	H00023435-M01	IP		1:1000
rabbit polyclonal C-terminal TDP-43	256-296	Proteintech	12892-1-AP		WB	1:1000
Mouse monoclonal phosphor TDP-43	S409/410	CosmoBio	TIP-PTD-M01		WB	1:500

All primary antibodies were raised in mouse or rabbit, followed by an anti-rabbit or anti-mouse IgG secondary antibody (diluted 1:10.000). The amino acid binding site also shown in Figure 1.2. is given. The catalogue number (CatNo) and the usage as capture antibody in immunoprecipitation (IP) or detection antibody for western immunoblotting (WB) is given.

2.1.5. Silver Staining

Total protein amounts were visualised by silver staining using a ProteoSilver Silver Stain kit (Sigma-Aldrich) as per the manufacturer's protocol and using solutions provided in the kit.

Briefly, after electrophoresis, gels were fixed overnight at room temperature in fixing solution (10% acetic acid (Millipore), 50% Ethanol (VWR) in MilliQ water). The gels were incubated in 10 minutes washes of, consecutively, 30% Ethanol, MilliQ water, sensitizer solution, and silver solution. Staining was visualised by incubating with developer solution for 30-70 seconds, the reaction was stopped by addition of ProteoSilver Stop solution and by washing with MilliQ water for 15 minutes.

2.1.6. Serial extraction of soluble and insoluble protein fractions from tissue

Frozen tissues from cortex and spinal cord of all groups of subjects were homogenized in 1:1 volume:tissue weight low-salt homogenization-solubilization (LS) buffer (10mM Tris pH 8.0 (Invitrogen), 5mM EDTA (Invitrogen), 1mM dithiothreitol (Alfa Alsar)) supplemented with protease and phosphatase inhibitors (100x HALT Protease&Phosphatase Inhibitor, ThermoFisher), 0.2mM Sodium orthovanadate and 0.3Unit/µl benzonase nuclease (Sigma-Aldrich) and 10% sucrose (Neumann *et al.*, 2006). For the discovery experiments in Chapter 3 0.5mg -1g of whole thoracic spinal cord or 1mg of whole frontal lobe cortex tissue were homogenized with LS buffer using pestles. For the targeted proteomics experiments in Chapter 4 approximately 0.5mg-1g of motor cortex tissues were homogenized using steel beads in a TissueLyser system (Qiagen) and centrifuged at 21,000g for 30 minutes at 4°C. The pellets were homogenized in Triton-X (TX) buffer (1% Triton X-100, 0.5M NaCl in LS buffer). Protein amount was determined by BCA assay (ThermoFisher) and all samples were equalized to 20mg of total protein in a final volume of 3ml TX buffer. Tissue homogenates were centrifuged at 180,000g for 30 minutes at 4°C in thin-wall polypropylene tubes (Beckman Coulter) in swinging buckets in an Optima MAX-XP ultracentrifuge (Beckman Coulter). Supernatants, corresponding to the soluble proteins, were saved as the Triton-X fraction (TX). Pellets were washed in TX buffer supplemented with 30% of sucrose (Sigma-

Aldrich). Pellets were subsequently resuspended in sarkosyl buffer (1% N-lauroyl-sarcosine (Sigma), 0.5M NaCl in LS buffer), briefly sonicated, and incubated at 37°C on a shaker (160rpm) for 30 minutes followed by centrifugation at 180,000g for 30 minutes at 22°C. Supernatants were saved as the sarkosyl fraction (Sark), while the pellets were resuspended in urea buffer (7M urea (Sigma), 2M Thiourea (Sigma), 4% CHAPS (ThermoFisher), 30mM Tris pH 8 (Invitrogen)) supplemented with protease and phosphatase inhibitors. Samples were sonicated and centrifuged for 30 minutes at 21,000g at room temperature. The supernatant, corresponding to the insoluble fraction, was saved as the urea-soluble fraction (Urea) and frozen at -80°C prior to use. For the discovery experiment in Chapter 3 350µl 7M urea buffer were used to resolve the pellet, 100µl were subjected to immunoblotting and 200µl were used for the preparation of in-solution or in-gel sample digestion for mass spectrometry. For Chapter 4 300µl 7M urea buffer were used to resolve the pellet.

2.1.7. Sample preparation for mass spectrometry – in-solution digest

Urea fractions were thawed on ice. For PRM 150µl (of 300µl) were topped up with 7M Urea to reach a 200µl final volume. The urea sample was reduced by incubation with 5mM dithiothreitol (DTT, Alfa Alsar) for 30 minutes at room temperature, followed by alkylation by incubating samples with 20mM iodoacetamide (IAA, Sigma-Aldrich) for a further 30 minutes at room temperature. Samples were subsequently precipitated by methanol-chloroform extraction by addition of three volumes of methanol (Millipore), one volume of chloroform (Sigma-Aldrich), and four volumes of MilliQ water, vortex and centrifugation for 2 minutes at full speed. The organic phase was washed in four volumes of methanol and centrifuged for 5 minutes at full speed. Pellets were fully resuspended by addition of 6M Urea (Sigma-Aldrich) and brief sonication. 50mM TEAB (Sigma-Aldrich) was subsequently added to reduce the final concentration of urea to 1M. Half the volume of the

samples were incubated with 2µg trypsin (Promega) while the other half was incubated with 2µg chymotrypsin (Promega), at 37°C and 22°C, respectively, in a shaker for 14-16 hours (approximately 1/250 protease to protein ratio). The reaction was stopped by addition of formic acid (Millipore) to lower the pH below 4. Samples were desalted using SOLA SPE columns (ThermoFisher), dried in a speed-vac (ThermoFisher) and pellets were resuspended in 10µl of Buffer A (2% acetonitrile (Sigma-Aldrich) with 0.1% formic acid diluted in MilliQ water). The peptide amount per sample was measured using a quantitative colorimetric peptide assay (Pierce) as per manufacturer's protocol. For PRM the final cortex samples in Buffer A were diluted 1:10 prior to mass spectrometry.

For the *biofluid* discovery proteomics in Chapter 3.2.2.1 TDP-43 immunoprecipitates from CSF and serum were eluted from the Protein A/G magnetic beads and the eluates dried in a speedVac as per manufacturer's instruction (ThermoFisher MS compatible IP KIT). Dried samples were resuspended in 10µL of 6M Urea in 50mM TEAB at pH 8.5 and vortexed to mix. 10µl of 10mM TCEP were added to each sample and incubated at 37°C for 30 minutes at 1000rpm. 1µL of IAA solution was added to the sample and incubate at room temperature for 30 minutes protected from light. Immediately 45µL of 50mM TEAB at pH 8.5 were added to each sample to bring urea concentration to <1M. 200ng of elastase (20ng/µl) diluted in 50mM TEAB at pH 8.5 was added and samples digested overnight (16-18 hours) at 37°C in a shaker at 300rpm.

2.1.8. Sample preparation for mass spectrometry – in-gel digest

Gel bands were excised with a scalpel and gel pieces rinsed in 200µl wash solution (50% methanol, 5% acetic acid in MilliQ water) overnight and again 3 hours at room temperature the next day. The wash solution was removed and 200µl acetonitrile added to dehydrate the

gel pieces for 5 minutes at room temperature. Samples were reduced by incubation with 5mM DTT for 30 minutes at room temperature, followed by alkylation by incubation with 20mM IAA for a further 30 minutes at room temperature. Samples were dehydrated with 200µl acetonitrile and rehydrated in 200µl 100mM ammonium bicarbonate for 10 minutes at room temperature. Samples were dehydrated with 200µl acetonitrile and 30µl of 200ng/µl of trypsin or chymotrypsin (Promega) in 50mM ammonium bicarbonate added for 10 minutes. Excess was removed and 5µl of 50mM ammonium bicarbonate added to the sample with digest carried out overnight at 37°C for 14-16 hours. The next day 50µl of 50mM ammonium bicarbonate buffer was added to the samples and incubated for 10 minutes, supernatant was collected in a 1.5ml collection tube. 50µl of extraction buffer 1 (50% acetonitrile, 5% formic acid in MilliQ water) was added, incubated for 10 minutes and collected. 50µl of extraction buffer 2 (85% acetonitrile, 5% formic acid in MilliQ water) was added, incubated for 10 minutes and collected. Samples were then dried in a speedVac (ThermoFisher) overnight and resuspended in 10µl of Buffer A.

2.1.9. Mass spectrometry and analysis

Liquid-chromatography tandem mass spectrometry (LC-MS/MS) was used to analyse all digested samples. Tandem mass spectrometry measures the m/z of all precursor ions electro-sprayed into the mass spectrometer at a given time (MS1). Selected precursor ions are then fragmented and the m/z of the fragment ions are measured in the MS2 spectrum. From the MS2 spectrum an amino acid peptide sequence is obtained, which can be used for protein identification (Kapp et al. 2007). The mass spectrometers used were the Q Exactive HF Hybrid Quadrupole-Orbitrap and the Orbitrap Fusion Lumos (ThermoFisher). Both have a quadrupole mass filter (used for precursor ion selection) and an orbitrap mass analyser that can be used for the acquisition of both MS1 and MS2 spectra. The Lumos instrument has a

dual-pressure linear ion trap to capture and fragment ions with highest sensitivity and resolution. For fragmentation usually the most abundant precursor ions of a given m/z and retention time window are selected and fragmented by collisional dissociation. Fragmentation generates multiple N-Terminus (b) and C-Terminus (y) ions. Multiple ion pairs are generated each with a different m/z, each ion pair resulting in a different amino acid. Together the MS2 spectrum generates a short amino acid sequence also called peptide. Obtained peptides are then compared to reference peptides in a protein database, e.g. the UniProt human or mouse reference proteome as used in this thesis. Commercially available search algorithms such as PEAKS DB (Bioinformatics Solutions Inc) or Mascot v2.5.1 (Matrix Science) compare the observed fragmentation pattern of peptides to theoretical fragmentation patterns of peptides given in the protein sequence database. To estimate the proportion of false positive peptides in a dataset the false discovery rate (FDR, mostly 1%) is calculated from a decoy database. A match in the decoy database is an estimate of the number of false positives that are present in the results from the target database (Elias and Gygi, 2007).

2.1.10 Digestion and peptide generation

Mass spectrometry in all discovery proteomic experiments was based on bottom-up (shotgun) proteomics meaning that all proteins were digested by a specific protease into peptides prior to analysis. All proteases had specific cleavage sites within an amino acid sequence (Table 2.1.). However, peptide generation can be more complicated, when considering that mis-cleavage or nonspecific cleavage might occur during digestion. Also, the efficiency of cleavage varies between proteases and can result in different peptide coverages of the protein. This thesis was focused on a technique to identify nonspecific cleavage sites of peptides, based on the assumption that specific lower molecular weight

species of our target protein TDP-43 were generated by endogenous truncation prior to digestion (Fig. 2.1.). Therefore, peptides were searched that had one protease specific cleavage site, but also one protease nonspecific site, to potentially reflect the endogenously truncated end of the TDP-43 protein. Therefore, the search algorithms included nonspecific cleaved peptides in Chapter 3 section 3.2.2.4..

Table 2.2. Proteases and cleavage sites

Description	Company	pH	Cleavage after amino acids
Trypsin [a)]	Promega	7.6	C-terminal side of lysine (K) and arginine (R)*
Chymotrypsin	Promega	7.6	C-terminal side of phenylalanine (F), tryptophan (W), and tyrosine (Y)*, rarely leucine (L)
Elastase	Worthington	9	C-terminal side of alanine (A), valine (V), serine (S), glycine (G), leucine (L) or isoleucine (I)

All proteases used and their cleavage sites. * If a proline residue is on the carboxyl side of the cleavage site, the cleavage will not occur. a) Unmodified trypsin is subject to auto-proteolysis. Promega Sequencing Grade Modified Trypsin is porcine trypsin modified by reductive methylation, rendering it resistant to proteolytic digestion.

Fig. 2.1. Specific and semi-specific peptide detection by LC-MS/MS and the underlying hypothesis of endogenous truncation

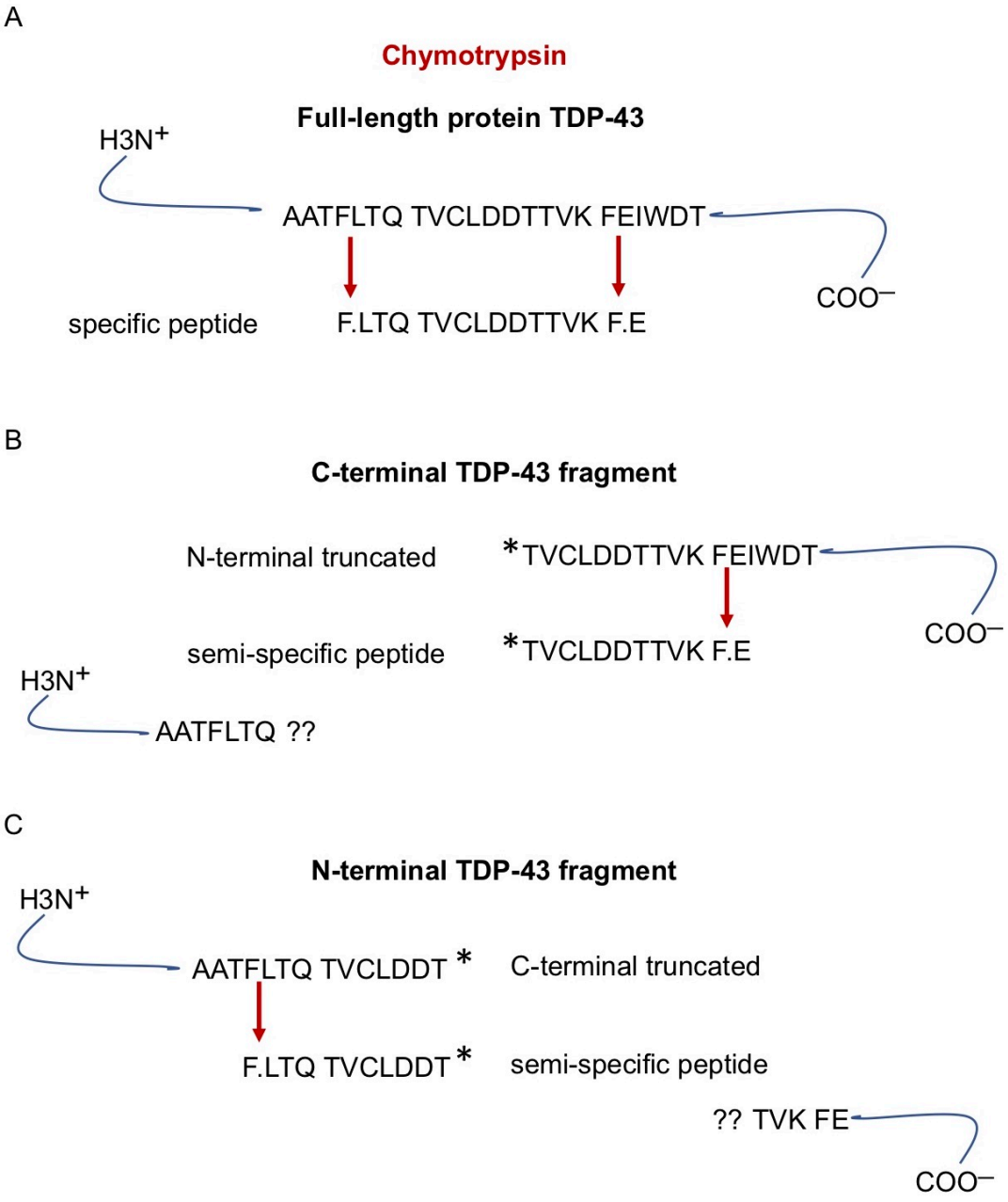


Fig. 2.1. Discovery of specific and semi-specific peptides by nonspecific cleavage sites. Chymotrypsin cleaves after amino acids phenylalanine (F), tryptophan (W), and tyrosine (Y), if not followed by proline (P). **A** Chymotryptic digest of the above protein sequence results in a specific chymotryptic peptide cleaved after F. **B** Chymotryptic digest of a *truncated* protein can result in the generation of a semi-specific peptide, where one end is cleaved independent of the protease (*, nonspecific cleavage site). The N-terminal semi-specific peptide suggests that the C-terminus of the protein exists normally. The nonspecific N-terminal cleavage site suggests endogenous truncation. **C** The C-terminal nonspecific cleavage site suggests an N-terminal protein fragment with a potential C-terminal endogenous truncation site.

2.2. Quantification of TDP-43 peptides by targeted mass spectrometry

2.2.1. Heavy isotope-labelled peptides

Heavy isotope-labelled, AQUA-grade peptides (heavy peptides) (ThermoFisher) were used for the relative and absolute quantitation of endogenous proteins. Heavy peptides were synthesized using Fmoc solid-phase technology and purified by HPLC as per manufacturer's protocol (ThermoFisher). AQUA-grade peptides are delivered in solution with a concentration of 5pmol/µl per peptide.

2.2.2. Sample preparation for parallel reaction monitoring

Human cortex *post mortem* tissue was prepared as described in Chapter 2.1.6 and 2.1.7.. For targeted proteomics it was important to equalize the protein amount to 20mg of the soluble TX fraction between all samples prior to the subsequent fractionation resulting in the insoluble pellet. The workflow for PRM experiments is described in Figure 2.2.. All soluble TX and insoluble urea fractions were immunoblotted using 30µl of the samples and silver stained using 0.5µl of the TX and 1µl of the urea fractions.

2.2.3. Parallel reaction monitoring

1µl of trypsin- or chymotrypsin-digested and desalted samples (diluted 1:10) were injected in a nano liquid-chromatography system coupled to an Orbitrap Fusion Lumos mass spectrometer (ThermoFisher). A time schedule targeted MS/MS method was used with peptide-specific parameters as described in Table 4.3.. To allow absolute quantification, 0.2µl of the heavy peptide mastermix (50fmol peptide concentration) equal to a 10fmol heavy peptide, was injected prior to each sample. As a technical quality check, pools of samples for each group were prepared and loaded every 10th run to determine the reproducibility of the assay. MS data processing was conducted using the software package Skyline and R.

Fig. 2.2. Workflow for parallel reaction monitoring

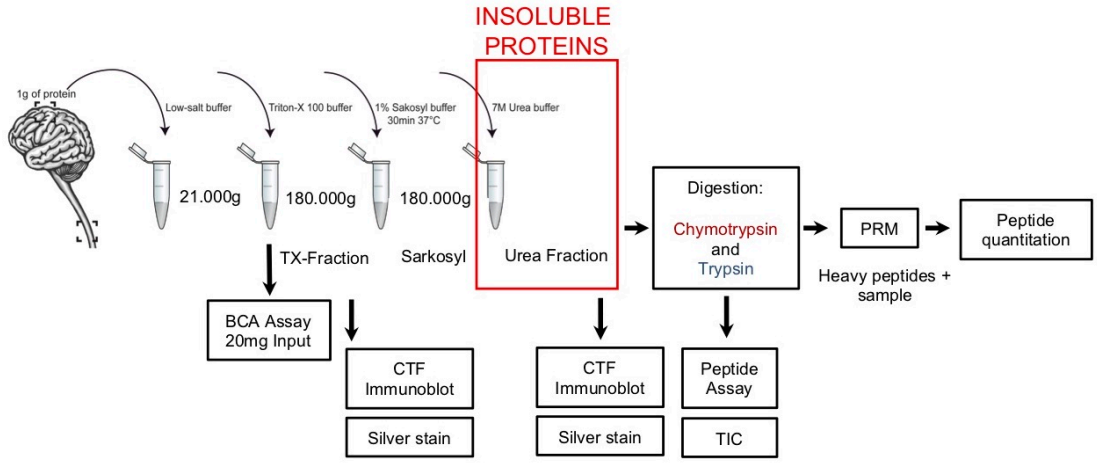


Fig. 2.2. Up to 1g of tissue from motor cortex or if unavailable frontal cortex (see table 4.3.) was used for sequential fractionation. Tissue was homogenized in low-salt buffer, centrifuged and the pellet resolved in 500µl Triton X-100 buffer and protein concentrations equalized to 20mg of starting material for the subsequent fractionations. After the first ultracentrifugation supernatants were saved as the Triton-X fraction (TX), corresponding to the soluble protein fraction, which were immunoblotted and silver stained. Fractionation was continued, the final pellets resolved in 7M urea buffer and the supernatants saved as urea fraction, corresponding to the insoluble protein fractions. Urea fractions were immunoblotted to confirm C-terminal fragment (CTF) pathology and silver stained. The main urea fractions were equally distributed to trypsin and chymotrypsin digestion for subsequent parallel reaction monitoring. Digestion efficiency of pooled digests was determined by total ion chromatography (TIC) and of individual digests by peptide assay. Parallel reaction monitoring (PRM) was performed using heavy isotope-labelled peptides and endogenous light peptide ratios were determined.

Very briefly, Skyline was used to export ion chromatogram data for the light and heavy versions of each peptide in each analysis run. Then the elution peaks of each light and heavy peptide pair were located in each sample. Pairs in each sample were filtered to remove those with insufficient signal for quantitation (minimum 2 monitorable fragment ion values measured over at least 3 collected spectra) or poor-quality data (pearson correlation between light and heavy chromatogram data less than 0.5). Elution peak boundaries were assigned at the point where the heavy peptide signal dipped below 1% of its max intensity in that sample. Finally, a light-heavy ratio was calculated for each peptide by finding the gradient of a fitted simple linear model with no intercept (L = mH) to the light and heavy data points at each time point. The absolute amount (fmol) of each peptide was calculated by dividing the peptide ratio by 10 according to the concentration of the heavy peptide (10fmol).

2.2.4. Statistical analysis

For interpretation of the PRM results across diagnostic groups, absolute abundances of light peptides (log10 ratio (light/heavy peptide)) were compared by testing significant differences between ALS to all other diagnostic groups using one-way ANOVA with Dunnett's multiple comparison test. The C-to N-terminal peptide ratio was calculated (non-log C-terminal peptide ratio/ non-log N-terminal peptide ratio) and compared between ALS and all other diagnostic groups using one-way ANOVA with Dunnett's multiple comparison test. For interpretation of the immunoblots the ratios of the intensities of the C-terminal fragments over full-length TDP-43 from ALS were compared against all other diseases using one-way ANOVA with Dunnett's multiple comparison test.

2.3. Studying the human TDP-43 interactome by mass spectrometry

2.3.1. Motor neuron cultures from mouse embryonic stem cells

MESC-derived motor neurons were generated from the same ESC lines (IDG26.10-3) originally used in the creation of a bacterial artificial chromosome (BAC)-transgenic mouse model (RRID:IMSR_JAX:029266) carrying human YPet-tagged TDP-43$^{WT/-}$ or *TDP-43*$^{M337V/-}$ as previously described (Wiese *et al.*, 2010; Gordon *et al.*, 2019). Briefly, mouse ESCs were expanded on irradiated CF1 mouse embryonic fibroblasts (Gibco, RRID:CVCL_RB05) in Knockout DMEM (Invitrogen) containing 15% ESC-screened fetal bovine serum (10439024, ThermoFisher), 2mML-glutamine (10378-016, Invitrogen), 0.01% MEM non-essential amino acids (11140035, Invitrogen), 1ng/ml leukaemia inhibitory factor (LIF, ESG1107, Millipore), 0.01% EmbryoMax ESC qualified nucleosides (ES-008-D, Millipore) and 0.1mM 2-mercaptoethanol (ES-008-DInvitrogen). After two days embryoid bodies were separated from the feeder layer by treatment with 0.25% trypsin-EDTA (25200-056, Gibco) and single cell suspension plated into 10cm dishes (Corning) in 50% advanced DMEM/F-12 (12634010, Gibco), 50% Neurobasal medium (21103049, Gibco), 10% Knockout serum replacement (10828028, Gibco), 2mM L-glutamine, 0.01% Penicillin-streptomycin and 0.1mM 2-mercaptoethanol (ADFNK medium). 1µM retinoid acid (R2625, Sigma) and 0.5µM smoothened agonist (56660, Merck) was added on day four and embryoid bodies were split on day six and eight. Embryoid bodies were collected and disaggregated on day nine. Embryoid bodies were collected and settled by gravity, washed with PBS and incubated with 2ml of Accumax (Sigma) for 10 minutes at 37°C. Cells were filtered through a 40µm cell strainer (Corning) and plated on poly-L-ornithine (P4957, Sigma) and laminin (23017015, Gibco) -coated plates in ADFNK medium plus retinoid acid, smoothened agonist and growth factors (10ng/ml GDNF, 10ng/ml BDNF, 25ng/ml CNTF and 10ng/ml NT-3; all from Pepro-Tech). Mature motor neurons were ready for analysis

after two days on day eleven. To examine the effect of oxidative stress, motor neurons were treated with 0.5mM sodium arsenite (NaAs; Sigma) in growth media for 30 or 60 minutes. Cultured cells were then washed with PBS and either fixed with 4% PFA for immunocytochemistry or lysed with 1% NP-40 buffer for protein extraction and co-immunoprecipitation. Survival was assessed over 24 hours after 0.5mM NaAs treatment measuring resazurin metabolism (alamar blue Ex560 Em 590) normalized to an untreated sample. The cultures were kept at 37 °C and 5% CO_2 for the duration of the experiments.

2.3.2. Mass spectrometry and bioinformatics

For the study of the TDP-43 interactome, a total of 3 differentiations of mouse ESC-derived motor neurons harbouring human *TDP-43*$^{WT/-}$ or *TDP-43*$^{M337V/-}$ with or without 0.5mM NaAs treatment for 60 minutes were generated. Cells were washed with PBS, incubated with 1% NP-40 buffer with 100x HALT protease phosphatase inhibitor (ThermoFisher) for 5 minutes on ice, cells were scraped and centrifuged for 10 minutes at 10,000 g at 4°C. 500µg of protein lysate was used per immunoprecipitation reaction. YPet-tagged human TDP-43 was co-immunoprecipitated using GFP antibody-coated magnetic-agarose beads for 1 hour (GFP Trap, Chromotek, Germany). Beads were washed three times with wash buffer (10 mM Tris/Cl, 150 mM NaCl, 0.5 mM EDTA pH 7.5) and immunoprecipitated proteins bound to YPet-TDP-43 were directly digested with trypsin/lysinC using in-StageTip method and frozen at -80°C prior to elution for mass spectrometry following the manufacturer's instructions (Preomics, Germany). Interactors of human TDP-43 were identified by high performance liquid-chromatography tandem mass spectrometry (LC-MS/MS) using an Orbitrap Fusion Lumos mass spectrometer (Thermo Scientific). Raw MS data were analysed using Progenesis QI for Proteomics software v3.0 (Nonlinear Dynamics). MS/MS spectra were searched against the Mus musculus reference proteome (retrieved 15/11/2016) including the YPet-sequence using Mascot v2.5.1 (Matrix Science) allowing for a precursor

mass tolerance of 10ppm and a fragment ion tolerance of 0.5Da. Carbamidomethylation on cysteines was defined as fixed modification and variable modification included deamidation on asparagine and glutamine and oxidation on methionine.

The peptide false discovery rate (FDR) was set at 1% and all peptides with an ion score higher than 20 were imported into Progenesis QIP. To further improve confidence in protein identification at least two peptides were required for protein identification, with 0.1% peptide FDR and 1% protein FDR. Protein abundance values were normalised to the median abundance of the 90 % of proteins with the lowest variance across all runs and compared by t-test, with a FDR-adjusted p-value of ≤0.05 for significant differences and fold changes between TDP-43^{WT} and TDP-43^{M337V} interactors were calculated. For interactors where ion abundances were missing approximate quantification by peptide spectral count was used. A protein was defined as putative interactor with at least 2 unique peptide spectral counts, when 0 or 1 in the other interactome, or 1 unique peptide spectral count, when completely absent in the other interactome.

2.3.3. Gene ontology (GO) enrichment analysis

Gene ontology (GO) enrichment analysis was performed using TopGO (R-studio Version 1.1.383) applying a target-background approach at the gene level, with specific interactors of the TDP-43^{WT} (> 3 peptide spectral counts) or TDP-43^{M337V} +/- NaAs interactome as the foreground list. The background list comprised all proteins identified over all twelve samples combined. Proteins of the interactomes significantly annotated to a GO term were determined by Fisher's exact test with a p-value <0.05. The odds ratio (OR) indicates the ratio of significant identified proteins in the foreground list to the expected presence of proteins. Calculations were made to identify overrepresented biological processes, cellular components and molecular functions. The top results are shown with the number of significant proteins (p<0.05) identified in each GO term annotated using ggplot2 version

0.9.0 (R-studio Version 1.1.383, H. Wickham. ggplot2: Elegant Graphics for Data Analysis. Springer-Verlag New York, 2016). A visual network of protein-protein interactions was generated by STRING (consortium 2019) utilized through Cytoscape v3.3.0 selecting Mus musculus organism and high confidence interactions.

2.3.3. Immunohistochemistry and confocal microscopy

Cells cultured on glass coverslips were fixed with 4% PFA-PBS for 15 minutes and blocked with 5% normal donkey serum with 0.1% Triton X-100 for one hour at room temperature (RT). The cells were incubated overnight with primary antibody diluted in 1% donkey serum (Table 2.3.). After washing with 0.1% Triton-X/PBS for ten minutes three times the samples were incubated with Alexa Fluor 488 or Alexa Fluor 568 conjugated donkey anti-rabbit, anti-mouse or anti-goat secondary antibodies (Life Technologies, 1:1000) for one hour at room temperature. After washing with 0.1% Triton-X/PBS for ten minutes twice, nuclei were stained with 4',6-Diamidino-2-Phenylindole (DAPI) for ten minutes. Coverslips were mounted and fluorescence was visualized using a confocal microscope Zeiss LSM. Cells from six randomly chosen-fields were counted and averaged for each differentiation. Statistical analysis compared average values from each differentiation (total differentiations per experiment n=3). The number and area of stress granules per motor neuron were assessed by an automated macro analysis programmed for the recognition of stress granules of the size from 100nm^2 to 1.5µm^2 (Fiji version 1.0 of ImageJ).

Table 2.3. Primary antibodies for immunohistochemistry

Description	Company	CatNo	Dilution
rabbit polyclonal GFP	Invitrogen	10474172	1:1000
mouse monoclonal Islet1	Developmental Studies Hybridoma Bank	40.2D6-A	1:1000
goat polyclonal ChAT	Millipore	ab144P	1:500
mouse monoclonal Tuj1	Covance	MMS-435P	1:1000
rabbit polyclonal cleaved caspase-3	Cell signaling	9661	1:1000
rabbit polyclonal PABPc	Abcam	Ab21060	1:1000
mouse monoclonal G3BP	Abcam	ab56574	1:1000

All primary antibodies were followed by Alexa Fluor anti-host IgG secondary antibody (diluted 1:1000). The catalogue number (CatNo) is given.

2.4. Validation of proteomic data and studying cellular pathways derived from the human TDP-43 interactome

2.4.1. Co-Immunoprecipitation for immunoblotting

In this Chapter co-immunoprecipitation was applied with the aim to detect interactors by western immunoblotting. Depending on the bait protein different antibody-coated beads and immunoprecipitation approaches were used. Cell lysates were prepared as previously described using 1% NP-40 buffer with 100x HALT protease phosphatase inhibitor (ThermoFisher). Cells were incubated with the lysis buffer for 5 minutes on ice, scraped and centrifuged for 10 minutes at 10,000g at 4°C. For immunoblots at least 1000µg of protein lysate was used per immunoprecipitation reaction. For RNase treatment protein extracts were incubated with either vehicle (10mM Tris-HCl, pH 7.5, 15mM NaCl) or 330µg of RNase A (Roche) for 10 minutes at 37°C on a shaker. After samples have been cooled on

ice co-immunoprecipitation was performed. YPet-tagged human TDP-43 and EGFP-tagged human C-terminal TDP-43 were co-immunoprecipitated using 25µl of GFP antibody-coated magnetic-agarose beads per sample (GFP Trap, Chromotek, Germany). TurboGFP-tagged human TDP-43 was immunoprecipitated using 25µl of turboGFP (tGFP) antibody-coated magnetic-agarose beads (TurboGFP Trap, Chromotek, Germany). Beads were washed three times with wash buffer (10mM Tris/Cl, 150mM NaCl, 0.5mM EDTA pH 7.5) and incubated with the sample for 45 minutes at 4°C. The beads were collected with a magnetic stand, the supernatant saved and beads washed 3 times with 500µl of wash buffer. The beads were then directly taken up in 30µl 2x LDS sample and cooked for 10 minutes at 95°C prior to immunoblotting. Human TDP-43 and PABPc reverse Co-immunoprecipitations were performed by incubating lysates with 5µg of rabbit anti-TDP-43 (Proteintech) or rabbit anti-PABPc protein (Abcam) at 4° overnight and binding to protein A/G magnetic beads (ThermoFisher) for one hour at room temperature the following day. Beads were washed and antibody-bound proteins eluted using the MS-Compatible Magnetic IP Kit (ThermoFisher). Eluates were dried in a speedVac (ThermoScientific) and IP-eluates were directly resuspended in 30µl 2x LDS sample buffer and 7.5µl of 4x LDS buffer was added to 19µl of the supernatants. All LDS sample buffers were supplemented with 10x reducing agent (Invitrogen) and boiled at 95 °C for 7 minutes. Sample were run on a 4-12% gradient precast gel (Invitrogen) at 135V for 2.5 hours in MOPS running buffer (Invitrogen). Membranes were blocked in TBS protein free blocking buffer (ThermoFisher) and incubated overnight with primary antibody, as follows: rabbit anti-GFP, which sufficiently detects the YPet and EGFP tag (Invitrogen, 1:1000), rabbit ant-turboGFP (Invitrogen, 1:1000) rabbit anti-PABPc (Abcam, 1:1000), rabbit anti-TDP-43 (Proteintech, 1:1000), rabbit anti-C-terminal TDP-43 (Proteintech, 1:1000) diluted in protein free blocking buffer followed by respective secondary antibodies (Novus Biologicals, 1:10000). ECL (GE Healthcare) signal was visualised using the BioRad ChemiDoc imaging system.

After immunodetection of the co-immunoprecipitated prey protein, all membranes were stripped with restore stripping buffer (ThermoFisher) for ten minutes and immunoblotted for the immunoprecipitated bait protein. This was repeated for immunoblotting ß-tubulin for loading control. Signal intensity was quantified using the Fiji version 1.0 of ImageJ. After immunoblotting the immunoreactivity of the co-immunoprecipitated prey protein was semi-quantified relative to the normalized immunoreactivity of the immunoprecipitated bait protein.

2.4.2. Cloning human TDP-43 constructs

2.4.2.1. cDNA Plasmid constructs

The cDNA plasmid of full-length human TDP-43 ORF clone in a pCMV6-AC-GFP tagged cloning vector was purchased from OriGene Technologies, Inc. (Rockville, USA) (Fig. 2.3. A). The C-terminal TDP-43 (NM_007375) from amino acid 257-414 construct 5 in a pEGFP-N1 vector delivered as bacterial agar stock was a gift from Zuoshang Xu (Addgene plasmid # 28198; http://n2t.net/addgene:28198; RRID:Addgene 28198) (Fig. 2.3. B). Both constructs express TDP-43 under the CMV promoter.

Fig. 2.3. Human TDP-43 constructs for transient transfection of HEK293T cells

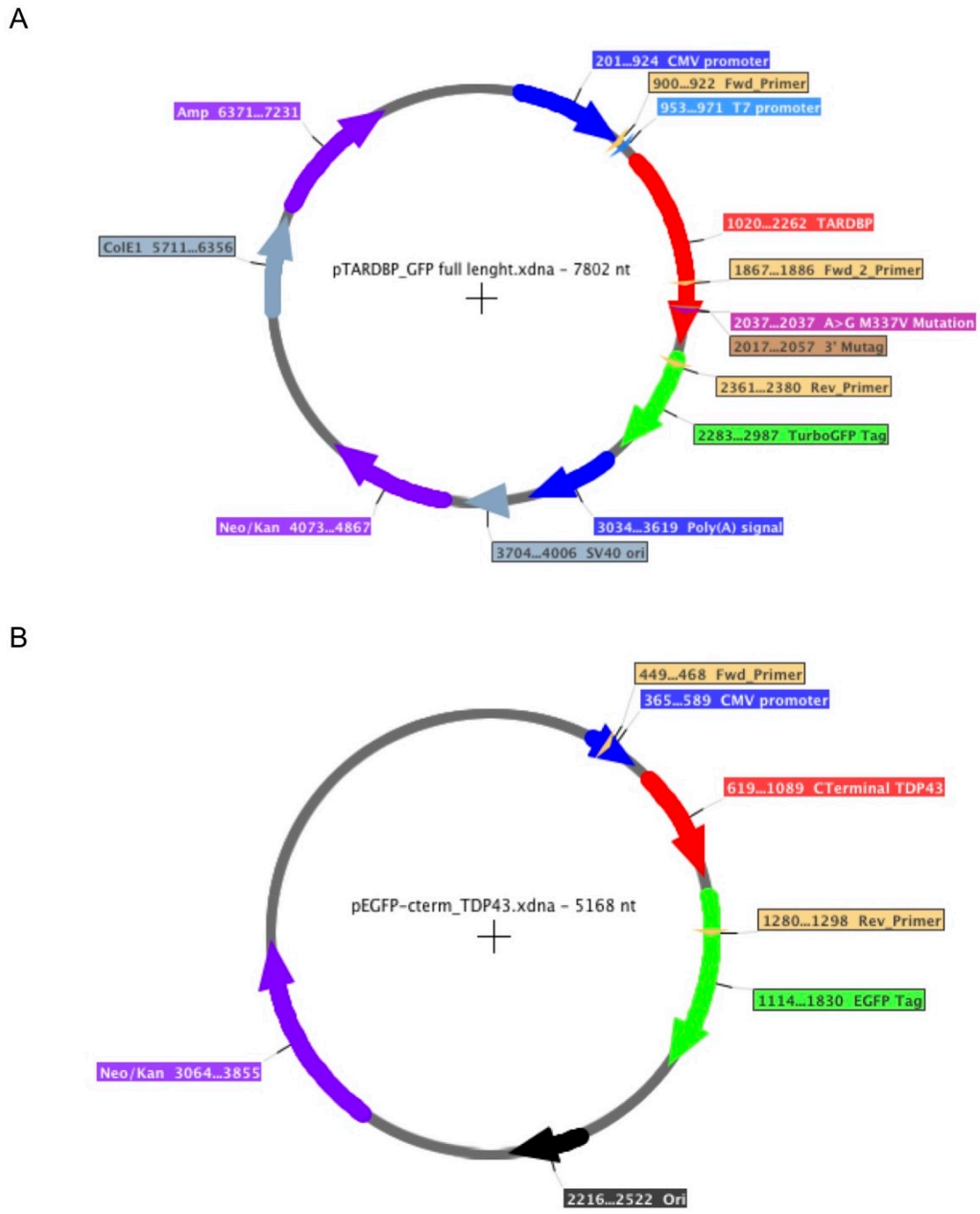


Fig. 2.3. **A** The cDNA plasmid of full-length human TDP-43 ORF in a pCMV6-AC-turboGFP-tagged cloning vector. This vector was used for expression of full-length TDP-43, site-directed mutagenesis of the M337V mutation (A>G missense mutation) and restriction of the TDP-43 sequence to obtain an empty vector control **B** The C-terminal TDP-43 (amino acid 257-414) construct in a pEGFP-N1 vector. Forward and reverse primers used for sequencing are indicated. Abbreviations: ORF, open reading frame; Fwd, forward; Rev, reverse; Kan, Kanamycin and Amp, Ampicillin antibiotic resistance; Ori, origin of replication.

2.4.2.2. Subcloning of chemically component cells

50µl of subcloning efficiency Stbl3 chemically competent E. coli (ThermoFisher) were used for transformation of 2µl DNA (1-10ng). Cells were thawed on ice and DNA added for 30 minutes on ice with intermediate tabbing, then the cells were heat shocked at 42°C for 45 seconds and put back on ice for 2 minutes. Each transformation was resuspended in 250µl of 37°C prewarmed SOC medium and incubated at 37°C on a 225rpm shaker for 1 hour. 50µl of three densities were platted on three separate LB agar petri dishes containing ampicillin and colonies were grown upside down at 37°C overnight. The next day the transfection efficiency was evaluated by assessing the number of colonies. A small amount of the C-terminal TDP-43 bacterial agar stock was directly streaked with a loop at decreasing concentrations on LB agar petri dishes containing kanamycin and colonies were grown upside down at 37°C overnight.

2.4.2.3. DNA extraction

2.4.2.3.1. Plasmid DNA mini preparation

A single bacterial colony was seeded in 4ml of LB culture containing the appropriate antibiotic and grown overnight at 37°C with shaking. To extract the DNA 1.5ml of the culture were prepared with PureLink Quick Plasmid Miniprep Kit (K210010, Invitrogen) while a stock of 1ml of the culture was snap frozen with 75µl DMSO at -80°C.

2.4.2.3.2. Plasmid DNA maxi preparation

A single bacterial colony was seeded in 300ml of LB culture containing the appropriate antibiotic and grown overnight at 37°C with shaking. To extract the DNA NucleoBond Xtra Midi EF / Maxi EF (Macherey and Nagel, Düren, Germany) while a stock of 1ml of the culture was snap frozen with 75µl DMSO at -80°C.

2.4.2.4. Restriction digests of plasmid DNA

The restriction enzymes and buffers were purchased from New England Biolabs (NEB). Restriction digests were prepared by adding the given components in Table 2.4..

When miniprep DNA was used, 1µg of miniprep DNA were digested. The digestion mix with DNA were incubated at 37°C for 1 hour and the results were analysed by agarose gel electrophoresis. 1% agarose gels plus 12µl of ethidium bromide (for 300ml volume) were prepared and 16µl of restriction digest samples mixed with 4µl of sample loading buffer were run at 200V in 1xTBE buffer.

Table 2.4. Protocol for restriction enzymes

Components	Per reaction
DNA from maxi prep	1µg
10x Buffer	5µl
(High fidelity) restriction enzyme(s)	1µl
H2O	up to 50µl

2.4.2.5. Sanger sequencing

The region of interest to be sequenced was taken to the sequencing facility (Weatherall Institute of Molecular Medicine, Oxford, UK) using the following primers (Table 2.5.):

Table 2.5. Oligomers for Sanger Sequencing

Primers	sequence	Tm	GC%
Fwd_seq_primer Cterm TDP	AATGGGAGTTTGTTTTGGCA	64	40
Rev_seq_primer Cterm TDP	ACGAGGGTGGGCCAGGGCA	76	74
Fwd_primer_TDP	CGGTGGGAGGTCTATATAAGCAG	74	52
Rev_primer_TDP	CCCACCAGCTCGAACTCCAC	74	65

2.4.2.6. Site-directed mutagenesis

Site-directed mutagenesis was done by using QuikChange Lightning Site-Directed Mutagenesis Kit (Agilent) applying the following oligomers (Table 2.6.).

After amplification the PCR product was purified (Qiagen PCR purification KIT) 1µl of Dpn1 restriction enzyme was added to 1µg of DNA and incubated for 15 minutes at 37°C, then heat-inactivated at 80°C for 20 minutes. To check the PCR production of mutated plasmids, 5µl of each PCR mix were separated on a 1% agarose gel. The mutation was confirmed by Sanger sequencing using the respective TDP-43 primers (Table 2.5.).

Table 2.6. Oligomers for site-directed mutagenesis

Primers	sequence	Tm	GC
5'_mutagenesis_S_M337V_TDP	TACAGAGCAGTTGGGGTATGGTGGG CATGTTAGCCAGCCAG	88	56
3'_mutagenesis_A_M337V_TDP	CTGGCTGGCTAACATGCCCACCATA CCCCAACTGCTCTGTA	88	56

2.4.2.7. Ligation

To circularize linear DNA T4 DNA Ligase was used in a 5 minutes reaction. Most ligations performed using the T4 DNA Ligase and 5X Rapid Ligation Buffer reach an end point at 5 minutes or less at 25°C.

2.4.3. Human cellular models

All fibroblasts were derived from skin biopsies from patients attending the Oxford Motor Neuron Disease clinic and taken under ethical approval granted by the South Wales NHS Research Ethics Committee (Ref 12/WA/0186). Fibroblasts from two male healthy control

patients: 841, OX03, and from one male ALS patient with a *M337V TDP-43* gene mutation: 03-03 (clone 3), were cultured in Dulbecco's modified Eagle's medium (Gibco) with 10% US-approved fetal bovine serum (16000036, Gibco) and 1% antibiotic-antimycotic (15240062, Life technologies).

HEK293T cells were transfected using 12µl Lipofectamine 2000 (Invitrogen) with 3.5µl of the following constructs as described above: C-terminal turboGFP-tagged full-length human TDP-43 plasmid +/- M337V mutation inserted by site-directed mutagenesis, the TDP-43 empty vector control and C-terminal EGFP-tagged C-terminal TDP-43. Transfection media was left on overnight and harvested 48h after transfection.

All iPSC lines were reprogrammed from skin biopsy fibroblasts in the James Martin Stem Cell Facility, University of Oxford, using standardized protocols as previously described (Dafinca *et al.*, 2016). Human motor neurons (MNs) were differentiated from iPSCs for 30 days before conditioned media was retrieved for vesicle experiments, as previously described (Maury *et al.*, 2015). Briefly, monolayers of iPSCs were induced in DMEM/F12/Neurobasal with N2 supplement (Life Technologies), B27 supplement (Life Technologies), ascorbic acid (0.5µM), 2-mercaptoethanol (Life Technologies), 1µM compound C (Millipore) and 3µM Chir99021 (Bio-Techne) for four days. After four days in culture, 1µM retinoic acid (Sigma-Aldrich) and 500nM smoothened agonist (SAG, Bio-Techne) were added to the medium. On day five, Chir99021 and compound C were removed from the medium, and the cells were cultured for another four to five days. Neural precursors were then dissociated and plated at a low density for seven days. The medium was supplemented with 10ng/mL BDNF (Life Technologies), 10ng/mL GDNF (Life Technologies), 10µM N-[N-(3,5-Difluorophenacetyl)-L-alanyl]-S-phenylglycine t-butyl ester (DAPT), and laminin (0.5mg/mL). After seven days, DAPT was removed from the

medium, and the neurons were allowed to mature for another two weeks before functional experiments.

2.4.4. Ultrafiltration liquid chromatography and extracellular vesicle characterization

Extracellular vesicle (EV) characterizations were performed in EV-depleted media prepared by ultracentrifugation for respective cell culture mediums centrifuged at 120,000g for 18 hours (Beckman Coulter, Optima MAX-XP Ultracentrifuge). Motor neuron cultures were plated at equal density on a 6-well plate. On day eleven motor neuron cultures were exposed to EV-depleted conditioned media +/- 0.5mM NaAs for 60 minutes, the media was then collected and immediately frozen at -80°C. Collected media was then defrosted on ice and centrifuged and following filtration (0.22µm), samples were filtered using Amicon Ultra-15 100kDa molecular weight cut-off (MWCO) centrifugal filters (Merck Millipore) at 3,500 g for eight minutes, washed with PBS and centrifuged at 3,500 g for four minutes. Retentate volume was adjusted to 800µL with PBS, injected into a 24ml size exclusion column packed with sepharose 4 fastflow (mean particle size 90µm, exclusion limit 3×10^7) and eluted with 40ml PBS at 0.5ml per minute using an AKTA pure chromatography system (GE Life Sciences). Two microliter fractions were collected from six to 40ml elution volume. Extracellular size distribution and concentration was ascertained using nanoparticle tracking analysis (NTA) using a NanoSight NS500 (Malvern Ltd) and NTA 2.3 software. Size distribution was averaged across three 30 seconds recordings per sample (Thompson *et al.*, 2018). EV-containing fractions (fraction 2–3) were concentrated for further analysis using Amicon Ultra-15 10kDa MWCO centrifugal filters. Samples were subsequently dried in a speedVac (Thermo Scientific) and the vesicle pellet was resolved in 30µl of 2x LDS sample buffer and immunoblotted with anti-Flotillin-1 antibody (BD Transduction Laboratories, 610821, 1:1000).

2.4.5. Quantification and statistical analysis

Proteomic analysis is detailed above. Data are presented as mean and standard deviation and unpaired t-test was used to assess significant differences ($p<0.05$). One-way ANOVA analysis was used to determine statistical differences between three or more groups. Sidak's multiple comparisons test was used to assess differences in survival. The exact value of the number of replicates and the statistical test and result are given in the figure legends. Statistical analysis was carried out using R-Studio and GraphPad Prism 7 (version7b, 2016).

Chapter 3: Detection of pathological TDP-43 peptides by mass spectrometry

3.1. Introduction and Aims

The diagnosis of ALS is clinical and monitoring the disease in terms of disease progression or effects of treatments relies on clinical output measures often subjective or lengthy as a result. Biomarkers are needed to facilitate diagnosis and enable effective therapy development. Neuronal and glial cytoplasmic aggregation of ubiquitinated TDP-43 can be found in nearly all cases and is a unifying pathological event across the expanding clinical heterogeneity of ALS, including overlap with FTD (Neumann *et al.*, 2006). By immunoblotting TDP-43 from human ALS brains, specific pathologically altered forms of TDP-43 have been observed. This includes full-length phosphorylated TDP-43 (45kDa), TDP-43 truncated C-terminal fragments (20-30kDa) and a high molecular weight smear representing ubiquitinated TDP-43. The detection and measurement of the pathological forms of TDP-43 would have a major diagnostic and possible prognostic value. Studies investigating concentrations of TDP-43 in plasma and CSF by antibody-based methods have had variable results so far. Most currently available antibodies recognise both the full-length form and smaller pathological fragments of TDP-43, thus making it difficult to differentiate patients from controls. A further challenge is the low concentration of pathological TDP-43 in respective biofluids.

Identification of TDP-43 by mass spectrometry is an alternative approach to antibody-based methods. When TDP-43 had been discovered, its protein sequence was confirmed by mass spectrometry from extracts of FTLD brains with TDP-43 pathology (Neumann *et al.*, 2006). Later a case study investigated pathological forms of TDP-43 extracted from ALS brains by

mass spectrometry and discovered potential new truncation and phosphorylation sites of TDP-43 (Kametani *et al.*, 2016). However, these findings are not yet validated and are restricted to a small discovery cohort. All these studies depend on the enrichment of the pathological TDP-43 prior to mass spectrometry. Identification of a protein by mass spectrometry requires the digestion of proteins into peptides and subsequent discovery of unique peptides to the target protein.

The aim of this chapter is to enrich TDP-43 and its pathological forms in order to detect TDP-43 and its most abundant peptides by mass spectrometry. This chapter also aims to detect TDP-43 peptides that are ALS-specific, mainly focusing on the enrichment of the C-terminal TDP-43 fragments and the detection of peptides that flank new truncation sites of TDP-43. The detection of TDP-43 from biofluids would provide the most useful information for biomarker development. However, the most abundant source of pathological TDP-43 in ALS is the central nervous system tissue with confirmed TDP-43 pathology and this must therefore be used for the detection of disease-specific TDP-43 peptides. In this chapter, TDP-43 is systematically enriched over a range of ALS-related biofluids and tissue. The discovery of TDP-43 peptides from ALS biosamples can then be used to develop a more sensitive and targeted proteomic method to study their specificity in more detail.

3.2. Results

3.2.1. Enrichment of TDP-43 for mass spectrometric detection

Previous studies have shown that TDP-43 in biofluids is low abundant and solubility of pathological aggregated TDP-43 relies on treatment with buffers with strong detergents. To detect TDP-43 or pathological TDP-43 by mass spectrometry enrichment by affinity purification is a valuable method for sample preparation prior to mass spectrometry to specifically enrich for TDP-43 and increase the chance of detection.

3.2.1.1. Specificity of antibodies for affinity enrichment of human TDP-43

To test if antibody-based methods are specific to enrich for human TDP-43, brain homogenates from mice (BAC)-transgenic for human YPet-tagged TDP-43 were used.

Western immunoblotting using a polyclonal TDP-43 detection antibody showed that both endogenous mouse TDP-43 and human YPet-tagged TDP-43 is present in homogenates from mouse brain (Fig. 3.1. A). Immunoprecipitation with a monoclonal antibody (mab) against TDP-43 showed a highly specific pull down of human YPet-tagged TDP-43 at 72kDa. The supernatant was almost devoid of human TDP-43, but still contained the endogenous mouse Tdp-43 at 48kDa, suggesting selective depletion. The negative immunoprecipitation control with an IgG instead of the TDP-43 capture antibody did not show any reaction for TDP-43. The same result was achieved for immunoprecipitation with a polyclonal TDP-43 antibody, however this antibody was less specific to human TDP-43 shown by an additional mouse Tdp-43 band present in the immunoprecipitation (Fig. 3.1. B). In both immunoblots using the polyclonal TDP-43 detection antibody a slight nonspecific reaction at 50kDa was observed corresponding to IgG present in the negative immunoprecipitation control sample.

In TDP-43 immunoprecipitations a slight IgG heavy chain reaction at 50kDa was expected due to some co-elution of IgG antibody chains with the bait protein. This together indicates a less specific reaction of the polyclonal TDP-43 capture antibody to human TDP-43 and a nonspecific reaction of the polyclonal TDP-43 detection antibody to IgG.

Fig. 3.1. Affinity enrichment of human TDP-43 from (BAC)-transgenic mouse brain homogenates and human biofluids

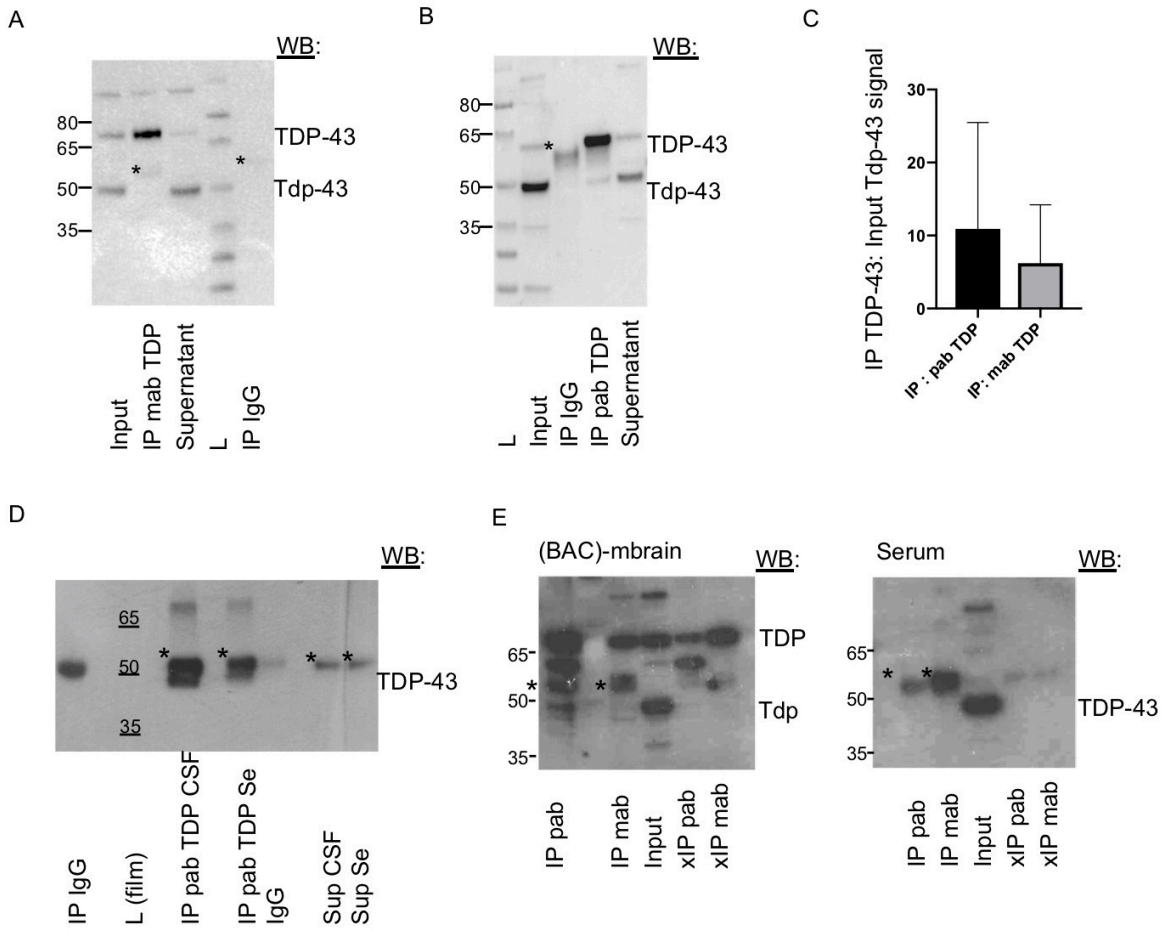


Fig. 3.1. For immunoblotting the polyclonal primary antibody against full-length TDP-43 was applied, Gels 4-12% using MOPS buffer, Spectra multicolor ladder (L), IgG heavy chain (*) at 55kDa. IP, immunoprecipitation.

A Characterization of TDP-43 immunoreactivity following IP of human GFP-tagged TDP-43 (BAC)-transgenic mouse brain. The input mouse brain homogenate (10µg) shows mouse Tdp-43 at 48kDa and human TDP-43 at 72kDa. IP with the monoclonal full-length TDP-43 bait antibody shows a strong reaction for human TDP-43 at 72kDa, mouse Tdp-43 at 48kDa was not recognized. IP supernatant shows depletion of human TDP-43 but remaining mouse Tdp-43. Negative control IP with IgG1 rabbit isotype control shows no TDP-43 reactivity at 48kDa and 72kDa, but a nonspecific reaction to co-eluted IgG at 55kDa (*).

B IP with the polyclonal full-length TDP-43 shows human TDP-43 at 72kDa and a slight mouse Tdp-43 reaction at 48kDa. IP supernatant shows still a slight reaction of human GFP-tagged TDP-43 and the remaining mouse Tdp-43.

C The ratio human TDP-43 IP signal to the TDP-43 input signal is not significantly different between the polyclonal and monoclonal TDP-43 antibodies (n=3, p=0.65).

D Immunoprecipitation from serum and CSF using 5µg of a polyclonal TDP-43 antibody: IP from pooled ALS CSFs (n=5) shows a nonspecific reactivity for IgG at 55kDa and a strong immunoreactive band for TDP-43 at 48kDa. IP of pooled ALS sera (n=5) shows nonspecific reactivity for IgG and a faint immunoreactive band for TDP-43 at 48kDa. IgG at 55kDa. IP supernatants show IgG at 55kDa.

E IPs with the poly- and monoclonal TDP-43 bait antibody from mouse brain show enrichment for human TDP-43 at 72kDA and nonspecific detection of IgG at 55kDa. After crosslinking (xIP) no IgG at 55kDa is detected. IP of TDP-43 from serum shows unspecific IgG immunoreactivity, not TDP-43. XIP reduces IgG.

3.2.1.2. Efficiency of antibodies for affinity enrichment of human TDP-43

Antibody efficiencies to pull-down human TDP-43 were determined relative to the amount of TDP-43 from 10µg of brain homogenate. All immunoprecipitations (IP) were performed from 1000µg total protein of brain homogenates and resulted in an increased signal intensity of human TDP-43 after immunoprecipitation. The median signal intensity ratio (signal of TDP-43 from IP: signal of TDP-43 from 10µg of input) from three separate experiments was 10.9 using the polyclonal TDP-43 capture antibody and 6.2 using the monoclonal TDP-43 capture antibody (Figure 3.1. C) ($p=0.65$). Both antibodies had the same efficiency to enrich for human TDP-43.

3.2.1.3. Antibody-based methods are limited for the enrichment of TDP-43 from human biofluids

The same immunoprecipitation approach as described above was used to enrich TDP-43 from human biofluids. The detection of TDP-43 between patients and samples can be variable, therefore I generated a pool of samples of serum and CSF from different patients with ALS and healthy controls to increase the likelihood to detect TDP-43. I have randomly selected five samples per pool, the ALS samples were from fast progressing patients. Western immunoblotting showed no result to detect TDP-43 in samples immunoprecipitated by the monoclonal TDP-43 antibody (data not shown). The polyclonal TDP-43 antibody immunoprecipitated TDP-43 at 48kDa from CSF and serum samples (Figure 3.1. D). The enrichment of TDP-43 from serum samples was decreased compared to CSF shown by a less intense TDP-43 signal in the immunoblot. In both immunoprecipitations an additional strong reaction for IgG heavy chain at 50kDa was observed indicating strong nonspecific binding of the antibody to immunoglobulin heavy chain or albumin. Only the application of high resolution 10% gels allowed the separation of the IgG heavy chain (50kDa) from the

TDP-43 (48kDa) band. A relatively high proportion of IgG was left in the remaining supernatant, suggesting that the binding of IgG to the antibody reached saturation. Crucially immunoprecipitation of TDP-43 by the polyclonal TDP-43 and the detection of a TDP-43-positive band by immunoblotting varied between samples. This experiment was therefore not reproducible in individual samples and only with high variability in pooled samples. Immunoprecipitation of TDP-43 from biofluids shows enrichment of the full-length form of TDP-43, pathological truncated forms are not observed in both serum and CSF samples. In summary the enrichment of human TDP-43 with a monoclonal TDP-43 antibody was not successful from both CSF and serum, while the polyclonal TDP-43 antibody yielded inconsistent results for the enrichment of full-length TDP-43 with strong nonspecific binding to IgG heavy chains.

Clearly the IgG heavy chain reaction was much more pronounced in biofluids where IgG and albumin are abundant compared to immunoprecipitates from tissue. Therefore, it is unlikely that all of the IgG observed in biofluids can be explained by co-elution of antibody chains as the same methods were applied. However, to clarify, if some IgG reaction can be reduced by avoiding co-elution of antibody chains, the antibody was crosslinked to the beads using DMP (Fig. 3.1. E). Crosslinking the antibodies to the magnetic beads prior to elution resulted in a decrease of IgG at 50kDa for both monoclonal and polyclonal TDP-43 antibodies, when immunoprecipitated from mouse tissue (Fig 3.1. E). This confirms that some IgG heavy chain reaction is explained by co-elution from beads. Crosslinking of antibodies reduced IgG heavy chain elution in immunoprecipitates from biofluids, however no immunoreactive signal for TDP-43 was observed.

3.2.1.4. Serial fractionation of ALS post mortem tissue with TDP-43 pathology enables the detection of disease-specific TDP-43 forms

Limitations of commercially available antibodies to specifically extract pathological forms of TDP-43 and the limitation of antibodies to be used in biofluids, ask for the need of an alternative method to identify TDP-43 and its disease-defining peptide signature. The most abundant source of pathological TDP-43 is human ALS brain tissue. Using a well-established sequential biochemical fractionation enabled the extraction of the soluble nuclear and cytoplasmic proteins (high-salt Triton X-100-soluble fraction, TX fraction) as well as the insoluble proteins (urea fraction) (Figure 3.2. A). By serial fractionation a defined proteome was obtained from extracts of the final insoluble protein pellet, shown by a clear banding pattern in silver stains (Fig. 3.2. A). In addition, the extraction of the insoluble protein fraction from ALS *post mortem* tissue enabled the detection of the characteristic pathological TDP-43 pattern.

Immunoblotting the urea fraction extracted from 1g of ALS cortex tissue using a polyclonal TDP-43 antibody detected full-length TDP-43 at 48kDa and at 52kDa suggesting pathological phosphorylated TDP-43 (Fig. 3.2. B). Additionally, a lower molecular TDP-43 band was detected at 28kDA suggesting truncated TDP-43. The urea fraction extracted from 1g of healthy control cortex tissue showed immunoreaction for full-length TDP-43 at 48kDa, but no higher or lower molecular weight bands were present. The TDP-43 immunoreactivity was also enriched in ALS urea fractions suggesting that more TDP-43 is present in the insoluble protein fraction compared to controls.

A more detailed analysis of TDP-43 in urea fractions from ALS cortex tissue was performed by using a C-terminal TDP-43 antibody binding to aa256-296 (C-TDP). The C-terminal antibody detected the full-length form of TDP-43 at 48kDa and lower molecular weight bands of TDP-43 at 20, 25, 28kDa (Fig. 3.2. C). This suggest that insoluble TDP-43 in ALS is also N-terminal truncated resulting in C-terminal lower molecular weight fragments. After

stripping the membrane and probing for phosphorylated TDP-43 using an antibody against the phosphorylation site of amino acid serine at position 409/410 of TDP-43 (P-TDP), a banding pattern corresponding to the C-terminal bands, but with a slight shift towards a higher molecular weight, was observed suggesting posttranslational modified TDP-43.

Fig. 3.2. Serial fractionation of ALS *post mortem* tissue with TDP-43 pathology enables the detection of disease-specific TDP-43 forms

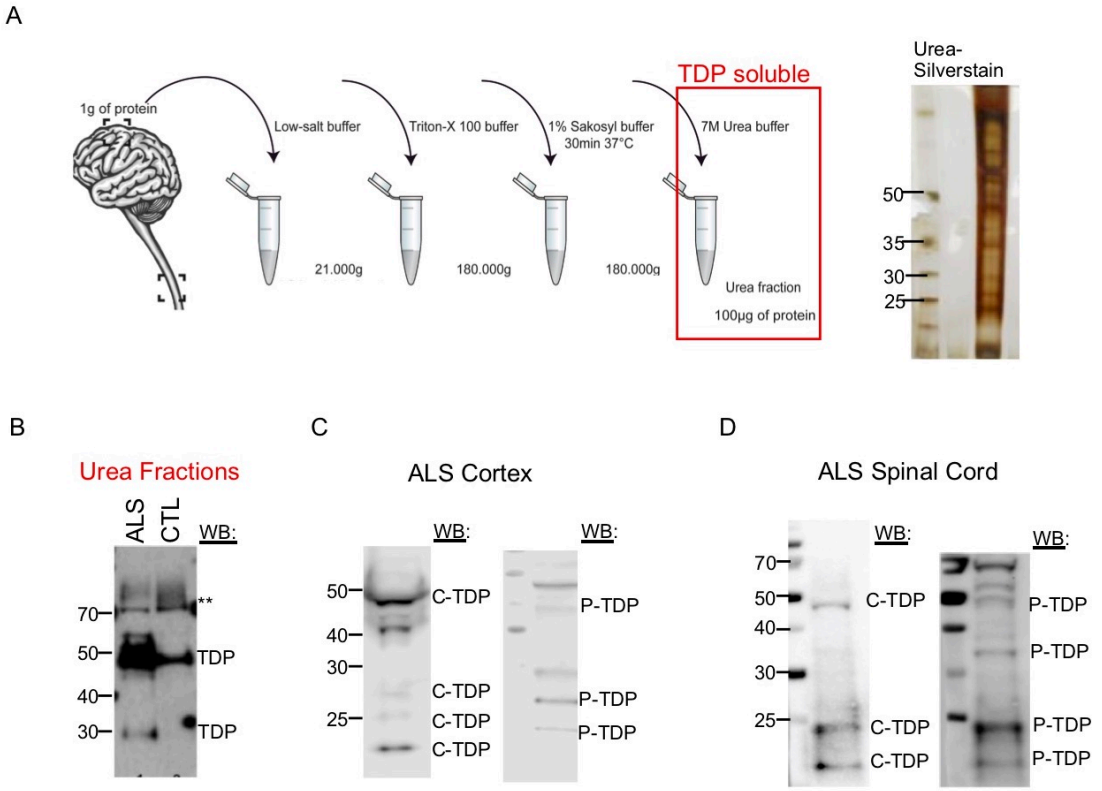


Fig. 3.2. A Serial fractionation of human motor cortex and spinal cord tissue (500mg-1g starting material) by ultracentrifugation and biochemical extraction of soluble and insoluble protein fractions. Red box indicates urea fraction with solubilised pathological TDP-43. Silver stain shows urea fraction with depletion of abundant proteins. **B** Western immunoblotting (WB) of sarkosyl-insoluble urea-soluble fractions on 4-12% gels using MES buffer, Spectra multicolor ladder (L). Full-length TDP-43 antibody (TDP) detects full-length TDP-43 at 48kDa, disease-specific phosphorylated TDP-43 at 50kDa and high molecular weight smear of posttranslational modified TDP-43 (**), as well as truncated TDP-43 at 28kDa from ALS spinal cord compared to full-length TDP-43 at 48kDa from healthy control (CTL). **C** A C-terminal specific TDP-43 antibody (C-TDP) detects full-length TDP-43 at 48kDa and low molecular C-terminal fragments at 20, 25 and 28kDa from an ALS cortex urea fraction. After stripping a phospho-specific TDP-43 antibody (P-TDP) detects corresponding bands. **D** The C-terminal antibody detects full-length and truncated TDP-43 at 24 and 20kDa from an ALS spinal cord urea fraction. Corresponding bands are detected after stripping and re-probing with P-TDP antibody.

Immunoblots of urea fractions from ALS spinal cord tissue using a C-terminal TDP-43 antibody showed full-length TDP-43 at 48kDa and lower molecular weight TDP-43 bands at 20 and 24kDa, possibly 27kDa (Fig. 3.2. D). After stripping and re-probing the membrane a corresponding banding pattern was observed with the TDP-43 antibody against phosphorylated serine indicating pathological phosphorylation of the C-terminal lower molecular weight bands. This finding indicates that C-terminal TDP-43 fragments are also present in the insoluble protein fraction of ALS spinal cords. The size of the C-terminal fragments varies between cortex and spinal cord samples suggesting different causes of cleavage.

3.2.2. Detection of TDP-43 and its pathological peptides by mass spectrometry

3.2.2.1. TDP-43 was not detected in human biofluids

Immunoprecipitations of human TDP-43 from serum samples with the monoclonal and polyclonal TDP-43 antibody were separated by electrophoresis on 10% high resolution gels and the purity of the eluates was evaluated by a whole protein gel stain using silver stain (Fig. 3.3.A). The results demonstrate that the immunoprecipitation enrichment is not specific for TDP-43 at 48kD with a high nonspecific enrichment of proteins of the size between 50kDa and 60kDa, likely reflecting heavy chain IgG and albumin, which are abundant in serum samples. For the subsequent discovery of TDP-43 from human ALS biofluids by mass spectrometry two approaches were applied 1.) TDP-43 was immunoprecipitated from native serum and CSF samples by a polyclonal TDP-43 antibody as this antibody yielded best results for TDP-43 immunoreactivity in western immunoblotting and eluates were directly referred to in-solution digest and mass spectrometry. 2.) Immunoprecipitation eluates were separated by electrophoresis on 10% high resolution gels to separate proteins by size and to perform in-gel digestion of the TDP-43 target band at 48kDa for mass spectrometry.

Fig. 3.3. In-Gel size separation of immunoprecipitations from biofluids does not separate a TDP-43 molecular weight band at 48kDa

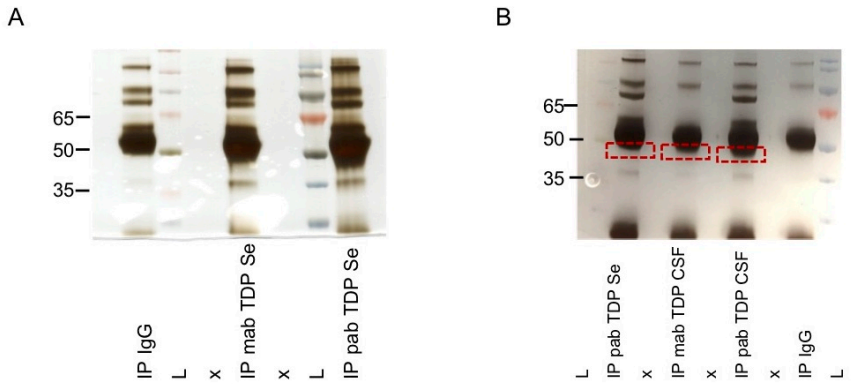


Fig. 3.3. A Electrophoretic separation on 10% gels and silver stains of TDP-43 IPs from serum using monoclonal (mab) or polyclonal (pab) TDP-43 antibodies show no clear separation of a molecular weight band at 48kDa which is the expected molecular weight of TDP-43. A strong staining at 50kDa is present suggesting co-eluted IgG heavy chain. The negative IP from serum with IgG1 does not show staining below 50kDa. **B** TDP-43 was immunoprecipitated from serum and CSF using mab and pab TDP-43 antibodies. Detection by silver stain shows a slight staining at 48kDa, but no distinct separation from the 50kDa signal. The 48kDa molecular weight signal was excised (red box) for in-gel digestion and subsequent mass spectrometry analysis. PageRuler prestain ladder (L). IP, immunoprecipitation.

All samples were digested with elastase, which has been chosen for the biofluid experiments, because it sufficiently cleaves the C-terminal region of TDP-43 into peptides. However, elastase is less specific and therefore has not been pursued further for the tissue experiments. The digestion was performed overnight for 16-18 hours. LC-MS/MS analysis was performed on the Lumos and data was analysed with PEAKS. Mass spectrometry of the in-solution digested samples identified a total of 523 proteins from serum and 659 proteins from CSF samples, but TDP-43 was not identified. The most abundant proteins, with a protein confidence score (-10lgP) well above the filtering threshold, were immunoglobulin gamma and immunoglobulin heavy chains, confirming the nonspecific reaction of the polyclonal TDP-43 antibody to IgG (Table 3.1.). Electrophoretic separation and silver stains of the immunoprecipitates did not allow a clear separation of the 48kDa band, which is the expected molecular weight band of TDP-43 (Fig. 3.3. A). Instead, the 48kDa band merged with the protein band at 50kDa. The 50kDa band stained much stronger in the silver stain, which is directly related to the protein amount. Despite this problem, the TDP-43 target protein bands were excised and digested with elastase and analyzed by mass spectrometry (Fig. 3.3. B). As anticipated TDP-43 was not detected in both serum and CSF in-gel digested samples after immunoprecipitation with the polyclonal TDP-43 antibody. TDP-43 was also not identified in in-gel digested samples from CSF using a monoclonal TDP-43 antibody for immunoprecipitation. Immunoglobulins were abundant in in-gel digests suggesting that the recovery of TDP-43 from the gel fractions was not sufficient or too low for proteomic identification (Table 3.2.).

Table 3.1. Mass spectrometric results from TDP-43 IP from serum and in-solution digest

Description	-10lgP	Coverage (%)	#Peptides	#Unique	Avg. Mass
Ig heavy constant gamma 1	248.35	33	18	2	36106
Ig heavy constant gamma 1	248.35	27	18	2	43912
Ig heavy constant gamma 2	247.95	30	17	1	35901
Ig heavy constant gamma 4	242.99	28	15	1	35941
Ig kappa constant	179.45	29	6	6	11765
Ig kappa variable 4-1	148.15	11	2	2	13380
Ig heavy variable 2-5	144.26	18	2	2	13231

Table 3.2. Mass spectrometric results from TDP-43 IP from CSF and in-solution digest

Description	-10lgP	Coverage (%)	#Peptides	#Unique	Avg. Mass
Ig heavy constant gamma 1	204.55	23	9	1	36106
Ig heavy constant gamma 1	204.55	19	9	1	43912
Ig heavy constant gamma 3	176.16	14	6	1	41287
Ig kappa constant	160.17	17	4	4	11765
Ig kappa variable 4-11	157.34	17	4	4	13380
Ig kappa variable 3D-11	124.33	7	2	2	12625
Ig kappa variable 3-11	124.33	7	2	2	12575

Description: Protein's header information as in FASTA database. -10lgP: The protein confidence score. A supporting peptide is considered as of high-confidence if it has a peptide -10lgP score above the filtering threshold. Coverage: The percentage of the protein sequence covered by supporting peptides. # peptides: The number of high-confidence supporting peptides. # unique: The number of high-confidence supporting peptides that are uniquely mapped to the protein group. Unique peptides with same sequence but different modifications are only counted once in this number. Avg. mass: Protein mass calculated using average mass. Ig, immunoglobulin; IP, immunoprecipitation.

3.2.2.2. Serial fractionation of ALS post mortem tissue enables the detection of TDP-43

500mg of human *post mortem* motor spinal cord tissue from ALS and healthy controls underwent serial fractionation resulting in the soluble protein fractions, as well as the insoluble protein urea fraction. The urea fractions were in-solution digested using trypsin a highly efficient protease. Trypsin is less specific to cleave the C-terminal region of TDP-43, as not many arginine or lysine amino acids are present in the C-terminal region. However, its digest efficiency and its specificity to cleave peptides increased the chance to detect TDP-43. Two independent mass spectrometric analysis were performed each consisting of urea fractions extracted from ALS and healthy control spinal cord tissue (Table 3.3.). In all samples more than 1000 proteins were identified by mass spectrometry. TDP-43 was discovered in both ALS and healthy control urea fractions. This indicates a sufficient enrichment of TDP-43 by serial fractionation for proteomic identification of TDP-43. The peptide coverage of TDP-43 varied between both mass spectrometric runs. In the first run TDP-43 peptide coverage was only >20% in both ALS and healthy control samples. In the second run the peptide coverage of TDP-43 was much higher reaching 50% (Table 3.3.). All peptides identified from in-solution digestion of tissue urea fractions showed trypsin-specific cleavage sites cutting after amino acids lysine (L) or arginine (R). The peptide coverage of TDP-43 analysed by PEAKS was shown for an in-solution digest of the urea fraction from an ALS patient (Fig. 3.4.). The coverage was 50% and it included tryptic peptides located at its N-terminal and C-terminal regions. The region closer to the C-terminal end was not covered by peptides, because of its low lysine and arginine content. A summary of all samples and the respective tryptic peptides that have been robustly identified for TDP-43 with a confidence score of -10lgP above the filter threshold are given in table 3.3..

Table 3.3. Detection of TDP-43 peptides from in-solution digest of urea fractions

ID	TDP-43 coverage in %	peptide length	peptide location	-10lgP	RT	m/z	Mass
1 ALS	23	TSDLIVLGLPWK	N-terminal	59.7	66.79	671.3928	1340.77
		FGGNPGGFGNQGGFGNSR	C-terminal	75.24	42.18	863.8885	1725.761
1 Ctrl	29	TSDLIVLGLPWK	N-terminal	53.56	66.59	671.3928	1340.77
		FGGNPGGFGNQGGFGNSR	C-terminal	71.31	41.56	863.8885	1725.761
2 ALS	50	TSDLIVLGLPWK	N-terminal	62.09	66.29	671.3928	1340.77
		FGGNPGGFGNQGGFGNSR	C-terminal	81.1	40.92	863.8885	1725.761
		VTEDENDEPIEIPSEDDGTVLLSTVTAQFPGACGLR	N-terminal	44.45	75.74	1292.279	3873.81
2 Ctrl	40	TSDLIVLGLPWK	N-terminal	65.31	66.39	671.3928	1340.77
		FGGNPGGFGNQGGFGNSR	C-terminal	69.82	41.19	863.8885	1725.761
		VTEDENDEPIEIPSEDDGTVLLSTVTAQFPGACGLR	N-terminal	42.17	75.9	1292.279	3873.81

Mass spectrometry data of the in-solution trypsin digests of urea fractions from ALS and healthy control spinal cord tissue obtained in two separate LC-MS/MS runs (run 1 and 2). Shown is the percentage of the TDP-43 protein sequence covered by supporting peptides. Listed are unique peptides that have been robustly identified for TDP-43. All peptides show the expected trypsin cleavage sites after amino acids Arginine (R) and Lysine (K). The -10lgP for the peptides is above the filter -10lgP (>14) indicating high-confidence peptides. The retention time (RT), m/z and mass of each peptide are given.

Fig. 3.4. Serial fractionation of ALS *post mortem* tissue enables the detection of TDP-43 by mass spectrometry

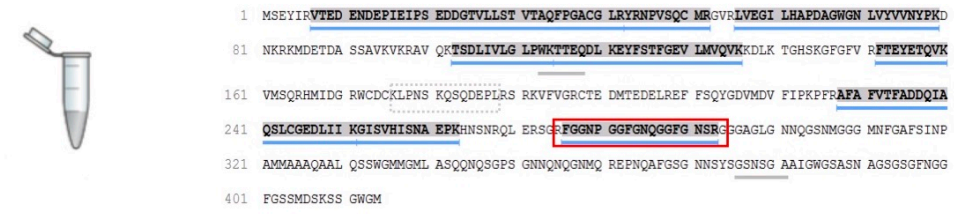


Fig. 3.4. Mass spectrometry of the in-solution trypsin digest of the urea fraction obtained from ALS spinal cord tissue detects TDP-43. Shown is the peptide coverage of TDP-43 analysed by PEAKS. The percentage of the protein sequence covered by supporting peptides is 50%. All peptides that are identified are unique for TDP-43 and show the expected trypsin cleavage sites at amino acids arginine (R) and lysin (K). The coverage is visualized by a colour bar. Each blue bar indicates an identified peptide sequence. Red boxes indicate example peptides that were reliable detected in subsequent LC-MS/MS runs and also used for heavy isotope-labelled peptide synthesis.

3.2.2.3. TDP-43 is detected in the disease-specific low molecular weight fractions

After human *post mortem* spinal cord tissue from ALS patients underwent serial fractionation the soluble protein fractions (LS and TX), the sarkosyl-soluble (Sark) and the sarkosyl-insoluble urea-soluble fractions (urea) were separated by electrophoresis on 10% high resolution gels. All four fractions were immunoblotted, while two lanes of the gel with 100µl urea fraction each were separated from the gel prior to membrane transfer and prepared for silver staining. Using a C-terminal specific TDP-43 antibody (green) the full-length TDP-43 at 48kDa and smaller TDP-43 fragments at 23kDa and 28kDa were detected in the sarkosyl and more pronounced in the urea fraction, but not in the soluble protein fractions (Fig. 3.5. A). This suggests the increased detection of TDP-43 and truncated TDP-43 fragments in insoluble protein fractions from tissue where TDP-43 pathology is present. The characteristic pathological pattern was further confirmed by a phosphorylation-specific TDP-43 antibody, which detected full-length and truncated TDP-43 bands (red) in sarkosyl and more pronounced in the urea fraction. This immunopattern was used as a reference to excise the corresponding low molecular weight TDP-43 bands of the silver stained urea fractions for in-gel digestion (Fig. 3.5. B). However instead of excising only the 23 and 26-28kDa bands an additional band at 25kDa was excised. The digestion of gel bands was done with chymotrypsin a protease that sufficiently cleaves the C-terminal region of TDP-43. By mass spectrometry TDP-43 was detected in the 23kDa and 26-28kDa low molecular weight bands. TDP-43 was not detected in the 25kDa band. In addition to TDP-43, more than 500 other proteins were detected from all in-gel digested bands by mass spectrometry. The detection and peptide coverage of TDP-43 were lower compared to in-solution samples suggesting an incomplete recovery of TDP-43 from silver stains (table 3.4.).

Fig. 3.5. TDP-43 is detected in the disease-specific low molecular weight TDP-43 fractions

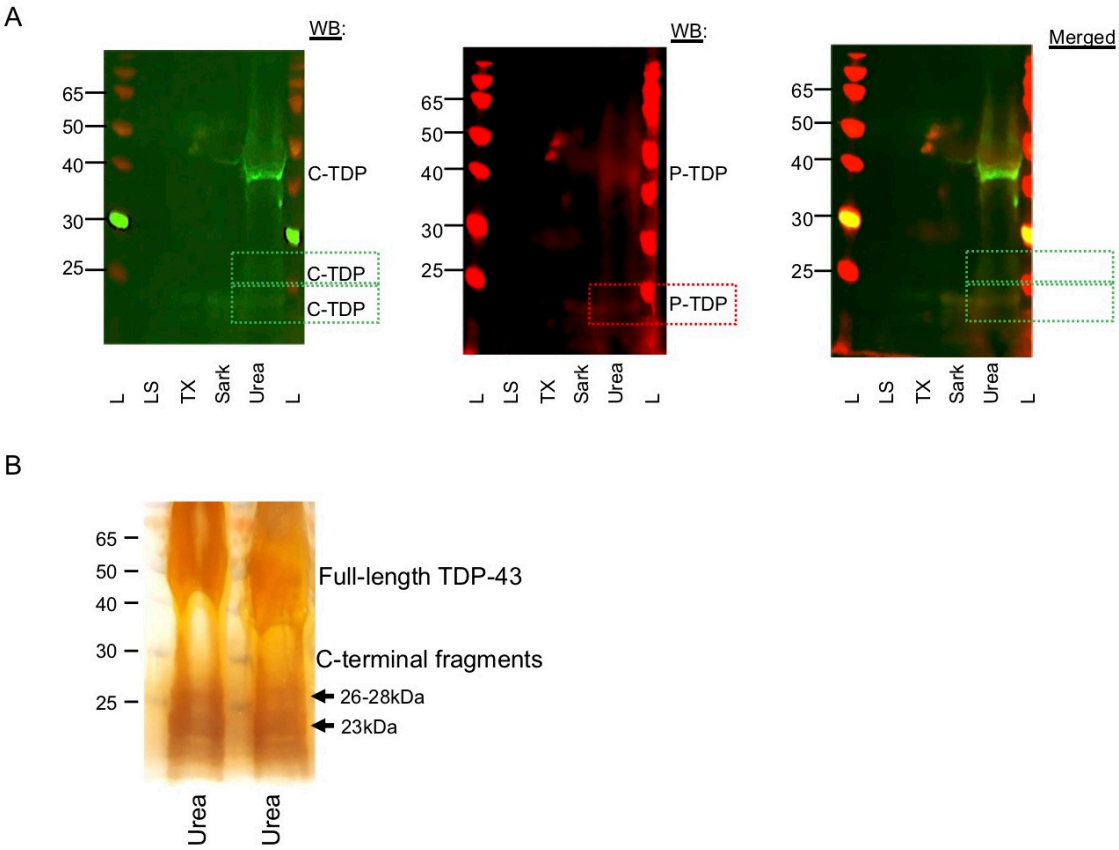


Fig. 3.5. Immunoblots and silver stains of soluble and insoluble protein fractions from ALS spinal cord tissue. PageRuler prestain ladder (L) on 10% gels. **A** Immunoblotting with a C-terminus specific TDP-43 antibody (C-TDP, green) shows increased detection of full-length TDP-43 at 48kDa and low molecular weight TDP-43 C-terminal fragments at 23 and 28kDa from soluble (LS and TX) to insoluble protein fractions (sarkosyl and Urea). A slightly higher immunoreaction is observed for phosphorylated full-length TDP-43 at 50kDa (P-TDP, red) and TDP-43 fragments. The overlay of C-terminal TDP-43 and phosphorylated TDP-43 suggests an enrichment of both pathological TDP-43 forms in urea fractions. **B** Corresponding silver stain of the immunoblot for in-gel digestion of the low molecular TDP-43 fragments (arrows) and LC-MS/MS for detection of TDP-43 peptides. Semi-specific peptides were discovered from 23kDa and 26-28kDa bands, suggesting endogenous truncation sites. Boxes indicate C-terminal low molecular weight bands used for in-gel digestion.

Table 3.4. Detection of semi-specific TDP-43 peptides from in-gel digest of urea fractions

mol. weight band (kDa)	TDP-43 coverage in %	Peptide length	Peptide location	-10lgP	RT	m/z	Mass
23	30	VQVKKDLKTGHSKGF	N-terminal	52.6	22.39	418.7	1670.9
23		RGVRLVEGILHAPDAGWGNLVY	N-terminal	43.6	56.46	598.8	2391.3
23		AFVTFADDQIAQSLCGEDLIIKGISVH	C-terminal	27.5	69.6	983.2	2946.5
26-28	10	SNRQLERSGRF	C-terminal	30.5	23.09	450.6	1348.7
26-28		ISNAEPKHNSNRQLERSGRF	C-terminal	15.53	22.8	585.8	2339.2

Mass spectrometry data of the in-gel chymotrypsin digests of urea fractions from ALS spinal cord tissue. Shown is the percentage of the TDP-43 protein sequence covered by supporting peptides. Listed are unique semi-specific peptides that have been robustly identified for TDP-43. All peptides show the expected chymotrypsin cleavage site after amino acids phenylalanine (F), tryptophan (W), and tyrosine (Y) and one nonspecific cleavage site suggesting truncation. The -10lgP for the peptides is above the filter -10lgP (>14) indicating high-confidence peptides. The retention time (RT), m/z and mass of each peptide are given.

3.2.2.4. Mass spectrometry has the potential to detect truncation of TDP-43 fragments by semi-specific peptide identification

TDP-43 was detected from in-gel digestions of TDP-43 low molecular weight bands as described above. The low molecular weight TDP-43 fragments were recognized by a C-terminus specific antibody (aa256-296) arguing for a N-terminal truncation with remaining C-terminal fragments. Mass spectrometry was now used to identify chymotrypsin semi-specific peptides for the potential identification of a truncation site. This was done by including peptides with one nonspecific cleavage site (semi-specific peptides) in the database search. In-gel digests from two different molecular weight bands ranging from 23 to 28kDa have led to the identification of five different TDP-43 semi-specific peptides (Fig. 3.5. B). Four of the semi-specific peptides had N-terminal nonspecific cleavage sites. Two of the N-terminal nonspecific cleaved peptides were located more towards the N-terminal of TDP-43 (around aa100), two N-terminal and one C-terminal nonspecific cleaved peptides were located towards the more C-terminal end of TDP-43 (from aa200 onwards). The assumption is that nonspecific cleavage has occurred prior to enzymatic digestion and therefore reflects pathologic truncation. The accumulation of semi-specific peptides towards the C-terminal end of TDP-43 could indicate a susceptible region of TDP-43 for truncation. Interestingly this region contains the C-terminal antibody recognition sequence. The calculated molecular weight of TDP-43 fragments derived from truncation result in an approximate 28kDa N-terminal fragment and 18kDa C-terminal fragment.

3.3. Conclusion

Previous studies measuring TDP-43 in CSF and serum using antibody-based methods have revealed inconsistent results due to the non-specific binding of antibodies to full-length and pathologically altered TDP-43 (Steinacker et al., 2008; Feneberg et al., 2014). This Chapter shows that TDP-43 from biofluids cannot be detected by affinity-enrichment mass spectrometry using antibodies that are commercially available. To overcome this problem, a similar approach to Kametani et al. has been applied to demonstrate that TDP-43 from brain tissue can be detected by mass spectrometry (Kametani *et al.*, 2016). This led to the discovery of new disease-relevant TDP-43 peptides that can now be used for further validation and quantification by targeted proteomics.

This study demonstrates that the use of commercially available antibodies to enrich TDP-43 from biofluids is limited and not sufficient for proteomic detection. In line with multiple previous studies that have tried to use these antibodies to detect TDP-43 in biofluids from ALS (Noto *et al.*, 2011; Suarez-Calvet *et al.*, 2014; Kuiperij *et al.*, 2017), the detection of TDP-43 was variable, the pathological signature cannot be recapitulated and the antibodies interfered with albumin and immunoglobulins (Steinacker *et al.*, 2008; Feneberg *et al.*, 2014).

However, the direct enrichment of pathological TDP-43 from ALS brains and spinal cords by a well-established biochemical fractionation is a reliable method to identify pathological TDP-43 without the use of antibodies (Neumann *et al.*, 2006). Our results support the findings from other proteomic studies that used FTLD, but also ALS *post mortem* brain tissue, that TDP-43 can be detected in the insoluble protein urea fraction (Kametani *et al.*, 2016). Further this chapter recapitulates that disease-specific peptides with nonspecific cleavage sites can be identified from low molecular weight TDP-43 fragments extracted

from ALS tissue (Kametani *et al.*, 2016). In this chapter I have identified new specific and semi-specific peptides with an indication for pathological truncation, which have not been described before.

Interestingly, one new truncation site lies within the recognition region of the C-terminal antibody used for detection of the truncated C-terminal fragment at 28kDa by in-gel digestion. This can suggest an off-target effect of the antibody. It can also suggest homodimerization of different C-Terminal fragments, which can be post-translationally modified, as the calculated molecular weight of the C-terminal fragment generated by the new truncation is only 18kDa (Neumann *et al.*, 2009; Prasad *et al.*, 2018). The latter is supported by the detection of other truncation site-specific peptides within the same in-gel molecular weight range.

However, if the truncation site-specific peptides are artefacts generated by mis-cleavage of the enzyme used for digestion cannot be excluded from bottom-up mass spectrometry (Chiva *et al.*, 2014) and requires further validation to proof disease-specificity. To investigate if semi-specific peptides are representative of C-terminal fragments of TDP-43 and if this leads to a decrease of the N-terminal end of TDP- 43 due to degradation has to be further validated. The divergence of proteomics findings with immunoblotting is also suggestive that the resolution of the latter might be less accurate compared to mass spectrometry that is able to detect proteins at femtomolar concentrations. That in mind the specificity of the truncation site-specific peptides needs to be proven by an independent method and compared across different diagnostic groups where pathology is present or absent. Secondly, protein degradation and truncation occur naturally, therefore absolute quantification of truncation site-specific peptides and their pathological relevance in disease compared to healthy controls is necessary.

Chapter 4: Quantification of TDP-43 peptides and its pathological forms in ALS

4.1. Introduction and Aims

The discovery of TDP-43 from ALS post mortem tissue after enriching pathologically altered TDP-43 by mass spectrometry enabled the identification of peptides that are unique to TDP-43. Studying in-gel digests of low molecular TDP-43 bands has led to the identification of semi-specific peptides that are able to indicate pathological truncation sites. A previous study demonstrated similar results by detecting peptides indicative of truncation sites, however without validation of the findings in a larger cohort or by an independent method (Kametani *et al.*, 2016). To test, if the peptides detected by the previous study and the peptides from my own discovery experiments of Chapter 3 are specific to ALS and to exclude technical artefacts, an independent method was applied to quantify peptides across different diagnostic groups. A method for absolute quantification of proteins is PRM, which is a targeted proteomic approach. This method utilises heavy isotope-labelled peptides (heavy peptides) of a known concentration to quantify the corresponding endogenous peptides (light peptides).

It has been recently described that TDP-43 pathology was present in approximately 20% of a *post mortem* cohort of individuals with clinical Alzheimer's dementia (Nelson *et al.*, 2019). Therefore, it is important to quantify the most promising peptides across a range of neurodegenerative diseases and healthy controls. By quantitation of peptides covering the TDP-43 sequence and truncation sites the detection of *decreased* full-length, but *increased* truncated TDP-43 would be expected in insoluble protein fractions extracted from *post mortem* tissue with TDP-43 pathology (Laferriere *et al.*, 2019). However, it has been described that cleavage is necessary to maintain TDP-43 homeostasis, which suggests a

degree of TDP-43 degradation products such as TDP-43 fragments also in physiological conditions (Li *et al.*, 2015).

The aims of the work described in this Chapter are:

1. To establish heavy isotope-labelled peptides for the quantification of TDP-43 by PRM
2. To quantify endogenous peptides of TDP-43 in urea fractions extracted from *post mortem* tissue across diagnostic groups

4.2. Results

4.2.1. Construction of heavy isotope-labelled TDP-43 peptides for the quantification of TDP-43

4.2.1.2. Biochemical characteristics of heavy isotope-labelled TDP-43 peptides

TDP-43 peptide sequences were synthesized with a heavy isotope label for absolute quantification of corresponding endogenous TDP-43 peptides (light peptides) by targeted LC-MS/MS. Heavy isotope labels were added to amino acids arginine (R) and lysine (K), or glycine (G), when R and K were absent. All heavy peptides were either fully tryptic, or chymotryptic, or contained one N- or C-terminal cleavage site that was nonspecific to trypsin or chymotrypsin (semi-specific heavy peptides), enabling the detection of potential endogenous truncation sites. In total 19 heavy peptides were synthesized according to the sequences of endogenous peptides that were detected by mass spectrometry in Chapter 3, those that have been previously published or were *in silico* constructed (Table 4.1., ***sequence redacted for confidentiality**).

Table 4.1. Characteristics of all heavy isotope-labelled peptides (on the next page)

Peptide Origin	Protease	Digestion	Sequence	Modification	Length	Labelled Residue	Detected	Light	Heavy	L:H
N-Terminus in silico	Trypsin	Specific	MSEYI(R)		6	Arginine (R), +10Da	y	n	y	
N-Terminus in silico	Trypsin	Specific	MSEYI(R)	Methylation M1	6	Arginine (R), +10Da	y	n	y	
N-Terminus in silico	Trypsin	Specific	NPVSQCM(R)		8	Arginine (R), +10Da	n	n	n	
N-Terminus in silico	Trypsin	Specific	NPVSQCM(R)	Methylation M7	8	Arginine (R), +10Da	n	n	n	
N-Terminus	Trypsin	Specific	LVEGILHAPDAGWGNLVYVVNYP(K)		24	Lysine (K), +8Da	n	x	x	
N-Terminus	Trypsin	Specific	TSDLIVLGLPW(K)		12	Lysine (K), +8Da	y	y	y	8.19
C-Terminus in silico	Trypsin	Specific	SS(G)WGM	Methylation M6	6	Glycine (G), +3Da	y	n	n	
Kametani et al.	Trypsin	N-Terminal Nonspecific	EFFSQYGDVMDVFIPKPF(R)		19	Arginine (R), +10Da	n	x	x	
Kametani et al.	Trypsin	N-Terminal Nonspecific	GDVMDVFIPKPF(R)		13	Lysine (K), +8Da	y	n	y	
Kametani et al.	Trypsin	N-Terminal Nonspecific	GDVMDVFIPKPF(R)	Methylation M4	13	Lysine (K), +8Da	y	n	n	
Kametani et al.	Trypsin	N-Terminal Nonspecific	FGGNPGGFGNQGGFGNS(R)		18	Arginine (R), +10Da	y	y	y	0.29
Kametani et al.	Trypsin	C-Terminal Nonspecific	FGGNP(G)GFGNQGGFGN		16	Glycine (G), +3Da	y	n	y	
Kametani et al.	Trypsin	N-Terminal Nonspecific	PGGFGNQGGFGNS(R)		14	Arginine (R), +10Da	y	n	y	
N-Terminus	Chymotrypsin	Specific	I(R)VTEDENDEPIEIPSEDDGTVL		23	Arginine (R), +10Da	y	y	y	0.68
N-Terminus in silico	Chymotrypsin	Specific	(R)NPVSQCMRGVRL		13	Arginine (R), +10Da	n	x	x	
N-Terminus in silico	Chymotrypsin	Specific	HAPDA(G)W		7	Glycine (G), +3Da	y	n	y	
C-Terminus in silico	Chymotrypsin	Specific	SGSNS(G)AAIGW		11	Glycine (G), +3Da	y	y	y	0.10
C-Terminus in silico	Chymotrypsin	Specific	GSASNA(G)SGSGF		12	Glycine (G), +3Da	y	n	n	
C-Terminus in silico	Chymotrypsin	Specific	SSMDSKSS(G)W		10	Glycine (G), +3Da	y	n	y	
C-Terminus in silico	Chymotrypsin	Specific	SSMDSKSS(G)W	Methylation M3	10	Glycine (G), +3Da	y	n	y	
Kametani et al.	Chymotrypsin	N-Terminal Nonspecific	CDC(K)LPNSKQSQDEPL		16	Lysine (K), +8Da	n	x	x	
Kametani et al.	Chymotrypsin	N-Terminal Nonspecific	(K)LPNSKQSQDEPL		13	Lysine (K), +8Da	y	n	y	
N-Terminus	Chymotrypsin	N-Terminal Nonspecific	SNRQLERSG(R)F		11	Lysine (K), +8Da	y	y	y	0.09

Their origin, biochemical characteristics, detection of the heavy peptide and corresponding endogenous light peptide and signal intensities for quantification (light (L) to heavy (H) peptide ratio) were determined by mass spectrometry in urea fraction test matrices. The signal of each heavy peptide was determined at a concentration of 10fmol. Eleven of the initial 19 heavy peptides were not detected by mass spectrometry and removed from the final peptide list. Nine heavy peptides were detected and quantifiable by PRM (Table 4.2.). Figure 4.1. B shows the retention times and intensities of one representative chymotryptic and tryptic peptide measured in urea fractions. All heavy peptides and retention times are given in Table 4.2..

Table 4.2. Characteristics of final heavy isotope-labelled peptide selection for absolute quantification

Peptide Origin	Protease	Digestion pattern	Sequence or length of peptide	Labelled Residue	RT (min)
N-Terminus	Trypsin	Specific	TSDLIVLGLPW(K)	Lysine (K), +8Da	54
C-Terminus ***in silico***	Trypsin	Specific	SS(G)WGM	Glycine (G), +3Da	38.5
Kametani ***et al.***	Trypsin	N-Terminal Nonspecific	FGGNPGGFGNQGGFGNS(R)	Arginine (R), +10Da	35
Kametani ***et al.***	Trypsin	C-Terminal Nonspecific	FGGNP(G)GFGNQGGFGN	Glycine (G), +3Da	42
Kametani ***et al.***	Trypsin	N-Terminal Nonspecific	PGGFGNQGGFGNS(R)	Arginine (R), +10Da	30
N-Terminus	Chymotrypsin	Specific	I(R)VTEDENDEPIEIPSEDDG TVL	Arginine (R), +10Da	47.5
C-Terminus ***in silico***	Chymotrypsin	Specific	SGSNS(G)AAIGW	Glycine (G), +3Da	40.5
Kametani ***et al.***	Chymotrypsin	N-Terminal Nonspecific	(K)LPNSKQSQDEPL	Lysine (K), +8Da	25.5
C-Terminus Truncation	Chymotrypsin	N-Terminal Nonspecific	SNRQLERSG(R)F	Lysine (K), +8Da	22.5

Abbreviation: RT, retention time in minutes.

Fig. 4.1. Characteristics of heavy isotope-labelled TDP-43 peptides

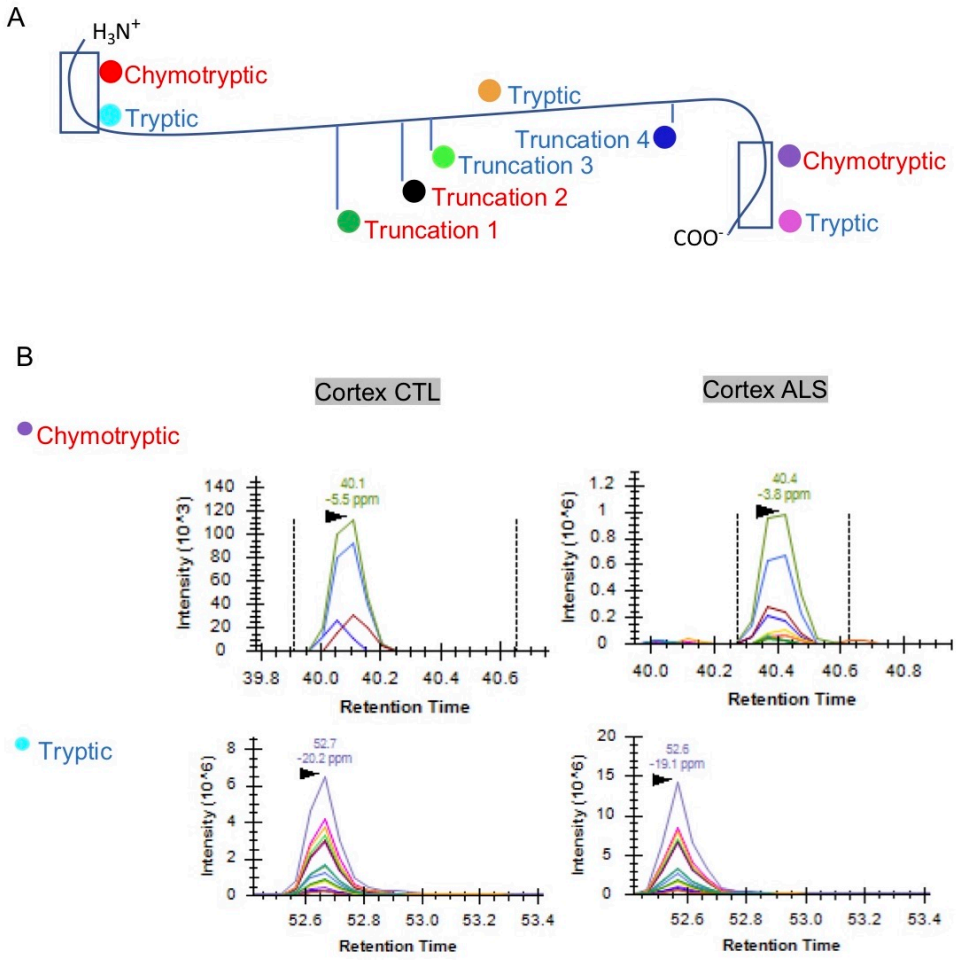


Fig. 4.1. A Schematic of the distribution of the final heavy isotope-labelled peptides within the full sequence of TDP-43 used for absolute quantification by parallel reaction monitoring. Showing fully chymotryptic or tryptic peptides located at the C-terminal and N-terminal end of TDP-43 as well as one middle tryptic peptide. In addition semi-tryptic and semi-chymotryptic peptides with an N- (Truncation 1, 2 and 3) or C-terminal (Truncation 4) nonspecific cleavage site, suggesting truncation sites, are shown. **B** Parallel reaction monitoring of a chymotryptic or tryptic digested urea fraction from healthy control (CTL) or ALS cortex tissue. Data processing was conducted using the software package Skyline. The graphs show peak intensities and areas under the curve for each heavy and light fragment ion of the indicated peptide at a defined retention time. Area under the curves were exported and used to calculate the absolute concentrations of endogenous light peptides per sample.

4.2.1.1. Heavy isotope-labelled TDP-43 peptides for the quantification of TDP-43 and pathological truncation sites

Nine heavy peptides fulfilled biochemical characteristic for signal detection and quantification (Table 4.2.). Only one peptide contained methionine (M) and resulted in a split signal due to oxidation and was therefore restricted in reliability, though included for final quantification. The final heavy peptides within the full sequence of TDP-43 used for absolute quantification comprised five *tryptic* heavy peptides with one N-terminal peptide detected in Chapter 3, one in silico constructed C-terminal peptide, two semi-tryptic peptides each consisting of a nonspecific and tryptic cleavage site and one tryptic heavy peptide covering both semi-tryptic peptides (Fig. 4.1. A). The two semi-tryptic peptides and the tryptic heavy peptide covering both semi-tryptic peptides were previously described by Kametani *et al.* (Kametani *et al.*, 2016). The first semi-tryptic peptide had a N-terminal nonspecific cleavage site at aa279 (Truncation 3), the second semi-tryptic peptide had a C-terminal nonspecific cleavage site at aa291 (Truncation 4).

In order to enhance the detection of the C-terminal end of TDP-43, *chymotryptic* heavy peptides were used in addition as many of them were located towards the C-terminal end of TDP-43. The first chymotryptic heavy peptide covered a region of the very N-terminal end of TDP-43 and was detected in Chapter 3. The other chymotryptic heavy peptide was located at the C-terminal end of TDP-43 and constructed *in silico*. Two heavy peptides were semi-chymotryptic. One with a N-terminal nonspecific cleavage site at aa175 (Truncation 1) previously described by Kametani *et al*. (Kametani *et al.*, 2016). The second semi-chymotryptic heavy peptide had a N-terminal nonspecific cleavage (Truncation 2) and was detected in Chapter 3.

4.2.2. Quantification of endogenous TDP-43 peptides by targeted mass spectrometry

TDP-43 peptide concentrations were determined relative to heavy peptides in urea fractions of ALS *post mortem* tissue with confirmed TDP-43 pathology (n=16), Parkinson's Disease (PD, n=8), Alzheimer's Disease (AD, n=8) and healthy controls (CTL, n=8) (Table 4.3.). The ALS cases included patients that were enrolled in a longitudinal biomarker collection and therefore enable the unique possibility of comparing the tissue data in matched *in vivo* biofluids. These cases were clinically well-characterised, but included more male than female cases. Some ALS cases were primarily chosen, because of the more severe TDP-43 pathology, but not all clinical data (progression rate, ALSFRS and side of onset) were available. The median age of the healthy control group was 65.9, of the PD group 76.9, and the ALS group 65.6 years. The AD group was significantly older with a mean age of 84.3 years compared to all other groups ($p<0.001$). Two PD cases had also neuropathologically confirmed Lewy-Body dementia.

Table 4.3. Clinical data and tissue regions of ALS *post mortem* tissue

Type	sex	Age (yrs)	PM time (hrs)	Duration (days)	PR	ALSFRS	Onset	Tissue Regions
ALS	m	57	48	1085	0.45	29	RLL	Motor cortex A1P1
ALS	f	64	48	591	1.6	21	Bulbar	Motor cortex
ALS	m	64	24	629	1.76	18	LUL	Motor cortex A1P1
ALS	m	59	96	1840	0.72	19	Bulbar	Frontal cortex
ALS	m	76	48	1312	0.68	20	LUL	Motor cortex
ALS	m	64	n/a	1478	0.55	21	LLL	Frontal cortex
ALS	m	62	72	1861	0.5	17	LLL	Frontal cortex
ALS	m	52	46	389			na	Motor cortex M1S1
ALS	f	76	na	183			na	Motor cortex M1S1
ALS	f	71	57	438			Bulbar	Motor cortex M1S1
ALS	f	49	11	849			Bulbar	Motor cortex M1S1
ALS	m	59	24	1058			na	Motor cortex M1S1
ALS	m	59	na	na			na	Motor cortex M1S1
ALS	f	86	42	na			na	Motor cortex M1S1
ALS	m	69	25	3285			na	Motor cortex M1S1

Abbreviations: m, male; f, female; yrs, years; PR, progression rate; RLL, right lower limb; LLL, left lower limb; RUL, right upper limb; LUL, left upper limb; PM, *post mortem.*

4.2.2.1. Pre-analytical screening of samples and digest sufficiency

Pre-analytical screening prior to TDP-43 quantification by PRM included three steps of technical controls. Firstly, silver stains of all soluble (TX) and final insoluble (urea) protein fractions were performed at equal volumes to verify the recovery of protein prior to digestion. Secondly, the digest efficiency was tested by plotting the peptide ion elution using mass spectrometry and peptide concentrations were measured after digestion.

Silver stains were used for visualisation of the total protein amount recovered per sample. The total amount of proteins determined by silver staining varied between samples. A decrease in total protein was observed from the soluble (TX) to the insoluble (urea) protein fractions. However, in urea fractions a more condensed staining of proteins of the same size was observed indicating specific enrichment of a protein population specific to the insoluble protein fraction (Fig. 4.2. A). Digest efficiency was determined from a pool of all trypsin and chymotrypsin digested samples. The total ion chromatogram for trypsin and chymotrypsin digested samples shows the maximal distribution of ion abundances between 25 and 75 minutes, when peptides elute. Larger fragments that derive from incomplete digestion would be expected to elute from the electrospray column after approximately 75 minutes (Fig. 4.2. B). The peptide concentrations for each urea digested sample ranged from 0.5 - 14μg/μl for cortex samples (Fig. 4.2. C). The differences in peptide concentrations were expected as the amount of insoluble protein recovered by fractionation prior to digestion varies between samples as also demonstrated by silver stains.

Fig. 4.2. Pre-analytical screening and digest sufficiency for parallel reaction monitoring

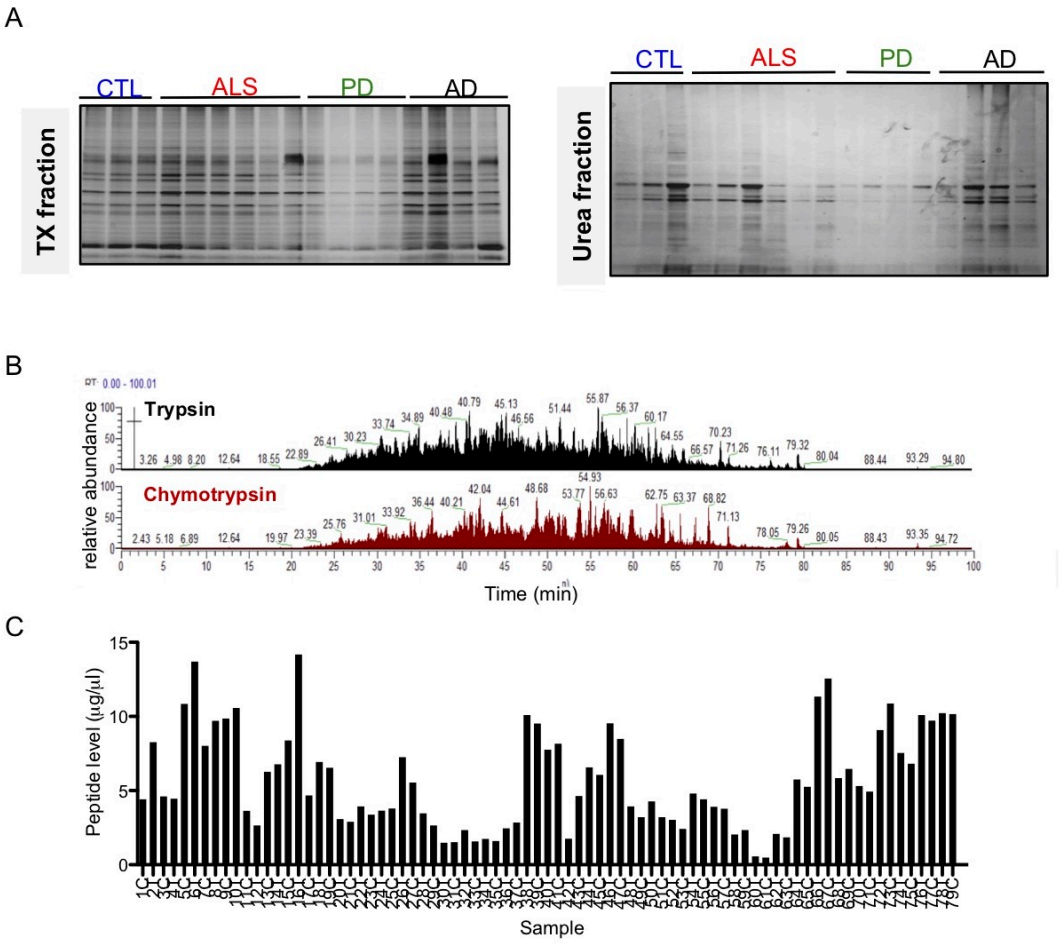
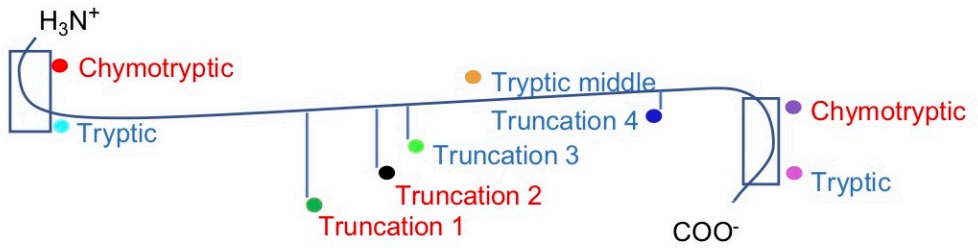


Fig. 4.2. A Representative silver stains demonstrate the total protein amount of 0.5µl of the soluble (TX) and 1µl of the insoluble (urea) protein fractions extracted from cortex *post mortem* tissue of CTL, ALS, PD and AD patients used for PRM analysis. **B** Total ion chromatograms of a pool from all trypsin (black) and chymotrypsin (red) digested cortex urea samples show relative ion abundances of a correct peptide spectrum between 25 and 75 minutes. **C** Peptide levels of all cortex urea chymotrypsin (C) or trypsin (T) digests 1-79 as run on mass spectrometer for PRM.

4.2.2.2. Quantification of endogenous TDP-43 peptides in tryptic and chymotryptic digested urea fractions across diagnostic groups

Quantification of endogenous TDP-43 peptides across diagnostic groups was done by comparing the log2 ratios of the TDP-43 light to TDP-43 heavy peptides, resulting in absolute abundances per diagnostic group. However, not all of the chymotryptic or tryptic peptides were specific to the corresponding protease, which is an indicator of miss quantification of light peptides. The chymotryptic peptide Truncation 1 was identified in trypsin digested samples. The tryptic peptide Truncation 4 and Truncation 3 were identified in the chymotryptic digested samples (Fig 4.3. A). The chromatographic point shift, an indicator of how much the light differs from the heavy peptide signal, was high for the tryptic peptide Truncation 4 limiting its quantification (Fig. 4.3. B). The high divergence of the Truncation 4 and middle tryptic (orange) light peptide to the corresponding heavy peptide signal with a correlation coefficient r <0.5 restricted the signal detection and reliable quantification (Fig 4.3. C). The chymotryptic peptides C-Terminus, Truncation 2 and N-Terminus fulfilled all criteria for specificity including the correct identification in chymotrypsin digested samples, small chromatographic shifts and zero divergence from the heavy-labelled peptides, which made them the strongest candidates for quantification.

Fig. 4.3. Quantification of TDP-43 peptides



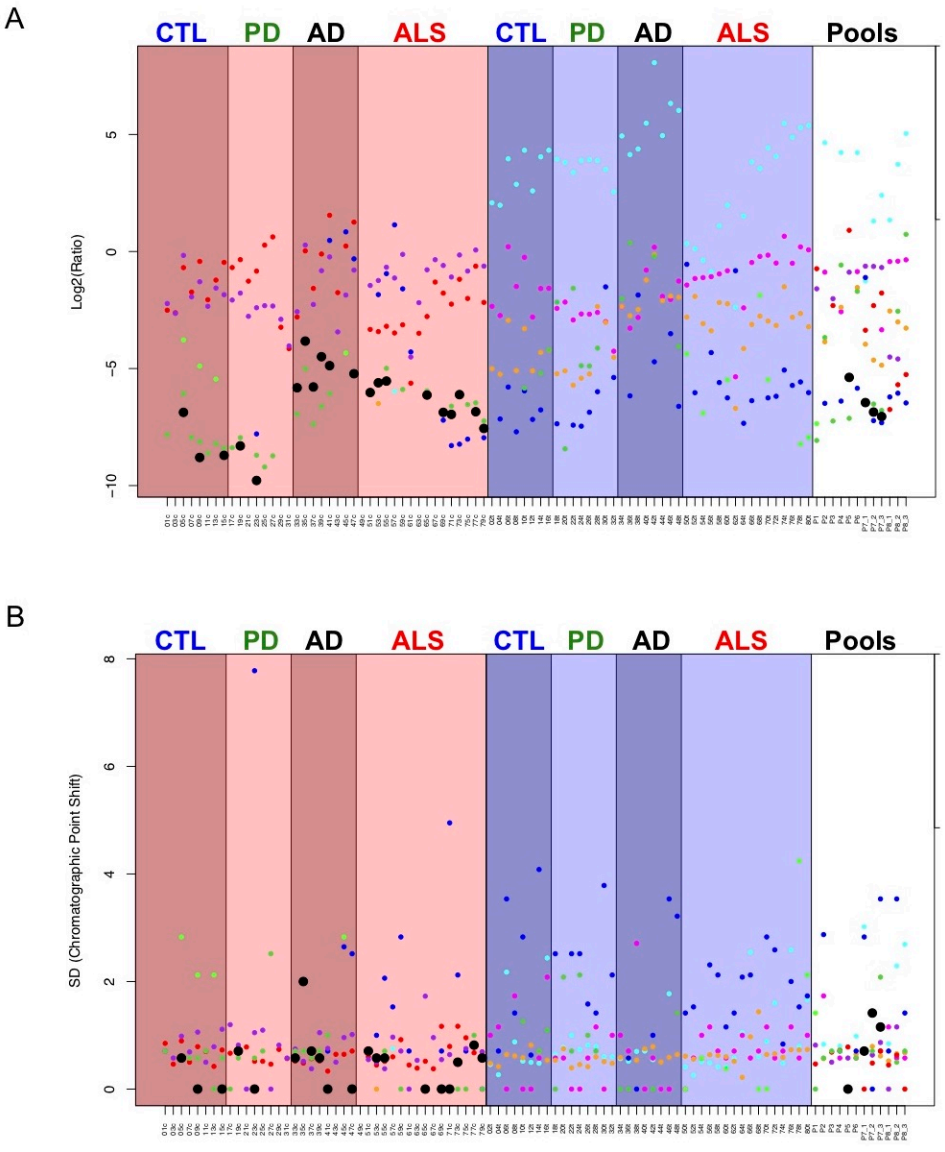


Fig. 4.3. to be continued on next page

Fig. 4.3. continued. Quantification of TDP-43 peptides

C

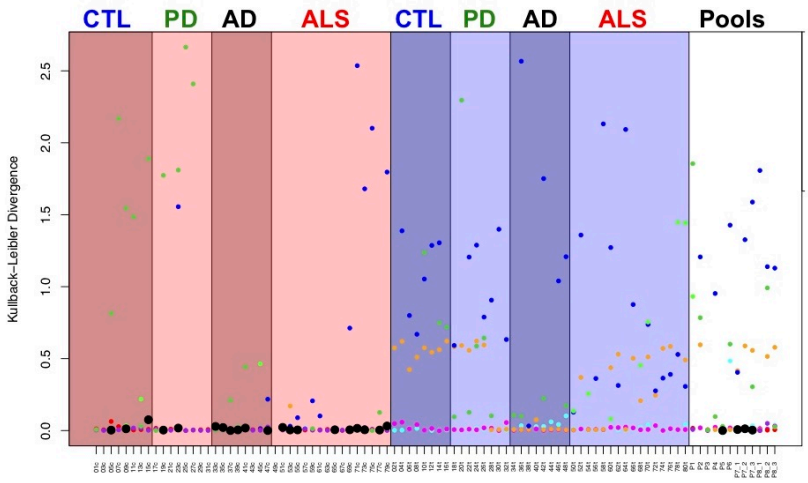


Fig. 4.3. Endogenous TDP-43 peptides are represented by colour coding as indicated in the schematic. The graphs show cortex samples on the x-axis ordered by protease and diagnostic groups (red, chymotrypsin digested samples; blue, trypsin digested samples). At the end of each graph sample pools consisting of 10 samples of each diagnostic group are shown for an additional positive control of peptide detection. **A** The first graph shows the log2 abundance of the light (endogenous) peptide to heavy peptide ratio. The black dots represent the newly detected truncation site-specific peptide, which is highly abundant in ALS and AD samples. **B** The chromatographic time shift of the light peptide from the heavy peptide is expected to be minimal for good quantification. **C** The Kullback-Leibler divergence is an indicator of how much the light peptide differs from the expected heavy peptide signal. Peptides with low values in B and C have a clear signal for good quantification by PRM.

4.2.3. The C-terminal end of TDP-43 is increased in ALS urea fractions

4.2.3.1. Absolute quantification shows a disease-specific peptide signature in ALS

Absolute quantification was performed by measuring endogenous TDP-43 peptides relative to heavy peptides (log10 of the light peptide/heavy peptide ratio) in urea fractions extracted from ALS, AD, PD and CTL tissue (Fig. 4.4. A). The most reliable quantification was retrieved from the chymotryptic peptides (Fig. 4.4. B). Compared to ALS, quantification showed a significant decrease of the chymotryptic N-terminal peptide in ALS compared to ALS ($p=0.001$). The chymotryptic C-terminal peptide was increased in ALS compared to PD ($p=0.004$). I then calculated the ratio of the chymotryptic C-terminal peptide to N-terminal peptide to detect, if the C-terminal end of TDP-43 is enriched in ALS urea fractions. The C- to N-terminal peptide ratio was significantly increased in ALS compared to CTL, PD and AD ($p<0.0001$, respectively). This suggests that the N-terminal peptide is less abundant compared to the relative level of the C-terminal peptide in urea fractions of ALS patients, suggesting C-terminal fragment enrichment and possible degradation of the cleaved N-terminal end. In line with this finding the truncation site-specific peptide 1 (Truncation 1) was increased in ALS compared to PD ($p<0.0001$) and CTL ($p=0.0008$). Also, Truncation 1 was restricted in reliability as indicated in Chapter 4.2.2.2.. The truncation site-specific peptide 2 (Truncation 2) was increased in ALS compared to PD ($p=0.002$) and CTL ($p=0.02$). Surprisingly, both truncation site-specific peptides were also increased in AD, with a significant increase in AD compared to ALS for truncation peptide 2 ($p=0.01$). However, the C-terminal to N-terminal peptide ratio was unaltered in AD, which was different to what was observed in ALS, suggesting the presence of full-length TDP-43 in AD. The quantification of tryptic peptides was limited due to the lack of technical confidence assessed by the chromatographic shift and Kullback-Leibler divergence (see section 4.2.2.2.) and the

bias of oxidation of the amino acid Methionine from the C-terminal end peptide (Fig. 4.4. C).

When quantified the C-terminal tryptic peptide showed an increase in ALS compared to AD ($p=0.04$), PD ($p=0.006$) and CTL ($p=0.02$), confirming the increase towards the C-terminus of TDP-43. The truncation site peptide 4 (Truncation 4), the only peptide with a C-terminal truncation was unaltered between ALS an all other groups. The C-terminal end peptide was increased in ALS compared to PD ($p<0.002$). However, these results could be false positive and for further experiments the tryptic peptides will be excluded.

Fig. 4.4. Quantification of TDP-43 peptides in human post mortem cortex tissue

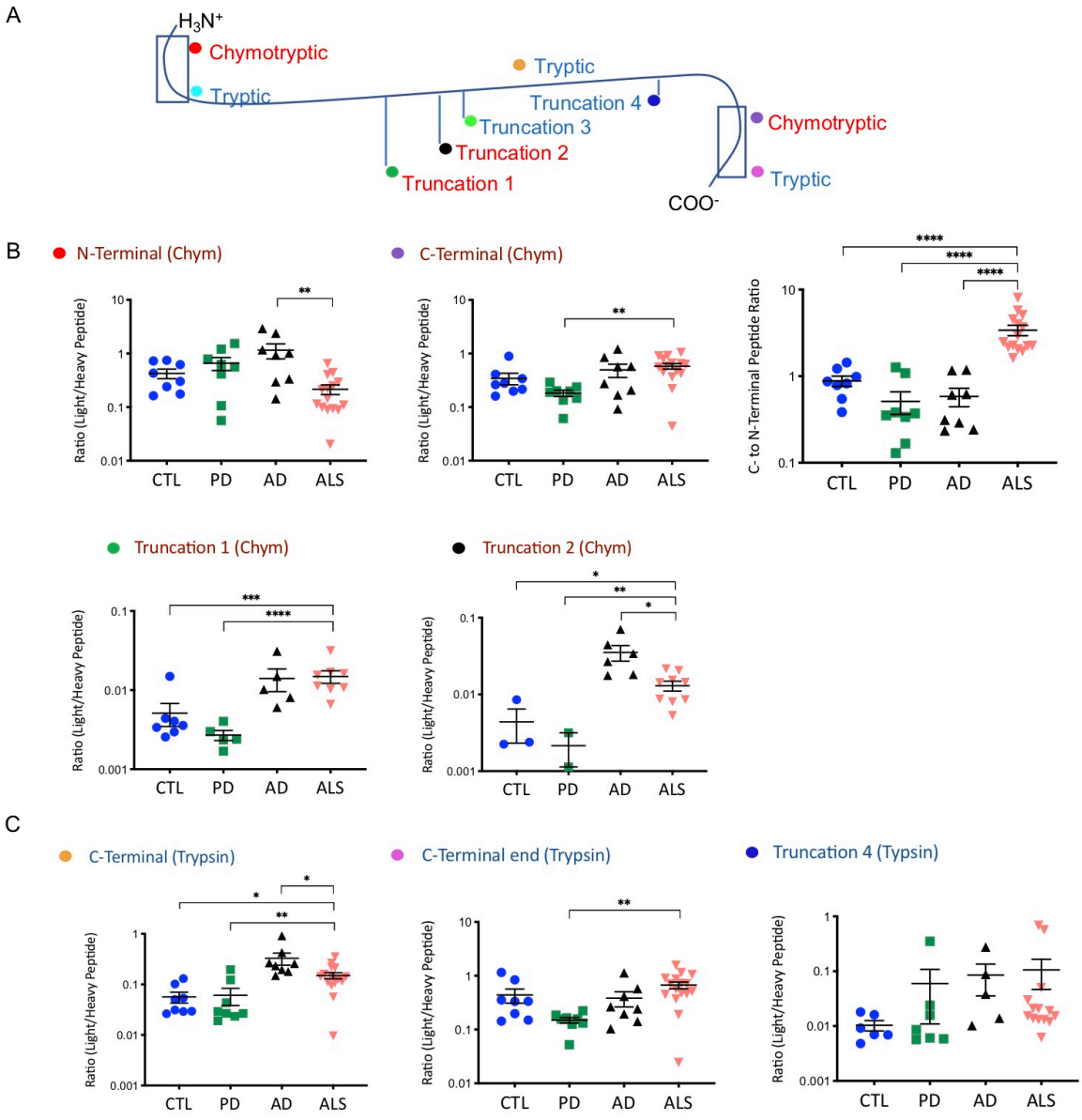


Fig. 4.4. Quantification of chymotryptic and tryptic TDP-43 peptides by parallel reaction monitoring. **A** Peptide localisation within the TDP-43 sequence is indicated by the schematic. **B and C** Quantification of individual peptides in urea fractions from 8 ALS cortex tissues compared to 8 CTL, 8 PD and 8 AD samples (1-way ANOVA Dunnett's multiple comparison). **B** Chymotryptic peptides: The N-terminal peptide is decreased in ALS compared to ALS ($p=0.001$). The C-terminal peptide is higher in ALS compared to PD ($p>0.004$). The calculated C-terminal to N-terminal peptide ratio is significantly increased in ALS compared to CTL, PD and AD ($p<0.0001$ respectively). Truncation 1 is increased in ALS compared to PD (both $p<0.0001$) and CTL ($p=0.0008$). Truncation 2 (detected in Chapter 3) is increased in ALS compared to PD ($p=0.002$) and CTL ($p=0.015$). Truncation 2 is decreased in ALS compared to AD ($p=0.01$).
C Tryptic peptides: The C-terminal peptide is increased in ALS compared to AD ($p=0.04$), PD ($p=0.006$) and CTL ($p=0.02$). The C-terminal end peptide is increased in ALS compared to PD ($p<0.002$). The Truncation 4 is unaltered between ALS and all other groups. Data are represented as mean±SEM.

4.2.3.2. The absolute amount of disease-specific TDP-43 peptides in ALS cortex tissue was higher compared to controls

The abundances of chymotryptic peptides were assessed. However, using absolute amounts without a recombinant protein as standard within the sample is inaccurate and only serves as an estimate. For the chymotryptic N-terminal peptide the mean values for CTL were 4.3±2.4, for PD 6.6±5.1, for AD 11.5±10.10 and for ALS 2.2±1.7. For the chymotryptic C-terminal peptide the mean values were for CTL 3.4±2.3, for PD 1.8±0.7, for AD 4.9±3.8, and for ALS 5.8±2.7. For the chymotryptic truncation peptide 1 (Truncation 1) the mean values (fmol) for CTL were 0.05±0.04 and for PD 0.03±0.01, while the mean values for AD were 0.14±0.1 and for ALS 0.15±0.08. For the chymotryptic truncation peptide 2 (Truncation 2) the mean values for CTL were 0.04±0.03 and for PD 0.02±0.01, while the mean values for AD were 0.35±0.2, and for ALS 0.13±0.06.

Considering that all samples were diluted 1:10 prior to PRM, conversion of truncation peptide 2 (Truncation 2) in fg (0.1fmol/µl = 130fg/µl) resulted in a mean value of 4.5fg for AD, 1.7fg for ALS compared to 0.26fg for PD and 0.53fg for CTL.

Fig. 4.5. Absolute amounts of TDP-43 peptides in human *post mortem* cortex tissue (fmol)

● Chymotryptic N-term

CTL	PD	AD	ALS
1.7567	6.2180	1.4369	
1.6289	7.8512	10.1956	0.9952
6.2048	4.1556	3.3521	0.9329
3.0079	5.5930	9.2840	1.0925
7.4571	12.0750	29.2213	0.8962
2.4009	15.4021	2.9603	1.1404
4.2908	1.0619	11.7479	0.2027
7.2408	0.5634	23.8586	0.8894
			1.4593
			4.0466
			2.9159
			2.1052
			4.3934
			2.4894
			6.4765
			2.2163

● Chymotryptic C-term

CTL	PD	AD	ALS
2.147	2.376	1.682	
1.601	2.917	12.089	3.658
8.917	1.468	2.084	4.237
2.614	1.891	5.671	6.280
4.082	2.011	8.517	4.561
1.975	1.990	0.925	9.185
3.386	1.343	2.757	0.440
2.786	0.611	5.774	2.198
			5.820
			7.843
			6.612
			4.696
			9.023
			5.604
			10.457
			6.487

● Truncation 1

CTL	PD	AD	ALS
0.044	0.030	0.081	
	0.040	0.310	
0.149		0.061	
0.041	0.024	0.102	0.315
0.036	0.017	0.149	0.168
0.026	0.024		
0.034			
0.030			
			0.161358
			0.1026662
			0.1545331
			0.107596
			0.1131486
			0.06640074

● Truncation 2

CTL	PD	AD	ALS
		0.17689814	
		0.70421669	0.15362091
0.08540208	0.03165064	0.18116765	0.20510032
		0.44386268	0.21573501
0.0224525	0.0113574	0.34034506	
0.02389684		0.26820364	
			0.1426138
			0.08542222
			0.080379
			0.14434377
			0.0869863
			0.05303604

Fig. 4.5. Shown are only the chymotryptic peptides. The absolute amount of each peptide was calculated by dividing the peptide ratio by the amount of heavy peptide injected (10fmol).

4.2.4. C-terminal fragments are increased in ALS urea fractions by immunoblotting

C-terminal TDP-43 fragments (CTF) have been shown to accumulate in the insoluble protein urea fraction of cortex tissue of patients with FTLD (Igaz *et al.*, 2008). Western blotting of the soluble proteins extracted by high-salt buffer (TX fraction) from the cortex of CTL, ALS, PD and AD patients confirmed the presence of full-length or disease-specific TDP-43 forms. When using an antibody that detects the C-Terminus of TDP-43, 35kDa and 25kDa low molecular weight bands were present in the cortex TX samples in addition to the 43kDa full-length TDP-43 form. A multiple band pattern was present in the control, ALS, PD and AD samples (Fig. 4.6. A). Given that low molecular weight bands have been previously suggested as associated with TDP-43 proteinopathy with C-terminal TDP-43 fragments, the ratio of the low molecular weight band intensities at 35kDa (CTF-35) or at 25kDa (CTF-25) over full-length TDP-43 (TDP-43 FL) at 45kDa intensities were calculated for all samples. In the soluble protein fraction the CTF-35/TDP-43 FL ratio was unaltered between ALS and CTL, PD or AD (all $p=0.9$). A slight increase in CTF-25/TDP-43 FL ratio was seen in the cortex of patients with AD and PD, but this was not significant (both ALS versus PD or AD $p=0.2$; ALS versus CTL $p=0.9$). Therefore, CTF-25 and CTF-35 do not seem to be associated with disease, when present in the soluble protein fraction. However, when similar experiments and quantifications were performed on the insoluble protein urea fractions, a significant increase in the level of CTF-25 over the level of full-length TDP-43 was observed in ALS compared to CTL ($p=0.03$), PD ($p=0.02$) and AD ($p=0.048$) (Fig. 4.6. B). The CTF-35 over the level of full-length TDP-43 was unaltered between ALS and CTL ($p=0.25$) or AD ($p=0.9$), but higher in ALS compared to PD ($p=0.03$). Together, these data show that mainly CTF-25 present in the insoluble protein fraction is associated with ALS with confirmed TDP-43 pathology.

Fig. 4.6. Quantification of C-terminal TDP-43 fragments in soluble and insoluble protein fractions

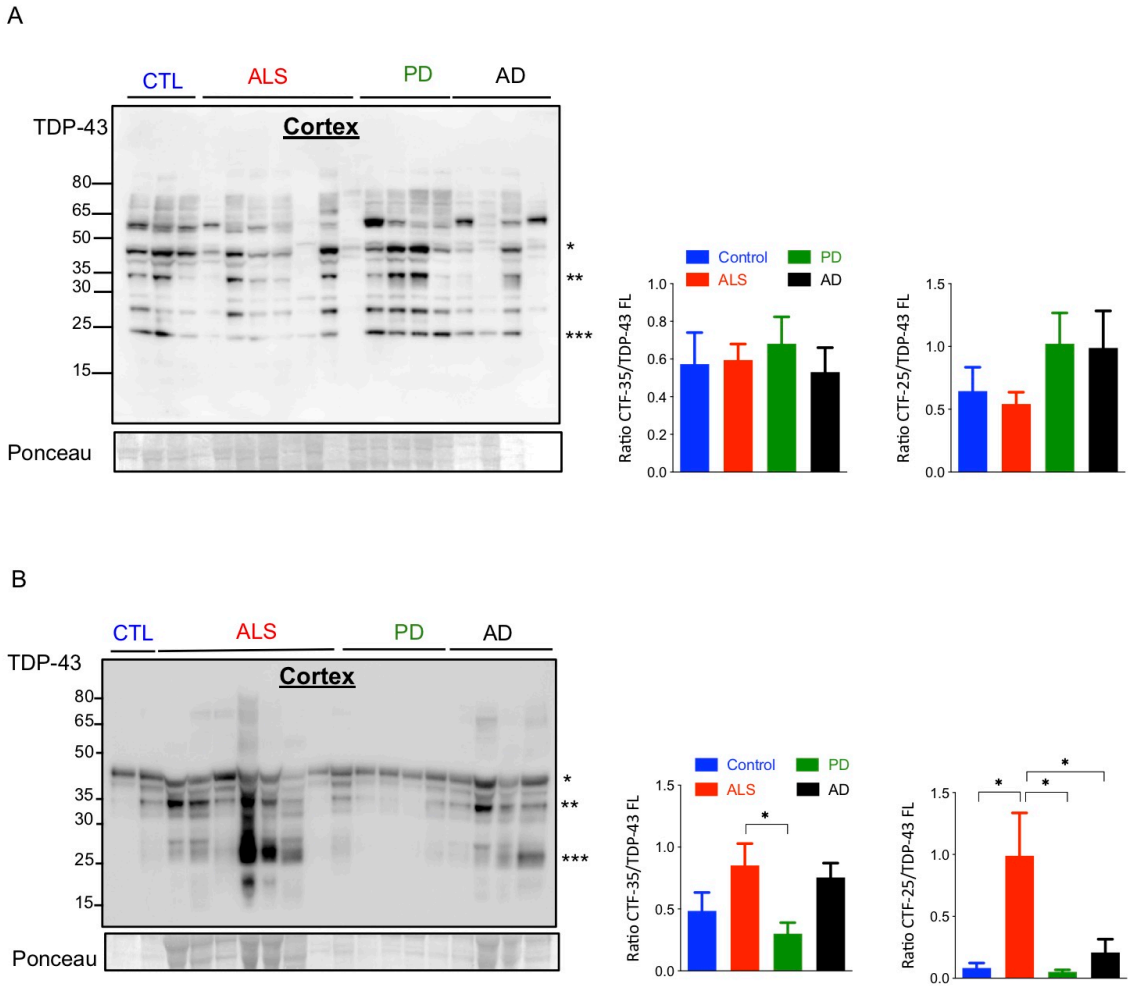


Fig. 4.6. Representative western immunoblots of samples from the PRM cohort of CTL, ALS, PD and AD cases. For immunoblotting the polyclonal primary antibody against C-terminal TDP-43 was applied. Gels 10% using MOPS buffer, Spectra multicolor ladder (L). **A** Shown are immunoblots of the soluble protein TX fractions from cortex tissue with multiple bands. The ratio of the intensities of the C-terminal TDP-43 band at 35kDa (CTF-35, **) over full-length TDP-43 band at 45kDa (TDP-43 FL*) were not significantly different between ALS and other disease groups (all p=0.9). The ratio of the intensities of the C-terminal TDP-43 band at 25kDa (CTF-25, ***) over TDP-43 FL* were increased in PD and AD, without reaching significance (p=0.2).
B Shown are immunoblots of the insoluble protein urea fractions from cortex tissue with a more concentrated banding pattern. The ratio of CTF-35** over TDP-43 FL* were not significantly different between ALS and CTL (p=0.2) or AD (p=0.9), but increased between ALS and PD (p=0.03). The ratio of the intensities of CTF-25 *** over TDP-43 FL * was significantly increased in ALS compared to CTL (p=0.03), PD (p=0.02) or AD (p=0.048).

4.3. Conclusion

In this Chapter for the first time a sophisticated targeted proteomic approach to validate disease-specific TDP-43 peptides by absolute quantification across an independent *post mortem* tissue cohort has been applied for the identification of an ALS-specific peptide signature in brain urea fractions. Further this technique allowed the detection of pathological processing in Alzheimer's disease, which is in line with the co-segregation of TDP-43 pathology in some pre-dominant Amyloid-ß and Protein Tau proteinopathies (Nelson *et al.*, 2019).

Peptides were quantified using targeted proteomics to investigate the presence of amino acid sequences of relevance to the disease-specific signature of TDP-43 pathology. This included peptides that were located at the N-Terminus, a peptide region that is recognized by an antibody specifically detecting full-length TDP-43 (Kwong *et al.*, 2014) and the C-Terminus of TDP-43, which is often found increased in TDP-43 insoluble aggregates in the brain (Igaz *et al.*, 2008). In addition, peptides which have the potential to reflect pathological truncation sites as described in Chapter 3 and by Kametani *et al.* were measured to assess their disease-specificity (Kametani *et al.*, 2016). The chymotryptic peptides used in this analysis were technically proven to be highly reliable and were therefore used for the interpretation of data. The combined peptide approach enabled the demonstration of the C-terminal to N-terminal peptide ratio being increased in ALS. This increase of the C-Terminus and decrease of the N-Terminus of TDP-43 protein in urea fractions from ALS *post mortem* tissue suggests decreased levels of full-length TDP-43 with potential pathological N-terminal truncation of TDP-43 leading to the degradation of the N-Terminus as recently also described by a different approach to isolate pathological TDP-43 (Laferriere *et al.*, 2019). Truncation as the disease-specific pathomechanism was further corroborated by data showing an increase of truncation site-specific peptides in ALS and in AD samples. These truncation site-specific peptides should not be observed in the presence of full-length TDP-43, because normal

digestion with chymotrypsin does exclude their production from the full sequence. Further immunoblotting confirmed that C-terminal TDP-43 bands at 25kDa were significantly increased in ALS insoluble urea fractions where TDP-43 pathology is expected. However, a general conclusion of the comparison between PRM and immunoblots is that the PRM might be a more sensitive method to detect pathological TDP-43. A drawback of the data presented is the lack of power to observe significant differences, when analysing absolute amounts of peptides. Many samples of the CTL and the PD group had missing values for the truncation site-specific peptides, which is most likely due to the very low abundance of these peptides and therefore not reaching the detection threshold by mass spectrometry. In future, larger cohorts are needed to validate these findings. However, the pre-analytical protocol is lengthy and a more sophisticated method to measure peptides in native *post mortem* tissue is needed. It also has to be kept in mind that all samples were treated with 7M urea. Therefore, detection of peptides in a native sample may be more complicated as the region of interest may not be exposed especially, when TDP-43 is aggregated.

The ultimate aim of the PRM technique developed in this thesis is to measure the chymotryptic peptides in CSF to enable an *in vivo* diagnostic test for TDP-43 pathology. From all *post mortem* tissues investigated in this thesis I have access to matched CSF samples. This is a unique possibility to investigate the peptide signature in CSF samples and compare it with *post mortem* tissue. The development of the PRM method to measure CSF samples is currently ongoing and I will compare ALS with PD and CTL samples. Another interesting prospect is to compare motor cortex with spinal cord tissue. I have prepared urea fractions from cortex matched ALS, AD, PD and AD spinal cord tissues and I am currently investigating the peptide signature by PRM.

Another interesting finding of this Chapter was the increase of peptides that reflect TDP-43 truncation in AD samples. However, in AD no increase of the C-Terminus to N-Terminus peptide ratio was observed, which might suggest a different underlying pathomechanism of

TDP-43 processing compared to ALS. TDP-43 pathology has been recently described in clinical AD and further neuropathological examinations are underway to look for any co-existing TDP-43 neuropathology in those AD cases used in this thesis in more detail (James *et al.*, 2016; Nelson *et al.*, 2019). The underlying pathology is important to assess the specificity of the peptides for TDP-43 proteinopathies. Ultimately the peptides identified offer targets for antibody development specific for the detection of pathologically altered TDP-43, leading to a more sensitive assay for ALS and possibly sub-types of AD with mixed neuropathology.

Chapter 5: The interactome of human TDP-43 in a cellular model of ALS

5.1. Introduction and aims

TDP-43 is a ubiquitously expressed heterogeneous nuclear ribonucleoprotein (hnRNP) (Ou *et al.*, 1995) containing two highly conserved RNA-recognition motifs (RRM) and a C-terminal glycine-rich domain (Kato *et al.*, 2012). It regulates key cellular functions such as alternative splicing and translation, but has a multiplicity of other functions (Buratti and Baralle, 2008; Ling *et al.*, 2013). The C-terminal region of TDP-43 has been demonstrated to be involved in protein-protein interactions, which mediate important cellular functions (Buratti *et al.*, 2005; Ayala *et al.*, 2011). Notably, ALS-associated mutations in TDP-43 are consistently located in the C-Terminus, suggesting that this region is critical for protein interactions relevant for ALS (Sreedharan *et al.*, 2008). Thus, the study of how pathologically altered TDP-43 affects protein-protein interactions and therefore its function is important in understanding ALS pathogenesis. The interactome of TDP-43 has to date been mostly studied in cellular models that overexpress human TDP-43 (Freibaum *et al.*, 2010; Li *et al.*, 2016). Overexpression of proteins has a major impact on cell homeostasis and only partially reflects the disease pathology found in humans. In this thesis a unique cellular model for ALS was used. Motor neurons were differentiated from mESCs harbouring a single copy stably-integrated bacterial artificial chromosome (BAC) transgene expressing human YPet-tagged *TDP-43$^{WT/-}$* or *TDP-43$^{M337V/-}$* (Gordon *et al.*, 2019). BAC-transgenic human *TDP-43$^{M337V/-}$* mice show motor function deficits at the age of six months and reduced survival in the absence of TDP-43 insoluble aggregates or motor neuron cell death. These ES-derived cells therefore provide a unique tool to compare the interactome of human TDP-43^{WT} and TDP-43^{M337V} under conditions close to physiological expression patterns, with an exogenous tag for highly specific affinity purification (Poser *et al.*, 2008).

This study allows to define the functional connectivity of human TDP-43 in well-characterized motor neuron cultures in which ALS-relevant phenotypes are present.

The aims of the work described in this Chapter are:

3. To define the normal TDP-43 interactome under resting conditions and in response to oxidative stress.
4. To identify how an ALS-causing mutation in TDP-43 alters the interactome.

5.2. Results

5.2.1. The characterisation of motor neurons derived from human YPet-tagged TDP-43 (BAC)-transgenic mESCs

In order to allow interpretation of interactome changes in the context of the mutation associated cellular phenotypes, I first characterised the motor neuron cultures with regards to the effect of the specific expression of human wild-type or M337V mutant TDP-43. Furthermore, the effects of oxidative stress, as a well-established pathway implicated in the pathogenesis of ALS, on survival and apoptosis of motor neuron cultures were studied prior to interpretation of the interactome data.

5.2.1.1. MESC-derived motor neurons express human wild-type and M337V mutant TDP-43

The (BAC)-transgenic mouse model expresses human TDP-43 with a C-terminal fluorescent tag (YPet) from a genomic insert integrated into the Rosa26 (Gt(ROSA26)Sor) locus of the mouse genome as a single stable copy, leading to expression levels below that of endogenous Tdp-43 (Gordon *et al.*, 2019). Mouse motor neurons were tested by PCR to confirm the

heterozygous state for YPet-tagged human *TDP-43*$^{WT/-}$ or *TDP-43*$^{M337V/-}$ inserted at the Rosa26 locus by PCR. A positive DNA product for the YPet-tagged *TDP-43*$^{WT/–}$ or *TDP-43*$^{M337V/–}$ and the Rosa26 locus confirmed heterozygosity (Fig. 5.1. A). By Sequencing the missense mutation A>G in exon 6 of human *TARDBP* (*TDP-43*) gene was confirmed for *TDP-43*$^{M337V/-}$ motor neurons (Fig.5.1. A).

5.2.1.2. Differentiated mouse embryonic stem cells express neuronal and motor neuronal marker and low levels of human TDP-43

After two days of motor neuron specification, cell cultures were assessed for the expression of neuronal and motor neuronal markers by immunohistochemistry (Fig. 5.1. B and C). 73% of *TDP-43*$^{WT/–}$ and 89% of *TDP-43*$^{M337V/–}$ cells co-expressed the neuronal marker Tuj1 and the early motor neuronal marker Islet1. There was no significant difference in expression between genotypes (p=0.196). 72% of *TDP-43*$^{WT/–}$ and 71% of *TDP-43*$^{M337V/–}$ cells co-expressed Tuj1 and the mature motor neuronal marker ChAT. 68% of the non-transgenic differentiated motor neurons also expressed ChAT and Tuj1 (p=0.557). Immunoblotting showed human YPet-tagged TDP-43^{WT} or TDP-43^{M337V} protein (72kDa) to be 0.78 and 0.74 times the level of mouse endogenous Tdp-43 (48kDa) respectively (p=0.85), and absent in cell lysates from motor neuron cultures from non-transgenic mESC (Fig. 5.1. D).

Fig. 5.1. Characterisation of motor neuron cultures from (BAC)-transgenic mouse embryonic stem cells that express human wild-type and M337V mutant TDP-43 at low levels

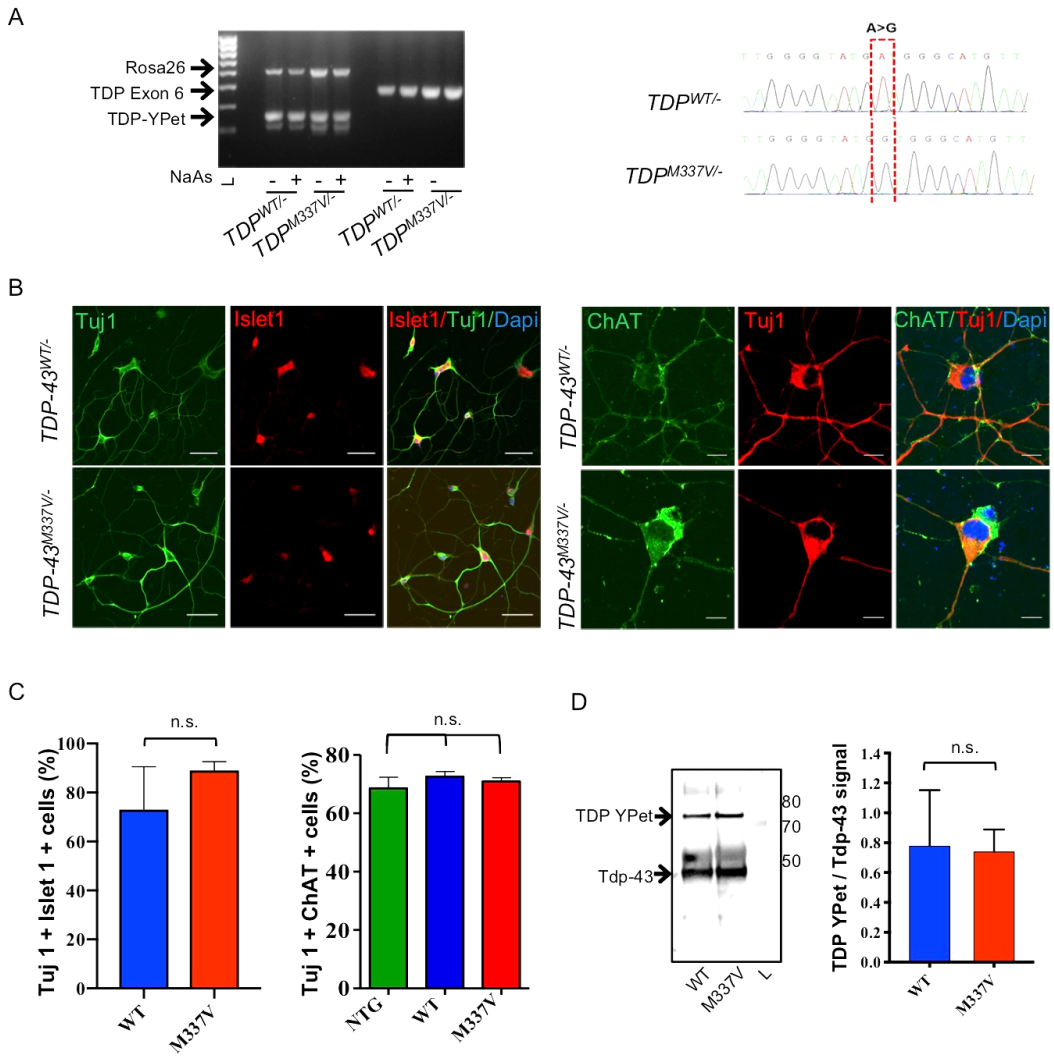


Fig. 5.1. **A** Mouse MNs +/- 0.5mM NaAs treatment were tested heterozygous for YPet-tagged human *TDP-43*$^{WT/-}$ or *TDP-43*$^{M337V/-}$ inserted at the Rosa26 locus by PCR. The heterozygosity is shown by the presence of the Rosa26 and YPet-tagged TDP-43 sequence. By Sequencing the missense mutation A>G in exon 6 of human TDP-43 was confirmed for *TDP-43*$^{M337V/-}$. **B** Immunostaining for Islet1 and Tuj1 in TDP-43$^{WT/-}$ and *TDP-43*$^{M337V/-}$ cell lines. Scale bar 50µm. Immunostaining for ChAT and Tuj1 in *TDP-43*$^{WT/-}$ and *TDP-43*$^{M337V/-}$ cell lines. Scale bar 10µm. **C** Quantification of Tuj1- and Islet1-positive cells shows 73% *TDP-43*$^{WT/-}$ and 89% *TDP-43*$^{M337V/-}$ cells are MNs with no differences between the genotypes (p>.05, unpaired t-test). Quantification of ChAT- and Tuj1-positive cells shows that 68% of the non-transgenic, 72% of *TDP-43*$^{WT/-}$ and 71% of *TDP-43*$^{M337V/-}$ cells are MNs with nonsignificant differences between the genotypes (p>.05, one-way ANOVA). **D** Immunoblotting with anti-TDP-43 full-length antibody. *TDP-43*$^{WT/-}$ and *TDP-43*$^{M337V/-}$ MN whole cell lysates show lower expression levels of human YPet-tagged TDP-43 compared to endogenous mouse Tdp-43 at 45kDa. The ratio of TDP-YPet to Tdp-43 was 0.78 and 0.74 respectively (p>.05, unpaired t-test). Data are represented as mean±SD. MN, motor neuron.

5.2.1.3. Low-level expression of human TDP-43$^{M337V/-}$ in (BAC)-transgenic motor neuron cultures leads to reduced survival in response to oxidative stress

Given the role of oxidative stress in neurodegeneration, the TDP-43 interactome was investigated under conditions which induce stress granules by treating cells with 0.5mM NaAs for 60 minutes as previously described by Gordon et al. (Gordon *et al.*, 2019). This treatment was associated with the expression of cleaved-caspase 3 in less than 20% of cells in either genotype (p=0.088) (Fig. 5.2. A). There was no difference in survival between genotypes at two hours (p=0.78) and seven hours (p=0.16) after treatment, but a significantly reduced survival of *TDP-43$^{M337V/-}$* compared to *TDP-43$^{WT/-}$* motor neurons was observed at 24 hours (p=0.02) (Fig. 5.2. B). The expression of human YPet-tagged TDP-43 showed a predominantly nuclear distribution in both *TDP-43$^{WT/-}$* or *TDP-43$^{M337V/-}$* motor neurons in basal conditions and was not altered after oxidative stress treatment with 0.5mM NaAs. However, this experiment was not systematically quantified (Fig. 5.2. C).

Fig. 5.2. Human *TDP-43$^{M337V/-}$* (BAC)-transgenic motor neurons in response to oxidative stress

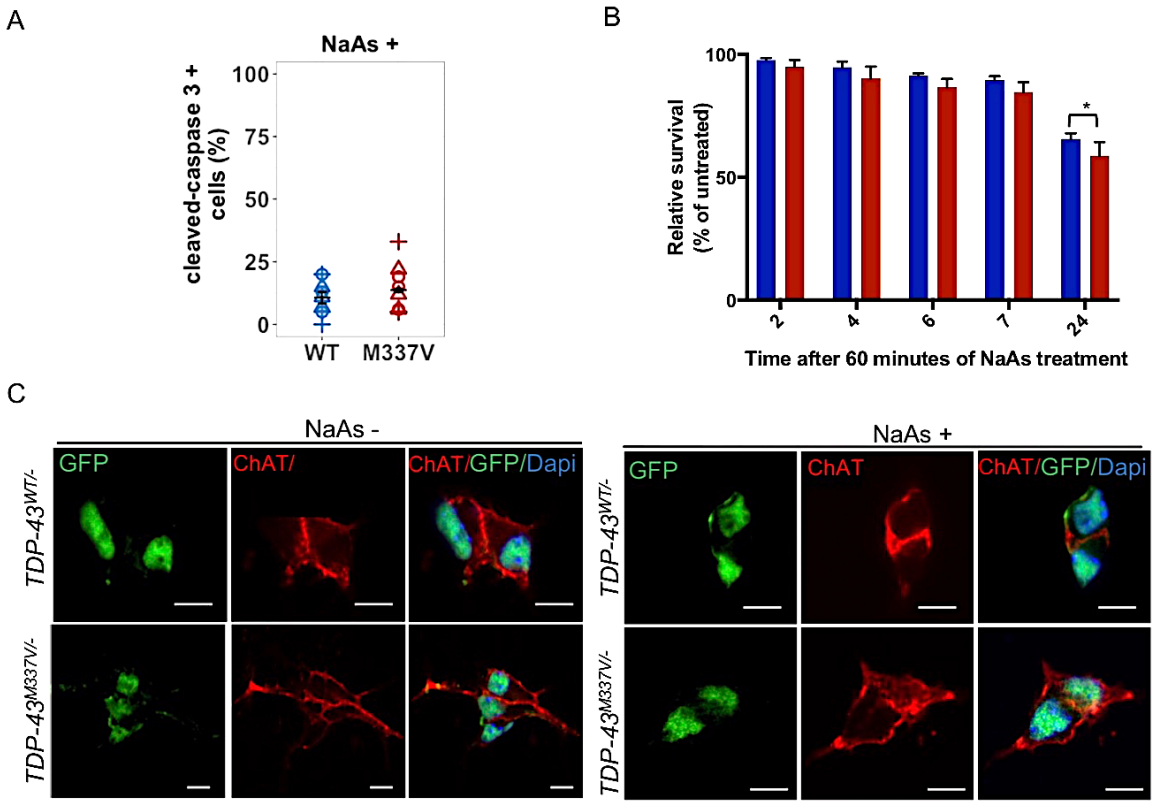


Fig. 5.2. **A** Quantification of cleaved-caspase 3 positive cells after 60 minutes of 0.5mM NaAs treatment shows 15% *TDP-43$^{WT/-}$* and 11% *TDP-43$^{M337V/-}$* cells are apoptotic with no differences between the genotypes (p>.05, unpaired t-test). Symbols (+,o,∇) represent number of positive stained cells per field and differentiation. **B** The relative survival is shown over a 24 hours time course after 60 minutes of 0.5 mM NaAs treatment with a significant difference between *TDP-43$^{WT/-}$* and *TDP-43$^{M337V/-}$* MNs after 24 hours (*, p<.05, Sidak's multiple comparison test). n=3 independent differentiations; Data are represented as mean±SD. **C** Motor neurons stained for ChAT and GFP, which detects YPet-tagged human TDP-43. Human TDP-43 was observed in the nucleus +/- 0.5mM NaAs treatment. Scale bar 10µm. Abbreviations: DAPI, 40,6-Diamidino-2-Phenylindole; MNs, motor neurons.

5.2.2. Co-Immunoprecipitation of human YPet-tagged TDP-43 and identification of protein-protein interactions by mass spectrometry

5.2.2.1. Affinity enrichment of human YPet-tagged TDP-43 from mouse motor neuron lysates

To study protein-protein interactions human wild-type or mutant M337V YPet-tagged TDP-43 was immunoprecipitated from motor neuron lysates using anti-GFP antibody-coated beads, which detect the YPet-tag of human TDP-43. The efficiency of the immunoprecipitation was confirmed by immunoblotting and detection of the YPet-tagged TDP-43. Immunoprecipitations of equal input amounts showed specific enrichment of human YPet-tagged TDP-43 (72kDa) with complete depletion from the supernatant, which contained the residual endogenous Tdp-43 (48kDa) (Fig. 5.3. A). Human YPet-tagged TDP-43 was immunoprecipitated from motor neuron lysates before and after treatment with 0.5mM NaAs.

Fig. 5.3. Human YPet-tagged TDP-43 is sufficiently immunoprecipitated from (BAC)-transgenic motor neuron lysates

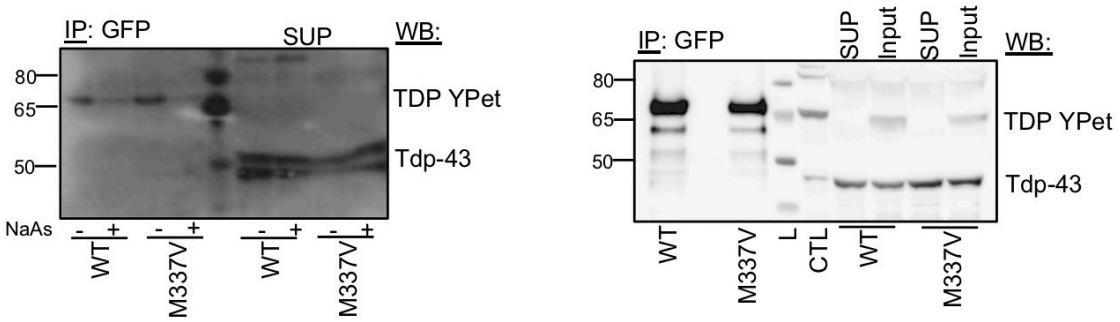


Fig. 5.3. Immunoblotting with anti-TDP-43 full-length antibody shows immunoprecipitated samples with enrichment of YPet-tagged human TDP-43^{WT} and TDP-43^{M337V} at 72kDA. The left WB shows enrichment of human TDP-43 after immunoprecipitation from *TDP-43$^{WT/-}$* and *TDP-43$^{M337V/-}$* motor neuron lysate -/+ 0.5mM NaAs treatment, with a slight decrease in NaAs treated samples. The supernatants (SUP) after immunoprecipitation are depleted from human TDP-43, with mouse Tdp-43 at 48kDa remaining in the sample. The right WB shows immunoprecipitation of human YPet-tagged TDP-43 at 72kDa, a positive control and the input sample of the immunoprecipitations with mouse Tdp-43 at 48kDa and human TDP-43 at 72kDa; The SUP after immunoprecipitation is depleted from human TDP-43. WB, western blot; Gels 4-12% using MOPS buffer, Spectra multicolor ladder (L).

5.2.2.2. Mass spectrometric analysis of the human TDP-43 interactome

Human wild-type or mutant TDP-43 were immunoprecipitated from motor neuron lysates under conditions promoting preservation of its protein-protein interactions using anti-GFP antibody-coated beads and a low-stringency 1% NP-40 buffer. To determine the effect of oxidative stress, experiments were repeated in motor neuron cultures treated with 0.5mM NaAs. Across all GFP-immunoprecipitated samples, a total of 534 proteins were co-immunoprecipitated and identified by mass spectrometry. As expected, the YPet bait was detected equally in all samples. While some proteins were equally abundant between genotypes, a range of specific proteins were differentially abundant in motor neurons expressing either TDP-43^{WT} or TDP-43^{M337V}. In figure 5.4. A hierarchical clustering of protein ion abundancies on the y-axis and sample per genotype on the x-axis shows proteins with missing ion abundancies (white spaces) at the bottom of the graph and a cluster of the TDP-43^{M337V} (red) samples where the majority of proteins with missing ion abundancies was found.

5.2.2.3. Human wild-type and mutant TDP-43 have a shared background proteome and genotype-specific interacting proteins that are unique binding partners

To quantify the presence or absence of an interactor in the human TDP-43^{WT} or TDP-43^{M337V} +/- NaAs interactomes label-free quantification by peptide spectral counts was used. Only those proteins with positive spectral counts in both the TDP-43^{WT} and TDP-43^{M337V} samples were additionally tested for significant differences by ion abundancies.

As shown in the Venn diagrams, label-free quantification identified 249 interactors that were abundant in the TDP-43^{WT} interactome, but not present in the TDP-43^{M337V} interactome. In contrast, only 43 interactors were abundant in the TDP-43^{M337V} interactome, but not in the TDP-43^{WT} interactome (Fig. 5.4. B).

Fig. 5.4. LC-MS/MS identification of proteins that bind to human TDP-43 and how the M337V mutation affects its binding capacity

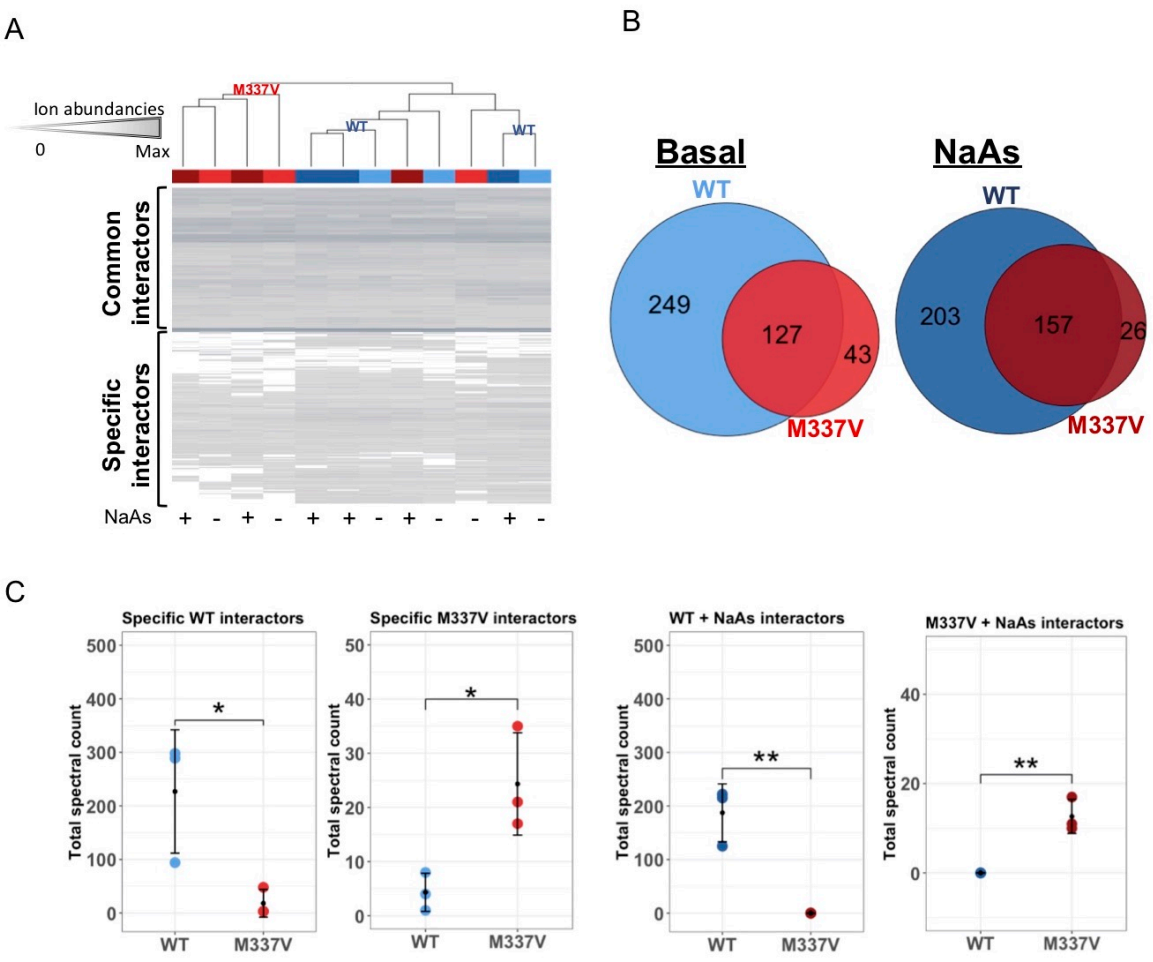


Fig. 5.4. **A** After immunoprecipitation of YPet-tagged TDP-43 and LC-MS/MS analysis 534 proteins were identified to co-immunoprecipitate over all samples. The graph shows a hierarchical cluster of TDP-43^{WT} (blue), TDP-43^{WT} + NaAs (dark blue), TDP-43^{M337V} (red), TDP-43^{M337V} + NaAs (dark red) samples by protein ion abundances. Empty fields indicate that a protein was not detected in a sample (ion abundance = 0). A cluster is shown for TDP-43^{M337V} samples where the majority of co-immunoprecipitated proteins were not detected. **B** Venn diagrams show the total number of proteins identified by **l**abel-free identification using spectral counts in the TDP-43^{WT} or TDP-43^{M337V} interactome (left) and the NaAs treated interactomes (right) with a reduction of proteins identified for TDP-43^{M337V}. Overlap indicates common interactor, while non-overlap indicates proteins that specifically immunoprecipitated with TDP-43^{WT} or TDP-43^{M337V}. **C** The total spectral counts of the specific TDP-43^{WT} or TDP-43^{M337V} interactomes are higher (both *, p<.05, unpaired t-test). The same is shown for TDP-43^{WT} + NaAs and TDP-43^{M337V} + NaAs interactors (**, p<.001, unpaired t-test). For mass spectrometry analysis n=3 independent differentiations for + and - NaAs treated cultures. Data are represented as mean±SD.

127 proteins were abundant in both interactomes using spectral counts, therefore ion abundancies were used to test for significant differences. Only four proteins had a significantly higher abundance, the remainder of the 127 proteins were unaltered between genotypes and therefore considered to be the nonspecific background proteome.

The TDP-43^{WT} + NaAs interactome contained 203 uniquely abundant interactors, while the TDP-43^{M337V} interactome with NaAs treatment had only 26 unique interactors. 157 proteins were common between both interactomes with NaAs stress treatment and not significantly different according to ion abundancies.

An additional test to show that the 249 proteins were specifically bound to TDP-43^{WT}, was to compare the total spectral counts obtained from three separate TDP-43^{WT} samples to the total spectral counts of those interactors in the TDP-43^{M337V} samples (Fig. 5.4. C). As anticipated, total spectral counts for those interactors were close to zero in the TDP-43^{M337V} samples and significantly increased in the TDP-43^{WT} samples. This was also shown for the proteins specifically bound to TDP-43^{M337V} and for the proteins bound to TDP-43^{WT} or TDP-43^{M337V} treated with 0.5mM NaAs (Fig. 5.4. C).

5.2.3. The ALS-associated C-terminal mutation M337V alters the normal interactome of human TDP-43

5.2.3.1. C-terminal mutation of TDP-43 leads to a reduction in protein-protein interactions

As described above, the number of proteins that were bound to human TDP-43 was reduced in the presence of the C-terminal M337V mutation. A 4x4 Chi-square test with a resultant p-value of 0.0001 demonstrated a significant relationship between the number of interactors and the human TDP-43 genotype, with a reduction of interactors observed in the TDP-43^{M337V} +/- NaAs interactome. In figure 5.5. examples of proteins that are differentially

bound to TDP-43^{WT} and TDP-43^{M337V} are given. Proteins that were bound to TDP-43^{WT} were serine/arginine-rich splicing factors (Srsf 7) and eukaryotic translation initiation factors (If 4a1) that reflect the physiological function of TDP-43 (Fig. 5.5. A). Binding to Hnrnpa2, as previously reported, was not altered by the M337V mutation (Buratti *et al.*, 2005; D'Ambrogio *et al.*, 2009). Interestingly, complexes of the dihydropyrimidinase-related proteins, Dpysl1 (Crmp1) and Dpysl3, were highly abundant in the TDP-43^{M337V} interactome. These proteins are known to be modified in neurodegeneration and are involved in several ALS-associated pathways including axonal transport, glutamate excitotoxicity and oxidative stress (Blasco *et al.*, 2013). To investigate how the TDP-43^{WT} and TDP-43^{M337V} interactomes +/- NaAs differ, gene ontology enrichment analysis was performed on both interactomes (Fig. 5.5.).

5.2.3.2. Gene ontology enrichment analysis reveals impairment of the normal cellular function of human wild-type TDP-43 and links the M337V mutation to ALS associated pathways

Gene ontology (GO) enrichment analysis of the putative interactors specific for either TDP-43^{WT} or TDP-43^{M337V} demonstrated differences in their functional role. Proteins bound to TDP-43^{WT} were enriched for terms including ‘transcription’ (odds ratio, OR 5.5, p=0.03), ‘translation’ (OR 3.2, p=0.02), ‘ribosome formation’ (OR 1.8, p=0.003), ‘Poly(A)-RNA binding’ (OR 1.4, p=0.004) and ‘extracellular exosome’ (OR 1.3, p=0.0003) (Fig. 5.5. A and 5.6. A). In contrast, the TDP-43^{M337V} interactome in basal conditions was enriched for different GO terms including ‘protein folding’ (OR 13.3, p=0.006) and ‘filamin binding’ (OR 13.3, p=0.005) (Fig. 5.5. A).

Fig. 5.5. The TDP-43 interactome is altered by the C-terminal TDP-43 mutation

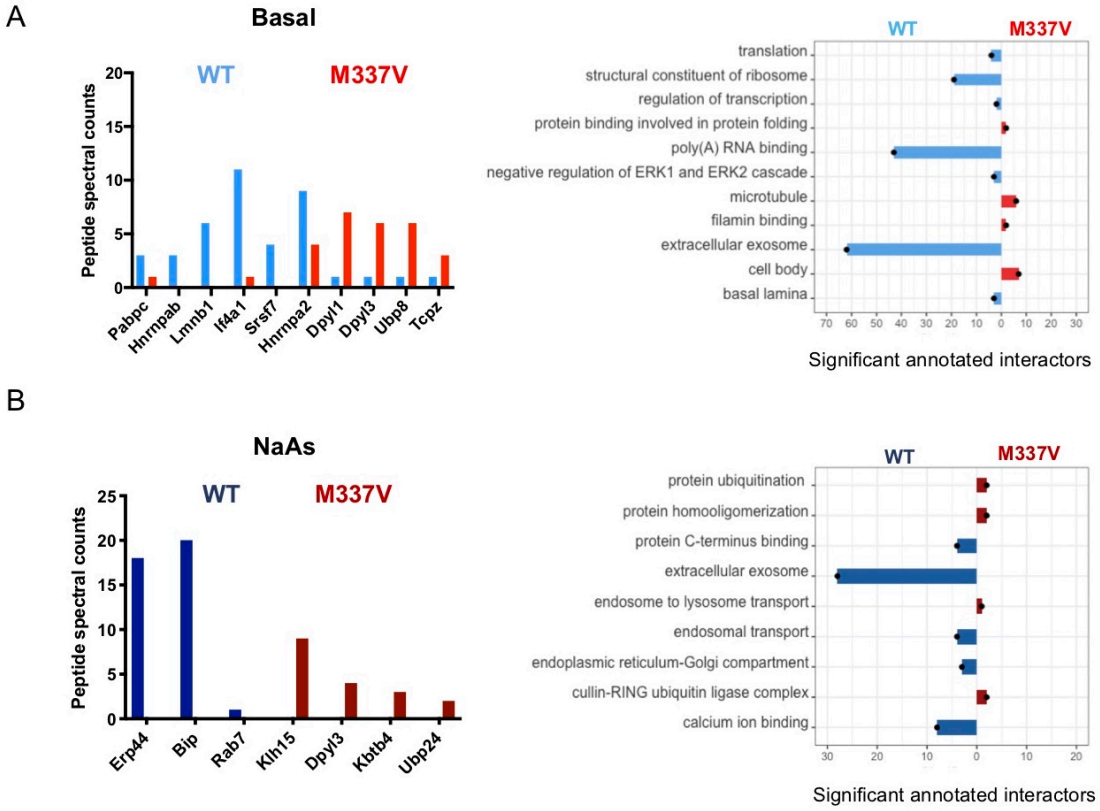


Fig. 5.5. **A** The bar graph shows examples of proteins bound to TDP-43^{WT} (blue), TDP-43^{M337V} (red) or both. Proteins with a spectral count of 1 were considered as absent if the protein was 2-fold increased in the other sample. Gene Ontology enrichment analysis is shown for significant terms ($p<.05$, Fisher's exact test) by number of annotated interactors from the human TDP-43^{WT} and TDP-43^{M337V} interactome **B** The bar graph shows examples of proteins bound to TDP-43^{WT} + NaAs (dark blue), TDP-43^{M337V} + NaAs (dark red). Gene Ontology enrichment analysis is shown for the TDP-43^{WT} + NaAs and TDP-43^{M337V} + NaAs interactomes. Abbreviations: Lamin-B1 (Lamnb1), ubiquitin carboxyl-terminal hydrolase (Ubp), T-complex protein 1 subunit zeta (Tcpz), endoplasmic reticulum resident protein 44 (Erp44), endoplasmic reticulum chaperone (Bip), kelch-like protein (Klhl15), kelch repeat and BTB domain-containing protein (Kbtb).

In response to NaAs stress treatment the TDP-43^{WT} interactome shifts towards proteins enriched for terms including 'endoplasmic reticulum' (OR 4.5, p=0.02), 'calcium binding' (OR 3.5, p=0.001) and 'endosomal transport' (OR 3.5, p=0.03) (Fig. 5.5. B and 5.6. A). Importantly, in response to stress the TDP-43^{M337V} interactome revealed significant GO terms distinct from those seen with TDP-43^{WT}, with high odds ratios for protein ubiquitination (OR 28, p=0.001), protein homo-oligomerization (OR 50, p= 0.0001) and endosomal to lysosomal transport (OR 8, p=0.02) (Fig. 5.5.B). This indicates that the M337V mutation disturbs the normal TDP-43 interactome in a way that is likely to affect its downstream function, with a shift towards pathways that have been previously established to have a role in ALS pathogenesis.

5.2.3.3. The physiological function of TDP-43 demonstrated by human TDP-43^{WT} interactors is disturbed by the M337V mutation

The reduced number of interactions for TDP-43^{M337V} and its altered binding partners, suggests a disruption of the normal physiological function of TDP-43, which was therefore further investigated in basal conditions and in response to stress by the analysis of the TDP-43^{WT} interactome. In the Venn diagram (Fig. 5.6. A) it is shown that the TDP-43^{WT} and the TDP-43^{WT} + NaAs treatment interactomes partly overlap, but TDP-43^{WT} also gained 92 new interactors in response to stress. By comparing the non-overlapping interactors, significant GO terms differed between basal and stress conditions (as also described above). When the TDP-43^{WT} interactomes without and with NaAs treatment were compared, the terms transcription and translation in basal conditions were replaced by endosomal transport and endoplasmic reticulum-Golgi compartment terms in response to stress. Detailed network analysis of the TDP-43^{WT} interactomes confirmed strong connectivity between interacting proteins (Fig. 5.6. B). In basal conditions, two main clusters of proteins were identified,

reflecting proteins involved in transcription and translation, or ribosome formation. In response to stress these clusters of proteins resolved, possibly reflecting a cellular response to stress through arresting translation and transcription, consistent with a shift towards protein-protein interactions that are involved in endosomal-exosomal transport pathways. This suggests potentially distinct condition-dependent functions of TDP-43^{WT} in motor neurons, with a predominant role in DNA/RNA metabolism in basal conditions and a shift in function towards intracellular trafficking in response to stress, which is disturbed by a pathogenic mutation in TDP-43.

Fig. 5.6. The physiological function of TDP-43 demonstrated by human TDP-43^{WT} interactors and its potentially distinct condition-dependent functions

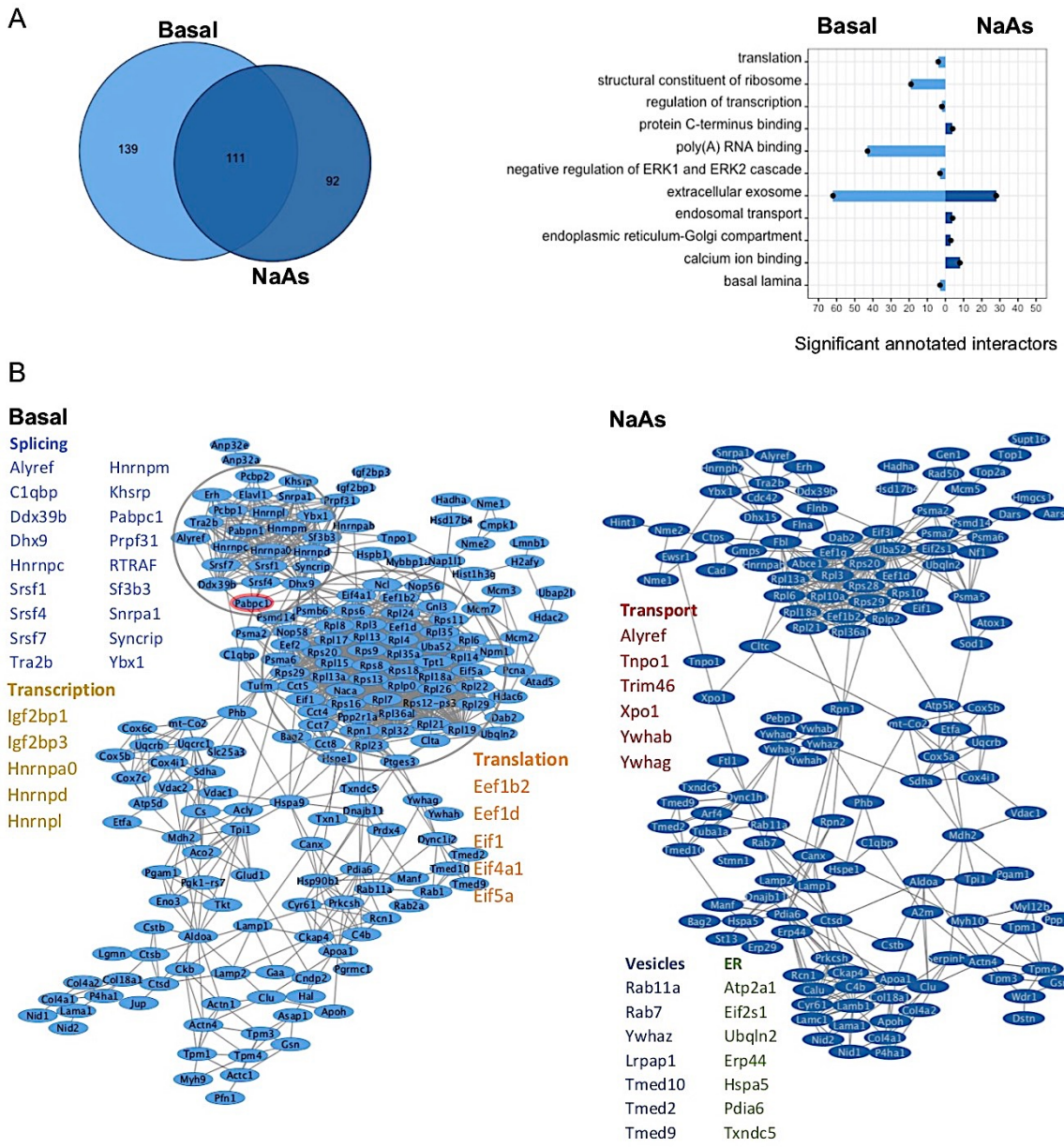


Fig. 5.6. **A** The human TDP-43^{WT} interactome changes in response to stress. Stress altered the interactome and revealed 92 new putative interactors. GO enrichment analysis shows significant terms (*, p<.05, Fisher's exact test) are altered in response to stress. Basal conditions show terms for translation and transcription, stress treatment shows terms for the endoplasmic reticulum and endosomal transport. **B** Protein-protein interaction network analysis shows a cluster of protein-protein interactions for proteins involved in transcription and splicing, ribosome formation and translation, (left); in response to stress those clusters resolve (right), while interactions of the endosomal-exosomal pathway form. Pabpc1 is indicated by a red circle. For better visualization coloured lists of proteins are given sorted by their attributed gene ontology function analysed by STRING network analysis. ER, endoplasmic reticulum.

5.3. Conclusion

Together our analysis highlights a functional interaction network involving human TDP-43, which regulates key cellular pathways, and that a mutation in the C-terminal region of TDP-43, which is important for protein-protein interactions, affects its interactome with implications for ALS pathogenesis in a mouse model relevant to motor neuron disease.

A major challenge in neurodegenerative disease is to link cellular phenotypes in model systems directly with molecular mechanisms driving loss of homeostasis and cell failure. The key question of how ALS-determining mutations are tolerated for long periods before triggering motor neuron degeneration requires models in which TDP-43 overexpression itself is not a significant factor in toxicity. Here a transgenic mouse model of ALS was studied, in which a genomic construct is site-specifically integrated as a single copy to drive human TDP-43 from its native promotor without the confounding effect of major protein overexpression (Gordon *et al.*, 2019). At the same time this model enabled direct comparison of the TDP-43^{WT} and TDP-43^{M337V} interactome under normal conditions and under an additional oxidative stress factor, which has been shown to be relevant to the pathogenesis of ALS (Shaw *et al.*, 1995).

In this study, I have shown that TDP-43^{WT} is a highly interactive protein. As demonstrated previously, human TDP-43^{WT} under basal conditions co-immunoprecipitates with proteins involved in transcription, splicing and translation (Freibaum *et al.*, 2010; Blokhuis *et al.*, 2016). However, these studies were based on transient overexpression of TDP-43 in HEK293T cells or N2A cells and the expression of the mutant TDP-43 had no effect on interactors (Freibaum *et al.*, 2010). In comparison to already published results, I demonstrated that the specification of motor neurons where human TDP-43 is expressed at low levels throughout differentiation has the potential to reveal genotype dependent changes

on protein-protein interactions. Here, the C-terminal mutation M337V of human TDP-43 had a significant effect on the reduction of established TDP-43^{WT} interactors.

It was confirmed that TDP-43^{M337V} binding to previously reported interactors such as Hnrnpa2 was maintained (Buratti *et al.*, 2005; D'Ambrogio *et al.*, 2009), while other interactors such as splicing factors (nuclear export factors) (Srsf7, Srsf4, Sf3b3) and translation initiation factors (If4a1, If5a1, Eif1, Eif2a,) were not present in the TDP-43^{M337V} interactome, suggesting potential contributions from dysregulated splicing and mRNA export dysfunction to ALS pathogenesis (Tollervey *et al.*, 2011; Colombrita *et al.*, 2012; Muller-McNicoll *et al.*, 2016).

Furthermore, in this thesis I investigated changes to both the wild-type and M337V mutant TDP-43 interactomes in direct response to oxidative stress. This led to a reorganisation of the TDP-43^{WT} interactome. Interactors for transcription and translation decreased in response to stress. This is in keeping with the protective response of general downregulation of translation in the cell under oxidative stress, which is at the same time often facilitated by the formation of stress granules (Guil *et al.*, 2006). Interactors involved in the endoplasmic reticulum-unfolded protein response, endosomal transport and extracellular exosome increased, suggesting a functional role of TDP-43 in these pathways (Schwenk *et al.*, 2016; Lindholm *et al.*, 2017). Strikingly, oxidative stress exposure leads to an enrichment of TDP-43^{M337V} interactors, which were relevant to known ALS pathways, notably protein-ubiquitination and a shift to lysosomal degradation (Wang *et al.*, 2010).

It is still a matter of debate, whether a loss of function of TDP-43 through an impaired capacity for RNA-binding, translation and splicing dysfunction or a toxic gain of function drives ALS pathology (Lee *et al.*, 2011; Ling *et al.*, 2013). This study provides further evidence that pathological changes within TDP-43 can have direct functional consequences

in the absence of protein mislocalisation or aggregation of TDP-43 (Gordon *et al.*, 2019). Previous studies confirmed the importance of an intact C-terminal tail of TDP-43 in biding to other hnRNPs or mRNA (Buratti *et al.*, 2005; Buratti and Baralle, 2008). Also, aberrant control of protein translation has been linked to ALS and very recently been shown to be relevant for the pathogenesis of the most frequent genetic mutation C9orf72 (Kapur *et al.*, 2017; Butti and Patten, 2018; Moens *et al.*, 2019). Whether a single nucleotide exchange causes these alterations or the M337V mutation leads to altered TDP-43 protein confirmation and folding that leads to its loss of interactions, as it has been shown for the RNA-binding protein FUS, remains to be investigated (Marrone *et al.*, 2019).

Chapter 6: The interactome of human TDP-43 reveals important cellular pathways with implications for possible therapeutic targets in ALS

6.1. Introduction and Aims

By mass spectrometry analysis human TDP-43 binding proteins were identified and gene ontology enrichment analysis was used to describe the potential role the binding proteins have within cellular pathways. In motor neurons the M337V mutation interrupted some protein-protein interactions, therefore suggesting that TDP-43 mutations may act in part through altering normal TDP-43 function. To validate results from the detailed proteomic analysis by co-immunoprecipitation, I looked at the interaction between TDP-43 and Pabpc, which is an established interactor of full-length TDP-43 (Freibaum *et al.*, 2010), to show the potential of the M337V mutation to alter its interaction.

The human TDP-43 (BAC)-transgenic mouse model enables the study of human M337V mutant TDP-43 on the basis of low expression. TDP-43 abnormalities have been confirmed in TDP-43^{M337V} primary motor neurons cultured from spinal cords of the human *TDP-43$^{M337V/-}$* (BAC)-transgenic mice, with TDP-43 mislocalized to the cytoplasm of motor neurons expressing the mutation, but not in those expressing wild-type TDP-43 (Gordon *et al.*, 2019). It was also shown that stress granule dynamics were altered in response to oxidative stress. Altered stress granule dynamics have been linked to TDP-43 pathology in ALS (Colombrita *et al.*, 2009; Liu-Yesucevitz *et al.*, 2010; McDonald *et al.*, 2011; Khalfallah *et al.*, 2018). It is known, that RNA-binding proteins are important for the regulation of stress granule dynamics (Markmiller *et al.*, 2018). The preceding chapter describes how TDP-43^{WT} interactors were significantly enriched for RNA-metabolism

pathways, which were then altered in response to stress, but the TDP-43^{M337V} interactome was lacking these interactions. To investigate how the M337V mutation in resting, but also in stress conditions, disturbs protein interactions, Pabpc was chosen as a target protein for further study. Pabpc is involved in both translation and in the formation of stress granules and therefore indicative of a disturbed interaction with possible functional consequences (Kedersha *et al.*, 2000). In addition, the TDP-43^{WT} interactome revealed high abundance of proteins involved in the extracellular exosome and this was not the case for the TDP-43^{M337V} interactome. Secretion of extracellular vesicles has a role in many neurodegenerative diseases and there is evidence that this is relevant for intercellular transmission of disease proteins (Feiler *et al.*, 2015; Thompson *et al.*, 2016). Reduced vesicle secretion has been shown for human fibroblasts from patients with the C9orf72 mutation (Aoki *et al.*, 2017). Therefore, this pathway was also selected for further functional analysis.

The aims of the work described in this Chapter are:

1. To validate the disruption of the TDP-43 interactor Pabpc by the M337V mutation in mouse motor neurons and human cellular models
2. To link alterations of protein-protein interactions to specific phenotypic changes to provide insights into ALS pathogenesis.

   i) To explore Pabpc-positive stress granule dynamics in *TDP-43$^{M337V/-}$* and *TDP-43$^{WT/-}$* motor neurons.

   ii) To investigate, if extracellular vesicles secretion is altered in *TDP-43$^{M337V/-}$* mouse motor neurons and human ALS *TDP-43$^{M337V/-}$* iPSC-derived motor neurons.

6.2. Results

6.2.1. Validation of the TDP-43^{WT} interactor Poly(A)-binding protein in mouse motor neurons

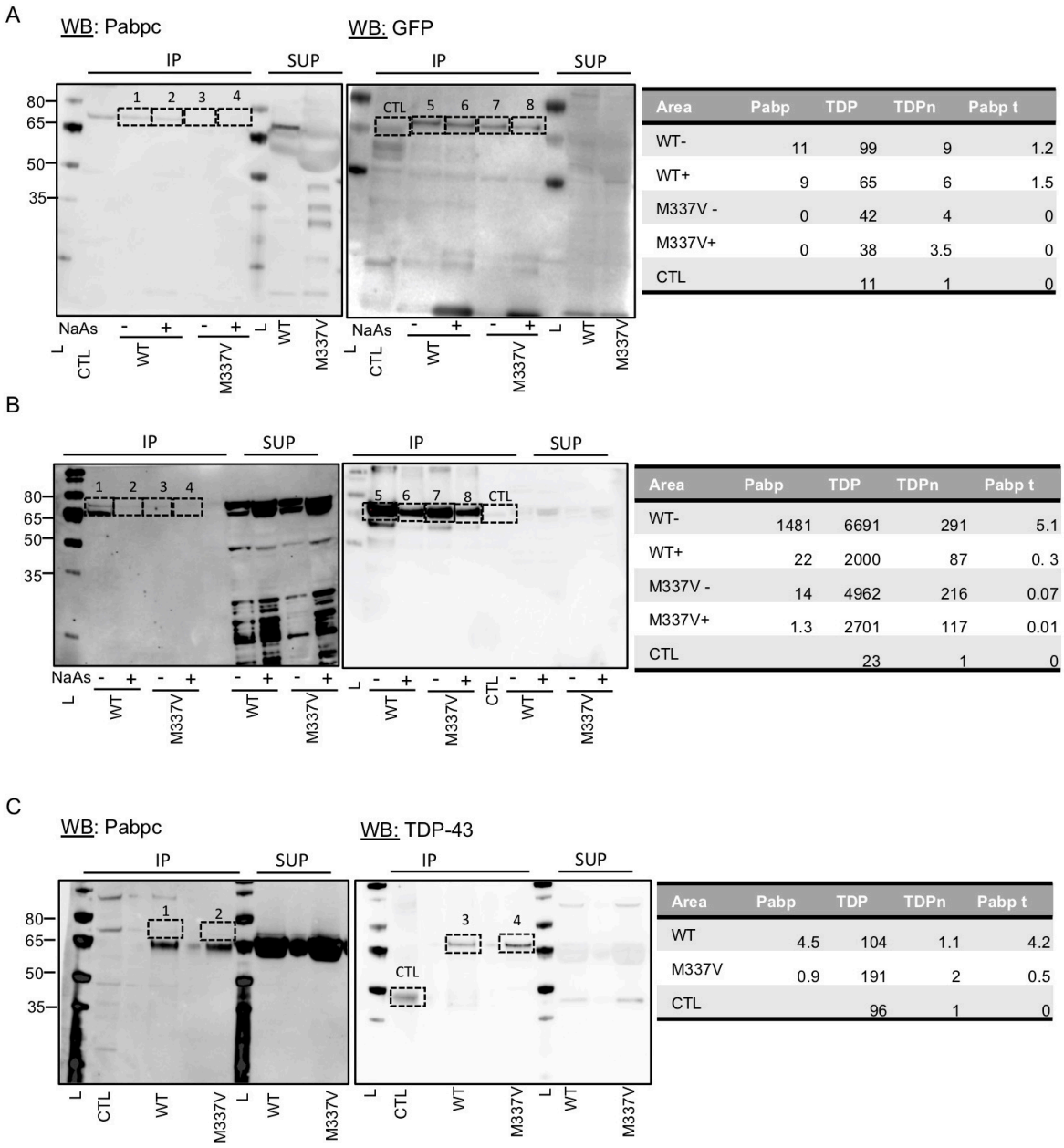
In the previous Chapter it was observed that TDP-43^{WT} showed a greater number of specific interactors than TDP-43^{M337V}. The main finding was that TDP-43^{WT} is important for binding to proteins that are involved in transcription and translation. It has also been shown that in response to oxidative stress TDP-43^{WT} interactors shift towards proteins that are relevant to cellular stress pathways, such as constituents of the endoplasmic reticulum and possible endosomal and extracellular vesicle pathways. At the same time significant interactions with proteins involved in RNA/DNA-metabolism decreased. To verify this data, I focused on the validation of the TDP-43^{WT} interactor Pabpc, a protein that is involved in translation and stress granule formation, and then investigated, how the M337V mutation affects this interaction.

6.2.1.1. The TDP-43^{WT} interaction with Poly(A)-binding protein is disrupted by the M337V mutation in mouse motor neurons

Our mass spectrometry data identified Pabpc as a TDP-43^{WT} binding protein. Pabpc has an important role in protein translation by binding to the poly(A)-tail, but also is an important component of stress granules, which are formed in response to stress and often are accompanied by arrest of translation (Markmiller *et al.*, 2018). To validate the TDP-43 and Pabpc interaction, co-immunoprecipitation experiments were performed from mouse motor neuron lysates. Co-immunoprecipitations required at least 1000µg of input protein for western immunoblot detection of the Pabpc prey protein. This was achieved by the appropriate expansion of mouse motor neuron cultures using at least two vials of $2x10^6$ mESCs. However, the additional oxidative stress treatment required a two-fold higher yield.

Therefore, co-immunoprecipitation of 0.5mM NaAs treated samples was limited to n=2 differentiations. Immunoprecipitations of human TDP-43^{WT} and TDP-43^{M337V} were performed using anti-GFP antibody-coated beads directed against the YPet tag. The eluates of the immunoprecipitations were first immunoblotted for the Pabpc prey protein and subsequently immunoblotted for the levels of the human YPet-tagged TDP-43 bait protein. To account for variations of human TDP-43 immunoprecipitated per sample, the ratio of Pabpc to normalized human TDP-43 was compared. This confirmed the co-immunoprecipitation of Pabpc with human TDP-43^{WT} in basal conditions, while a reduction or absence of Pabpc co-immunoprecipitation was observed with human TDP-43^{M337V} (n=3, p=0.049) (Fig. 6.1.). Immunoprecipitation of TDP-43^{WT} and TDP-43^{M337V} from 0.5mM NaAs stress treated samples led to lower Pabpc levels in both genotypes and no differences in the levels of Pabpc were observed between genotypes (n=2, p=0.286). In figure 6.1. full western blots are shown for all immunoprecipitation experiments from motor neuron cultures (Fig. 6.1. A), while the second part of the figure demonstrates an enlarged and cropped image with graphical quantification of the results from all experiments (Fig. 6.1. D). Mouse Pabpc immunoreaction is shown at 75kDa, while human TDP-43 immunoprecipitation is shown at 72kDa. When immunoblotting with a TDP-43 antibody instead of using the YPet-specific anti-GFP antibody, endogenous mouse Tdp-43 is not detected in immunoprecipitates, showing that only the interaction of human TDP-43 to mouse Pabpc was investigated (Fig. 6.1. C). In one immunoprecipitation a nonspecific immunoreaction with the antibody against Pabpc was observed at a molecular weight band at 65kDa, which was not considered as the specific Pabpc band at 75kDa (Fig. 6.1. C).

Fig. 6.1. The interaction of mouse Poly(A)-binding protein to human TDP-43 is disrupted by the M337V mutation in mouse motor neurons



Area	Pabp	TDP	TDPn	Pabp t
WT-	11	99	9	1.2
WT+	9	65	6	1.5
M337V -	0	42	4	0
M337V+	0	38	3.5	0
CTL		11	1	0

Area	Pabp	TDP	TDPn	Pabp t
WT-	1481	6691	291	5.1
WT+	22	2000	87	0. 3
M337V -	14	4962	216	0.07
M337V+	1.3	2701	117	0.01
CTL		23	1	0

Area	Pabp	TDP	TDPn	Pabp t
WT	4.5	104	1.1	4.2
M337V	0.9	191	2	0.5
CTL		96	1	0

Fig. 6.1. to be continued on next page

Fig. 6.1. continued. The interaction of Poly(A)-binding protein to human TDP-43 is disrupted by the M337V mutation in mouse motor neurons

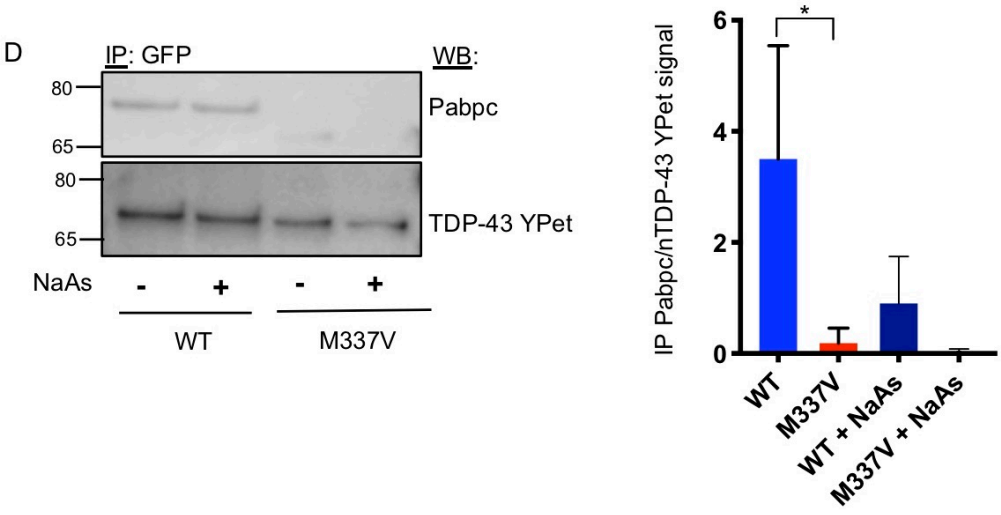


Fig. 6.1. Co-IP of human YPet-tagged TDP-43 from mouse MN lysates analysed for immunoreactivity of mouse Pabpc at 75kDa (left membrane). After stripping immunoreactivity of anti-GFP antibody, that detects human YPet-tagged TDP-43 at 72kDa confirms efficiency of the IP (right membranes). Supernatants after IP show that Pabpc is equally expressed and YPet-tagged TDP-43 depleted. The tables show the signal intensity of the bands outlined with dashed lines and total Pabpc levels (Pabp t) co-immunoprecipitated relative to the control (CTL) normalized human YPet-tagged TDP-43 levels.
A Co-IPs of human YPet-tagged TDP-43^{WT} and TDP-43^{M337V} +/- NaAs were compared. Here the supernatant after TDP-43^{M337V} IP contained less Pabpc. Equal levels of YPet-tagged TDP-43 of both genotypes were immunoprecipitated. Pabpc levels were reduced in TDP-43^{M337V} IPs +/- NaAs.
B Co-IPs of human YPet-tagged TDP-43^{WT} and TDP-43^{M337V} +/- NaAs were compared. A strong reaction of Pabpc was present in all supernatants, the immunoprecipitated levels of YPet-tagged TDP-43 varied between samples and demonstrates the importance of normalizing total co-IP Pabpc levels. Pabpc levels were reduced in TDP-43^{M337V} IPs +/- NaAs.
C Co-IPs of human YPet-tagged TDP-43^{WT} and TDP-43^{M337V} were compared. There was an nonspecific reaction at 65kDa after IP, but a clear 75kDa band was present in the human YPet-tagged TDP-43^{WT} immunoprecipitated sample representing Pabpc. The right membrane was immunoblotted with anti-TDP-43 antibody and showed equal enriched YPet-tagged TDP-43 levels at 72kDa, while mouse Tdp-43 at 45kDa remains depleted.
D Enlargement of representative YPet-tagged TDP-43 IP immunoblot (A) for detection of Pabpc signal relative to human YPet-tagged TDP-43. Quantification of all immunoblots (A-C) shows that Pabpc levels relative to normalized human YPet-tagged TDP-43 are significantly lower in TDP-43^{M337V} compared to TDP-43^{WT} IPs (*, $p<.05$, unpaired t-test). n=3 independent differentiations. After 60 minutes of 0.5mM NaAs treatment Pabpc levels are lower in TDP-43^{M337V} +NaAs IPs ($p>.05$, unpaired t-test). n=2 differentiations.
Abbreviations: IP, immunoprecipitation; WB, western immunoblot; MN, motor neuron.

6.2.2. The M337V mutation alone is not sufficient to cause an interruption of exogenous expressed TDP-43 and PABPc binding in HEK293T cells

To see if the binding of Pabpc to TDP-43 was directly interrupted by the M337V mutation full-length TDP-43, TDP-43 with the M337V mutation and an N-terminal truncated TDP-43 constructs were expressed in human HEK293T cells to investigate the direct protein interaction of exogenously expressed TDP-43 and PABPc and whether this interaction is RNA dependent.

6.2.2.1. Expression of exogenous TDP-43 constructs in HEK293T cells

Different constructs of TDP-43, each with a C-terminal protein tag, were cloned and expressed in HEK293T cells. First, a DNA vector with human full-length TDP-43 with a C-terminal turboGFP protein tag was commercially obtained to transform Stbl3 chemically competent E. coli. DNA from selected bacterial clones was extracted and digested with restriction enzymes to confirm the vector DNA. According to the vector sequence Nde1 restriction lead a 1.0kb and 6.8kb DNA fragment on agarose gel (Fig. 6.2. A). Age1 and Not1 restriction lead to fragments of the expected molecular weights of 6.5kb and 1.3kb. The DNA of selected clones were then sent for Sanger sequencing using primers flanking TDP-43 (Table 2.5.) and the sequence of human full-length TDP-43 was confirmed. To obtain a vector without human TDP-43 for empty control transfections, human TDP-43 was excised from the vector applied above using ACC651 and BsiWi restriction enzymes under preservation of the turboGFP protein tag. Restriction enzymes successfully excised a 1200bp fragment, corresponding to human full-length TDP-43, with the remainder open vector at 7000bp confirmed on an agarose gel.

Fig. 6.2. Cloning for expression of human full-length TDP-43, M337V mutant TDP-43 and N-terminal truncated C-terminal TDP-43 in HEK293T cells

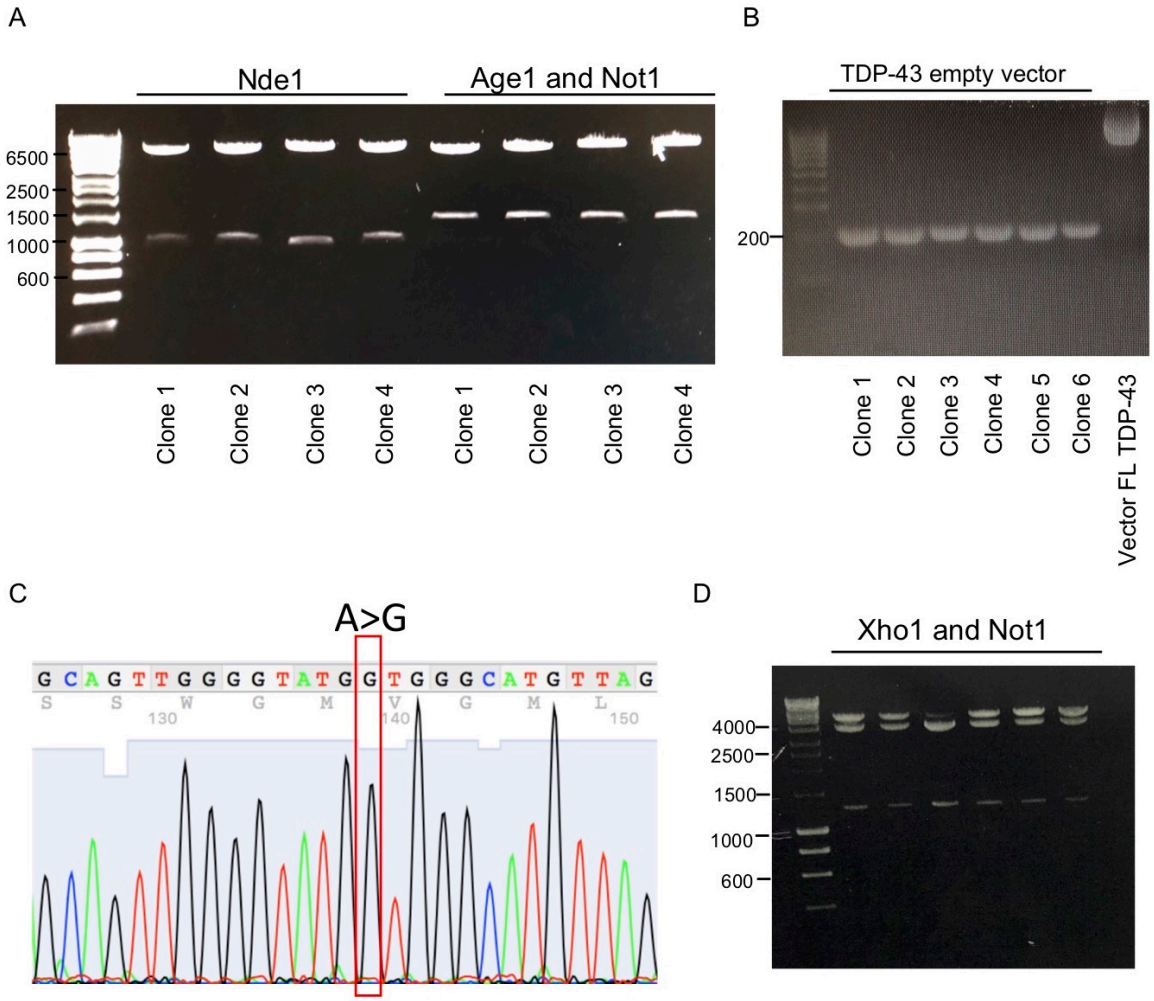


Fig. 6.2. A Restriction enzyme digests of plasmid DNA with turboGFP-tagged full-length TDP-43 shows expected restriction fragments at 1000 and 6800bp for Nde1, and 1300bp and 6500bp for Age1 and Not1 after digestion on agarose gels. **B** After excision of human TDP-43 from the background vector, a PCR with primers flanking the human TDP-43 sequence results in a shorter PCR product of 238bps. **C** Sanger Sequencing after site-directed mutagenesis confirms missense mutation A>G in the human full-length TDP-43 sequence. **D** Restriction enzyme digest of plasmid DNA with the EGFP-tagged C-terminal TDP-43 shows the expected restriction fragments at 1222bp and 3946bp for Xho1 and Not1 on an agarose gel.

After extraction of the 7000bp open vector DNA from the gel, the open vector ends were ligated and used for transformation. PCR of the human TDP-43 empty vector DNA amplified the expected shorter 238bp DNA sequence, when using the primers originally flanking the 1400bp human TDP-43 sequence (Fig. 6.2. B). Only successfully ligated vectors were taken up by the bacteria during transformation and conferred antibiotic resistance, resulting in fewer bacterial colonies. DNA extracted from the selected colonies was sent for Sanger sequencing using the same primer pairs as for the sequencing of TDP-43 to confirm its absence. Next, the full-length TDP-43 construct underwent site-directed mutagenesis to obtain the missense mutation M337V by exchange of the base A>G. After cloning the TDP-43 missense mutation A>G at position 139 was confirmed by Sanger sequencing (Fig 6.2. C). Last, the C-terminal TDP-43 construct ranging from amino acid 257-414 with a C-terminal EGFP protein tag was commercially purchased on agar and used for bacterial expansion. Individual clones were picked and the DNA extracted for Sanger sequencing to confirm the C-terminal TDP-43 sequence.

6.2.2.2. The interaction of TDP-43 with Poly(A)-binding protein is not abrogated by the M337V mutation, when expressed exogenously in HEK293T cells

All TDP-43 constructs were transfected into HEK293T cells to explore the interaction of TDP-43 and PABPc. First turboGFP-tagged full-length TDP-43 and TDP-43 with the M337V mutation were compared, with additional use of the human TDP-43 empty control vector. Of note, the human TDP-43 empty vector still contained the turboGFP tag to allow affinity enrichment. First, turboGFP was immunoprecipitated using anti-turboGFP antibody-coated beads to investigate the binding of PABPc to full-length TDP-43 and M337V mutant TDP-43. Then the reverse experiment was conducted by

immunoprecipitating PABPc to confirm the binding of human TDP-43 to PABPc. Immunoprecipitation of turboGFP from the TDP-43 empty vector transfected cells led to an enrichment of the turboGFP tag at 30kDa (Fig. 6.3. B). Immunoprecipitation of turboGFP from cells transfected with turboGFP-tagged full-length or M337V mutant TDP-43 led to the immunoprecipitation of both full-length TDP-43 and M337V mutant TDP-43 at 72kDa (Fig. 6.3. A). At the same time PABPc co-immunoprecipitated with both TDP-43 forms. However, HEK293T cells expressing M337V mutant TDP-43 showed a slight reduction of PABPc interaction without reaching statistical significance (n=2) (Fig. 6.3. A). Equal levels of PABPc were present in the input samples, which were loaded at the same amount confirmed by equal ß-tubulin levels. In these experiments the binding of PABPc to exogenous expressed full-length TDP-43 forms was investigated, while the endogenous TDP-43 was not immunoprecipitated using anti-turboGFP antibody-coated beads. In the reverse experiment endogenous PABPc was immunoprecipitated and immunoblots analysed for co-immunoprecipitation of the turboGFP-tagged TDP-43 constructs. Relative to the immunoprecipitated PABPc levels turboGFP-tagged full-length, but also M337V mutant TDP-43 bound equally to PABPc (Fig. 6.3. C). It was also confirmed that PABPc does not bind to the turboGFP tag of the TDP-43 empty vector, which proves that the binding of PABPc to TDP-43 is specific. Together this data indicates that the M337V mutation of in exogenously expressed full-length TDP-43 is not sufficient to interrupt the binding of PABPc in HEK293T cells.

Fig. 6.3. The interaction of Poly(A)-binding protein and human TDP-43 is unaltered by the M337V mutation, when transiently expressed in HEK293T cells

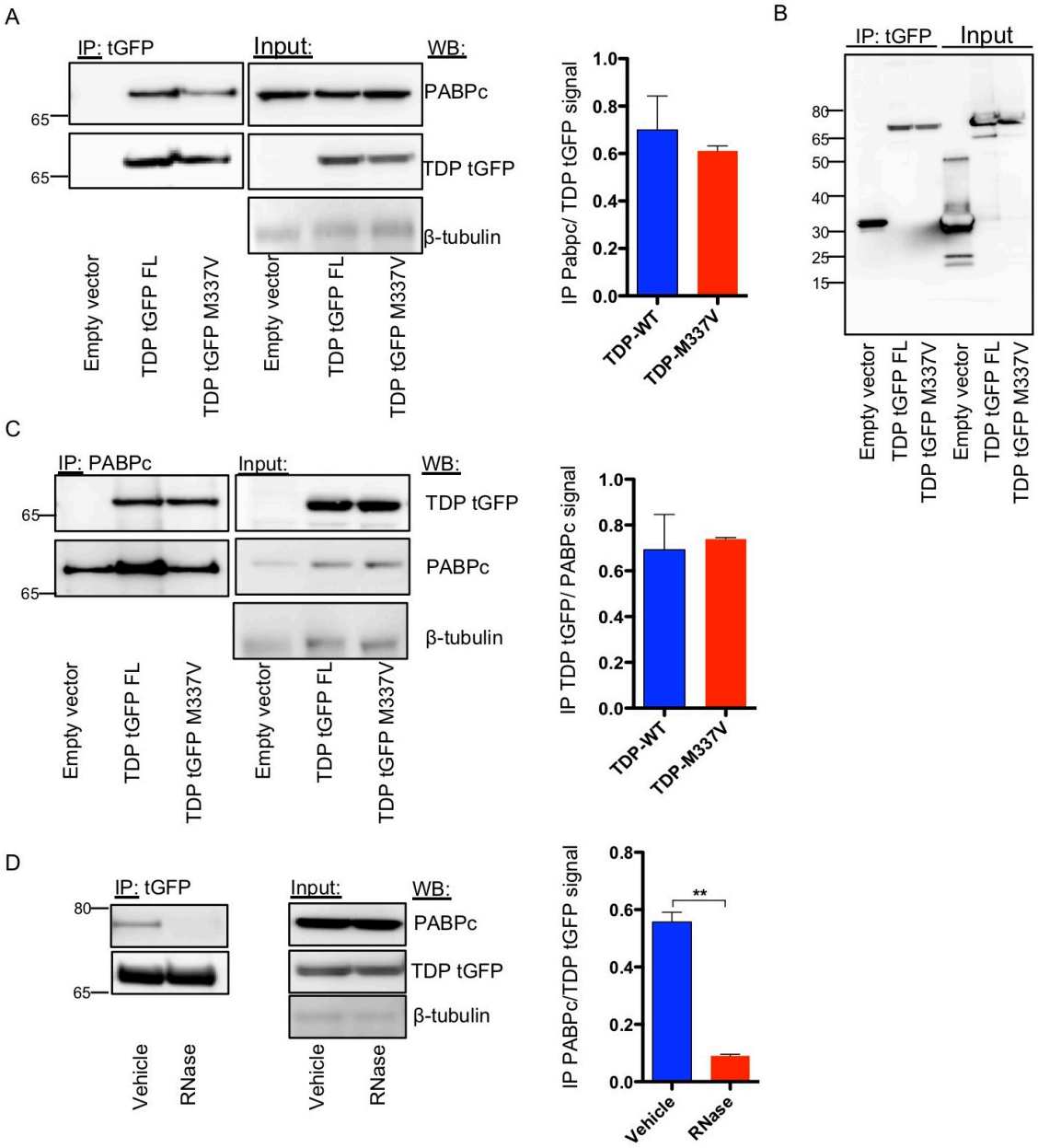


Fig. 6.3. A Co-IP of turboGFP from human turboGFP-tagged full-length or M337V mutant TDP-43 transfected HEK293T cell lysates. Immunoblot for PAPBc shows immunoreactivity in both full-length and M337V mutant IPs. PABPc does not bind to the empty vector which contains turboGFP. The interaction of overexpressed human full-length TDP-43 and Pabpc is disrupted by the M337V mutation but not abolished. Co-IP of PABPc from GFPturbo-tagged human TDP-43 +/- M337V transfected HEK293T cells shows lower PABPc levels bound to TDP-43^{M337V}. Equal immunoreactivity levels of GFPturbo-tagged TDP-43 at 72kDa confirm the efficiency of the IP. Input shows equal levels for TDP-43, PABPc and ß-Tubulin. Quantification shows PABPc levels are marginally lower in human TDP-43 M337V overexpressed samples ($p>0.05$, unpaired t-test). n=2 differentiations. **B** Full western blot of A anti turboGFP antibody reaction shows turboGFP is immunoprecipitated from empty vector transfected cell lysates at 30kDa. **C** Reverse Co-IP of PABPc. The interaction of human full-length TDP-43 and PABPc is unaltered by the M337V mutation ($p>0.05$, unpaired t-test). n=2 differentiations. **D** Samples +/- RNase treatment were immunoprecipitated for human turboGFP-tagged TDP-43. Immunoreactivity for PABPc at 75kDa was abolished by RNAse treatment of TDP-43^{WT} samples (**, $p<0.001$, unpaired t-test). n=2 differentiations. Abbreviations: IP, immunoprecipitation; WB, western immunoblot; FL, full-length; TDP tGFP, turboGFP-tagged TDP-43.

6.2.2.3. The binding of Poly(A)-binding to N-terminal truncated TDP-43 is reduced

To test, if PABPc binds to the C-terminal region of TDP-43, a N-terminal truncated TDP-43 construct of TDP-43 covering amino acid 257-414 with a C-terminal EGFP tag was expressed in HEK293T cells. This region of TDP-43 is N-terminally truncated excluding most of the second RNA-recognition motif. Expression lead to immunoreaction at 47kDa which is the size of the C-terminal fragment (17kDa) plus the EGFP tag (30kDa). Notably, this molecular weight overlaps with the size of endogenous TDP-43 (48kDa). Immunoprecipitation using anti-GFP antibody-coated beads shows a strong enrichment of the EGFP-tagged C-terminal TDP-43 at 47kDa, with a few lower molecular bands ranging around 25kDa (Fig. 6.4. A). At the same time a slight reaction for co-immunoprecipitated PABPc at 75kDa is present and also a lower band for PABPc at 50kDa, that has not been observed in co-immunoprecipitations of full-length TDP-43. The input levels of PABPc were equally distributed at 75kDa. When conducting the reverse immunoprecipitation with an antibody directed against PABPc, a slight co-immunoprecipitation of the EGFP-tagged C-terminal TDP-43 was observed (Fig. 6.4. B). However, compared to the input sample, which shows a strong expression level of the EGFP-tagged C-terminal TDP-43 at 47kDa, and the interaction that was observed for full-length TDP-43, the binding of the C-terminal TDP-43 to PABPc was weak. It can be concluded that PABPc does bind to the C-terminal region (aa 257-414) of TDP-43, however the binding is weaker compared to full-length TDP-43.

Fig. 6.4. The interaction of Poly(A)-binding protein to N-terminal truncated TDP-43 is reduced in HEK293T cells

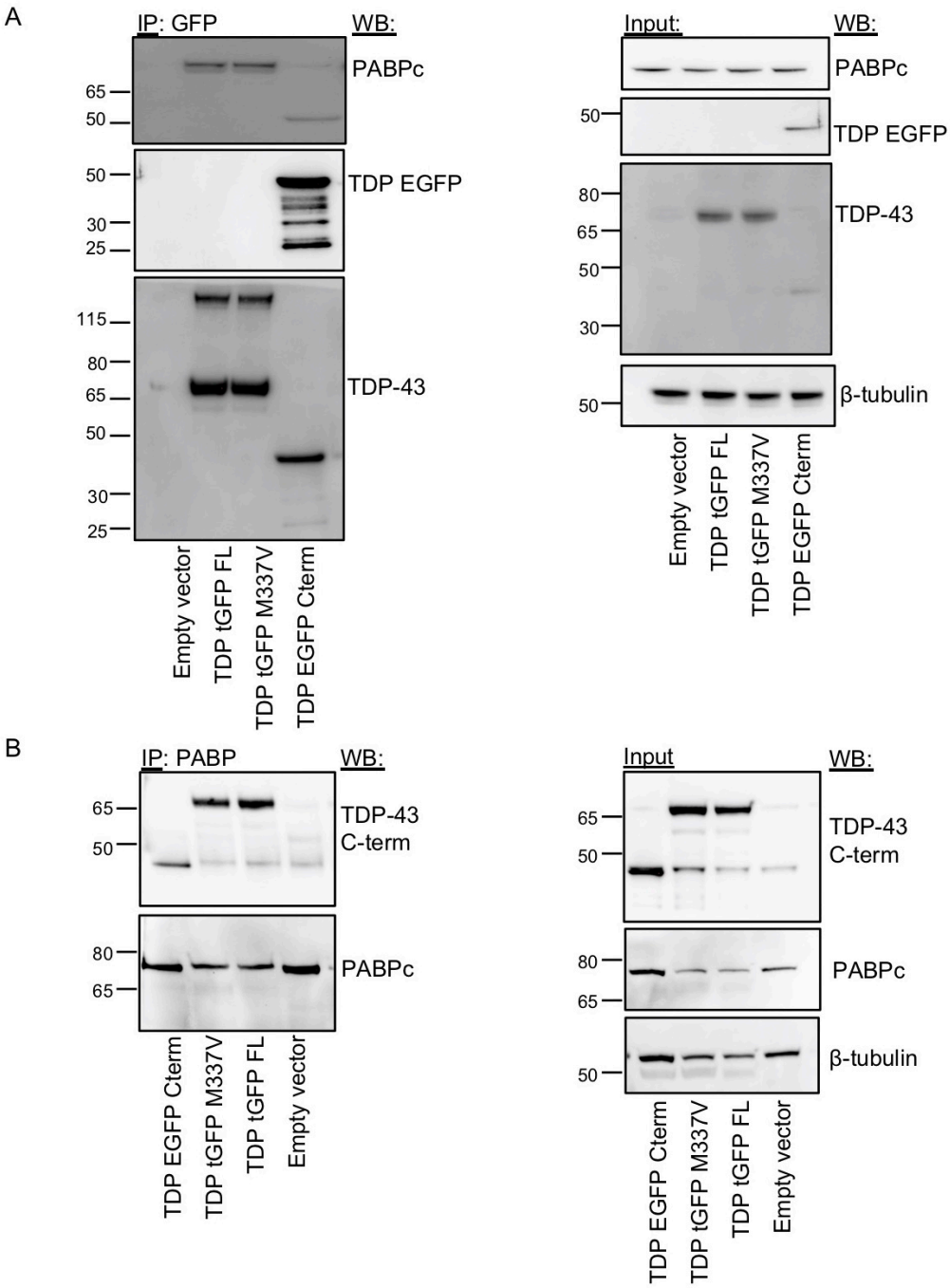


Fig. 6.4. A Co-IP of turboGFP or EGFP from tGFP-tagged FL, M337V mutant or EGFP-tagged C-terminal TDP-43 transfected HEK293T cell lysates. Immunoblot for PAPBc shows immunoreactivity in both FL and M337V mutant TDP-43 IPs. PABPc does not bind to the TDP-43 empty vector. PABPc immunoreactivity at 75kDa is lower in the C-terminal TDP-43 IP and has an additional band at 50kDa. EGFP-tagged C-terminal TDP-43 at 48kDa (EGFP and TDP-43 WB) and tGFP-tagged TDP-43 at 72kDa (TDP-43 WB) are enriched after IP (left membrane). Inputs show that PABPc, tGFP-tagged TDP-43 and EGF-tagged C-terminal TDP-43 are equally expressed (right membrane). **B** Reverse Co-IP of PABPc and subsequent immunoblotting using an anti-C-terminal TDP-43 antibody shows that both human FL and M337V mutant TDP-43 are equally co-immunoprecipitated with PABPc, while the C-terminal TDP-43 is reduced, suggesting impaired interaction. PABPc IP from empty vector transfected cells shows a slight nonspecific reaction to endogenous TDP-43 at 45kDa. IPs are enriched for PABPc at 75kDa (left membrane). Input samples show equal expression of all target proteins (right membrane). The loading control with ß-tubulin immunoreacts at 52kDa. Abbreviations: IP, immunoprecipitation; WB, western immunoblot; FL, full-length; TDP tGFP, turboGFP-tagged TDP-43; TDP EGFP, EGFP-tagged TDP-43.

6.2.2.4. Interaction of Poly(A)-binding protein to TDP-43 is RNA dependent

PABPc is a protein involved in translation and binds to the poly(A)-tail of RNA. At the same time TDP-43 is involved in translation and has two RNA-recognition motifs for regulation. To test if the binding of PABPc to full-length TDP-43 is RNA dependent, immunoprecipitation experiments were conducted in the absence and presence of RNase. In this experiment lysates were exposed to RNase prior to immunoprecipitation (n=2). The turboGFP-tagged full-length and M337V mutant TDP-43 interaction with PABPc was almost entirely abrogated by RNase treatment (p=0.006) (Fig. 6.3. D). Again, the levels of PABPc and full-length TDP-43 or M337V mutant TDP-43 were equally expressed after RNase treatment as shown in the input samples. This suggests that the binding of PABPc to TDP-43 is RNA-dependent, in accordance with the well-established role of TDP-43 as an RNA-binding protein. This would also explain why the C-terminal TDP-43 construct lacking its RNA-recognition motifs is not capable of binding PABPc to the same extent as full-length TDP-43.

6.2.2.5. Immunoprecipitation of TDP-43 from human fibroblasts derived from an ALS patient with the heterozygous TDP-43$^{M337V/-}$ mutation is impaired

Given that the transient expression of human TDP-43^{M337V} in HEK293T cells was not sufficient to cause an interruption of the interaction with PABPc compared to *TDP-43$^{M337V/-}$* (BAC)-transgenic mouse motor neurons, human fibroblasts from an ALS patient carrying the *TDP-43 M337V* mutation were investigated. ALS fibroblasts were compared with two separate healthy control lines. However, Immunoprecipitation of TDP-43 from ALS fibroblast lysates was impaired compared to healthy control. Due to the different levels of immunoprecipitated TDP-43 the interaction with PABPc between healthy control and ALS fribroblasts could not be investigated (Fig. 6.5.). Impaired immunoprecipitation of

endogenous TDP-43 from the human *TDP-43*$^{M337V/-}$ fibroblast lysates may suggest that antibody-binding is impaired resulting in less TDP-43 protein levels bound. This might suggest that TDP-43^{M337V} in human ALS fibroblasts is pathological altered or undergoes change in protein confirmation or turnover.

Fig. 6.5. Immunoprecipitation of TDP-43 from human ALS fibroblasts with a heterozygous *TDP-43 M337V* mutation is impaired

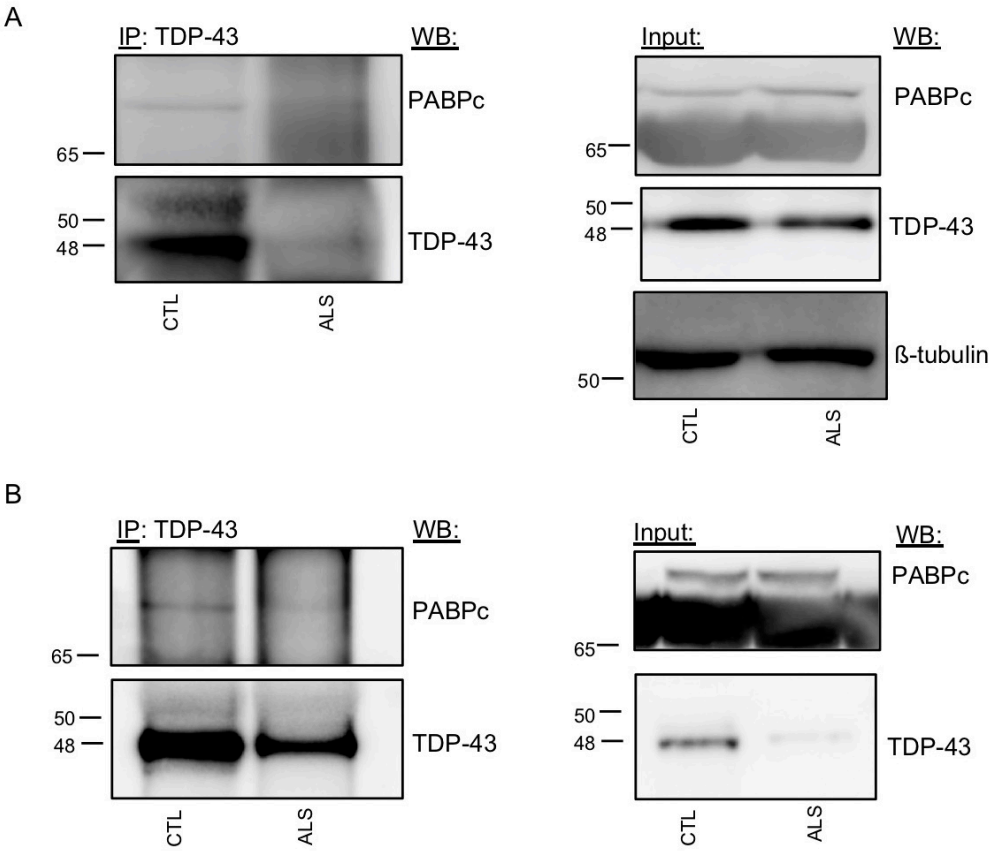


Fig. 6.5. A Human endogenous TDP-43 Co-IP showed a reduced enrichment of TDP-43 from ALS compared to a healthy control (CTL) fibroblast lysates. Inputs showed equal levels of TDP-43, PABPc and ß-Tubulin. The binding between PABPc and TDP-43 was not comparable due to different immunoprecipitated TDP-43 levels between genotypes. **B** TDP-43 Co-IP showed slightly lower endogenous TDP-43 levels in ALS compared to CTL. The binding of PABPc to TDP-43 was not evaluated. Input showed equal levels of PABPc, but less TDP-43 in the ALS input lysate compared to CTL.

6.2.3. Phenotypic characterization of *TDP-43$^{M337V/-}$* motor neurons reveal impaired functions relevant to identified pathways containing human TDP-43 interactors

The interactome data revealed that many interactors were affected by the M337V mutation. The disturbance of Pabpc binding, an important interaction of TDP-43, was validated by co-immunoprecipitation experiments. To investigate the functional consequences of disturbed protein-protein interactions, mouse motor neurons were screened for phenotypic changes. Based on the interactome data I focused on the formation of Pabpc-positive stress granules and on extracellular vesicle secretion.

6.2.3.1. Reduced formation of stress granules in response to oxidative stress treatment

Stress granules are RNA-containing cytoplasmic foci formed through liquid-liquid phase separation, and are enriched for low complexity domain-containing proteins, including TDP-43 and Pabpc, a well-established stress granule marker (Colombrita *et al.*, 2009). It has been demonstrated that stress granule formation is impaired in M337V mutant primary motor neurons from the (BAC)-transgenic mouse model in response to oxidative stress (Gordon *et al.*, 2019). It has also been shown that the number of *TDP-43$^{M337V/-}$* (BAC)-transgenic mESC-derived motor neurons with stress granules is reduced compared to *TDP-43$^{WT/-}$* motor neurons after 60 minutes of 0.5mM sodium arsenite (NaAs) treatment. Therefore, I investigated if the impaired interaction between TDP-43^{M337V} and Pabpc resulted in the same functional consequences under those stress conditions and if the stress granule number and size per motor neuron is different between genotypes.

To observe stress granule formation motor neuron cultures were immunostained for Pabpc and the neuronal marker Tuj1. Although Tuj1 is not a motor neuron-specific marker, it was shown in the previous Chapter that more than 70% of Tuj1-positive neurons overlap with

the early motor neuron-specific marker Islet1. Tuj1 has a good staining quality and was therefore preferred for the co-immunostaining with Pabpc. First the time evolution of stress granules was investigated by immunostaining. Neurons were stained in basal conditions, 30 and 60 minutes after 0.5mM NaAs stress treatment and 6 hours after recovery. In basal conditions, Pabpc was constitutively expressed in the cytoplasm of Tuj1-positive mouse neurons. After 30 and 60 minutes of NaAs treatment Pabpc-positive stress granules formed, which were largely resolved after 6 hours of stress recovery (Fig. 6.6.). To quantify motor neurons with stress granules between genotypes, the experiment was restricted to basal conditions and 60 minutes of NaAs stress treatment. After 60 minutes of treatment with 0.5mM NaAs a reduction in the number of motor neurons with Pabpc-positive stress granules was found in *TDP-43*$^{M337V/-}$ compared to *TDP-43*$^{WT/-}$ cultures, suggesting that stress granule assembly is impaired by the mutation ($p=0.0004$) (Fig. 6.7. A). Using an automated macro-analysis for the detection of stress granules, individual stress granules can be detected, when they are in the size range between 200nm to 1.5µm (Fig. 6.7. B). With this analysis individual neuronal cells stained with Tuj1 were assessed for the number of stress granules per cell and the area per stress granule. This automated experiment confirmed a decreased number of Pabpc-positive stress granules per neuron in *TDP-43*$^{M337V/-}$ cultures ($p=0.019$) and a decreased total stress granule area per neuron, with a mean area of 376nm^2 in *TDP-43*$^{M337V/-}$ neurons compared to 806nm^2 in *TDP-43*$^{WT/-}$ neurons ($p=0.013$). Together, these data suggest that altered binding of human TDP-43^{M337V} to Pabpc, potentially affects an established physiological role of these proteins in early stress granule formation. Co-localization experiments were performed using human TDP-43 (BAC)-transgenic HEK293T cells. While in response to NaAs stress treatment for 60 minutes a positive co-localization signal of the stress granule markers PABPc and G3BP was shown in human *TDP-43*$^{WT/-}$ and *TDP-43*$^{M337V/-}$ HEK293T cells, no co-localization signal was present for human YPet-tagged TDP-43 and PABPc during the formation of stress granules (Fig 6.8.).

This result was expected due to the preserved nuclear localisation of human TDP-43 in (BAC)-transgenic mouse motor neurons in response to oxidative stress as shown in the previous Chapter (Fig. 5.2. C).

Fig. 6.6. Time course of Poly(A)-binding protein-positive stress granule formation in response to 0.5mM NaAs treatment in *TDP-43$^{WT/-}$* and *TDP-43$^{M337V/-}$* mouse motor neurons

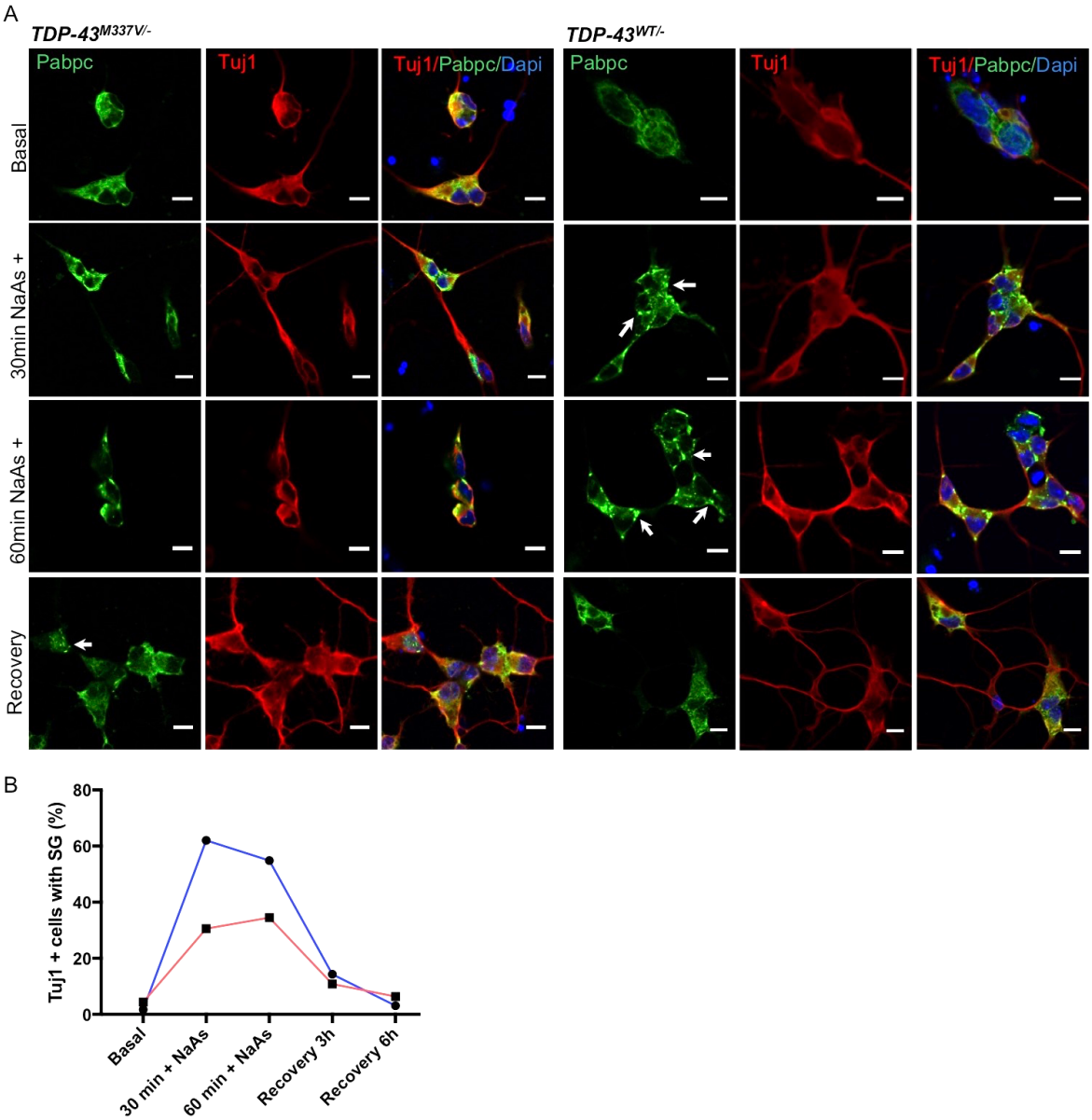


Fig. 6.6. A The formation of Pabpc-positive stress granules in response to different times of 0.5mM NaAs treatment in human *TDP-43$^{M337V/-}$* (left panel) and *TDP-43$^{WT/-}$* (right panel) mouse motor neurons. Immunohistochemistry for Pabpc (green) and neuronal marker Tuj1 (red). Basal, 30 minutes or 60 minutes of 0.5mM NaAs exposed cultures and cultures recovered for 6 hours from NaAs treatment. **B** When exposed to 0.5mM NaAs treatment for 30 and 60 minutes a reduced formation of Pabpc-positive stress granules was observed in the *TDP-43$^{M337V/-}$* motor neurons (red line) compared to *TDP-43$^{WT/-}$* motor neurons (blue line). Arrows indicate Pabpc-positive stress granules (n=1 differentiation). Scale bar 50µm. Abbreviations: DAPI, 40,6-Diamidino-2-Phenylindole; MNs, motor neurons.

Fig. 6.7. Poly(A)-binding protein-positive stress granule formation is reduced in *TDP-43$^{M337V/-}$* motor neurons treated with 0.5mM NaAs

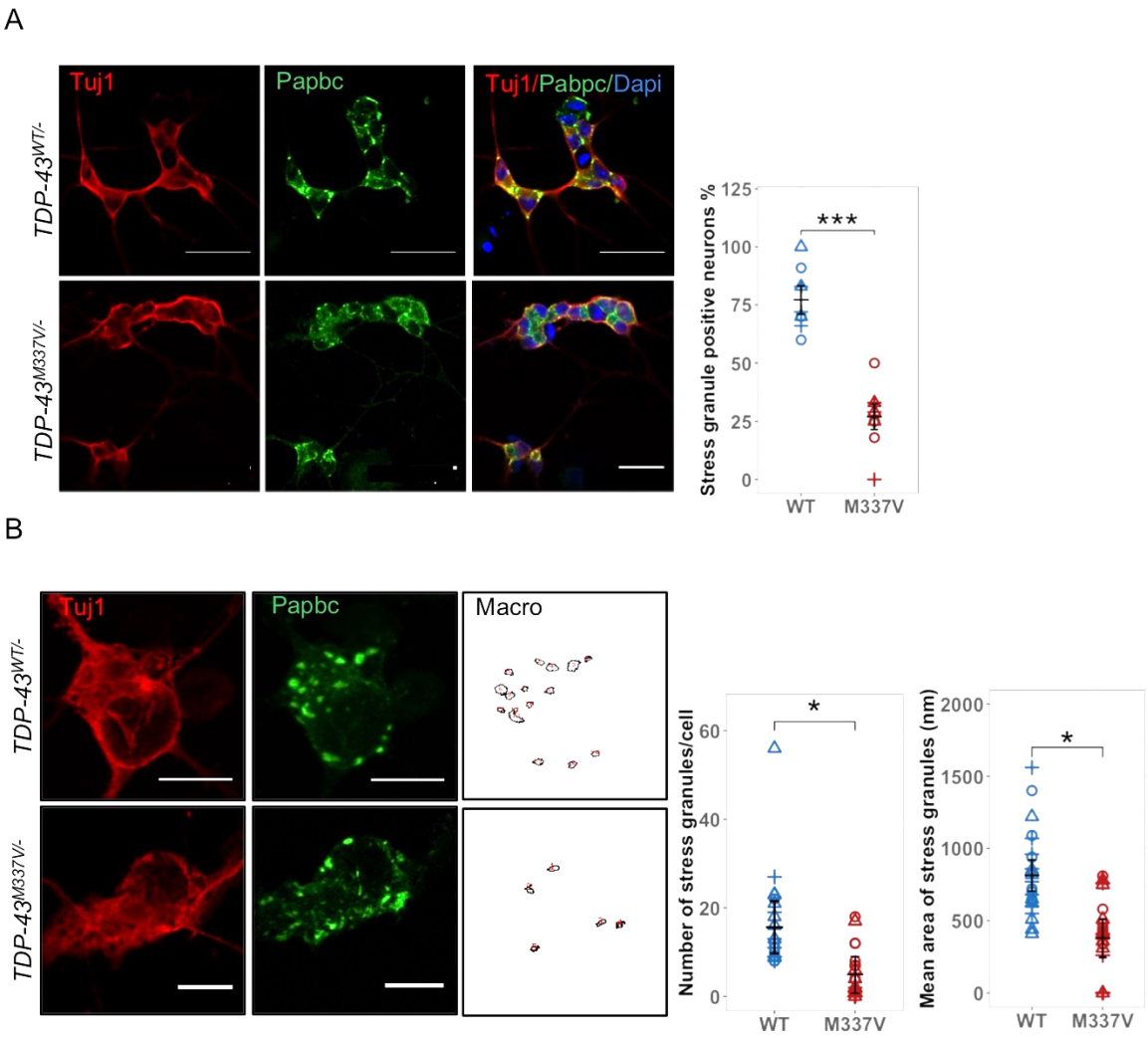


Fig. 6.7. A Immunostaining for Tuj1 and Pabpc in *TDP-43$^{WT/-}$* and *TDP-43$^{M337V/-}$* cell lines after 60 minutes of NaAs treatment, showing that *TDP-43$^{M337V/-}$* Tuj1-positive neurons with stress granules are reduced (***, p<0.001, unpaired t-test). Scale bar 30µm. Tuj1-positive neurons with Pabpc-positive stress granules are reduced in TDP-43$^{M337V/-}$ cells over time. **B** Immunostaining of Tuj1- and Pabpc-positive neurons for automated macro analysis to assess the number and size of stress granules per cell. Scale bar 10µm. Quantification shows the number and average area (nm) of stress granules per neuron are reduced in *TDP-43$^{M337V/-}$* motor neurons (both *, p<.05, unpaired t-test). n=3 independent differentiations. Data are represented as mean±SD.

Fig. 6.8. Human YPet-tagged TDP-43 does not co-localize with Poly(A)-binding protein-positive stress granules

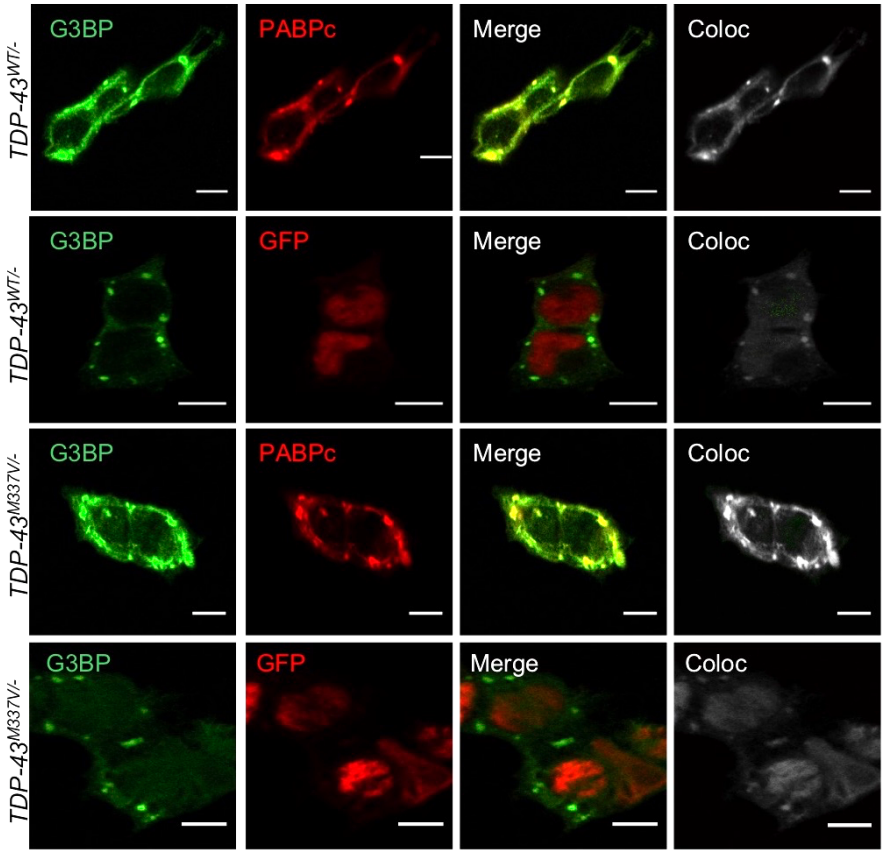


Fig. 6.8. Co-localisation of PABPc and G3BP in human *TDP-43$^{WT/-}$* and *TDP-43$^{M337V/-}$* (BAC)-transgenic HEK293T cells is shown in the top row for each genotype representing stress granule formation after treatment with 0.5mM NaAr for 60 minutes. In comparison, human YPet-tagged TDP-43 stained with an anti-GFP antibody and G3BP is shown in the bottom row of each genotype and is negative for any co-localisation signal. Scale bar 10µm. Abbreviations: Coloc, Co-localisation signal.

6.2.3.2. Reduced vesicle secretion in response to stress treatment

In response to stress the TDP-43^{WT} interactome was highly enriched in proteins of the endosomal-exosomal pathway. Notably, Rab-GTPase7, which functions to target endosomal trafficking towards extracellular secretion, was found as a putative interactor of TDP-43^{WT}. Other important proteins such as Rab-GTPase11a involved in late endosomal pathways, but also Transmembrane emp24 domain-containing proteins involved in the early secretory pathways, the Golgi apparatus and also in the processing of amyloid, were found in the TDP-43^{WT} interactome (Vetrivel *et al.*, 2007). By mass spectrometry it was also shown that these interactions are abolished by the TDP-43^{M337} mutation, which showed a shift towards VPS41 regulation of endosomal-lysosomal degradation. The relevance of endosomal trafficking and extracellular vesicles secretion in TDP-43 pathology was therefore explored in *TDP-43$^{M337V/-}$* mouse motor neuron cultures by studying the effect of the M337V mutation on extracellular vesicles secretion.

To investigate secretion of extracellular vesicles, this study aimed to enumerate the number of vesicles secreted within a defined time in the presence or absence of stress exposure into the culture condition media. To guarantee equal numbers of motor neurons for the collection of conditioned media, precursor cells were initially plated at the same density and after conditioned media collection the final number of cells grown per dish was confirmed by cell counting after trypsinization. This ensured that in all experiments, culture media was collected from equal amounts of plated mouse motor neurons, with no differences occurring between genotypes after trypsinization ($p=0.372$) (Table 6.1.). Conditioned media of each condition was prepared and referred to ultrafiltration liquid chromatography and the number of extracellular vesicles was quantified by nanoparticle tracking analysis (NTA). Under basal conditions, no difference in the total number of extracellular vesicles recovered per ml of conditioned media was detectable between genotypes ($p= 0.56$) (Fig. 6.9. A). However,

after 60 minutes of 0.5mM NaAs stress treatment, a reduction in the number of vesicles was seen in conditioned media from *TDP-43$^{M337V/-}$* cells across a total of four separate differentiations (p=0.048). This suggests that the M337V mutation affects extracellular vesicle secretion in the context of cellular stress. To verify that the reduced number derives from extracellular vesicles, the concentrated extracellular vesicle peak fractions were analysed by size using NTA. The size distribution in both genotypes was characteristic of a mixed population of extracellular vesicles. The number of vesicles in the size range 40-100nm, which is typical of exosomes arising from endosomal pathways, and vesicles of the size range typical of a mixed population of extracellular vesicles (>100nm) were significantly decreased in mouse *TDP-43$^{M337V/-}$* motor neurons (Fig. 6.9. B) (Thery *et al.*, 2006).

Table 6.1. Cell number and viability per plate

Differentiations (n=4)	Number of cells Plated/ Well	Number of cells Trypsinization/ Well	Condition media Volume total (ml)
TDP-43$^{M337V/-}$	1Mio	230.000/	6
TDP-43$^{WT/-}$	1Mio	250.000	6
TDP-43$^{M337V/-}$	1Mio	260.000	7
TDP-43$^{WT/-}$	1Mio	220.000	7
TDP-43$^{M337V/-}$	1Mio	250.000	6
TDP-43$^{WT/-}$	1Mio	300.000	6
TDP-43$^{M337V/-}$	1Mio	250.000/	6
TDP-43$^{WT/-}$	1Mio	300.000	6

Fig. 6.9. In response to stress extracellular vesicle secretion is decreased in *TDP-43$^{M337V/-}$* mouse and ALS iPSC-derived motor neurons

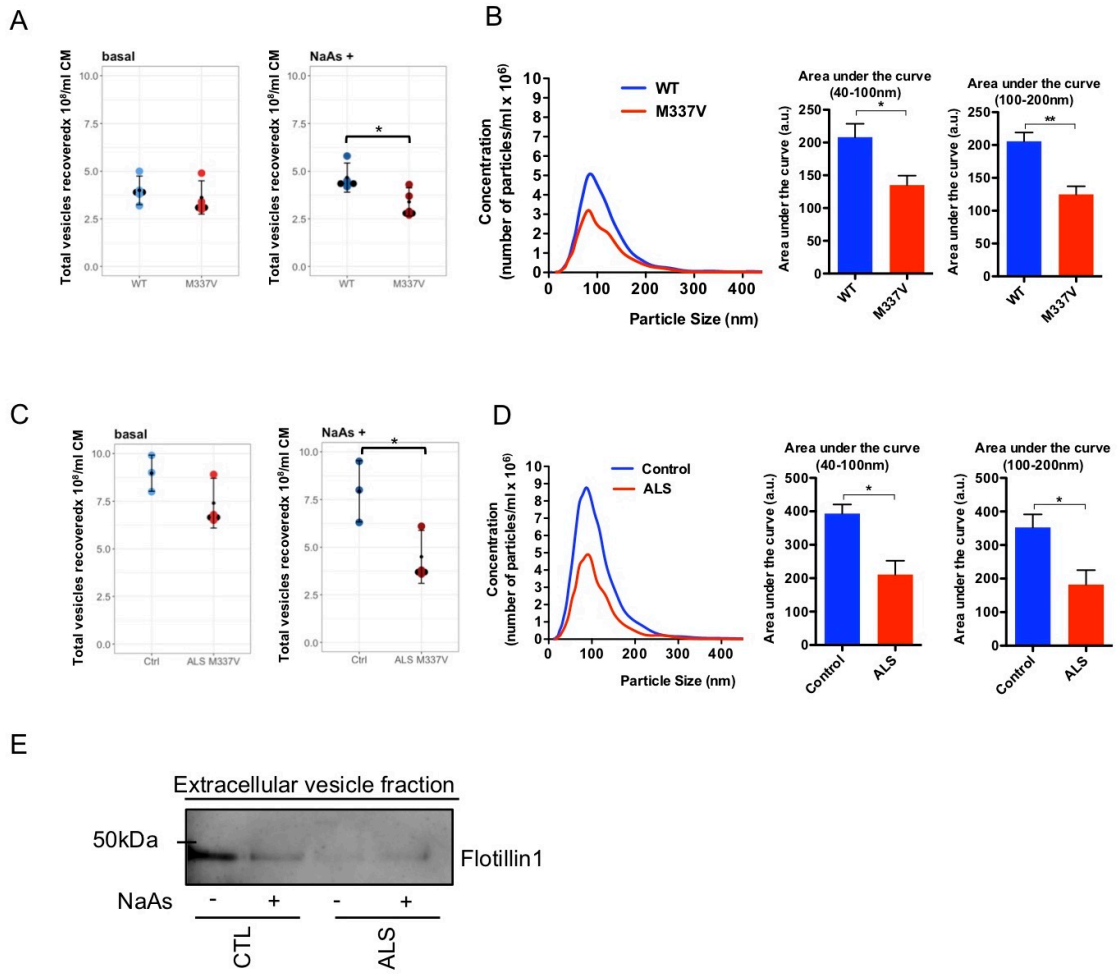


Fig. 6.9. A Total number of vesicles recovered per ml of condition media *TDP-43$^{M337V/-}$* and *TDP-43$^{WT/-}$* mouse motor neurons in basal condition (p>.05) and in response to 60 minutes of 0.5mM NaAs (*, p<.05, unpaired t-test). n=4 independent differentiations **B** Size distribution of extracellular vesicles given as total number per ml of conditioned media in response to stress. Extracellular vesicle peak at 85nm is decreased for conditioned media from *TDP-43$^{M337V/-}$* motor neurons. The Area under the curve for exosomes (40-100nm) and a mixed population of extracellular vesicles (100-200nm) is significantly decreased for *TDP-43$^{M337V/-}$* motor neurons (*p<.05 and **, p<.01, unpaired t-test) **C** Total number of vesicles recovered from hiPSC-derived motor neuron conditioned media from three healthy control lines and three clonal lines of an ALS patient with the M337V mutation in basal condition (p>.05) and in response to stress (*, p<.05, unpaired t-test). n=3 independent differentiations **D** Size distribution of extracellular vesicles given as total number per ml of conditioned media in response to stress. Extracellular vesicle peak at 93nm is decreased for conditioned media from ALS motor neurons. The Area under the curve for exosomes (40-100nm) and a mixed population of extracellular vesicles (100-200nm) is significantly decreased for ALS motor neurons (both *p<.05, unaired t-test). **E** Immunoblot shows Flotillin-1 positive bands for combined vesicle fractions two and three from control and ALS hiPSC-derived motor neurons +/- NaAs. Data are represented as mean±SD. Abbreviations: hiPSC, human induced pluripotent stem cells.

6.2.3.3. Extracellular vesicles secretion is decreased in human iPSC-derived motor neurons from an ALS patient with the heterozygous TDP-43$^{M337V/-}$ mutation

To further validate mass spectrometry data derived from mouse motor neurons in human cellular models, human iPSC-derived motor neurons from an ALS patient and healthy controls were additionally investigated for phenotypes explored in the ALS mouse model. The use of conditioned media of motor neuron cultures to enumerate extracellular vesicles has been previously shown in C9orf72 fibroblasts (Aoki *et al.*, 2017), however this has never been performed on iPSC-derived motor neuron cultures. Therefore, extracellular vesicles were extracted from conditioned media of equal density plated motor neuron cultures and enumerated for the total number of vesicles per ml conditioned media by NTA. The results showed a reduction in the total number of vesicles of a total of three separate differentiations in response to NaAs treatment in conditioned media from iPSC-derived motor neurons from an ALS patient with the M337V mutation compared to controls (three M337V ALS clone lines and 3 separate control lines) ($p=0.049$) (Fig. 6.9.C). This suggests that the M337V mutation affects extracellular vesicle secretion in human motor neurons when under stress. The size distribution showed that vesicles in the range between 40-100nm and 100-200nm, representative for exosomes and mixed extracellular vesicles, are reduced in *TDP-43$^{M337V/-}$*-derived motor neurons (Fig. 6.9. D). Extracellular vesicle fractions were confirmed by immunoblotting with an antibody against the exosome marker protein Flotillin-1 (Fig. 6.9. E). These results suggest that extracellular vesicle formation or release is impaired in human ALS iPSC-derived motor neurons by TDP-43^{M337V} and confirmed our findings from mouse motor neurons that a disruption of elements of the TDP-43^{WT} interactome in response to cellular stress alters cellular phenotypes.

6.3. Conclusion

This Chapter shows the validation of mutation dependent changes of the proteomic interactome data. First Pabpc, a known TDP-43 interactor, was investigated since abnormalities in stress granule dynamics have been previously identified as a robust *in vitro* phenotype in *TDP-43$^{M337V/-}$* mouse motor neurons (Freibaum *et al.*, 2010; Gordon *et al.*, 2019). I showed that the M337V mutation in mouse motor neurons affects its interaction, which is in contrast to previous data from overexpression models (Freibaum *et al.*, 2010) and related this to the known pathogenic phenotype of reduced stress granule formation. In addition, I showed that in response to stress extracellular exosome secretion (a pathway within the TDP-43^{WT} interactome that was affected by the M337V mutation, as described in Chapter 5) is reduced in *TDP-43$^{M337V/-}$* motor neurons.

The impaired interaction with Pabpc also suggests an important role of RNA processing in ALS, because of its function in translation initiation and mRNA decay regulation. Pabpc is known to assemble in polysomes with other proteins implicated in translational dysregulation in ALS including Ataxin 2 and Matrin 3 (Nonhoff *et al.*, 2007; Boehringer *et al.*, 2017). Binding of TDP-43 to Pabpc may therefore be an important mediator of RNA processing in the cytoplasm of motor neurons (Craig *et al.*, 1998; Ayala *et al.*, 2011; He *et al.*, 2014; Zhang *et al.*, 2014). This Chapter describes, how the interaction of human TDP-43^{M337V} with Pabpc is impaired in mouse motor neurons and ALS fibroblasts. However, this was not recapitulated, when TDP-43 with the M337V mutation was transiently overexpressed in HEK293T cells. This indicates that the M337V mutation is not in itself sufficient to interrupt the binding of PABPc to TDP-43, but according to this work and others, depends on the presence of RNA (Freibaum *et al.*, 2010). In (BAC)-transgenic mouse motor neurons TDP-43^{M337V} led to decrease in protein-protein interactions possibly altering its normal function. Many interactors which were affected by the M337V mutation are

important mediators of RNA-metabolism, among them Pabpc. The RNA-dependence of the PABPc and TDP-43 interaction was further evidenced showing that truncated TDP-43 lacking RNA-recognition motifs reduces the interaction. Hence it can be speculated that TDP-43^{M337V} affects normal RNA-binding in mouse motor neurons and human ALS fibroblasts leading to impaired interaction of Pabpc. This would also support the observation that proteins involved in ALS are less interactive and subsequently are able to cause translational repression as shown in the context of the C9orf72 mutation (Moens *et al.*, 2019).

To further investigate the direct functional consequence of the impaired binding of TDP-43^{M337V} to Pabpc, this thesis focused on the investigation of a phenotype of stress granule formation as read-out for Pabpc function. Oxidative stress is an important mediator of pathological processes and increases with aging. It has been shown as an important contributing factor to the pathology of neurodegenerative conditions and a potent trigger to stress granule formation (Guil *et al.*, 2006). Impaired binding of TDP-43^{M337V} to Pabpc in the (BAC)-transgenic mouse model is associated with altered stress granule formation in motor neurons, a phenotype that has also been described in other ALS disease models, and may be mediated by the dynamic interaction of a wide repertoire of cytoplasmic RNA-binding proteins (Markmiller *et al.*, 2018). Based on this study it was hypothesised that reduced binding between mutant TDP-43^{M337V} and Pabpc may impair the initial assembly of stress granules, ultimately resulting in a decreased number of motor neurons exhibiting stress granules. Of note, a direct interaction of human TDP-43^{WT} with the late core stress granule marker G3BP has not been observed (Freibaum *et al.*, 2010). Furthermore, the TDP-43^{M337V} interactome contained proteins that are known to inhibit the formation of stress granules such as the chaperonin-containing T complex (CCT complex) (Leitner *et al.*, 2012; Jain *et al.*, 2016), while chaperones including HSP90b1 and HSP90ab1 that are known to be

important for the assembly of stress granules were found to bind preferentially to TDP-43^{WT} (Matsumoto *et al.*, 2011). In TDP-43 overexpression models, stress granule formation has often been reported as increased and associated with toxic aggregate formation, giving rise to the theory that stress granules seed TDP-43 aggregation (Liu-Yesucevitz *et al.*, 2010; Li *et al.*, 2013; Chew *et al.*, 2019). However, a recent model in which TDP-43 proteinopathy is driven by optogenetic control has demonstrated that pathological aggregation of TDP-43 may occur independently of stress granule formation (Mann *et al.*, 2019). This together with the current data suggests that altered protein interactions of TDP-43^{M337V} may impair the immediate assembly of stress granule shells promoted by Pabpc (Kedersha and Anderson, 2002), and that this occurs prior to significant protein aggregation.

In response to oxidative stress TDP-43^{M337V} interacted with proteins of the ubiquitin-proteasome and lysosome, which have been independently linked to ALS pathogenesis (Wang *et al.*, 2010). As shown in the literature knock-down of TDP-43 has a direct impact on endosomal trafficking suggesting it has a role in this pathway (Schwenk *et al.*, 2016). Consistent with this observation this study showed that in response to stress TDP-43^{WT} interacts with the Ras-related protein 7 that targets vesicle transport to the plasma membrane and that the M337V mutation abolishes this interaction (Farg *et al.*, 2017). TDP-43^{WT} also interacted with proteins of the endosomal and endoplasmic reticulum pathways. In response to stress, *TDP-43$^{M337V/-}$* motor neurons showed a decrease in extracellular vesicle secretion compared to *TDP-43$^{WT/-}$* motor neurons. This was confirmed in human iPSC-derived motor neurons from an ALS patient with the M337V mutation. This suggests that recognition of TDP-43^{M337V} by the endosomal sorting complexes required for transport and secretion is impaired in ALS neurons (Colombo *et al.*, 2013). Whether this is due to a direct interaction such as the Ras-related proteins as suggested previously (Aoki *et al.*, 2017) or through an indirect mechanism such as activation of the proteasome-ubiquitin pathway by TDP-

43^{M337V}, as shown by our mass spectrometry data, remains to be investigated. Exosome secretion is known to be promoted by inhibiting proteasome pathways (Iguchi *et al.*, 2016). Ultimately, reduced cytoplasmic trafficking of TDP-43 is likely to be a factor in the formation of cytoplasmic TDP-43 aggregates observed in 95% of ALS cases and therefore could reflect a common therapeutic target upstream of protein aggregation (Winton *et al.*, 2008; Chen-Plotkin *et al.*, 2010). This chapter demonstrates that a single C-terminal mutation has multiple functional consequences resulting in a pathological stress response which, under chronic conditions, might ultimately result in decreased survival of motor neurons.

7. Discussion

The aim of the studies described in this thesis was to develop TDP-43 as a biomarker in ALS. My novel contributions to this field have been:

1. Detection of a disease-associated TDP-43 peptide from human ALS *post mortem* tissue
2. Quantification of an ALS disease-specific TDP-43 peptide signature by targeted proteomics
3. Identification of the human TDP-43 interactome in a (BAC)-transgenic mouse model
4. Characterisation of motor neuron phenotypes which are linked to altered TDP-43 interactome pathways

This chapter will discuss my results in the wider context of ALS research and outline suggestions for the direction of future research.

7.1. The current understanding of ALS and the relevance of studying TDP-43 as a disease-specific marker in ALS

ALS is a devastating neurodegenerative disease that leads to the degeneration of motor neurons. Motor neurons are post-mitotic cells, that are no longer able to divide, which makes them more vulnerable with age. They are the largest cells within the central nervous system that may have to supply distal muscles with processes of the length of up to one meter (Shaw, 1999). Remarkably, within the motor system there are neuronal subgroups which are more resistant to degeneration, such as the oculomotor neurons and motor neurons innervating slow-twitch muscles (Nijssen *et al.*, 2017). Although non-cell autonomous mechanisms have an effect on vulnerability such as interneurons, e.g. GABAergic inhibitory neuronal circuits, influencing excitability (Nihei *et al.*, 1993; Petri *et al.*, 2003; Turner and Kiernan, 2012) or

inflammatory cells as possible disease modulators (Thompson and Turner, 2019). Age is a risk factor of ALS, although some cases are observed in younger people (Baumer *et al.*, 2010), but molecular pathways are likely to underpin the susceptibility to age-related changes (Alonso *et al.*, 2009; Niccoli *et al.*, 2017). In 10% of cases a positive family history is reported, and in about 70% of the familial cases a causative single gene can be identified. The most frequent gene is *C9orf72* which causes both MND and FTD (Renton *et al.*, 2011), in rare cases also associated with neuropsychiatric diseases or Parkinsonism (Byrne *et al.*, 2013). In a significant minority of cases a gene mutation can be found despite a negative family history, likely to be explained by missing family histories or reduced penetrance leading to ALS that skips a generation. It has been proposed that ALS develops in a multistep process (Al-Chalabi *et al.*, 2014) and that risk of sporadic ALS increases on a certain genetic background multiplied by environmental factors (Al-Chalabi and Hardiman, 2013). When a common gene can be identified the threshold to develop the disease is much lower (Chio *et al.*, 2018). Also, there is an intrinsic variance between genes in disease penetrance, with some *SOD1* gene mutations have a strong disease determining effect, for example, with a penetrance of about 80% at the age of 60 years. In contrast, the figure for *C9orf72* is 60% at age 60, rising to >90% by the age of 85 years, and at 60% at the age of 80 years, even lower for $TARDBP^{A382T}$ (Aggarwal and Nicholson, 2005; Chio *et al.*, 2011a; Majounie *et al.*, 2012). This heterogeneity raises questions about mechanisms and gene modifiers that regulate the development of ALS within individuals and especially within gene carriers (Diekstra *et al.*, 2012; Gijselinck *et al.*, 2016; Kramer *et al.*, 2016). The evolution of the first symptom suggests a sudden decompensation, possibly of a system that has slowly accumulated vulnerability over time (Benatar *et al.*, 2019). On this background, detecting changes that are disease-specific and independent of neuronal damage, which often already reflects the symptomatic phase, becomes more important (Weydt *et al.*, 2016). New therapies that target the treatment of genetic mutations require specific disease markers that

can indicate a turning point from health to disease before incurable damage has occurred. The heterogeneity of ALS makes this difficult. One approach to this, is to focus on TDP-43 as a disease-specific biomarker that reflects the common underlying pathology in 97% of ALS cases.

The two trajectories followed in this thesis were

1. To measure the most valuable and disease-specific maker in ALS based on the underlying neuropathology by detecting pathological TDP-43 from human ALS post-mortem tissue and investigating disease-specific TDP-43 peptides to enable quantification across diagnostic groups by targeted proteomics.
2. To discover cellular targets that are disturbed by the expression of pathologically altered TDP-43 in order to find pathways relevant for drug target development by exploring the effects of human mutant TDP-43 on protein-protein interactions and its cellular pathways in an ALS disease model with low and motor neuron specific expression.

7.2. The concept of measuring disease-specific TDP-43 from human *post mortem* tissue

Previous studies measuring TDP-43 in CSF and serum using antibody-based methods have revealed inconsistent results due to the non-specific binding of antibodies to full-length and pathologically altered TDP-43 (Steinacker *et al.*, 2008; Feneberg *et al.*, 2014). To overcome this problem my work demonstrated that TDP-43 from brain tissue can be detected by mass spectrometry, which led to the discovery of a potentially pathognomonic truncation site-specific TDP-43 peptide. Furthermore, I was able to quantify those disease-relevant TDP-43 peptides across diagnostic groups by using targeted mass spectrometry which enabled the

identification of an ALS-specific peptide signature in brain urea fractions. This ultimately can be used to develop a more disease-specific assay for *in vivo* biomarker detection.

When TDP-43 was first described as pathologically altered in ALS and FTD in 2006, mass spectrometry was used to verify the protein amino acid sequence of TDP-43 in a 45kDa and a lower molecular weight gel band from TDP-43 immunoblotted urea fractions extracted from FTLD brain tissue, later characterised as full-length TDP-43 and C-terminal TDP-43 fragments (CTFs) (Neumann *et al.*, 2006). Nearly one decade later a study used a similar approach focusing on the investigation of pathological phosphorylated TDP-43 bands from ALS brain urea fractions determining phosphorylation sites and potential CTFs (Kametani *et al.*, 2016). However, this was based on two cases and the proteomic discovery of peptides was not validated by an independent method.

In this thesis I used a similar approach to identify disease-relevant TDP-43 peptides in urea fractions extracted from human ALS *post mortem* tissues. However, this was then followed by a sophisticated targeted proteomic approach for the validation of TDP-43 peptides and absolute quantification in a large and independent ALS *post mortem* tissue cohort, which has never been attempted on this scale before. I used autopsy-confirmed TDP-43-positive cases, which is important for the interpretation of the results (Foulds *et al.*, 2009; Kuiperij *et al.*, 2017). Targeted proteomics provided a successful and reliable alternative method to the initial approach in this thesis that focused on the use of commercially available antibodies to enrich TDP-43 directly from biofluids, which was not sufficient for proteomic detection of TDP-43 and confirmed findings from a previous study (Feneberg *et al.*, 2014).

7.3. The detection and quantification of TDP-43 peptides discriminate ALS from other diseases

My serial fractionations of human *post mortem* ALS cortex tissue confirmed the characteristics of TDP-43 pathology, namely phosphorylated full-length TDP-43 at 48kDa and smaller TDP-43 fragments at 25kDa and 28kDa by immunoblotting (Neumann *et al.*, 2006). From these urea fractions I was subsequently able to detect tryptic and chymotryptic specific TDP-43 peptide sequences by mass spectrometry. The peptides that were identified were located at the N- and C-terminus of TDP-43, as well as peptides revealing nonspecific cleavage sites suggesting endogenous truncation as an underlying pathomechanism. The development of heavy isotope-labelled peptides allowed for the absolute quantification of corresponding endogenous TDP-43 peptides by PRM. Compared to healthy controls, quantification of peptides in ALS showed an increase for truncation site- specific peptides and an increase in the C-terminal specific peptide relative to the N-terminal TDP-43 peptide, suggesting possible degradation of the N-terminal TDP-43 after truncation. The recognition of truncation site peptides together with the altered N- and C-terminal peptide ratio have the potential to be developed as a more specific ALS biomarker, using commercially available assay development.

The finding that truncation site-specific peptides were also increased in Alzheimer's Disease suggests that TDP-43 pathology might occur beyond ALS and FTLD. It has been described as a major component of the underlying pathology in a sub-group of patients who clinically presented like Alzheimer's Disease (Nelson *et al.*, 2019). This limbic-predominant age-related TDP-43 encephalopathy recently described as "LATE", affects more than 20% of people who are over 80 years, a frequency similar to that of Alzheimer's Disease. Also, I detected truncation site-specific TDP-43 peptides in

Alzheimer's Disease cases, the peptide signature was slightly different compared to the ALS cases. The N- to C-terminal ratio was normal in Alzheimer's Disease cases and might suggest a different underlying pathomechanism. Potentially, the findings described in Chapter 4 could offer a more sensitive method to detect mixed pathology in clinical Alzheimer's Disease (James *et al.*, 2016).

7.4. Implications for future TDP-43 assay developments

The production of more sensitive antibodies to detect pathological TDP-43 still remains a focus of research in the ALS biomarker field and has not yet revealed specific antibodies with common immunisation methods (Kwong *et al.*, 2014). Monoclonal antibodies could support the detection, but also the development of clinical immunisation studies to prevent the transmission of pathogenic forms of TDP-43. Rising TDP-43 antibodies in mice against recombinant TDP-43 protein forms including full-length TDP-43, N-terminal truncated TDP-43 (aa1-261) and C-terminal truncated protein (aa182- 414) has been one approach (Kwong *et al.*, 2014). From 168 antibodies only 45 clones showed immunoreactivity for TDP-43 with epitope mapping revealing just 34 antibodies that bound to the C-terminal region of TDP-43. Nevertheless, most of these antibodies did not specifically bind to pathological TDP-43. Promisingly, this study was the finding that an antibody that binds to the N-terminus of TDP-43 was highly specific for full-length TDP-43, but not to pathological phosphorylated or truncated TDP-43. This corroborates my finding that the N-terminal peptide was decreased in ALS urea fractions reflecting a decrease of full-length TDP-43 in the insoluble protein fraction, while the pathologically truncated, C-terminal TDP-43 fragments increase. However, the C-terminal monoclonal antibodies as described by Kwong *et al.* were less specific in detecting pathologically altered TDP-43 (Kwong *et al.*, 2014). This has important implications for my study as the truncation site-specific

peptide identified in this thesis, lies within this region. Future antibody production based on the identified peptide must therefore address a more specific region of TDP-43. The potential of aptamers, which ate small nucleic acid molecules, could be explored for a more specific detection of a single amino acid change. As truncation of the TDP-43 protein is likely to alter its confirmation, the use of an assay using these aptamers could allow for a more specific read-out (Mascini *et al.*, 2012). However, Kwong *et al.* also discovered a monoclonal antibody that detected the RRM 2, clearly the region before the truncated peptide, that was highly specific to pathologically altered TDP-43, but not full-length TDP-43 in FTLD brains (Kwong *et al.*, 2014). From these findings and also already suggested alternative truncation sites of TDP-43, corroborated by an ALS specific increase of a second truncation site-specific peptide in our study, it is likely that C-terminal fragments of different sizes exist in FTLD and possibly in ALS (Laferriere *et al.*, 2019). In terms of disease mechanisms there is no clear evidence of a protease that cleaves TDP-43 at the newly identified truncation site (https://web.expasy.org/peptide_cutter/) and alternative mechanisms that can lead to the generation of protein isoforms such as genetic variants (single-nucleotide-polymorphism) or alternative splice isoforms must be considered (Wang *et al.*, 2004; Ayala *et al.*, 2011; D'Alton *et al.*, 2015).

7.5. Studying the interactome of human TDP-43 in a mouse motor neuronal model elucidates pathways for the understanding of ALS pathogenesis

In the work described in this thesis, genetic engineering was used to maintain the expression of TDP-43 at a level which has the potential to verify the most physiologically relevant protein interactors, with the aim of translation into human disease modulators. The interactome of human TDP-43 was studied in a transgenic mouse model of ALS, where the human construct was site-specifically integrated as a single copy into the mouse genome

(Gordon *et al.*, 2019). The mass spectrometry data of the human TDP-43 interactome was derived from differentiated mouse motor neuron cultures comparing the human wild-type and M337V mutant TDP-43 interactomes. This enabled the elucidation of how a pathologic mutation in the C-terminal region of TDP-43 alters protein-protein interactions. Compared to previous studies (Freibaum *et al.*, 2010; Blokhuis *et al.*, 2016), this work focused on investigating the interactomes in a non-overexpressing model and importantly in a cellular model relevant to ALS by studying differentiated motor neurons (Gordon *et al.*, 2019). The model of human *TDP-43*$^{M337V/-}$ (BAC)-transgenic motor neurons allowed to observe disease-specific interactome changes that were associated with ALS-pathogenesis.

7.6. A C-terminal M337V mutation of TDP-43 alters the interactome of TDP-43

Mass spectrometry was used to identify the TDP-43 protein interactome, how it changed in response to oxidative stress, and how an ALS-causing mutation in TDP-43 might abrogate interactions of normal TDP-43. A strength of affinity-enrichment and bottom-up mass spectrometry is the ability to identify a vast range of proteins bound to the bait protein. By direct comparison between the wild-type and M337V mutant TDP-43 interactomes I demonstrated that there was a marked reduction of proteins bound to TDP-43^{M337V}. Therefore, the M337V mutation seems to affect cellular pathways which are important for the normal function of TDP-43. Further evidence of the validity of the model was given by demonstrating that oxidative stress shifted the wild-type interactome towards a normal stress response, while stress to *TDP-43*$^{M337V/-}$ mouse motor neurons altered the interactome towards pathways associated with ALS pathogenesis (Shaw *et al.*, 1995). I then focused on the validation of single interactors. This required state-of-the-art methods such as co-immunoprecipitation and detection of the bound prey protein by immunoblotting. Often these methods require the establishment of a protocol for each single prey (Phizicky and

Fields, 1995). This relies on the availability of antibodies and the generation of appropriate numbers of differentiations. In a more developed cellular model this is often challenging to achieve.

I attach great significance to the loss of interaction with Pabpc. Impaired stress granule assembly was described as a phenotype of the mouse cellular model and further corroborated in this thesis (Gordon *et al.*, 2019). I demonstrated an impaired interaction of Pabpc with TDP-43^{M337V} in mouse motor neurons as observed in the proteomic dataset. Disappointingly, there was a lack of altered interaction, when M337V mutant TDP-43 was transiently expressed in HEK293T cells and the binding of PABPc to overexpressed wild-type TDP-43 might be RNA-dependent. Although transient expression is a simple method to perform, overexpression of an RNA binding protein like TDP-43 is somewhat artificial, and the results therefore difficult to interpret with certainty. TDP-43^{M337V} in (BAC)-transgenic motor neurons may well lead to an indirect impairment of Pabpc with TDP-43 via multiple intermediary binding proteins such as proteins involved in RNA metabolism (Boehringer *et al.*, 2017; Moens *et al.*, 2019). The same holds true for the alteration in stress granule dynamics where Pabpc is an important mediator and well-established, but unlikely to be the sole pathway involved in stress granule formation. This suggests that the impaired interaction of Pabpc with TDP-43^{M337V} in mouse motor neurons is not directly affected by the mutation, but that a combined loss of several interactors may lead to an impairment of interaction with Pabpc. Another striking difference between the interactomes was the significant enrichment of proteins of the endosomal and extracellular-exosome pathway for TDP-43^{WT}. Intracellular trafficking has been associated with ALS pathogenesis in a knock-out model of TDP-43 (Schwenk *et al.*, 2016). Here I demonstrated reduced vesicle secretion in mouse and human iPSC-derived M337V mutant TDP-43 motor neurons, which has only been previously reported in human *C9orf72*-based pathology (Aoki *et al.*, 2017). This might

suggest that mutations in TDP-43 affect the secretion of pathological proteins and therefore increase the exposure to toxic protein deposits. So far, TDP-43 oligomers have been detected in exosomes (Feiler *et al.*, 2015) and it would be interesting to study how a decrease in vesicles affects the overall secretion of TDP-43 and if there is evidence of TDP-43 oligomers in our model or if I can detect the pathological TDP-43 peptide signature in those vesicles.

7.7. Towards the identification of protein-protein interactions linking phenotypes of M337V mutant TDP-43 mouse motor neurons

Impaired stress granule formation in *TDP-43*$^{M337V/-}$ motor neurons in response to oxidative stress treatment, which is sufficient to induce stress granules in wild-type TDP-43 motor neurons, was a major finding in the (BAC)-transgenic mouse cellular model and further supported by my work. The impaired interaction with Pabpc as an important stress granule marker appears to be supported by the observed cellular phenotype. However, other potential interactors involved in the formation of stress granules were also altered by the M337V mutation, which as a consequence of stress may become repressed and condensed into stress granules (Buchan and Parker, 2009), namely an interruption of the interaction of TDP-43^{M337V} with eIF2a or eIF4a1 could affect stress granule formation. Interestingly EIF4a1 is also upstream of the pathway to initiate translation in conjunction with Pabpc, possibly giving a further link towards the reduced binding of Pabpc to TDP-43^{M337V} (Rogers *et al.*, 2001). Another relevant area of future investigation is how stress alters the overall expression of proteins and how this affects interactors to TDP-43. I alluded to the fact that components of the stress granule inhibiting CCT complex are found in the M337V mutant TDP-43 interactome, but not in wild-type TDP-43 interactome, while Hsp90 chaperones which facilitate stress granule formation are found in the wild-type interactome (Matsumoto *et al.*, 2011; Leitner *et al.*, 2012). This points towards an important role of chaperones within

the interactomes. Chaperones have been under investigation for motor neuropathies and are important for the proteostasis of a cell (Lupo *et al.*, 2016) and loss of association with chaperones may render TDP-43^{M337V} less interactive more generally. GRP78 was highly upregulated in the wild-type interactome and is an important component of protein folding and quality control in the endoplasmic reticulum (Lee, 2005). Endoplasmic reticulum alterations and calcium signalling have been recently described to be altered in human iPSC-derived motor neurons from patients with a TDP-43 mutation (Bursch *et al.*, 2019). This is an important finding that should prompt further exploration of the role of oxidative stress in how TDP-43 interacts with the endoplasmic reticulum and influences endosomal trafficking. Similar interactome work may be directly used to explore targets within human cellular models, importantly in human iPSC-derived motor neurons from patients with the same TDP-43 mutation. This might enable the discovery of overlapping disease pathology and the establishment of novel human therapeutic targets.

7.8. Closing remarks

Although there is no highly-effective disease-modifying therapy for ALS today, an era of unprecedented molecular discovery is bringing new perspectives to one of the most devastating of the neurodegenerative diseases. Molecular heterogeneity is undoubtedly increasing in ALS, but understanding the wider cellular changes in the context of the consistent phenomenon of TDP-43 aggregation has potential to reveal the common downstream pathological pathways that may offer common therapeutic targets. Biomarker development is crucial to clinical translation and my thesis has demonstrated the value of integrating human tissue and cellular models towards a better future for those suffering from and those yet to develop ALS.

8. Publications arising from this research period

8.1. Original articles

E. Feneberg, P. D. Charles, M. J. Finelli, *et al.* (2020). "Detection and quantification of pathological C-terminal TDP-43 fragments in post mortem brain tissue". (submitted)

E. Feneberg, D. Gordon, A. G. Thompson, *et al.* (2020). "The TDP-43 interactome defines stress granule assembly and defective exosome secretion as key pathways in amyotrophic lateral sclerosis". (submitted)

M. Salter, E. Corfield . . . **E. Feneberg** et al. (2018). "Initial Identification of a Blood-Based Chromosome Conformation Signature for Aiding in the Diagnosis of Amyotrophic Lateral Sclerosis". In: *EBioMedicine* 33, pp. 169-184. doi: 10.1016/j.ebiom.2018.06.015

8.2. Review articles

E. Feneberg, E. Gray, O. Ansorge, *et al.* (2018). "Towards a TDP-43-Based Biomarker for ALS and FTLD". In: *Mol Neurobiol* 55, pp. 7789-7801. doi: 10.1007/s12035-018-0947-6

K. Talbot, **E. Feneberg**, J. Scaber, et al. (2018). "Amyotrophic lateral sclerosis: the complex path to precision medicine." In: *J Neurol* 265, pp. 2454-2462. doi: 10.1007/s00415-018-8983-8

References

Afroz T, Hock EM, Ernst P, Foglieni C, Jambeau M, Gilhespy LAB, Laferriere F, Maniecka Z, Pluckthun A, Mittl P, Paganetti P, Allain FHT, Polymenidou M. Functional and dynamic polymerization of the ALS-linked protein TDP-43 antagonizes its pathologic aggregation. Nat Commun 2017; 8(1): 45.

Aggarwal A, Nicholson G. Age dependent penetrance of three different superoxide dismutase 1 (sod 1) mutations. Int J Neurosci 2005; 115(8): 1119-30.

Al-Chalabi A, Calvo A, Chio A, Colville S, Ellis CM, Hardiman O, Heverin M, Howard RS, Huisman MHB, Keren N, Leigh PN, Mazzini L, Mora G, Orrell RW, Rooney J, Scott KM, Scotton WJ, Seelen M, Shaw CE, Sidle KS, Swingler R, Tsuda M, Veldink JH, Visser AE, van den Berg LH, Pearce N. Analysis of amyotrophic lateral sclerosis as a multistep process: a population-based modelling study. Lancet Neurol 2014; 13(11): 1108-13.

Al-Chalabi A, Hardiman O. The epidemiology of ALS: a conspiracy of genes, environment and time. Nat Rev Neurol 2013; 9(11): 617-28.

Al-Chalabi A, van den Berg LH, Veldink J. Gene discovery in amyotrophic lateral sclerosis: implications for clinical management. Nat Rev Neurol 2017; 13(2): 96-104.

Al-Sarraj S, King A, Troakes C, Smith B, Maekawa S, Bodi I, Rogelj B, Al-Chalabi A, Hortobagyi T, Shaw CE. p62 positive, TDP-43 negative, neuronal cytoplasmic and intranuclear inclusions in the cerebellum and hippocampus define the pathology of C9orf72-linked FTLD and MND/ALS. Acta Neuropathol 2011; 122(6): 691-702.

Almeida S, Gascon E, Tran H, Chou HJ, Gendron TF, Degroot S, Tapper AR, Sellier C, Charlet-Berguerand N, Karydas A, Seeley WW, Boxer AL, Petrucelli L, Miller BL, Gao FB. Modeling key pathological features of frontotemporal dementia with C9ORF72 repeat expansion in iPSC-derived human neurons. Acta Neuropathol 2013; 126(3): 385-99.

Alonso A, Logroscino G, Jick SS, Hernan MA. Incidence and lifetime risk of motor neuron disease in the United Kingdom: a population-based study. Eur J Neurol 2009; 16(6): 745-51.

Aoki Y, Manzano R, Lee Y, Dafinca R, Aoki M, Douglas AGL, Varela MA, Sathyaprakash C, Scaber J, Barbagallo P, Vader P, Mager I, Ezzat K, Turner MR, Ito N, Gasco S, Ohbayashi N, El Andaloussi S, Takeda S, Fukuda M, Talbot K, Wood MJA. C9orf72 and RAB7L1 regulate vesicle trafficking in amyotrophic lateral sclerosis and frontotemporal dementia. Brain 2017; 140(4): 887-97.

Armon C, Graves MC, Moses D, Forte DK, Sepulveda L, Darby SM, Smith RA. Linear estimates of disease progression predict survival in patients with amyotrophic lateral sclerosis. Muscle Nerve 2000; 23(6): 874-82.

Arnold ES, Ling SC, Huelga SC, Lagier-Tourenne C, Polymenidou M, Ditsworth D, Kordasiewicz HB, McAlonis-Downes M, Platoshyn O, Parone PA, Da Cruz S, Clutario KM, Swing D, Tessarollo L, Marsala M, Shaw CE, Yeo GW, Cleveland DW. ALS-linked TDP-43 mutations produce aberrant RNA splicing and adult-onset motor neuron disease without aggregation or loss of nuclear TDP-43. Proc Natl Acad Sci U S A 2013; 110(8): E736-45.

Ash PE, Bieniek KF, Gendron TF, Caulfield T, Lin WL, Dejesus-Hernandez M, van Blitterswijk MM, Jansen-West K, Paul JW, 3rd, Rademakers R, Boylan KB, Dickson DW, Petrucelli L. Unconventional translation of C9ORF72 GGGGCC expansion generates insoluble polypeptides specific to c9FTD/ALS. Neuron 2013; 77(4): 639-46.

Ayala YM, De Conti L, Avendano-Vazquez SE, Dhir A, Romano M, D'Ambrogio A, Tollervey J, Ule J, Baralle M, Buratti E, Baralle FE. TDP-43 regulates its mRNA levels through a negative feedback loop. EMBO J 2011; 30(2): 277-88.

Balendra R, Isaacs AM. C9orf72-mediated ALS and FTD: multiple pathways to disease. Nat Rev Neurol 2018; 14(9): 544-58.

Baumer D, Hilton D, Paine SM, Turner MR, Lowe J, Talbot K, Ansorge O. Juvenile ALS with basophilic inclusions is a FUS proteinopathy with FUS mutations. Neurology 2010; 75(7): 611-8.

Begley DJ, Brightman MW. Structural and functional aspects of the blood-brain barrier. Prog Drug Res 2003; 61: 39-78.

Benajiba L, Le Ber I, Camuzat A, Lacoste M, Thomas-Anterion C, Couratier P, Legallic S, Salachas F, Hannequin D, Decousus M, Lacomblez L, Guedj E, Golfier V, Camu W, Dubois B, Campion D, Meininger V, Brice A, French C, Genetic Research Network on Frontotemporal Lobar Degeneration/Frontotemporal Lobar Degeneration with Motoneuron D. TARDBP mutations in motoneuron disease with frontotemporal lobar degeneration. Ann Neurol 2009; 65(4): 470-3.

Benatar M, Turner MR, Wuu J. Defining pre-symptomatic amyotrophic lateral sclerosis. Amyotroph Lateral Scler Frontotemporal Degener 2019: 1-7.

Benatar M, Wuu J, Andersen PM, Lombardi V, Malaspina A. Neurofilament light: A candidate biomarker of presymptomatic amyotrophic lateral sclerosis and phenoconversion. Ann Neurol 2018; 84(1): 130-9.

Berning BA, Walker AK. The Pathobiology of TDP-43 C-Terminal Fragments in ALS and FTLD. Front Neurosci 2019; 13: 335.

Bilican B, Serio A, Barmada SJ, Nishimura AL, Sullivan GJ, Carrasco M, Phatnani HP, Puddifoot CA, Story D, Fletcher J, Park IH, Friedman BA, Daley GQ, Wyllie DJ, Hardingham GE, Wilmut I, Finkbeiner S, Maniatis T, Shaw CE, Chandran S. Mutant induced pluripotent stem cell lines recapitulate aspects of TDP-43 proteinopathies and reveal cell-specific vulnerability. Proc Natl Acad Sci U S A 2012; 109(15): 5803-8.

Blasco H, Bernard-Marissal N, Vourc'h P, Guettard YO, Sunyach C, Augereau O, Khederchah J, Mouzat K, Antar C, Gordon PH, Veyrat-Durebex C, Besson G, Andersen PM, Salachas F, Meininger V, Camu W, Pettmann B, Andres CR, Corcia P, French ALSSG.

A rare motor neuron deleterious missense mutation in the DPYSL3 (CRMP4) gene is associated with ALS. Hum Mutat 2013; 34(7): 953-60.

Blokhuis AM, Koppers M, Groen EJ, van den Heuvel DM, Dini Modigliani S, Anink JJ, Fumoto K, van Diggelen F, Snelting A, Sodaar P, Verheijen BM, Demmers JA, Veldink JH, Aronica E, Bozzoni I, den Hertog J, van den Berg LH, Pasterkamp RJ. Comparative interactomics analysis of different ALS-associated proteins identifies converging molecular pathways. Acta Neuropathol 2016; 132(2): 175-96.

Boehringer A, Garcia-Mansfield K, Singh G, Bakkar N, Pirrotte P, Bowser R. ALS Associated Mutations in Matrin 3 Alter Protein-Protein Interactions and Impede mRNA Nuclear Export. Sci Rep 2017; 7(1): 14529.

Bolognesi B, Lorenzo Gotor N, Dhar R, Cirillo D, Baldrighi M, Tartaglia GG, Lehner B. A Concentration-Dependent Liquid Phase Separation Can Cause Toxicity upon Increased Protein Expression. Cell Rep 2016; 16(1): 222-31.

Borroni B, Bonvicini C, Alberici A, Buratti E, Agosti C, Archetti S, Papetti A, Stuani C, Di Luca M, Gennarelli M, Padovani A. Mutation within TARDBP leads to frontotemporal dementia without motor neuron disease. Hum Mutat 2009; 30(11): E974-83.

Bose JK, Huang CC, Shen CK. Regulation of autophagy by neuropathological protein TDP-43. J Biol Chem 2011; 286(52): 44441-8.

Boylan KB, Glass JD, Crook JE, Yang C, Thomas CS, Desaro P, Johnston A, Overstreet K, Kelly C, Polak M, Shaw G. Phosphorylated neurofilament heavy subunit (pNF-H) in peripheral blood and CSF as a potential prognostic biomarker in amyotrophic lateral sclerosis. J Neurol Neurosurg Psychiatry 2013; 84(4): 467-72.

Brenner D, Sieverding K, Bruno C, Luningschror P, Buck E, Mungwa S, Fischer L, Brockmann SJ, Ulmer J, Bliederhauser C, Philibert CE, Satoh T, Akira S, Boillee S, Mayer B, Sendtner M, Ludolph AC, Danzer KM, Lobsiger CS, Freischmidt A, Weishaupt JH.

Heterozygous Tbk1 loss has opposing effects in early and late stages of ALS in mice. J Exp Med 2019; 216(2): 267-78.

Brenner D, Yilmaz R, Muller K, Grehl T, Petri S, Meyer T, Grosskreutz J, Weydt P, Ruf W, Neuwirth C, Weber M, Pinto S, Claeys KG, Schrank B, Jordan B, Knehr A, Gunther K, Hubers A, Zeller D, Kubisch C, Jablonka S, Sendtner M, Klopstock T, de Carvalho M, Sperfeld A, Borck G, Volk AE, Dorst J, Weis J, Otto M, Schuster J, Del Tredici K, Braak H, Danzer KM, Freischmidt A, Meitinger T, Strom TM, Ludolph AC, Andersen PM, Weishaupt JH, German ALSnMNDNET. Hot-spot KIF5A mutations cause familial ALS. Brain 2018; 141(3): 688-97.

Brettschneider J, Del Tredici K, Toledo JB, Robinson JL, Irwin DJ, Grossman M, Suh E, Van Deerlin VM, Wood EM, Baek Y, Kwong L, Lee EB, Elman L, McCluskey L, Fang L, Feldengut S, Ludolph AC, Lee VM, Braak H, Trojanowski JQ. Stages of pTDP-43 pathology in amyotrophic lateral sclerosis. Ann Neurol 2013; 74(1): 20-38.

Brettschneider J, Van Deerlin VM, Robinson JL, Kwong L, Lee EB, Ali YO, Safren N, Monteiro MJ, Toledo JB, Elman L, McCluskey L, Irwin DJ, Grossman M, Molina-Porcel L, Lee VM, Trojanowski JQ. Pattern of ubiquilin pathology in ALS and FTLD indicates presence of C9ORF72 hexanucleotide expansion. Acta Neuropathol 2012; 123(6): 825-39.

Brewis IA, Brennan P. Proteomics technologies for the global identification and quantification of proteins. Adv Protein Chem Struct Biol 2010; 80: 1-44.

Brooks BR. El Escorial World Federation of Neurology criteria for the diagnosis of amyotrophic lateral sclerosis. Subcommittee on Motor Neuron Diseases/Amyotrophic Lateral Sclerosis of the World Federation of Neurology Research Group on Neuromuscular Diseases and the El Escorial "Clinical limits of amyotrophic lateral sclerosis" workshop contributors. J Neurol Sci 1994; 124 Suppl: 96-107.

Brooks BR, Miller RG, Swash M, Munsat TL, World Federation of Neurology Research Group on Motor Neuron D. El Escorial revisited: revised criteria for the diagnosis of

amyotrophic lateral sclerosis. Amyotroph Lateral Scler Other Motor Neuron Disord 2000; 1(5): 293-9.

Buchan JR, Parker R. Eukaryotic stress granules: the ins and outs of translation. Mol Cell 2009; 36(6): 932-41.

Buratti E, Baralle FE. Multiple roles of TDP-43 in gene expression, splicing regulation, and human disease. Front Biosci 2008; 13: 867-78.

Buratti E, Brindisi A, Giombi M, Tisminetzky S, Ayala YM, Baralle FE. TDP-43 binds heterogeneous nuclear ribonucleoprotein A/B through its C-terminal tail: an important region for the inhibition of cystic fibrosis transmembrane conductance regulator exon 9 splicing. J Biol Chem 2005; 280(45): 37572-84.

Buratti E, Dork T, Zuccato E, Pagani F, Romano M, Baralle FE. Nuclear factor TDP-43 and SR proteins promote in vitro and in vivo CFTR exon 9 skipping. EMBO J 2001; 20(7): 1774-84.

Bursch F, Kalmbach N, Naujock M, Staege S, Eggenschwiler R, Abo-Rady M, Japtok J, Guo W, Hensel N, Reinhardt P, Boeckers TM, Cantz T, Sterneckert J, Van Den Bosch L, Hermann A, Petri S, Wegner F. Altered calcium dynamics and glutamate receptor properties in iPSC-derived motor neurons from ALS patients with C9orf72, FUS, SOD1 or TDP43 mutations. Hum Mol Genet 2019; 28(17): 2835-50.

Butti Z, Patten SA. RNA Dysregulation in Amyotrophic Lateral Sclerosis. Front Genet 2018; 9: 712.

Byrne S, Heverin M, Elamin M, Bede P, Lynch C, Kenna K, MacLaughlin R, Walsh C, Al Chalabi A, Hardiman O. Aggregation of neurologic and neuropsychiatric disease in amyotrophic lateral sclerosis kindreds: a population-based case-control cohort study of familial and sporadic amyotrophic lateral sclerosis. Ann Neurol 2013; 74(5): 699-708.

Caccamo A, Majumder S, Deng JJ, Bai Y, Thornton FB, Oddo S. Rapamycin rescues TDP-43 mislocalization and the associated low molecular mass neurofilament instability. J Biol Chem 2009; 284(40): 27416-24.

Cartegni L, Maconi M, Morandi E, Cobianchi F, Riva S, Biamonti G. hnRNP A1 selectively interacts through its Gly-rich domain with different RNA-binding proteins. J Mol Biol 1996; 259(3): 337-48.

Chang MC, Srinivasan K, Friedman BA, Suto E, Modrusan Z, Lee WP, Kaminker JS, Hansen DV, Sheng M. Progranulin deficiency causes impairment of autophagy and TDP-43 accumulation. J Exp Med 2017; 214(9): 2611-28.

Charcot JM. Sclérose des cordons latéraux de la moelle épinière chez une femme hystérique. (Par.),; 1865.

Charcot JM. Leçons sur les maladies du système nerveux : faites à la Salpétrière. Paris: V. Adrien Delahaye; 1875.

Chen-Plotkin AS, Lee VM, Trojanowski JQ. TAR DNA-binding protein 43 in neurodegenerative disease. Nat Rev Neurol 2010; 6(4): 211-20.

Chew J, Cook C, Gendron TF, Jansen-West K, Del Rosso G, Daughrity LM, Castanedes-Casey M, Kurti A, Stankowski JN, Disney MD, Rothstein JD, Dickson DW, Fryer JD, Zhang YJ, Petrucelli L. Aberrant deposition of stress granule-resident proteins linked to C9orf72-associated TDP-43 proteinopathy. Mol Neurodegener 2019; 14(1): 9.

Chio A, Borghero G, Pugliatti M, Ticca A, Calvo A, Moglia C, Mutani R, Brunetti M, Ossola I, Marrosu MG, Murru MR, Floris G, Cannas A, Parish LD, Cossu P, Abramzon Y, Johnson JO, Nalls MA, Arepalli S, Chong S, Hernandez DG, Traynor BJ, Restagno G, Italian Amyotrophic Lateral Sclerosis Genetic C. Large proportion of amyotrophic lateral sclerosis cases in Sardinia due to a single founder mutation of the TARDBP gene. Arch Neurol 2011a; 68(5): 594-8.

Chio A, Calvo A, Moglia C, Mazzini L, Mora G, group Ps. Phenotypic heterogeneity of amyotrophic lateral sclerosis: a population based study. J Neurol Neurosurg Psychiatry 2011b; 82(7): 740-6.

Chio A, Mazzini L, D'Alfonso S, Corrado L, Canosa A, Moglia C, Manera U, Bersano E, Brunetti M, Barberis M, Veldink JH, van den Berg LH, Pearce N, Sproviero W, McLaughlin R, Vajda A, Hardiman O, Rooney J, Mora G, Calvo A, Al-Chalabi A. The multistep hypothesis of ALS revisited: The role of genetic mutations. Neurology 2018; 91(7): e635-e42.

Chio A, Traynor BJ, Lombardo F, Fimognari M, Calvo A, Ghiglione P, Mutani R, Restagno G. Prevalence of SOD1 mutations in the Italian ALS population. Neurology 2008; 70(7): 533-7.

Chiva C, Ortega M, Sabido E. Influence of the digestion technique, protease, and missed cleavage peptides in protein quantitation. J Proteome Res 2014; 13(9): 3979-86.

Chou CC, Zhang Y, Umoh ME, Vaughan SW, Lorenzini I, Liu F, Sayegh M, Donlin-Asp PG, Chen YH, Duong DM, Seyfried NT, Powers MA, Kukar T, Hales CM, Gearing M, Cairns NJ, Boylan KB, Dickson DW, Rademakers R, Zhang YJ, Petrucelli L, Sattler R, Zarnescu DC, Glass JD, Rossoll W. TDP-43 pathology disrupts nuclear pore complexes and nucleocytoplasmic transport in ALS/FTD. Nat Neurosci 2018; 21(2): 228-39.

Cohen TJ, Hwang AW, Restrepo CR, Yuan CX, Trojanowski JQ, Lee VM. An acetylation switch controls TDP-43 function and aggregation propensity. Nat Commun 2015; 6: 5845.

Cohen TJ, Hwang AW, Unger T, Trojanowski JQ, Lee VM. Redox signalling directly regulates TDP-43 via cysteine oxidation and disulphide cross-linking. EMBO J 2012; 31(5): 1241-52.

Colombo M, Moita C, van Niel G, Kowal J, Vigneron J, Benaroch P, Manel N, Moita LF, Thery C, Raposo G. Analysis of ESCRT functions in exosome biogenesis, composition and

secretion highlights the heterogeneity of extracellular vesicles. J Cell Sci 2013; 126(Pt 24): 5553-65.

Colombrita C, Onesto E, Megiorni F, Pizzuti A, Baralle FE, Buratti E, Silani V, Ratti A. TDP-43 and FUS RNA-binding proteins bind distinct sets of cytoplasmic messenger RNAs and differently regulate their post-transcriptional fate in motoneuron-like cells. J Biol Chem 2012; 287(19): 15635-47.

Colombrita C, Zennaro E, Fallini C, Weber M, Sommacal A, Buratti E, Silani V, Ratti A. TDP-43 is recruited to stress granules in conditions of oxidative insult. J Neurochem 2009; 111(4): 1051-61.

Cooper-Knock J, Hewitt C, Highley JR, Brockington A, Milano A, Man S, Martindale J, Hartley J, Walsh T, Gelsthorpe C, Baxter L, Forster G, Fox M, Bury J, Mok K, McDermott CJ, Traynor BJ, Kirby J, Wharton SB, Ince PG, Hardy J, Shaw PJ. Clinico-pathological features in amyotrophic lateral sclerosis with expansions in C9ORF72. Brain 2012; 135(Pt 3): 751-64.

Corbier C, Sellier C. C9ORF72 is a GDP/GTP exchange factor for Rab8 and Rab39 and regulates autophagy. Small GTPases 2017; 8(3): 181-6.

Craig AW, Haghighat A, Yu AT, Sonenberg N. Interaction of polyadenylate-binding protein with the eIF4G homologue PAIP enhances translation. Nature 1998; 392(6675): 520-3.

Crockford C, Newton J, Lonergan K, Chiwera T, Booth T, Chandran S, Colville S, Heverin M, Mays I, Pal S, Pender N, Pinto-Grau M, Radakovic R, Shaw CE, Stephenson L, Swingler R, Vajda A, Al-Chalabi A, Hardiman O, Abrahams S. ALS-specific cognitive and behavior changes associated with advancing disease stage in ALS. Neurology 2018; 91(15): e1370-e80.

Cruts M, Gijselinck I, van der Zee J, Engelborghs S, Wils H, Pirici D, Rademakers R, Vandenberghe R, Dermaut B, Martin JJ, van Duijn C, Peeters K, Sciot R, Santens P, De Pooter T, Mattheijssens M, Van den Broeck M, Cuijt I, Vennekens K, De Deyn PP, Kumar-

Singh S, Van Broeckhoven C. Null mutations in progranulin cause ubiquitin-positive frontotemporal dementia linked to chromosome 17q21. Nature 2006; 442(7105): 920-4.

Cykowski MD, Powell SZ, Peterson LE, Appel JW, Rivera AL, Takei H, Chang E, Appel SH. Clinical Significance of TDP-43 Neuropathology in Amyotrophic Lateral Sclerosis. J Neuropathol Exp Neurol 2017; 76(5): 402-13.

D'Alton S, Altshuler M, Lewis J. Studies of alternative isoforms provide insight into TDP-43 autoregulation and pathogenesis. RNA 2015; 21(8): 1419-32.

D'Ambrogio A, Buratti E, Stuani C, Guarnaccia C, Romano M, Ayala YM, Baralle FE. Functional mapping of the interaction between TDP-43 and hnRNP A2 in vivo. Nucleic Acids Res 2009; 37(12): 4116-26.

Dafinca R, Scaber J, Ababneh N, Lalic T, Weir G, Christian H, Vowles J, Douglas AG, Fletcher-Jones A, Browne C, Nakanishi M, Turner MR, Wade-Martins R, Cowley SA, Talbot K. C9orf72 Hexanucleotide Expansions Are Associated with Altered Endoplasmic Reticulum Calcium Homeostasis and Stress Granule Formation in Induced Pluripotent Stem Cell-Derived Neurons from Patients with Amyotrophic Lateral Sclerosis and Frontotemporal Dementia. Stem Cells 2016; 34(8): 2063-78.

Daoud H, Valdmanis PN, Kabashi E, Dion P, Dupre N, Camu W, Meininger V, Rouleau GA. Contribution of TARDBP mutations to sporadic amyotrophic lateral sclerosis. J Med Genet 2009; 46(2): 112-4.

de Carvalho M, Swash M. The onset of amyotrophic lateral sclerosis. J Neurol Neurosurg Psychiatry 2006; 77(3): 388-9.

De Marco G, Lupino E, Calvo A, Moglia C, Buccinna B, Grifoni S, Ramondetti C, Lomartire A, Rinaudo MT, Piccinini M, Giordana MT, Chio A. Cytoplasmic accumulation of TDP-43 in circulating lymphomonocytes of ALS patients with and without TARDBP mutations. Acta Neuropathol 2011; 121(5): 611-22.

de Vries BS, Rustemeijer LMM, Bakker LA, Schroder CD, Veldink JH, van den Berg LH, Nijboer TCW, van Es MA. Cognitive and behavioural changes in PLS and PMA:challenging the concept of restricted phenotypes. J Neurol Neurosurg Psychiatry 2019; 90(2): 141-7.

DeJesus-Hernandez M, Mackenzie IR, Boeve BF, Boxer AL, Baker M, Rutherford NJ, Nicholson AM, Finch NA, Flynn H, Adamson J, Kouri N, Wojtas A, Sengdy P, Hsiung GY, Karydas A, Seeley WW, Josephs KA, Coppola G, Geschwind DH, Wszolek ZK, Feldman H, Knopman DS, Petersen RC, Miller BL, Dickson DW, Boylan KB, Graff-Radford NR, Rademakers R. Expanded GGGGCC hexanucleotide repeat in noncoding region of C9ORF72 causes chromosome 9p-linked FTD and ALS. Neuron 2011; 72(2): 245-56.

Diekstra FP, van Vught PW, van Rheenen W, Koppers M, Pasterkamp RJ, van Es MA, Schelhaas HJ, de Visser M, Robberecht W, Van Damme P, Andersen PM, van den Berg LH, Veldink JH. UNC13A is a modifier of survival in amyotrophic lateral sclerosis. Neurobiol Aging 2012; 33(3): 630 e3-8.

Doi Y, Atsuta N, Sobue G, Morita M, Nakano I. Prevalence and incidence of amyotrophic lateral sclerosis in Japan. J Epidemiol 2014; 24(6): 494-9.

Donnelly CJ, Zhang PW, Pham JT, Haeusler AR, Mistry NA, Vidensky S, Daley EL, Poth EM, Hoover B, Fines DM, Maragakis N, Tienari PJ, Petrucelli L, Traynor BJ, Wang J, Rigo F, Bennett CF, Blackshaw S, Sattler R, Rothstein JD. RNA toxicity from the ALS/FTD C9ORF72 expansion is mitigated by antisense intervention. Neuron 2013; 80(2): 415-28.

Eisenberg D, Jucker M. The amyloid state of proteins in human diseases. Cell 2012; 148(6): 1188-203.

Elias JE, Gygi SP. Target-decoy search strategy for increased confidence in large-scale protein identifications by mass spectrometry. Nat Methods 2007; 4(3): 207-14.

Farg MA, Sundaramoorthy V, Sultana JM, Yang S, Atkinson RAK, Levina V, Halloran MA, Gleeson PA, Blair IP, Soo KY, King AE, Atkin JD. C9ORF72, implicated in amytrophic

lateral sclerosis and frontotemporal dementia, regulates endosomal trafficking. Hum Mol Genet 2017; 26(20): 4093-4.

Feiguin F, Godena VK, Romano G, D'Ambrogio A, Klima R, Baralle FE. Depletion of TDP-43 affects Drosophila motoneurons terminal synapsis and locomotive behavior. FEBS Lett 2009; 583(10): 1586-92.

Feiler MS, Strobel B, Freischmidt A, Helferich AM, Kappel J, Brewer BM, Li D, Thal DR, Walther P, Ludolph AC, Danzer KM, Weishaupt JH. TDP-43 is intercellularly transmitted across axon terminals. J Cell Biol 2015; 211(4): 897-911.

Felgenhauer K. Protein size and cerebrospinal fluid composition. Klinische Wochenschrift 1974; 52(24): 1158-64.

Feneberg E, Gray E, Ansorge O, Talbot K, Turner MR. Towards a TDP-43-Based Biomarker for ALS and FTLD. Mol Neurobiol 2018a; 55(10): 7789-801.

Feneberg E, Oeckl P, Steinacker P, Verde F, Barro C, Van Damme P, Gray E, Grosskreutz J, Jardel C, Kuhle J, Koerner S, Lamari F, Amador MDM, Mayer B, Morelli C, Muckova P, Petri S, Poesen K, Raaphorst J, Salachas F, Silani V, Stubendorff B, Turner MR, Verbeek MM, Weishaupt JH, Weydt P, Ludolph AC, Otto M. Multicenter evaluation of neurofilaments in early symptom onset amyotrophic lateral sclerosis. Neurology 2018b; 90(1): e22-e30.

Feneberg E, Steinacker P, Lehnert S, Schneider A, Walther P, Thal DR, Linsenmeier M, Ludolph AC, Otto M. Limited role of free TDP-43 as a diagnostic tool in neurodegenerative diseases. Amyotroph Lateral Scler Frontotemporal Degener 2014; 15(5-6): 351-6.

Feneberg E, Steinacker P, Volk AE, Weishaupt JH, Wollmer MA, Boxer A, Tumani H, Ludolph AC, Otto M. Progranulin as a candidate biomarker for therapeutic trial in patients with ALS and FTLD. Journal of neural transmission 2016; 123(3): 289-96.

Filimonenko M, Stuffers S, Raiborg C, Yamamoto A, Malerod L, Fisher EM, Isaacs A, Brech A, Stenmark H, Simonsen A. Functional multivesicular bodies are required for autophagic clearance of protein aggregates associated with neurodegenerative disease. J Cell Biol 2007; 179(3): 485-500.

Fong GC, Cheng TS, Lam K, Cheng WK, Mok KY, Cheung CM, Chim CS, Mak W, Chan KH, Tsang KL, Kwan MC, Tsoi TH, Cheung RT, Ho SL. An epidemiological study of motor neuron disease in Hong Kong. Amyotroph Lateral Scler Other Motor Neuron Disord 2005; 6(3): 164-8.

Foulds P, McAuley E, Gibbons L, Davidson Y, Pickering-Brown SM, Neary D, Snowden JS, Allsop D, Mann DM. TDP-43 protein in plasma may index TDP-43 brain pathology in Alzheimer's disease and frontotemporal lobar degeneration. Acta Neuropathol 2008; 116(2): 141-6.

Foulds PG, Davidson Y, Mishra M, Hobson DJ, Humphreys KM, Taylor M, Johnson N, Weintraub S, Akiyama H, Arai T, Hasegawa M, Bigio EH, Benson FE, Allsop D, Mann DM. Plasma phosphorylated-TDP-43 protein levels correlate with brain pathology in frontotemporal lobar degeneration. Acta Neuropathol 2009; 118(5): 647-58.

Fratta P, Sivakumar P, Humphrey J, Lo K, Ricketts T, Oliveira H, Brito-Armas JM, Kalmar B, Ule A, Yu Y, Birsa N, Bodo C, Collins T, Conicella AE, Mejia Maza A, Marrero-Gagliardi A, Stewart M, Mianne J, Corrochano S, Emmett W, Codner G, Groves M, Fukumura R, Gondo Y, Lythgoe M, Pauws E, Peskett E, Stanier P, Teboul L, Hallegger M, Calvo A, Chio A, Isaacs AM, Fawzi NL, Wang E, Housman DE, Baralle F, Greensmith L, Buratti E, Plagnol V, Fisher EM, Acevedo-Arozena A. Mice with endogenous TDP-43 mutations exhibit gain of splicing function and characteristics of amyotrophic lateral sclerosis. EMBO J 2018; 37(11).

Freibaum BD, Chitta RK, High AA, Taylor JP. Global analysis of TDP-43 interacting proteins reveals strong association with RNA splicing and translation machinery. J Proteome Res 2010; 9(2): 1104-20.

Freibaum BD, Lu Y, Lopez-Gonzalez R, Kim NC, Almeida S, Lee KH, Badders N, Valentine M, Miller BL, Wong PC, Petrucelli L, Kim HJ, Gao FB, Taylor JP. GGGGCC repeat expansion in C9orf72 compromises nucleocytoplasmic transport. Nature 2015; 525(7567): 129-33.

Fujimori K, Ishikawa M, Otomo A, Atsuta N, Nakamura R, Akiyama T, Hadano S, Aoki M, Saya H, Sobue G, Okano H. Modeling sporadic ALS in iPSC-derived motor neurons identifies a potential therapeutic agent. Nat Med 2018; 24(10): 1579-89.

Gendron TF, Bieniek KF, Zhang YJ, Jansen-West K, Ash PE, Caulfield T, Daughrity L, Dunmore JH, Castanedes-Casey M, Chew J, Cosio DM, van Blitterswijk M, Lee WC, Rademakers R, Boylan KB, Dickson DW, Petrucelli L. Antisense transcripts of the expanded C9ORF72 hexanucleotide repeat form nuclear RNA foci and undergo repeat-associated non-ATG translation in c9FTD/ALS. Acta Neuropathol 2013; 126(6): 829-44.

Gendron TF, Chew J, Stankowski JN, Hayes LR, Zhang YJ, Prudencio M, Carlomagno Y, Daughrity LM, Jansen-West K, Perkerson EA, O'Raw A, Cook C, Pregent L, Belzil V, van Blitterswijk M, Tabassian LJ, Lee CW, Yue M, Tong J, Song Y, Castanedes-Casey M, Rousseau L, Phillips V, Dickson DW, Rademakers R, Fryer JD, Rush BK, Pedraza O, Caputo AM, Desaro P, Palmucci C, Robertson A, Heckman MG, Diehl NN, Wiggs E, Tierney M, Braun L, Farren J, Lacomis D, Ladha S, Fournier CN, McCluskey LF, Elman LB, Toledo JB, McBride JD, Tiloca C, Morelli C, Poletti B, Solca F, Prelle A, Wuu J, Jockel-Balsarotti J, Rigo F, Ambrose C, Datta A, Yang W, Raitcheva D, Antognetti G, McCampbell A, Van Swieten JC, Miller BL, Boxer AL, Brown RH, Bowser R, Miller TM, Trojanowski JQ, Grossman M, Berry JD, Hu WT, Ratti A, Traynor BJ, Disney MD, Benatar M, Silani V, Glass JD, Floeter MK, Rothstein JD, Boylan KB, Petrucelli L. Poly(GP) proteins are a useful pharmacodynamic marker for C9ORF72-associated amyotrophic lateral sclerosis. Sci Transl Med 2017; 9(383).

Gerber SA, Rush J, Stemman O, Kirschner MW, Gygi SP. Absolute quantification of proteins and phosphoproteins from cell lysates by tandem MS. Proc Natl Acad Sci U S A 2003; 100(12): 6940-5.

Gijselinck I, Van Mossevelde S, van der Zee J, Sieben A, Engelborghs S, De Bleecker J, Ivanoiu A, Deryck O, Edbauer D, Zhang M, Heeman B, Baumer V, Van den Broeck M, Mattheijssens M, Peeters K, Rogaeva E, De Jonghe P, Cras P, Martin JJ, de Deyn PP, Cruts M, Van Broeckhoven C. The C9orf72 repeat size correlates with onset age of disease, DNA methylation and transcriptional downregulation of the promoter. Mol Psychiatry 2016; 21(8): 1112-24.

Gitcho MA, Baloh RH, Chakraverty S, Mayo K, Norton JB, Levitch D, Hatanpaa KJ, White CL, 3rd, Bigio EH, Caselli R, Baker M, Al-Lozi MT, Morris JC, Pestronk A, Rademakers R, Goate AM, Cairns NJ. TDP-43 A315T mutation in familial motor neuron disease. Ann Neurol 2008; 63(4): 535-8.

Glick D, Barth S, Macleod KF. Autophagy: cellular and molecular mechanisms. J Pathol 2010; 221(1): 3-12.

Goh CW, Lee IC, Sundaram JR, George SE, Yusoff P, Brush MH, Sze NSK, Shenolikar S. Chronic oxidative stress promotes GADD34-mediated phosphorylation of the TAR DNA-binding protein TDP-43, a modification linked to neurodegeneration. J Biol Chem 2018; 293(1): 163-76.

Goldstein LH, Abrahams S. Changes in cognition and behaviour in amyotrophic lateral sclerosis: nature of impairment and implications for assessment. Lancet Neurol 2013; 12(4): 368-80.

Gomez-Deza J, Lee YB, Troakes C, Nolan M, Al-Sarraj S, Gallo JM, Shaw CE. Dipeptide repeat protein inclusions are rare in the spinal cord and almost absent from motor neurons in C9ORF72 mutant amyotrophic lateral sclerosis and are unlikely to cause their degeneration. Acta Neuropathol Commun 2015; 3: 38.

Goossens J, Vanmechelen E, Trojanowski JQ, Lee VM, Van Broeckhoven C, van der Zee J, Engelborghs S. TDP-43 as a possible biomarker for frontotemporal lobar degeneration: a systematic review of existing antibodies. Acta Neuropathol Commun 2015; 3: 15.

Gordon D, Dafinca R, Scaber J, Alegre-Abarrategui J, Farrimond L, Scott C, Biggs D, Kent L, Oliver PL, Davies B, Ansorge O, Wade-Martins R, Talbot K. Single-copy expression of an amyotrophic lateral sclerosis-linked TDP-43 mutation (M337V) in BAC transgenic mice leads to altered stress granule dynamics and progressive motor dysfunction. Neurobiol Dis 2019; 121: 148-62.

Guil S, Long JC, Caceres JF. hnRNP A1 relocalization to the stress granules reflects a role in the stress response. Mol Cell Biol 2006; 26(15): 5744-58.

Hasegawa M, Arai T, Nonaka T, Kametani F, Yoshida M, Hashizume Y, Beach TG, Buratti E, Baralle F, Morita M, Nakano I, Oda T, Tsuchiya K, Akiyama H. Phosphorylated TDP-43 in frontotemporal lobar degeneration and amyotrophic lateral sclerosis. Ann Neurol 2008; 64(1): 60-70.

He F, Krans A, Freibaum BD, Taylor JP, Todd PK. TDP-43 suppresses CGG repeat-induced neurotoxicity through interactions with HnRNP A2/B1. Hum Mol Genet 2014; 23(19): 5036-51.

Highley JR, Kirby J, Jansweijer JA, Webb PS, Hewamadduma CA, Heath PR, Higginbottom A, Raman R, Ferraiuolo L, Cooper-Knock J, McDermott CJ, Wharton SB, Shaw PJ, Ince PG. Loss of nuclear TDP-43 in amyotrophic lateral sclerosis (ALS) causes altered expression of splicing machinery and widespread dysregulation of RNA splicing in motor neurones. Neuropathol Appl Neurobiol 2014; 40(6): 670-85.

Hiji M, Takahashi T, Fukuba H, Yamashita H, Kohriyama T, Matsumoto M. White matter lesions in the brain with frontotemporal lobar degeneration with motor neuron disease: TDP-43-immunopositive inclusions co-localize with p62, but not ubiquitin. Acta Neuropathol 2008; 116(2): 183-91.

Hsiung GY, DeJesus-Hernandez M, Feldman HH, Sengdy P, Bouchard-Kerr P, Dwosh E, Butler R, Leung B, Fok A, Rutherford NJ, Baker M, Rademakers R, Mackenzie IR. Clinical and pathological features of familial frontotemporal dementia caused by C9ORF72 mutation on chromosome 9p. Brain 2012; 135(Pt 3): 709-22.

Hubner NC, Bird AW, Cox J, Splettstoesser B, Bandilla P, Poser I, Hyman A, Mann M. Quantitative proteomics combined with BAC TransgeneOmics reveals in vivo protein interactions. J Cell Biol 2010; 189(4): 739-54.

Igaz LM, Kwong LK, Chen-Plotkin A, Winton MJ, Unger TL, Xu Y, Neumann M, Trojanowski JQ, Lee VM. Expression of TDP-43 C-terminal Fragments in Vitro Recapitulates Pathological Features of TDP-43 Proteinopathies. J Biol Chem 2009; 284(13): 8516-24.

Igaz LM, Kwong LK, Lee EB, Chen-Plotkin A, Swanson E, Unger T, Malunda J, Xu Y, Winton MJ, Trojanowski JQ, Lee VM. Dysregulation of the ALS-associated gene TDP-43 leads to neuronal death and degeneration in mice. J Clin Invest 2011; 121(2): 726-38.

Igaz LM, Kwong LK, Xu Y, Truax AC, Uryu K, Neumann M, Clark CM, Elman LB, Miller BL, Grossman M, McCluskey LF, Trojanowski JQ, Lee VM. Enrichment of C-terminal fragments in TAR DNA-binding protein-43 cytoplasmic inclusions in brain but not in spinal cord of frontotemporal lobar degeneration and amyotrophic lateral sclerosis. Am J Pathol 2008; 173(1): 182-94.

Iguchi Y, Eid L, Parent M, Soucy G, Bareil C, Riku Y, Kawai K, Takagi S, Yoshida M, Katsuno M, Sobue G, Julien JP. Exosome secretion is a key pathway for clearance of pathological TDP-43. Brain 2016; 139(Pt 12): 3187-201.

Ince PG, Evans J, Knopp M, Forster G, Hamdalla HH, Wharton SB, Shaw PJ. Corticospinal tract degeneration in the progressive muscular atrophy variant of ALS. Neurology 2003; 60(8): 1252-8.

Jain S, Wheeler JR, Walters RW, Agrawal A, Barsic A, Parker R. ATPase-Modulated Stress Granules Contain a Diverse Proteome and Substructure. Cell 2016; 164(3): 487-98.

James BD, Wilson RS, Boyle PA, Trojanowski JQ, Bennett DA, Schneider JA. TDP-43 stage, mixed pathologies, and clinical Alzheimer's-type dementia. Brain 2016; 139(11): 2983-93.

Jantrapirom S, Lo Piccolo L, Yoshida H, Yamaguchi M. Depletion of Ubiquilin induces an augmentation in soluble ubiquitinated Drosophila TDP-43 to drive neurotoxicity in the fly. Biochim Biophys Acta Mol Basis Dis 2018; 1864(9 Pt B): 3038-49.

Jeon GS, Shim YM, Lee DY, Kim JS, Kang M, Ahn SH, Shin JY, Geum D, Hong YH, Sung JJ. Pathological Modification of TDP-43 in Amyotrophic Lateral Sclerosis with SOD1 Mutations. Mol Neurobiol 2019; 56(3): 2007-21.

Johanson CE, Stopa EG, McMillan PN. The blood-cerebrospinal fluid barrier: structure and functional significance. Methods Mol Biol 2011; 686: 101-31.

Josephs KA, Hodges JR, Snowden JS, Mackenzie IR, Neumann M, Mann DM, Dickson DW. Neuropathological background of phenotypical variability in frontotemporal dementia. Acta Neuropathol 2011; 122(2): 137-53.

Jucker M, Walker LC. Self-propagation of pathogenic protein aggregates in neurodegenerative diseases. Nature 2013; 501(7465): 45-51.

Junttila A, Kuvaja M, Hartikainen P, Siloaho M, Helisalmi S, Moilanen V, Kiviharju A, Jansson L, Tienari PJ, Remes AM, Herukka SK. Cerebrospinal Fluid TDP-43 in Frontotemporal Lobar Degeneration and Amyotrophic Lateral Sclerosis Patients with and without the C9ORF72 Hexanucleotide Expansion. Dement Geriatr Cogn Dis Extra 2016; 6(1): 142-9.

Kabashi E, Valdmanis PN, Dion P, Spiegelman D, McConkey BJ, Vande Velde C, Bouchard JP, Lacomblez L, Pochigaeva K, Salachas F, Pradat PF, Camu W, Meininger V, Dupre N, Rouleau GA. TARDBP mutations in individuals with sporadic and familial amyotrophic lateral sclerosis. Nat Genet 2008; 40(5): 572-4.

Kametani F, Nonaka T, Suzuki T, Arai T, Dohmae N, Akiyama H, Hasegawa M. Identification of casein kinase-1 phosphorylation sites on TDP-43. Biochem Biophys Res Commun 2009; 382(2): 405-9.

Kametani F, Obi T, Shishido T, Akatsu H, Murayama S, Saito Y, Yoshida M, Hasegawa M. Mass spectrometric analysis of accumulated TDP-43 in amyotrophic lateral sclerosis brains. Sci Rep 2016; 6: 23281.

Kanouchi T, Ohkubo T, Yokota T. Can regional spreading of amyotrophic lateral sclerosis motor symptoms be explained by prion-like propagation? J Neurol Neurosurg Psychiatry 2012; 83(7): 739-45.

Kapur M, Monaghan CE, Ackerman SL. Regulation of mRNA Translation in Neurons-A Matter of Life and Death. Neuron 2017; 96(3): 616-37.

Kasai T, Tokuda T, Ishigami N, Sasayama H, Foulds P, Mitchell DJ, Mann DM, Allsop D, Nakagawa M. Increased TDP-43 protein in cerebrospinal fluid of patients with amyotrophic lateral sclerosis. Acta Neuropathol 2009; 117(1): 55-62.

Kato M, Han TW, Xie S, Shi K, Du X, Wu LC, Mirzaei H, Goldsmith EJ, Longgood J, Pei J, Grishin NV, Frantz DE, Schneider JW, Chen S, Li L, Sawaya MR, Eisenberg D, Tycko R, McKnight SL. Cell-free formation of RNA granules: low complexity sequence domains form dynamic fibers within hydrogels. Cell 2012; 149(4): 753-67.

Kawahara Y, Mieda-Sato A. TDP-43 promotes microRNA biogenesis as a component of the Drosha and Dicer complexes. Proc Natl Acad Sci U S A 2012; 109(9): 3347-52.

Kedersha N, Anderson P. Stress granules: sites of mRNA triage that regulate mRNA stability and translatability. Biochem Soc Trans 2002; 30(Pt 6): 963-9.

Kedersha N, Cho MR, Li W, Yacono PW, Chen S, Gilks N, Golan DE, Anderson P. Dynamic shuttling of TIA-1 accompanies the recruitment of mRNA to mammalian stress granules. J Cell Biol 2000; 151(6): 1257-68.

Keilhauer EC, Hein MY, Mann M. Accurate protein complex retrieval by affinity enrichment mass spectrometry (AE-MS) rather than affinity purification mass spectrometry (AP-MS). Mol Cell Proteomics 2015; 14(1): 120-35.

Khalfallah Y, Kuta R, Grasmuck C, Prat A, Durham HD, Vande Velde C. TDP-43 regulation of stress granule dynamics in neurodegenerative disease-relevant cell types. Sci Rep 2018; 8(1): 7551.

Khalil M, Teunissen CE, Otto M, Piehl F, Sormani MP, Gattringer T, Barro C, Kappos L, Comabella M, Fazekas F, Petzold A, Blennow K, Zetterberg H, Kuhle J. Neurofilaments as biomarkers in neurological disorders. Nat Rev Neurol 2018; 14(10): 577-89.

Kiernan MC, Vucic S, Cheah BC, Turner MR, Eisen A, Hardiman O, Burrell JR, Zoing MC. Amyotrophic lateral sclerosis. Lancet 2011; 377(9769): 942-55.

Kim HJ, Kim NC, Wang YD, Scarborough EA, Moore J, Diaz Z, MacLea KS, Freibaum B, Li S, Molliex A, Kanagaraj AP, Carter R, Boylan KB, Wojtas AM, Rademakers R, Pinkus JL, Greenberg SA, Trojanowski JQ, Traynor BJ, Smith BN, Topp S, Gkazi AS, Miller J, Shaw CE, Kottlors M, Kirschner J, Pestronk A, Li YR, Ford AF, Gitler AD, Benatar M, King OD, Kimonis VE, Ross ED, Weihl CC, Shorter J, Taylor JP. Mutations in prion-like domains in hnRNPA2B1 and hnRNPA1 cause multisystem proteinopathy and ALS. Nature 2013; 495(7442): 467-73.

King OD, Gitler AD, Shorter J. The tip of the iceberg: RNA-binding proteins with prion-like domains in neurodegenerative disease. Brain Res 2012; 1462: 61-80.

Kiskinis E, Sandoe J, Williams LA, Boulting GL, Moccia R, Wainger BJ, Han S, Peng T, Thams S, Mikkilineni S, Mellin C, Merkle FT, Davis-Dusenbery BN, Ziller M, Oakley D, Ichida J, Di Costanzo S, Atwater N, Maeder ML, Goodwin MJ, Nemesh J, Handsaker RE, Paull D, Noggle S, McCarroll SA, Joung JK, Woolf CJ, Brown RH, Eggan K. Pathways disrupted in human ALS motor neurons identified through genetic correction of mutant SOD1. Cell Stem Cell 2014; 14(6): 781-95.

Kon T, Mori F, Oyama Y, Tanji K, Kimura T, Takahashi S, Wakabayashi K. An autopsy case of early-stage amyotrophic lateral sclerosis with TDP-43 immunoreactive neuronal, but not glial, inclusions. Neuropathology 2019; 39(3): 224-30.

Kramer NJ, Carlomagno Y, Zhang YJ, Almeida S, Cook CN, Gendron TF, Prudencio M, Van Blitterswijk M, Belzil V, Couthouis J, Paul JW, 3rd, Goodman LD, Daughrity L, Chew J, Garrett A, Pregent L, Jansen-West K, Tabassian LJ, Rademakers R, Boylan K, Graff-Radford NR, Josephs KA, Parisi JE, Knopman DS, Petersen RC, Boeve BF, Deng N, Feng Y, Cheng TH, Dickson DW, Cohen SN, Bonini NM, Link CD, Gao FB, Petrucelli L, Gitler AD. Spt4 selectively regulates the expression of C9orf72 sense and antisense mutant transcripts. Science 2016; 353(6300): 708-12.

Krecic AM, Swanson MS. hnRNP complexes: composition, structure, and function. Curr Opin Cell Biol 1999; 11(3): 363-71.

Kuhnlein P, Sperfeld AD, Vanmassenhove B, Van Deerlin V, Lee VM, Trojanowski JQ, Kretzschmar HA, Ludolph AC, Neumann M. Two German kindreds with familial amyotrophic lateral sclerosis due to TARDBP mutations. Arch Neurol 2008; 65(9): 1185-9.

Kuiperij HB, Versleijen AA, Beenes M, Verwey NA, Benussi L, Paterlini A, Binetti G, Teunissen CE, Raaphorst J, Schelhaas HJ, Kusters B, Pijnenburg YA, Ghidoni R, Verbeek MM. Tau Rather than TDP-43 Proteins are Potential Cerebrospinal Fluid Biomarkers for Frontotemporal Lobar Degeneration Subtypes: A Pilot Study. J Alzheimers Dis 2017; 55(2): 585-95.

Kwiatkowski TJ, Jr., Bosco DA, Leclerc AL, Tamrazian E, Vanderburg CR, Russ C, Davis A, Gilchrist J, Kasarskis EJ, Munsat T, Valdmanis P, Rouleau GA, Hosler BA, Cortelli P, de Jong PJ, Yoshinaga Y, Haines JL, Pericak-Vance MA, Yan J, Ticozzi N, Siddique T, McKenna-Yasek D, Sapp PC, Horvitz HR, Landers JE, Brown RH, Jr. Mutations in the FUS/TLS gene on chromosome 16 cause familial amyotrophic lateral sclerosis. Science 2009; 323(5918): 1205-8.

Kwong LK, Irwin DJ, Walker AK, Xu Y, Riddle DM, Trojanowski JQ, Lee VM. Novel monoclonal antibodies to normal and pathologically altered human TDP-43 proteins. Acta Neuropathol Commun 2014; 2: 33.

Kwong LK, Uryu K, Trojanowski JQ, Lee VM. TDP-43 proteinopathies: neurodegenerative protein misfolding diseases without amyloidosis. Neurosignals 2008; 16(1): 41-51.

Laferriere F, Maniecka Z, Perez-Berlanga M, Hruska-Plochan M, Gilhespy L, Hock EM, Wagner U, Afroz T, Boersema PJ, Barmettler G, Foti SC, Asi YT, Isaacs AM, Al-Amoudi A, Lewis A, Stahlberg H, Ravits J, De Giorgi F, Ichas F, Bezard E, Picotti P, Lashley T, Polymenidou M. TDP-43 extracted from frontotemporal lobar degeneration subject brains displays distinct aggregate assemblies and neurotoxic effects reflecting disease progression rates. Nat Neurosci 2019; 22(1): 65-77.

Lee AS. The ER chaperone and signaling regulator GRP78/BiP as a monitor of endoplasmic reticulum stress. Methods 2005; 35(4): 373-81.

Lee EB, Lee VM, Trojanowski JQ. Gains or losses: molecular mechanisms of TDP43-mediated neurodegeneration. Nat Rev Neurosci 2011; 13(1): 38-50.

Lee EB, Porta S, Michael Baer G, Xu Y, Suh E, Kwong LK, Elman L, Grossman M, Lee VM, Irwin DJ, Van Deerlin VM, Trojanowski JQ. Expansion of the classification of FTLD-TDP: distinct pathology associated with rapidly progressive frontotemporal degeneration. Acta Neuropathol 2017; 134(1): 65-78.

Lee KH, Zhang P, Kim HJ, Mitrea DM, Sarkar M, Freibaum BD, Cika J, Coughlin M, Messing J, Molliex A, Maxwell BA, Kim NC, Temirov J, Moore J, Kolaitis RM, Shaw TI, Bai B, Peng J, Kriwacki RW, Taylor JP. C9orf72 Dipeptide Repeats Impair the Assembly, Dynamics, and Function of Membrane-Less Organelles. Cell 2016; 167(3): 774-88 e17.

Lehmer C, Oeckl P, Weishaupt JH, Volk AE, Diehl-Schmid J, Schroeter ML, Lauer M, Kornhuber J, Levin J, Fassbender K, Landwehrmeyer B, German Consortium for Frontotemporal Lobar D, Schludi MH, Arzberger T, Kremmer E, Flatley A, Feederle R, Steinacker P, Weydt P, Ludolph AC, Edbauer D, Otto M. Poly-GP in cerebrospinal fluid links C9orf72-associated dipeptide repeat expression to the asymptomatic phase of ALS/FTD. EMBO Mol Med 2017; 9(7): 859-68.

Leibiger C, Deisel J, Aufschnaiter A, Ambros S, Tereshchenko M, Verheijen BM, Buttner S, Braun RJ. TDP-43 controls lysosomal pathways thereby determining its own clearance and cytotoxicity. Hum Mol Genet 2018; 27(9): 1593-607.

Leigh PN, Whitwell H, Garofalo O, Buller J, Swash M, Martin JE, Gallo JM, Weller RO, Anderton BH. Ubiquitin-immunoreactive intraneuronal inclusions in amyotrophic lateral sclerosis. Morphology, distribution, and specificity. Brain 1991; 114 (Pt 2): 775-88.

Leitner A, Joachimiak LA, Bracher A, Monkemeyer L, Walzthoeni T, Chen B, Pechmann S, Holmes S, Cong Y, Ma B, Ludtke S, Chiu W, Hartl FU, Aebersold R, Frydman J. The molecular architecture of the eukaryotic chaperonin TRiC/CCT. Structure 2012; 20(5): 814-25.

Li Q, Yokoshi M, Okada H, Kawahara Y. The cleavage pattern of TDP-43 determines its rate of clearance and cytotoxicity. Nat Commun 2015; 6: 6183.

Li Y, Collins M, An J, Geiser R, Tegeler T, Tsantilas K, Garcia K, Pirrotte P, Bowser R. Immunoprecipitation and mass spectrometry defines an extensive RBM45 protein-protein interaction network. Brain Res 2016; 1647: 79-93.

Li YR, King OD, Shorter J, Gitler AD. Stress granules as crucibles of ALS pathogenesis. J Cell Biol 2013; 201(3): 361-72.

Lindholm D, Korhonen L, Eriksson O, Koks S. Recent Insights into the Role of Unfolded Protein Response in ER Stress in Health and Disease. Front Cell Dev Biol 2017; 5: 48.

Ling JP, Pletnikova O, Troncoso JC, Wong PC. TDP-43 repression of nonconserved cryptic exons is compromised in ALS-FTD. Science 2015; 349(6248): 650-5.

Ling SC, Albuquerque CP, Han JS, Lagier-Tourenne C, Tokunaga S, Zhou H, Cleveland DW. ALS-associated mutations in TDP-43 increase its stability and promote TDP-43 complexes with FUS/TLS. Proc Natl Acad Sci U S A 2010; 107(30): 13318-23.

Ling SC, Polymenidou M, Cleveland DW. Converging mechanisms in ALS and FTD: disrupted RNA and protein homeostasis. Neuron 2013; 79(3): 416-38.

Liscic RM, Grinberg LT, Zidar J, Gitcho MA, Cairns NJ. ALS and FTLD: two faces of TDP-43 proteinopathy. Eur J Neurol 2008; 15(8): 772-80.

Liu Y, Pattamatta A, Zu T, Reid T, Bardhi O, Borchelt DR, Yachnis AT, Ranum LP. C9orf72 BAC Mouse Model with Motor Deficits and Neurodegenerative Features of ALS/FTD. Neuron 2016; 90(3): 521-34.

Liu-Yesucevitz L, Bilgutay A, Zhang YJ, Vanderweyde T, Citro A, Mehta T, Zaarur N, McKee A, Bowser R, Sherman M, Petrucelli L, Wolozin B. Tar DNA binding protein-43 (TDP-43) associates with stress granules: analysis of cultured cells and pathological brain tissue. PLoS One 2010; 5(10): e13250.

Logroscino G, Traynor BJ, Hardiman O, Chio A, Mitchell D, Swingler RJ, Millul A, Benn E, Beghi E, Eurals. Incidence of amyotrophic lateral sclerosis in Europe. J Neurol Neurosurg Psychiatry 2010; 81(4): 385-90.

Lomen-Hoerth C, Anderson T, Miller B. The overlap of amyotrophic lateral sclerosis and frontotemporal dementia. Neurology 2002; 59(7): 1077-9.

Lu CH, Macdonald-Wallis C, Gray E, Pearce N, Petzold A, Norgren N, Giovannoni G, Fratta P, Sidle K, Fish M, Orrell R, Howard R, Talbot K, Greensmith L, Kuhle J, Turner MR, Malaspina A. Neurofilament light chain: A prognostic biomarker in amyotrophic lateral sclerosis. Neurology 2015; 84(22): 2247-57.

Lukavsky PJ, Daujotyte D, Tollervey JR, Ule J, Stuani C, Buratti E, Baralle FE, Damberger FF, Allain FH. Molecular basis of UG-rich RNA recognition by the human splicing factor TDP-43. Nat Struct Mol Biol 2013; 20(12): 1443-9.

Lule DE, Aho-Ozhan HEA, Vazquez C, Weiland U, Weishaupt JH, Otto M, Anderl-Straub S, Semler E, Uttner I, Ludolph AC. Story of the ALS-FTD continuum retold: rather two distinct entities. J Neurol Neurosurg Psychiatry 2019; 90(5): 586-9.

Lupo V, Aguado C, Knecht E, Espinos C. Chaperonopathies: Spotlight on Hereditary Motor Neuropathies. Front Mol Biosci 2016; 3: 81.

Mackenzie IR, Arzberger T, Kremmer E, Troost D, Lorenzl S, Mori K, Weng SM, Haass C, Kretzschmar HA, Edbauer D, Neumann M. Dipeptide repeat protein pathology in C9ORF72 mutation cases: clinico-pathological correlations. Acta Neuropathol 2013; 126(6): 859-79.

Mackenzie IR, Bigio EH, Ince PG, Geser F, Neumann M, Cairns NJ, Kwong LK, Forman MS, Ravits J, Stewart H, Eisen A, McClusky L, Kretzschmar HA, Monoranu CM, Highley JR, Kirby J, Siddique T, Shaw PJ, Lee VM, Trojanowski JQ. Pathological TDP-43 distinguishes sporadic amyotrophic lateral sclerosis from amyotrophic lateral sclerosis with SOD1 mutations. Ann Neurol 2007; 61(5): 427-34.

Mackenzie IR, Frick P, Grasser FA, Gendron TF, Petrucelli L, Cashman NR, Edbauer D, Kremmer E, Prudlo J, Troost D, Neumann M. Quantitative analysis and clinico-pathological correlations of different dipeptide repeat protein pathologies in C9ORF72 mutation carriers. Acta Neuropathol 2015; 130(6): 845-61.

Mackenzie IR, Frick P, Neumann M. The neuropathology associated with repeat expansions in the C9ORF72 gene. Acta Neuropathol 2014; 127(3): 347-57.

Mackenzie IR, Neumann M. Molecular neuropathology of frontotemporal dementia: insights into disease mechanisms from postmortem studies. J Neurochem 2016; 138 Suppl 1: 54-70.

Mackenzie IR, Neumann M. Reappraisal of TDP-43 pathology in FTLD-U subtypes. Acta Neuropathol 2017; 134(1): 79-96.

Magnus T, Beck M, Giess R, Puls I, Naumann M, Toyka KV. Disease progression in amyotrophic lateral sclerosis: predictors of survival. Muscle Nerve 2002; 25(5): 709-14.

Majounie E, Renton AE, Mok K, Dopper EG, Waite A, Rollinson S, Chio A, Restagno G, Nicolaou N, Simon-Sanchez J, van Swieten JC, Abramzon Y, Johnson JO, Sendtner M, Pamphlett R, Orrell RW, Mead S, Sidle KC, Houlden H, Rohrer JD, Morrison KE, Pall H, Talbot K, Ansorge O, Chromosome ALSFTDC, French research network on FFA, Consortium I, Hernandez DG, Arepalli S, Sabatelli M, Mora G, Corbo M, Giannini F, Calvo A, Englund E, Borghero G, Floris GL, Remes AM, Laaksovirta H, McCluskey L, Trojanowski JQ, Van Deerlin VM, Schellenberg GD, Nalls MA, Drory VE, Lu CS, Yeh TH, Ishiura H, Takahashi Y, Tsuji S, Le Ber I, Brice A, Drepper C, Williams N, Kirby J, Shaw P, Hardy J, Tienari PJ, Heutink P, Morris HR, Pickering-Brown S, Traynor BJ. Frequency of the C9orf72 hexanucleotide repeat expansion in patients with amyotrophic lateral sclerosis and frontotemporal dementia: a cross-sectional study. Lancet Neurol 2012; 11(4): 323-30.

Mann JR, Gleixner AM, Mauna JC, Gomes E, DeChellis-Marks MR, Needham PG, Copley KE, Hurtle B, Portz B, Pyles NJ, Guo L, Calder CB, Wills ZP, Pandey UB, Kofler JK, Brodsky JL, Thathiah A, Shorter J, Donnelly CJ. RNA Binding Antagonizes Neurotoxic Phase Transitions of TDP-43. Neuron 2019; 102(2): 321-38 e8.

Markmiller S, Soltanieh S, Server KL, Mak R, Jin W, Fang MY, Luo EC, Krach F, Yang D, Sen A, Fulzele A, Wozniak JM, Gonzalez DJ, Kankel MW, Gao FB, Bennett EJ, Lecuyer E, Yeo GW. Context-Dependent and Disease-Specific Diversity in Protein Interactions within Stress Granules. Cell 2018; 172(3): 590-604 e13.

Marrone L, Drexler HCA, Wang J, Tripathi P, Distler T, Heisterkamp P, Anderson EN, Kour S, Moraiti A, Maharana S, Bhatnagar R, Belgard TG, Tripathy V, Kalmbach N, Hosseinzadeh Z, Crippa V, Abo-Rady M, Wegner F, Poletti A, Troost D, Aronica E, Busskamp V, Weis J, Pandey UB, Hyman AA, Alberti S, Goswami A, Sterneckert J. FUS pathology in ALS is linked to alterations in multiple ALS-associated proteins and rescued by drugs stimulating autophagy. Acta Neuropathol 2019; 138(1): 67-84.

Mascini M, Palchetti I, Tombelli S. Nucleic acid and peptide aptamers: fundamentals and bioanalytical aspects. Angew Chem Int Ed Engl 2012; 51(6): 1316-32.

Matsumoto K, Minami M, Shinozaki F, Suzuki Y, Abe K, Zenno S, Matsumoto S, Minami Y. Hsp90 is involved in the formation of P-bodies and stress granules. Biochem Biophys Res Commun 2011; 407(4): 720-4.

Maury Y, Come J, Piskorowski RA, Salah-Mohellibi N, Chevaleyre V, Peschanski M, Martinat C, Nedelec S. Combinatorial analysis of developmental cues efficiently converts human pluripotent stem cells into multiple neuronal subtypes. Nat Biotechnol 2015; 33(1): 89-96.

May S, Hornburg D, Schludi MH, Arzberger T, Rentzsch K, Schwenk BM, Grasser FA, Mori K, Kremmer E, Banzhaf-Strathmann J, Mann M, Meissner F, Edbauer D. C9orf72 FTLD/ALS-associated Gly-Ala dipeptide repeat proteins cause neuronal toxicity and Unc119 sequestration. Acta Neuropathol 2014; 128(4): 485-503.

McDonald KK, Aulas A, Destroismaisons L, Pickles S, Beleac E, Camu W, Rouleau GA, Vande Velde C. TAR DNA-binding protein 43 (TDP-43) regulates stress granule dynamics via differential regulation of G3BP and TIA-1. Hum Mol Genet 2011; 20(7): 1400-10.

McGoldrick P, Joyce PI, Fisher EM, Greensmith L. Rodent models of amyotrophic lateral sclerosis. Biochim Biophys Acta 2013; 1832(9): 1421-36.

McGurk L, Lee VM, Trojanowksi JQ, Van Deerlin VM, Lee EB, Bonini NM. Poly-A binding protein-1 localization to a subset of TDP-43 inclusions in amyotrophic lateral sclerosis occurs more frequently in patients harboring an expansion in C9orf72. J Neuropathol Exp Neurol 2014; 73(9): 837-45.

Michalski A, Damoc E, Hauschild JP, Lange O, Wieghaus A, Makarov A, Nagaraj N, Cox J, Mann M, Horning S. Mass spectrometry-based proteomics using Q Exactive, a high-performance benchtop quadrupole Orbitrap mass spectrometer. Mol Cell Proteomics 2011; 10(9): M111 011015.

Miller TM, Pestronk A, David W, Rothstein J, Simpson E, Appel SH, Andres PL, Mahoney K, Allred P, Alexander K, Ostrow LW, Schoenfeld D, Macklin EA, Norris DA, Manousakis G, Crisp M, Smith R, Bennett CF, Bishop KM, Cudkowicz ME. An antisense oligonucleotide against SOD1 delivered intrathecally for patients with SOD1 familial amyotrophic lateral sclerosis: a phase 1, randomised, first-in-man study. Lancet Neurol 2013; 12(5): 435-42.

Mitchell JD, Callagher P, Gardham J, Mitchell C, Dixon M, Addison-Jones R, Bennett W, O'Brien MR. Timelines in the diagnostic evaluation of people with suspected amyotrophic lateral sclerosis (ALS)/motor neuron disease (MND)--a 20-year review: can we do better? Amyotroph Lateral Scler 2010; 11(6): 537-41.

Mizielinska S, Lashley T, Norona FE, Clayton EL, Ridler CE, Fratta P, Isaacs AM. C9orf72 frontotemporal lobar degeneration is characterised by frequent neuronal sense and antisense RNA foci. Acta Neuropathol 2013; 126(6): 845-57.

Moens TG, Niccoli T, Wilson KM, Atilano ML, Birsa N, Gittings LM, Holbling BV, Dyson MC, Thoeng A, Neeves J, Glaria I, Yu L, Bussmann J, Storkebaum E, Pardo M, Choudhary JS, Fratta P, Partridge L, Isaacs AM. C9orf72 arginine-rich dipeptide proteins interact with ribosomal proteins in vivo to induce a toxic translational arrest that is rescued by eIF1A. Acta Neuropathol 2019; 137(3): 487-500.

Molliex A, Temirov J, Lee J, Coughlin M, Kanagaraj AP, Kim HJ, Mittag T, Taylor JP. Phase separation by low complexity domains promotes stress granule assembly and drives pathological fibrillization. Cell 2015; 163(1): 123-33.

Mori F, Tanji K, Zhang HX, Nishihira Y, Tan CF, Takahashi H, Wakabayashi K. Maturation process of TDP-43-positive neuronal cytoplasmic inclusions in amyotrophic lateral sclerosis with and without dementia. Acta Neuropathol 2008; 116(2): 193-203.

Mori K, Weng SM, Arzberger T, May S, Rentzsch K, Kremmer E, Schmid B, Kretzschmar HA, Cruts M, Van Broeckhoven C, Haass C, Edbauer D. The C9orf72 GGGGCC repeat is

translated into aggregating dipeptide-repeat proteins in FTLD/ALS. Science 2013; 339(6125): 1335-8.

Muller-McNicoll M, Botti V, de Jesus Domingues AM, Brandl H, Schwich OD, Steiner MC, Curk T, Poser I, Zarnack K, Neugebauer KM. SR proteins are NXF1 adaptors that link alternative RNA processing to mRNA export. Genes Dev 2016; 30(5): 553-66.

Nelson PT, Dickson DW, Trojanowski JQ, Jack CR, Boyle PA, Arfanakis K, Rademakers R, Alafuzoff I, Attems J, Brayne C, Coyle-Gilchrist ITS, Chui HC, Fardo DW, Flanagan ME, Halliday G, Hokkanen SRK, Hunter S, Jicha GA, Katsumata Y, Kawas CH, Keene CD, Kovacs GG, Kukull WA, Levey AI, Makkinejad N, Montine TJ, Murayama S, Murray ME, Nag S, Rissman RA, Seeley WW, Sperling RA, White Iii CL, Yu L, Schneider JA. Limbic-predominant age-related TDP-43 encephalopathy (LATE): consensus working group report. Brain 2019; 142(6): 1503-27.

Neumann M, Kwong LK, Lee EB, Kremmer E, Flatley A, Xu Y, Forman MS, Troost D, Kretzschmar HA, Trojanowski JQ, Lee VM. Phosphorylation of S409/410 of TDP-43 is a consistent feature in all sporadic and familial forms of TDP-43 proteinopathies. Acta Neuropathol 2009; 117(2): 137-49.

Neumann M, Sampathu DM, Kwong LK, Truax AC, Micsenyi MC, Chou TT, Bruce J, Schuck T, Grossman M, Clark CM, McCluskey LF, Miller BL, Masliah E, Mackenzie IR, Feldman H, Feiden W, Kretzschmar HA, Trojanowski JQ, Lee VM. Ubiquitinated TDP-43 in frontotemporal lobar degeneration and amyotrophic lateral sclerosis. Science 2006; 314(5796): 130-3.

Niccoli T, Partridge L, Isaacs AM. Ageing as a risk factor for ALS/FTD. Hum Mol Genet 2017; 26(R2): R105-R13.

Nicholson AM, Finch NA, Thomas CS, Wojtas A, Rutherford NJ, Mielke MM, Roberts RO, Boeve BF, Knopman DS, Petersen RC, Rademakers R. Progranulin protein levels are differently regulated in plasma and CSF. Neurology 2014; 82(21): 1871-8.

Nihei K, McKee AC, Kowall NW. Patterns of neuronal degeneration in the motor cortex of amyotrophic lateral sclerosis patients. Acta Neuropathol 1993; 86(1): 55-64.

Nijssen J, Comley LH, Hedlund E. Motor neuron vulnerability and resistance in amyotrophic lateral sclerosis. Acta Neuropathol 2017; 133(6): 863-85.

Nonaka T, Kametani F, Arai T, Akiyama H, Hasegawa M. Truncation and pathogenic mutations facilitate the formation of intracellular aggregates of TDP-43. Hum Mol Genet 2009; 18(18): 3353-64.

Nonaka T, Suzuki G, Tanaka Y, Kametani F, Hirai S, Okado H, Miyashita T, Saitoe M, Akiyama H, Masai H, Hasegawa M. Phosphorylation of TAR DNA-binding Protein of 43 kDa (TDP-43) by Truncated Casein Kinase 1delta Triggers Mislocalization and Accumulation of TDP-43. J Biol Chem 2016; 291(11): 5473-83.

Nonhoff U, Ralser M, Welzel F, Piccini I, Balzereit D, Yaspo ML, Lehrach H, Krobitsch S. Ataxin-2 interacts with the DEAD/H-box RNA helicase DDX6 and interferes with P-bodies and stress granules. Mol Biol Cell 2007; 18(4): 1385-96.

Noto Y, Shibuya K, Sato Y, Kanai K, Misawa S, Sawai S, Mori M, Uchiyama T, Isose S, Nasu S, Sekiguchi Y, Fujimaki Y, Kasai T, Tokuda T, Nakagawa M, Kuwabara S. Elevated CSF TDP-43 levels in amyotrophic lateral sclerosis: specificity, sensitivity, and a possible prognostic value. Amyotroph Lateral Scler 2011; 12(2): 140-3.

O'Toole O, Traynor BJ, Brennan P, Sheehan C, Frost E, Corr B, Hardiman O. Epidemiology and clinical features of amyotrophic lateral sclerosis in Ireland between 1995 and 2004. J Neurol Neurosurg Psychiatry 2008; 79(1): 30-2.

Oeckl P, Steinacker P, Otto M. Comparison of Internal Standard Approaches for SRM Analysis of Alpha-Synuclein in Cerebrospinal Fluid. J Proteome Res 2018; 17(1): 516-23.

Osaka M, Ito D, Suzuki N. Disturbance of proteasomal and autophagic protein degradation pathways by amyotrophic lateral sclerosis-linked mutations in ubiquilin 2. Biochem Biophys Res Commun 2016; 472(2): 324-31.

Otto M, Bowser R, Turner M, Berry J, Brettschneider J, Connor J, Costa J, Cudkowicz M, Glass J, Jahn O, Lehnert S, Malaspina A, Parnetti L, Petzold A, Shaw P, Sherman A, Steinacker P, Sussmuth S, Teunissen C, Tumani H, Wuolikainen A, Ludolph A. Roadmap and standard operating procedures for biobanking and discovery of neurochemical markers in ALS. Amyotroph Lateral Scler 2012; 13(1): 1-10.

Ou SH, Wu F, Harrich D, Garcia-Martinez LF, Gaynor RB. Cloning and characterization of a novel cellular protein, TDP-43, that binds to human immunodeficiency virus type 1 TAR DNA sequence motifs. J Virol 1995; 69(6): 3584-96.

Pesiridis GS, Tripathy K, Tanik S, Trojanowski JQ, Lee VM. A "two-hit" hypothesis for inclusion formation by carboxyl-terminal fragments of TDP-43 protein linked to RNA depletion and impaired microtubule-dependent transport. J Biol Chem 2011; 286(21): 18845-55.

Peters OM, Cabrera GT, Tran H, Gendron TF, McKeon JE, Metterville J, Weiss A, Wightman N, Salameh J, Kim J, Sun H, Boylan KB, Dickson D, Kennedy Z, Lin Z, Zhang YJ, Daughrity L, Jung C, Gao FB, Sapp PC, Horvitz HR, Bosco DA, Brown SP, de Jong P, Petrucelli L, Mueller C, Brown RH, Jr. Human C9ORF72 Hexanucleotide Expansion Reproduces RNA Foci and Dipeptide Repeat Proteins but Not Neurodegeneration in BAC Transgenic Mice. Neuron 2015; 88(5): 902-9.

Petri S, Krampfl K, Hashemi F, Grothe C, Hori A, Dengler R, Bufler J. Distribution of GABAA receptor mRNA in the motor cortex of ALS patients. J Neuropathol Exp Neurol 2003; 62(10): 1041-51.

Phizicky EM, Fields S. Protein-protein interactions: methods for detection and analysis. Microbiol Rev 1995; 59(1): 94-123.

Polymenidou M, Lagier-Tourenne C, Hutt KR, Huelga SC, Moran J, Liang TY, Ling SC, Sun E, Wancewicz E, Mazur C, Kordasiewicz H, Sedaghat Y, Donohue JP, Shiue L, Bennett CF, Yeo GW, Cleveland DW. Long pre-mRNA depletion and RNA missplicing contribute to neuronal vulnerability from loss of TDP-43. Nat Neurosci 2011; 14(4): 459-68.

Poser I, Sarov M, Hutchins JR, Heriche JK, Toyoda Y, Pozniakovsky A, Weigl D, Nitzsche A, Hegemann B, Bird AW, Pelletier L, Kittler R, Hua S, Naumann R, Augsburg M, Sykora MM, Hofemeister H, Zhang Y, Nasmyth K, White KP, Dietzel S, Mechtler K, Durbin R, Stewart AF, Peters JM, Buchholz F, Hyman AA. BAC TransgeneOmics: a high-throughput method for exploration of protein function in mammals. Nat Methods 2008; 5(5): 409-15.

Prasad A, Sivalingam V, Bharathi V, Girdhar A, Patel BK. The amyloidogenicity of a C-terminal region of TDP-43 implicated in Amyotrophic Lateral Sclerosis can be affected by anions, acetylation and homodimerization. Biochimie 2018; 150: 76-87.

Pringle CE, Hudson AJ, Munoz DG, Kiernan JA, Brown WF, Ebers GC. Primary lateral sclerosis. Clinical features, neuropathology and diagnostic criteria. Brain 1992; 115 (Pt 2): 495-520.

Proudfoot M, Jones A, Talbot K, Al-Chalabi A, Turner MR. The ALSFRS as an outcome measure in therapeutic trials and its relationship to symptom onset. Amyotrophic lateral sclerosis & frontotemporal degeneration 2016; 17(5-6): 414-25.

Radcliffe CB, Clarke JL. An Important Case of Paralysis and Muscular Atrophy, with Disease of the Nervous Centres. Br Foreign Med Chir Rev 1862; 30(59): 215-25.

Rascovsky K, Hodges JR, Knopman D, Mendez MF, Kramer JH, Neuhaus J, van Swieten JC, Seelaar H, Dopper EG, Onyike CU, Hillis AE, Josephs KA, Boeve BF, Kertesz A, Seeley WW, Rankin KP, Johnson JK, Gorno-Tempini ML, Rosen H, Prioleau-Latham CE, Lee A, Kipps CM, Lillo P, Piguet O, Rohrer JD, Rossor MN, Warren JD, Fox NC, Galasko D, Salmon DP, Black SE, Mesulam M, Weintraub S, Dickerson BC, Diehl-Schmid J, Pasquier F, Deramecourt V, Lebert F, Pijnenburg Y, Chow TW, Manes F, Grafman J, Cappa SF,

Freedman M, Grossman M, Miller BL. Sensitivity of revised diagnostic criteria for the behavioural variant of frontotemporal dementia. Brain 2011; 134(Pt 9): 2456-77.

Ravits J, Paul P, Jorg C. Focality of upper and lower motor neuron degeneration at the clinical onset of ALS. Neurology 2007; 68(19): 1571-5.

Ravits JM, La Spada AR. ALS motor phenotype heterogeneity, focality, and spread: deconstructing motor neuron degeneration. Neurology 2009; 73(10): 805-11.

Reijn TS, Abdo WF, Schelhaas HJ, Verbeek MM. CSF neurofilament protein analysis in the differential diagnosis of ALS. J Neurol 2009; 256(4): 615-9.

Renton AE, Majounie E, Waite A, Simon-Sanchez J, Rollinson S, Gibbs JR, Schymick JC, Laaksovirta H, van Swieten JC, Myllykangas L, Kalimo H, Paetau A, Abramzon Y, Remes AM, Kaganovich A, Scholz SW, Duckworth J, Ding J, Harmer DW, Hernandez DG, Johnson JO, Mok K, Ryten M, Trabzuni D, Guerreiro RJ, Orrell RW, Neal J, Murray A, Pearson J, Jansen IE, Sondervan D, Seelaar H, Blake D, Young K, Halliwell N, Callister JB, Toulson G, Richardson A, Gerhard A, Snowden J, Mann D, Neary D, Nalls MA, Peuralinna T, Jansson L, Isoviita VM, Kaivorinne AL, Holtta-Vuori M, Ikonen E, Sulkava R, Benatar M, Wuu J, Chio A, Restagno G, Borghero G, Sabatelli M, Consortium I, Heckerman D, Rogaeva E, Zinman L, Rothstein JD, Sendtner M, Drepper C, Eichler EE, Alkan C, Abdullaev Z, Pack SD, Dutra A, Pak E, Hardy J, Singleton A, Williams NM, Heutink P, Pickering-Brown S, Morris HR, Tienari PJ, Traynor BJ. A hexanucleotide repeat expansion in C9ORF72 is the cause of chromosome 9p21-linked ALS-FTD. Neuron 2011; 72(2): 257-68.

Rogers GW, Jr., Richter NJ, Lima WF, Merrick WC. Modulation of the helicase activity of eIF4A by eIF4B, eIF4H, and eIF4F. J Biol Chem 2001; 276(33): 30914-22.

Rosen DR, Siddique T, Patterson D, Figlewicz DA, Sapp P, Hentati A, Donaldson D, Goto J, O'Regan JP, Deng HX, et al. Mutations in Cu/Zn superoxide dismutase gene are associated with familial amyotrophic lateral sclerosis. Nature 1993; 362(6415): 59-62.

Rosenfeld J, Swash M. What's in a name? Lumping or splitting ALS, PLS, PMA, and the other motor neuron diseases. Neurology 2006; 66(5): 624-5.

Rosengren LE, Karlsson JE, Karlsson JO, Persson LI, Wikkelso C. Patients with amyotrophic lateral sclerosis and other neurodegenerative diseases have increased levels of neurofilament protein in CSF. J Neurochem 1996; 67(5): 2013-8.

Santos MO, Gromicho M, Pinto S, de Carvalho M. Very late-onset amyotrophic lateral sclerosis in a Portuguese cohort. Amyotroph Lateral Scler Frontotemporal Degener 2018; 19(7-8): 619-22.

Sasaki S. Autophagy in spinal cord motor neurons in sporadic amyotrophic lateral sclerosis. J Neuropathol Exp Neurol 2011; 70(5): 349-59.

Schludi MH, May S, Grasser FA, Rentzsch K, Kremmer E, Kupper C, Klopstock T, German Consortium for Frontotemporal Lobar D, Bavarian Brain Banking A, Arzberger T, Edbauer D. Distribution of dipeptide repeat proteins in cellular models and C9orf72 mutation cases suggests link to transcriptional silencing. Acta Neuropathol 2015; 130(4): 537-55.

Schwenk BM, Hartmann H, Serdaroglu A, Schludi MH, Hornburg D, Meissner F, Orozco D, Colombo A, Tahirovic S, Michaelsen M, Schreiber F, Haupt S, Peitz M, Brustle O, Kupper C, Klopstock T, Otto M, Ludolph AC, Arzberger T, Kuhn PH, Edbauer D. TDP-43 loss of function inhibits endosomal trafficking and alters trophic signaling in neurons. EMBO J 2016; 35(21): 2350-70.

Schymick JC, Yang Y, Andersen PM, Vonsattel JP, Greenway M, Momeni P, Elder J, Chio A, Restagno G, Robberecht W, Dahlberg C, Mukherjee O, Goate A, Graff-Radford N, Caselli RJ, Hutton M, Gass J, Cannon A, Rademakers R, Singleton AB, Hardiman O, Rothstein J, Hardy J, Traynor BJ. Progranulin mutations and amyotrophic lateral sclerosis or amyotrophic lateral sclerosis-frontotemporal dementia phenotypes. J Neurol Neurosurg Psychiatry 2007; 78(7): 754-6.

Scotter EL, Vance C, Nishimura AL, Lee YB, Chen HJ, Urwin H, Sardone V, Mitchell JC, Rogelj B, Rubinsztein DC, Shaw CE. Differential roles of the ubiquitin proteasome system and autophagy in the clearance of soluble and aggregated TDP-43 species. J Cell Sci 2014; 127(Pt 6): 1263-78.

Sha SJ, Miller ZA, Min SW, Zhou Y, Brown J, Mitic LL, Karydas A, Koestler M, Tsai R, Corbetta-Rastelli C, Lin S, Hare E, Fields S, Fleischmann KE, Powers R, Fitch R, Martens LH, Shamloo M, Fagan AM, Farese RV, Jr., Pearlman R, Seeley W, Miller BL, Gan L, Boxer AL. An 8-week, open-label, dose-finding study of nimodipine for the treatment of progranulin insufficiency from GRN gene mutations. Alzheimers Dement (N Y) 2017; 3(4): 507-12.

Shaw PJ. Motor neurone disease. BMJ 1999; 318(7191): 1118-21.

Shaw PJ, Ince PG, Falkous G, Mantle D. Oxidative damage to protein in sporadic motor neuron disease spinal cord. Ann Neurol 1995; 38(4): 691-5.

Sheets MD, Amersdorfer P, Finnern R, Sargent P, Lindquist E, Schier R, Hemingsen G, Wong C, Gerhart JC, Marks JD. Efficient construction of a large nonimmune phage antibody library: the production of high-affinity human single-chain antibodies to protein antigens. Proc Natl Acad Sci U S A 1998; 95(11): 6157-62.

Shi Y, Lin S, Staats KA, Li Y, Chang WH, Hung ST, Hendricks E, Linares GR, Wang Y, Son EY, Wen X, Kisler K, Wilkinson B, Menendez L, Sugawara T, Woolwine P, Huang M, Cowan MJ, Ge B, Koutsodendris N, Sandor KP, Komberg J, Vangoor VR, Senthilkumar K, Hennes V, Seah C, Nelson AR, Cheng TY, Lee SJ, August PR, Chen JA, Wisniewski N, Hanson-Smith V, Belgard TG, Zhang A, Coba M, Grunseich C, Ward ME, van den Berg LH, Pasterkamp RJ, Trotti D, Zlokovic BV, Ichida JK. Haploinsufficiency leads to neurodegeneration in C9ORF72 ALS/FTD human induced motor neurons. Nat Med 2018; 24(3): 313-25.

Sreedharan J, Blair IP, Tripathi VB, Hu X, Vance C, Rogelj B, Ackerley S, Durnall JC, Williams KL, Buratti E, Baralle F, de Belleroche J, Mitchell JD, Leigh PN, Al-Chalabi A,

Miller CC, Nicholson G, Shaw CE. TDP-43 mutations in familial and sporadic amyotrophic lateral sclerosis. Science 2008; 319(5870): 1668-72.

Steinacker P, Feneberg E, Weishaupt J, Brettschneider J, Tumani H, Andersen PM, von Arnim CA, Bohm S, Kassubek J, Kubisch C, Lule D, Muller HP, Muche R, Pinkhardt E, Oeckl P, Rosenbohm A, Anderl-Straub S, Volk AE, Weydt P, Ludolph AC, Otto M. Neurofilaments in the diagnosis of motoneuron diseases: a prospective study on 455 patients. J Neurol Neurosurg Psychiatry 2016; 87(1): 12-20.

Steinacker P, Hendrich C, Sperfeld AD, Jesse S, von Arnim CA, Lehnert S, Pabst A, Uttner I, Tumani H, Lee VM, Trojanowski JQ, Kretzschmar HA, Ludolph A, Neumann M, Otto M. TDP-43 in cerebrospinal fluid of patients with frontotemporal lobar degeneration and amyotrophic lateral sclerosis. Arch Neurol 2008; 65(11): 1481-7.

Strong MJ, Abrahams S, Goldstein LH, Woolley S, McLaughlin P, Snowden J, Mioshi E, Roberts-South A, Benatar M, HortobaGyi T, Rosenfeld J, Silani V, Ince PG, Turner MR. Amyotrophic lateral sclerosis - frontotemporal spectrum disorder (ALS-FTSD): Revised diagnostic criteria. Amyotroph Lateral Scler Frontotemporal Degener 2017; 18(3-4): 153-74.

Suarez-Calvet M, Dols-Icardo O, Llado A, Sanchez-Valle R, Hernandez I, Amer G, Anton-Aguirre S, Alcolea D, Fortea J, Ferrer I, van der Zee J, Dillen L, Van Broeckhoven C, Molinuevo JL, Blesa R, Clarimon J, Lleo A. Plasma phosphorylated TDP-43 levels are elevated in patients with frontotemporal dementia carrying a C9orf72 repeat expansion or a GRN mutation. J Neurol Neurosurg Psychiatry 2014; 85(6): 684-91.

Svahn AJ, Don EK, Badrock AP, Cole NJ, Graeber MB, Yerbury JJ, Chung R, Morsch M. Nucleo-cytoplasmic transport of TDP-43 studied in real time: impaired microglia function leads to axonal spreading of TDP-43 in degenerating motor neurons. Acta Neuropathol 2018; 136(3): 445-59.

Talbot K. Amyotrophic lateral sclerosis: cell vulnerability or system vulnerability? J Anat 2014; 224(1): 45-51.

Tanaka Y, Hasegawa M. Profilin 1 mutants form aggregates that induce accumulation of prion-like TDP-43. Prion 2016; 10(4): 283-9.

Taylor RC, Dillin A. Aging as an event of proteostasis collapse. Cold Spring Harb Perspect Biol 2011; 3(5).

Thery C, Amigorena S, Raposo G, Clayton A. Isolation and characterization of exosomes from cell culture supernatants and biological fluids. Curr Protoc Cell Biol 2006; Chapter 3: Unit 3 22.

Thompson AG, Gray E, Heman-Ackah SM, Mager I, Talbot K, Andaloussi SE, Wood MJ, Turner MR. Extracellular vesicles in neurodegenerative disease - pathogenesis to biomarkers. Nat Rev Neurol 2016; 12(6): 346-57.

Thompson AG, Gray E, Mager I, Fischer R, Thezenas ML, Charles PD, Talbot K, El Andaloussi S, Kessler BM, Wood M, Turner MR. UFLC-Derived CSF Extracellular Vesicle Origin and Proteome. Proteomics 2018; 18(24): e1800257.

Thompson AG, Turner MR. Untangling neuroinflammation in amyotrophic lateral sclerosis. J Neurol Neurosurg Psychiatry 2019; 90(12): 1303-4.

Tollervey JR, Curk T, Rogelj B, Briese M, Cereda M, Kayikci M, Konig J, Hortobagyi T, Nishimura AL, Zupunski V, Patani R, Chandran S, Rot G, Zupan B, Shaw CE, Ule J. Characterizing the RNA targets and position-dependent splicing regulation by TDP-43. Nat Neurosci 2011; 14(4): 452-8.

Tortelli R, Ruggieri M, Cortese R, D'Errico E, Capozzo R, Leo A, Mastrapasqua M, Zoccolella S, Leante R, Livrea P, Logroscino G, Simone IL. Elevated cerebrospinal fluid neurofilament light levels in patients with amyotrophic lateral sclerosis: a possible marker of disease severity and progression. Eur J Neurol 2012; 19(12): 1561-7.

Toth RP, Atkin JD. Dysfunction of Optineurin in Amyotrophic Lateral Sclerosis and Glaucoma. Front Immunol 2018; 9: 1017.

Traynor BJ, Codd MB, Corr B, Forde C, Frost E, Hardiman OM. Clinical features of amyotrophic lateral sclerosis according to the El Escorial and Airlie House diagnostic criteria: A population-based study. Arch Neurol 2000; 57(8): 1171-6.

Turner MR, Kiernan MC. Does interneuronal dysfunction contribute to neurodegeneration in amyotrophic lateral sclerosis? Amyotroph Lateral Scler 2012; 13(3): 245-50.

Turner MR, Talbot K. Mimics and chameleons in motor neurone disease. Pract Neurol 2013; 13(3): 153-64.

Van Deerlin VM, Leverenz JB, Bekris LM, Bird TD, Yuan W, Elman LB, Clay D, Wood EM, Chen-Plotkin AS, Martinez-Lage M, Steinbart E, McCluskey L, Grossman M, Neumann M, Wu IL, Yang WS, Kalb R, Galasko DR, Montine TJ, Trojanowski JQ, Lee VM, Schellenberg GD, Yu CE. TARDBP mutations in amyotrophic lateral sclerosis with TDP-43 neuropathology: a genetic and histopathological analysis. Lancet Neurol 2008; 7(5): 409-16.

van den Berg LH, Sorenson E, Gronseth G, Macklin EA, Andrews J, Baloh RH, Benatar M, Berry JD, Chio A, Corcia P, Genge A, Gubitz AK, Lomen-Hoerth C, McDermott CJ, Pioro EP, Rosenfeld J, Silani V, Turner MR, Weber M, Brooks BR, Miller RG, Mitsumoto H, Airlie House ALSCTGG. Revised Airlie House consensus guidelines for design and implementation of ALS clinical trials. Neurology 2019; 92(14): e1610-e23.

van Eersel J, Ke YD, Gladbach A, Bi M, Gotz J, Kril JJ, Ittner LM. Cytoplasmic accumulation and aggregation of TDP-43 upon proteasome inhibition in cultured neurons. PLoS One 2011; 6(7): e22850.

van Es MA, Hardiman O, Chio A, Al-Chalabi A, Pasterkamp RJ, Veldink JH, van den Berg LH. Amyotrophic lateral sclerosis. Lancet 2017; 390(10107): 2084-98.

Vance C, Rogelj B, Hortobagyi T, De Vos KJ, Nishimura AL, Sreedharan J, Hu X, Smith B, Ruddy D, Wright P, Ganesalingam J, Williams KL, Tripathi V, Al-Saraj S, Al-Chalabi A, Leigh PN, Blair IP, Nicholson G, de Belleroche J, Gallo JM, Miller CC, Shaw CE.

Mutations in FUS, an RNA processing protein, cause familial amyotrophic lateral sclerosis type 6. Science 2009; 323(5918): 1208-11.

Vatsavayai SC, Yoon SJ, Gardner RC, Gendron TF, Vargas JN, Trujillo A, Pribadi M, Phillips JJ, Gaus SE, Hixson JD, Garcia PA, Rabinovici GD, Coppola G, Geschwind DH, Petrucelli L, Miller BL, Seeley WW. Timing and significance of pathological features in C9orf72 expansion-associated frontotemporal dementia. Brain 2016; 139(Pt 12): 3202-16.

Verstraete E, Kuiperij HB, van Blitterswijk MM, Veldink JH, Schelhaas HJ, van den Berg LH, Verbeek MM. TDP-43 plasma levels are higher in amyotrophic lateral sclerosis. Amyotroph Lateral Scler 2012; 13(5): 446-51.

Vetrivel KS, Gong P, Bowen JW, Cheng H, Chen Y, Carter M, Nguyen PD, Placanica L, Wieland FT, Li YM, Kounnas MZ, Thinakaran G. Dual roles of the transmembrane protein p23/TMP21 in the modulation of amyloid precursor protein metabolism. Mol Neurodegener 2007; 2: 4.

Visser J, van den Berg-Vos RM, Franssen H, van den Berg LH, Wokke JH, de Jong JM, Holman R, de Haan RJ, de Visser M. Disease course and prognostic factors of progressive muscular atrophy. Arch Neurol 2007; 64(4): 522-8.

Walker LC, Jucker M. Neurodegenerative diseases: expanding the prion concept. Annu Rev Neurosci 2015; 38: 87-103.

Wang HY, Wang IF, Bose J, Shen CK. Structural diversity and functional implications of the eukaryotic TDP gene family. Genomics 2004; 83(1): 130-9.

Wang IF, Guo BS, Liu YC, Wu CC, Yang CH, Tsai KJ, Shen CK. Autophagy activators rescue and alleviate pathogenesis of a mouse model with proteinopathies of the TAR DNA-binding protein 43. Proc Natl Acad Sci U S A 2012; 109(37): 15024-9.

Wang X, Fan H, Ying Z, Li B, Wang H, Wang G. Degradation of TDP-43 and its pathogenic form by autophagy and the ubiquitin-proteasome system. Neurosci Lett 2010; 469(1): 112-6.

Webster CP, Smith EF, Bauer CS, Moller A, Hautbergue GM, Ferraiuolo L, Myszczynska MA, Higginbottom A, Walsh MJ, Whitworth AJ, Kaspar BK, Meyer K, Shaw PJ, Grierson AJ, De Vos KJ. The C9orf72 protein interacts with Rab1a and the ULK1 complex to regulate initiation of autophagy. EMBO J 2016; 35(15): 1656-76.

Wegorzewska I, Bell S, Cairns NJ, Miller TM, Baloh RH. TDP-43 mutant transgenic mice develop features of ALS and frontotemporal lobar degeneration. Proc Natl Acad Sci U S A 2009; 106(44): 18809-14.

Westeneng HJ, Debray TPA, Visser AE, van Eijk RPA, Rooney JPK, Calvo A, Martin S, McDermott CJ, Thompson AG, Pinto S, Kobeleva X, Rosenbohm A, Stubendorff B, Sommer H, Middelkoop BM, Dekker AM, van Vugt J, van Rheenen W, Vajda A, Heverin M, Kazoka M, Hollinger H, Gromicho M, Korner S, Ringer TM, Rodiger A, Gunkel A, Shaw CE, Bredenoord AL, van Es MA, Corcia P, Couratier P, Weber M, Grosskreutz J, Ludolph AC, Petri S, de Carvalho M, Van Damme P, Talbot K, Turner MR, Shaw PJ, Al-Chalabi A, Chio A, Hardiman O, Moons KGM, Veldink JH, van den Berg LH. Prognosis for patients with amyotrophic lateral sclerosis: development and validation of a personalised prediction model. Lancet Neurol 2018; 17(5): 423-33.

Weydt P, Oeckl P, Huss A, Muller K, Volk AE, Kuhle J, Knehr A, Andersen PM, Prudlo J, Steinacker P, Weishaupt JH, Ludolph AC, Otto M. Neurofilament levels as biomarkers in asymptomatic and symptomatic familial amyotrophic lateral sclerosis. Ann Neurol 2016; 79(1): 152-8.

Wiese S, Herrmann T, Drepper C, Jablonka S, Funk N, Klausmeyer A, Rogers ML, Rush R, Sendtner M. Isolation and enrichment of embryonic mouse motoneurons from the lumbar spinal cord of individual mouse embryos. Nat Protoc 2010; 5(1): 31-8.

Wijesekera LC, Mathers S, Talman P, Galtrey C, Parkinson MH, Ganesalingam J, Willey E, Ampong MA, Ellis CM, Shaw CE, Al-Chalabi A, Leigh PN. Natural history and clinical features of the flail arm and flail leg ALS variants. Neurology 2009; 72(12): 1087-94.

Williams SM, Khan G, Harris BT, Ravits J, Sierks MR. TDP-43 protein variants as biomarkers in amyotrophic lateral sclerosis. BMC Neurosci 2017; 18(1): 20.

Winton MJ, Igaz LM, Wong MM, Kwong LK, Trojanowski JQ, Lee VM. Disturbance of nuclear and cytoplasmic TAR DNA-binding protein (TDP-43) induces disease-like redistribution, sequestration, and aggregate formation. J Biol Chem 2008; 283(19): 13302-9.

Woerner AC, Frottin F, Hornburg D, Feng LR, Meissner F, Patra M, Tatzelt J, Mann M, Winklhofer KF, Hartl FU, Hipp MS. Cytoplasmic protein aggregates interfere with nucleocytoplasmic transport of protein and RNA. Science 2016; 351(6269): 173-6.

Xiao S, Sanelli T, Chiang H, Sun Y, Chakrabartty A, Keith J, Rogaeva E, Zinman L, Robertson J. Low molecular weight species of TDP-43 generated by abnormal splicing form inclusions in amyotrophic lateral sclerosis and result in motor neuron death. Acta Neuropathol 2015; 130(1): 49-61.

Xiao S, Sanelli T, Dib S, Sheps D, Findlater J, Bilbao J, Keith J, Zinman L, Rogaeva E, Robertson J. RNA targets of TDP-43 identified by UV-CLIP are deregulated in ALS. Mol Cell Neurosci 2011; 47(3): 167-80.

Yamashita T, Hideyama T, Hachiga K, Teramoto S, Takano J, Iwata N, Saido TC, Kwak S. A role for calpain-dependent cleavage of TDP-43 in amyotrophic lateral sclerosis pathology. Nat Commun 2012; 3: 1307.

Ying Z, Xia Q, Hao Z, Xu D, Wang M, Wang H, Wang G. TARDBP/TDP-43 regulates autophagy in both MTORC1-dependent and MTORC1-independent manners. Autophagy 2016; 12(4): 707-8.

Zhang HX, Tanji K, Mori F, Wakabayashi K. Epitope mapping of 2E2-D3, a monoclonal antibody directed against human TDP-43. Neurosci Lett 2008; 434(2): 170-4.

Zhang T, Baldie G, Periz G, Wang J. RNA-processing protein TDP-43 regulates FOXO-dependent protein quality control in stress response. PLoS Genet 2014; 10(10): e1004693.

Zhang YJ, Xu YF, Cook C, Gendron TF, Roettges P, Link CD, Lin WL, Tong J, Castanedes-Casey M, Ash P, Gass J, Rangachari V, Buratti E, Baralle F, Golde TE, Dickson DW, Petrucelli L. Aberrant cleavage of TDP-43 enhances aggregation and cellular toxicity. Proc Natl Acad Sci U S A 2009; 106(18): 7607-12.

Zoccolella S, Beghi E, Palagano G, Fraddosio A, Samarelli V, Lamberti P, Lepore V, Serlenga L, Logroscino G, registry S. Predictors of delay in the diagnosis and clinical trial entry of amyotrophic lateral sclerosis patients: a population-based study. J Neurol Sci 2006; 250(1-2): 45-9.

Zou ZY, Zhou ZR, Che CH, Liu CY, He RL, Huang HP. Genetic epidemiology of amyotrophic lateral sclerosis: a systematic review and meta-analysis. J Neurol Neurosurg Psychiatry 2017; 88(7): 540-9.